ORNL
MASTER COPY

ORNL-3492
UC-41 — Health and Safety
TID-4500 (22nd ed.)

HEALTH PHYSICS DIVISION
ANNUAL PROGRESS REPORT
FOR PERIOD ENDING JUNE 30, 1963

OAK RIDGE NATIONAL LABORATORY
operated by
UNION CARBIDE CORPORATION
for the
U.S. ATOMIC ENERGY COMMISSION

Printed in USA. Price: $3.00. Available from the
Office of Technical Services
U. S. Department of Commerce
Washington 25, D. C.

LEGAL NOTICE

This report was prepared as an account of Government sponsored work. Neither the United States, nor the Commission, nor any person acting on behalf of the Commission:

A. Makes any warranty or representation, expressed or implied, with respect to the accuracy, completeness, or usefulness of the information contained in this report, or that the use of any information, apparatus, method, or process disclosed in this report may not infringe privately owned rights; or

B. Assumes any liabilities with respect to the use of, or for damages resulting from the use of any information, apparatus, method, or process disclosed in this report.

As used in the above, "Person acting on behalf of the Commission" includes any employee or contractor of the Commission, or employee of such contractor, to the extent that such employee or contractor of the Commission, or employee of such contractor prepares, disseminates, or provides access to, any information pursuant to his employment or contract with the Commission, or his employment with such contractor.

ORNL-3492
UC-41 – Health and Safety
TID-4500 (22nd ed.)

Contract No. W-7405-eng-26

HEALTH PHYSICS DIVISION ANNUAL PROGRESS REPORT

For Period Ending June 30, 1963

K. Z. Morgan, Director
W. S. Snyder, Assistant Director
E. G. Struxness, Assistant Director

DATE ISSUED

SEP 23 1963

OAK RIDGE NATIONAL LABORATORY
Oak Ridge, Tennessee
operated by
UNION CARBIDE CORPORATION
for the
U. S. ATOMIC ENERGY COMMISSION

Summary

PART I. RADIOACTIVE WASTE DISPOSAL

1. Liquid Injection into Deep Permeable Formations

The Ca-Sr exchange properties of numerous minerals show that these two cations behave quite similarly in ion exchange reactions. In cases where precipitation of slightly soluble salts occurs, the relative behavior may differ appreciably; strontium is less likely to be removed from solution than calcium by calcium carbonate but more likely to be removed by phosphatic minerals.

Solution dispersion due to formation heterogeneities is likely to lead to radionuclide dispersion a few orders of magnitude greater than that observed in laboratory columns. As a result, the factors affecting dispersion in laboratory columns are likely to be of little influence in affecting radionuclide dispersion in the environment.

In order to study geometric effects of dispersion of radionuclides by porous media and to test the effectiveness of physical and chemical barriers on a laboratory scale, a sandstone model has been constructed. The kinetics of ion exchange reactions observed in linear-flow columns will be extrapolated to the two-dimensional flow system, and the calculated response compared to measured values.

2. Disposal by Hydraulic Fracturing

An acceptable waste mix has been developed that is usable with waste solutions having a wide range of concentrations and chemical compositions. It is probable that an equally acceptable, cheaper mix can be developed that will require less of the expensive fluid-loss additive.

An injection and an observation well have been drilled, logged, cased, and cemented. These wells are 1080 ft deep; the main casing string of the injection well is $5\frac{1}{2}$ in. OD, and the main casing string of the observation well is $2\frac{7}{8}$ in. OD.

The design of the injection plant is virtually complete. The equipment consists of waste storage tanks, a waste transfer pump, four bulk storage tanks to store the solid constituents of the mix, a jet mixer, a high-pressure injection pump, and a standby injection pump and mixer. The mixer, injection pump, and wellhead valving will be installed in cells to reduce radiation exposure and limit the area of possible contamination.

In the proposed experiments several 40,000-gal batches of intermediate-level waste solution will be mixed with cement and injected into a shale formation at an approximate depth of 900 ft. At some time after the completion of the third injection the formation will be core drilled to verify the location of the grout sheets and to evaluate the various mixes.

3. Disposal in Natural Salt Formations

A 2-ft-high by 8-ft-wide model room was cut into a pillar to a depth of 10 ft, and closure rates were measured both before and during heating of the room to 160°C. The floor-to-ceiling closure rate after 40 days of heating (5×10^{-3} in./day) was two orders of magnitude higher than that at ambient temperature. Continued flow at this rate would completely close the room in 12 yr.

Measurements of creep closure in the Hutchinson, Kansas, mine in rooms ranging in age from about 1 to 27 yr indicate that closure rates decrease with age but increase with increased salt extraction. The floor-to-ceiling closure rates range from 8×10^{-4} to 1×10^{-4} in./day.

A demonstration of disposal of high-level radioactive waste solids is being designed for the Carey Salt Company mine in Lyons, Kansas. The

purposes of the demonstration are to perfect equipment and techniques and to investigate the synergistic effects of heat, radiation, and pressure on plastic flow, salt stability, and chlorine production. The demonstration will consist of a seven-can array of fuel assemblies, an electrical-heat-equivalent array, and two sets of electrical heaters to heat a pillar between the two arrays. Fourteen irradiated Engineering Test Reactor fuel assemblies will provide radiation in lieu of actual solidified waste. The test will last 2 yr; then all fuel assemblies will be returned to the Idaho Chemical Processing Plant for recovery of unfissioned fuel.

High-temperature studies on the disposal of high-level solid wastes have continued. In tests with 6-in.-diam by 4-ft-long heat sources (in 10-in.-diam by 10-ft-deep holes in the floor and wall), the effects of salt temperatures up to 350°C were investigated. Shattering of salt *in situ* in the Hutchinson mine occurred at about 280°C, in comparison to a range of 260 to 320°C determined from samples in the laboratory. Maximum reduction in hole diameter was 15%, due to nonrecoverable thermal expansion at a salt temperature of 350°C. Nonrecoverable expansion of about ½ in. of the floor and wall around the holes was also observed.

Experimental work on KCl has been used to calculate total production of chlorine in irradiated NaCl. After 200 days, a total of 0.5 mole of oxidizing agent would be produced per 6-in.-diam by 12-ft-long can of hypothetical (expected to be produced about 1975) solid waste. Irradiation of NaCl indicates that these values are conservative and that for short-term storage of high-level wastes in salt, little or no production of free chlorine can be expected.

Creep measurements in the Hutchinson mine indicate that the greater the percent of extraction, the greater the creep, and the older the age of the excavation, the lower the creep, with an average closure rate of 5×10^{-4} in./day.

Cores taken from the floor and roof of the Lyons mine showed that the only extensive pure salt deposits in the formation are those currently being mined. Therefore it was concluded that the experiment should be run in the same salt bed previously mined.

4. Clinch River Study

Results from the first year's water-sampling program indicate that most of the radioactive material entering the Clinch River from ORNL passes out of the river system in the water phase. The second year's data indicate some anomalous results, but thorough sampling of potential routes of contamination failed to reveal any other source than the monitored flow through White Oak Dam. Sampling has been discontinued until a new sampling program, designed to proportionally sample the flow releases from Melton Hill Dam, is installed.

Core samples from the Clinch River system were taken to obtain the radioactive material profile in the river and to determine the radioactive inventory in the bottom sediments. Specially designed counting equipment has been installed to automatically count the core in preset increments for gross gamma and to gamma-scan specific portions of the core.

Correlation analyses of the radionuclides in the bottom sediments indicate that Cs^{137}, Ru^{106}, TRE, and Co^{60} are apparently deposited by similar mechanisms and that Zr^{95}-Nb^{95} and Sr^{90} are deposited by different mechanisms. It may be possible to predict movement of the group of nuclides by counting just one.

Melton Hill Dam, a peaking power plant, will affect the hydraulic regime in the Clinch River by the sudden changes in discharge. Flume tests indicate that the effect of these changes will not cause greater dispersion than that observed with steady flow.

A preliminary safety analysis of the discharge of radionuclides to the Clinch River has been made. Dosages were compiled for the bone, gastrointestinal tract, thyroid, gonads, and total body for people at Clinch River Miles 14.5 and 2.6 and Tennessee River Miles 529.9 and 465.5, the critical points on the river system. For drinking water the largest fraction of $(MPC)_w$ attained was 0.51 in 1954. Variations in intake for sex and age differences indicate that dosages different than those obtained by standard man are possible. Immersion in contaminated water resulted in a maximum dose of 0.027 millirad/day in 1960. The greatest dose from bottom sediments was 12 millirads per day of exposure in 1959. Other potential sources of exposure being investigated are those due to ingestion of irrigated crops and contaminated fish.

5. Study of White Oak Creek Drainage Basin

Analyses of a series of 250 core samples taken in the bed of former White Oak Lake showed that, as of December 1962, the soil contained 1038 curies of Ru^{106}, 704 curies of Cs^{137}, 152 curies of Co^{60}, 17 curies of the rare earths (exclusive of Y^{90}), and 15 curies of Sr^{90}. Approximately 65% of the activity was found in the upper 6 in. of soil.

Studies on the movement of radionuclides in White Oak Creek indicate that (1) the amount of activity transported downstream by suspended solids is small during low creek flow rates and/or low suspended-solids loads, but during high stream flow and/or high suspended-solids loads, significant quantities of strontium and practically all the cesium are associated with sediments; (2) suspended solids of less than 9 μ sorb considerably more activity than larger particles; and (3) the amount of cesium associated with suspended solids increases considerably with a rise in the creek, and the amount of strontium associated with the liquid phase shows a pronounced increase.

Mean velocities in White Oak Creek of 0.4 to 2.3 fps at discharges ranging from 4.5 to 200 cfs have been determined from time-of-travel studies.

Water levels were measured in the permanent wells in White Oak Creek Basin in March (the time of highest ground-water surface) and showed greater annual variations at the higher elevations above the valley floor than at the lower elevations.

6. Mineral Exchange Studies

Heat-treated gibbsite is highly selective for strontium in alkaline systems. The capacity of heat-treated gibbsite is approximately 4 meq/100 g for cesium and 12 meq/100 g for strontium. The affinity for strontium of the heat-treated material is reflected by the lessened ability of sodium ions to desorb the strontium. After the sorbent was leached with sodium equal to 23 meq of Na^+ per meq of sorbed Cs^+, 96% of the cesium was desorbed; but when strontium was sorbed, only 77% of the strontium was desorbed after leaching with sodium equal to 730 times the amount of strontium on the sorbent.

Several other hydrous oxide minerals were heated to 500°C in order to determine whether this heat treatment could improve their properties for sorbing strontium. Goethite ($HFeO_2$), diaspore ($HAlO_2$), and limonite ($Fe_2O_3 \cdot xH_2O$) were used; heat-treated limonite showed the best strontium-sorbing characteristics.

Strontium removals by four different sorbents were compared using column techniques. Tests were performed using a 0.5 *M* $NaNO_3$ solution adjusted to pH 10 and containing 10^{-5} *M* $Sr(NO_3)_2$; the flow rate was 3 ml min^{-1} cm^{-2}. Commercial-grade activated alumina was most efficient; the 50% breakthrough volume for 10 g of material was approximately 6500 cm^3; the same weight of Dowex 50-X12 treated 2600 cm^3 for the same breakthrough percentage.

Sorption of trace quantities of cesium by vermiculite can be improved by pretreatment with potassium to increase the number of collapsed lattices available for edge fixation. Continued leaching of the treated vermiculite with 0.5 *M* $NaNO_3$, containing traces of cesium (1.7×10^{-7} *M*), releases the interlayer potassium and negates the pretreatment. Addition of potassium in the influent was found effective in maintaining potassium-treated vermiculite in a collapsed state. A concentration of 0.0005 *M* KNO_3 in 0.5 *M* $NaNO_3$ gave optimum cesium sorption (K_d = 366 ml/g) and a final exchange capacity of 46.8 meq/100 g compared to the initial exchange capacity of the potassium-saturated vermiculite of 5.9 meq/100 g.

Interlayer fixation of trace quantities of strontium was not observed when the vermiculite lattice was collapsed by addition of 0.01 to 0.04 *M* KNO_3 to 0.5 *M* $NaNO_3$ influent. The sorption of strontium was reduced by increases in the potassium concentration of the influent, and approximately 80% of the strontium was removed during the determination of the exchange capacity following column saturation.

7. Engineering, Economic, and Safety Evaluations

Studies of interim storage of calcined wastes and the effects of fission product removal on waste-management costs have been completed.

Interim storage facilities were designed to handle calcined waste cylinders for assumed storage periods of 1, 3, 10, and 30 yr. The computed costs of storage of Purex and Thorex wastes together in the same facility ranged from 0.0015 mill/kwhr (electrical) for 1 yr storage to 0.0048 mill/kwhr (electrical) for 30 yr storage for the

calcined acid wastes, and from 0.0018 to 0.0063 mill/kwhr (electrical) for the calcined reacidified wastes.

The object of the fission-product-removal study was to compare the waste-management costs for wastes with 90 and 99% of the fission products removed with the costs for managing the original waste with all fission products present. In each case, costs were estimated for the interim storage of liquid waste, pot calcination of waste, shipment of the calcined solids, and disposal of the solids in a salt mine. Total waste-management costs for the waste depleted of 99% of the fission products were only about 7% lower than for the 90%-depleted wastes, and both fell in the range of 0.017 to 0.019 mill/kwhr (electrical). Management costs for the original waste [0.024 mill/kwhr (electrical)] were only about one-third higher.

The tank storage hazard study has resumed under a modified set of basic postulates. Possible exposures of large populations to radiation resulting from accidental large-scale activity releases are being considered theoretically.

8. Related Cooperative Projects

The U.S. Geological Survey has continued to obtain partial-record base-flow and crest-stage records for the area. In addition, a geologic map of White Oak Creek Basin, with an explanatory text, has been prepared.

The multiagency steering committee for the Clinch River Study has continued.

Three alien guests have been on assignment during the past year.

Several members of the Section have continued to participate in the following activities: the ASA Committee N5, the AEC Advisory Committee on Deep-Well Disposal, the ASCE Committee on Sanitary Engineering Aspects of Nuclear Energy, and various ORNL special committees; members have also contributed to the journal *Nuclear Safety*.

In addition, courses and lectures have been given for ORSORT, Vanderbilt University, and the U.S. Public Health Service.

PART II. RADIATION ECOLOGY

9. Radioactive Waste Area and Radiation Effects Studies

In new dosimetry studies, miniature metaphosphate glass rods are being used to estimate absorbed dose in air and in the plants and soils of White Oak Lake bed. Combined beta and gamma doses in the top inch of mineral soil ranged from 20 to 25 rads/day on the northwest edge of the lake bed where Ru^{106} seepage from higher ground is appreciable. Absorbed doses in air at the surface of marsh plants (*Typha latifolia* L.) in this area ranged vertically from 6.2 rads/day at ground level to 2.8 rads/day at 5 ft above the ground. Absorbed doses in stem tissue of these plants were 23% higher due to absorbed radionuclides, principally Ru^{106}. The dose to root systems was three to seven times higher than the dose to shoot components.

In food-chain studies of cotton rats maintained in pens on White Oak Lake bed and feeding on native vegetation, it was found that (1) the concentrations of radionuclides in tissues are positively correlated with the corresponding concentrations in stomach contents and plants, (2) the concentrations of radionuclides in tissues are not correlated with corresponding concentrations in soil, (3) Sr^{90} in femurs is the only radionuclide in the tissues which was in greater concentration than in food or plants, and (4) the placental and mammary barriers apparently were effective in reducing the concentration of Sr^{90} in fetuses and nursing young.

Blood samples were taken from the original cotton rats one week before release into pens and at 4- to 6-week intervals thereafter. Blood analyses were also made on samples from rats born in the pens. Analyses of erythrocyte and leucocyte counts, leucocyte differential counts, hematocrits, mean corpuscular volumes, cell-volume distributions, and total serum solids were performed. These analyses showed no apparent effects of ionizing radiation in the blood of cotton rats maintained in the pens for this first experiment.

Studies on hematology of native mammals continued to support the discovery last year that the number of erythrocytes is inversely related to species size and that the mean erythrocyte volume is directly related to the species size. This

relation was found to be present in the rodent families Muridae and Sciuridae, the shrew family Soricidae, and the primate family Cebidae. Seasonal effects on the blood of native mammals are being followed because of variations noted in cell counts and hematocrits of the blood of mammals trapped during various seasons of last year. Erythrocyte counts and hematocrits, for instance, in some species seem to be higher in the winter than during other seasons.

Use of trees as long-term monitors of radioactive seepage from underground waste pits was tested by sampling even-age pines growing around waste pit No. 5. Significant concentrations of four gamma-emitting radionuclides were found in these pine trees. These nuclides were Ru^{106}, Zr^{95}-Nb^{95}, Cs^{137}, and Ce^{144}. Concentration of Ce^{144} was between 100 and 200 $\mu\mu c$ per g of dry weight, which is the same as fallout levels. Cesium-137 concentration was uniform in all trees at 30 to 70 $\mu\mu c$ per g of dry weight. This amount could be attributed to blowout from three open pits which are due west of waste pit No. 5. Ruthenium-106 concentration varied from 0.02 μc per g of dry weight to fallout levels, which are 40 to 70 $\mu\mu c$ per g of dry weight. Twenty-three of the seventy-three trees collected showed a concentration of Ru^{106} greater than that which could be attributed to fallout or to blowout from the open pits. This higher concentration is attributed to seepage (and subsequent uptake by the tree) from waste pit No. 5. Five trees showed a concentration of Zr^{95}-Nb^{95} which was greater than fallout levels and also greater than Ru^{106} levels. The highest concentration of Zr^{95}-Nb^{95} was 771 $\mu\mu c$ per g of dry weight. Concentration of all the isotopes except Zr^{95}-Nb^{95} tended to be greater in needle material than in twig material.

Fission foil threshold detectors were used to determine the fast-neutron dose absorbed by white oak acorns irradiated in the ORNL Graphite Reactor. The acorns were irradiated in a $17 \times 8 \times 4.5$ in. box of boron carbide—impregnated Lucite, which absorbed thermal neutrons (over 50% of the total flux) but allowed fast neutrons to pass through the seed. Fission foils and pellets of S^{32} were placed under and on top of the sample to be irradiated — seed stacked to a depth of 4 in. After irradiation the foils and sulfur were counted immediately in the special fission foil counters of the Health Physics Division. Dose calculations were made according to the method of Hurst and Ritchie. The dose under 4 in. of acorns was 1755.8 rads/hr, whereas the dose over 4 in. was approximately 1250 rads/hr.

Use of biological elimination of radioisotopes in insects as indirect measures of metabolism under field conditions was continued with emphasis on the influence of temperature on elimination rates. In geometrid caterpillars the biological half-life of Cs^{137} was decreased by one-half for a 10° rise in temperature. Similar temperature-related trends were found for leaf beetles (*Chrysomela knabi*) and millipedes (*Dixidesmus erasus*).

10. Forest Studies

Computer feedback models have included compartments for woody materials, as a step toward interpreting patterns of forest growth. The positive feedback representing increased photosynthetic rate with increased foliage mass is counteracted by opposing negative feedbacks, representing not only the loss rates from respiration and other processes (litter fall, consumption, translocation) but also a "limiting feedback" related to the capabilities of an area for producing organic matter. Diurnal and seasonal cycles of production have been combined in the same model.

Further analyses of two- and three-year comparative experiments, in cooperation with the Botany Department of the University of Tennessee, showed different rates of breakdown for several kinds of deciduous leaves measured in the Oak Ridge Reservation and the Great Smoky Mountains. In all environments, leaf species showed large and consistent differences in weight loss of leaves confined in bags of nylon net. Mulberry decayed rapidly to black humus, losing 0.002 to 0.0046 of its total weight per day in different environments. Beech showed the slowest visible signs of decay, with fractional weight losses of only 0.0003 to 0.0012 per day. White oak, Shumard red oak, and sugar maple showed intermediate rates of weight loss and visible destruction. Yearly differences in decay rates emphasize the need for several-year experiments, using closely compared sets of techniques, for drawing generalizations about rates of ecological processes which affect the movement of nutrients or isotopes in contrasting environments.

Seasonal measurements of microbial populations of four leaf species in three contrasting forest

types during the first year showed a highly significant correlation between leaf weight loss and microbial respiration, especially that of bacteria. Seasonal fluctuations of microbial respiration were primarily correlated with temperature, but other significant correlations were found with bacterial counts, moisture content of the leaves, and age of the litter.

The first large-scale tracer experiment employing Cs^{137} in a small stand of yellow poplar is confirming the expectation of rapid circulation of Cs^{137} through the forest ecosystem. The rapid attainment of maximum foliage concentrations in June was followed by a decrease throughout the growing season. Evidence was found of a marked withdrawal of Cs^{137} from the leaves back into the trunk prior to leaf fall. Rainwater collections further supported the possibility that in late summer there is a period in which alkali metal reserves are remobilized into the tree. Paper chromatography analyses, autoradiograms, and column elution tests showed that the bulk of Cs^{137} activity is in the phloem tissue (parenchyma), where it exists only in the ionic form, and that only ionic bonding takes place between the cesium and the wood.

In addition to Cs^{137} income from rainfall and litter fall, downward movement of Cs^{137} in roots of tulip poplar apparently provides an important contribution of this nuclide into the soil (Emory silt loam) of the tagged forest. Early litter sampling on lines on a close spacing (2 cm) showed very abrupt variation, due partly to uneven movement of rainout over the incomplete litter cover of the mull humus. The extent of variation within centimeter distances was greater than two orders of magnitude. Early sampling indicated the importance of root contribution to the highly variable initial distribution. Root fragments which could be separated from inorganic soil particles contributed at least 90% of the total activity as of July 16, 1962. Fine rootlets that could not be separated from sieved mineral soil may already have contributed to radioactivity in this and subsequent samples.

Wide differences in concentrations of Cs^{137} were found in mushrooms growing on the tagged forest floor. This variability was not only the result of large differences among substrates but also the result of differences within one substrate at different locations. Concentrations of Cs^{137} in litter were from 0.1 to 68 times lower than the concentrations in the underlying soil and roots. Variations in concentrations of Cs^{137} in mineral soil exceeded two orders of magnitude for surface samples taken only 10 cm apart.

Two types of food chains are being compared in the tagged forest: the green foliage–herbivorous arthropod–predaceous arthropod type of food chain and the leaf litter–herbivorous arthropod–predaceous arthropod type. Cesium-137 concentrations were lower in the leaf litter–soil arthropod food chain than in the green foliage food chain, since leaching of cesium from green leaves was the radioisotope source for the litter layers. Radioisotope concentration in leaf litter increased gradually during the summer and abruptly during the early autumn as leaf fall progressed. During the summer months herbivores had Cs^{137} concentrations almost as high as the concentration in leaf litter. Herbivore radioactivity increased in the autumn but not as rapidly as did leaf litter radioactivity. Predators also showed an increase in Cs^{137} content during the summer and early autumn. During July and August the herbivore and predator parts of the leaf litter–soil arthropod food chain had an added input due to direct feeding on the green foliage. Phalangids (*Liobunum* sp.), for example, had Cs^{137} contents which were a factor of 2 or more higher than leaf litter concentrations. Also, some of the predators were evidently feeding in the green foliage food chain although they were trapped on the forest floor. The result was that the animal portions of the leaf litter food chain appeared abnormally high during July and August. In October the green foliage had disappeared, and the leaf litter food chain assumed a Cs^{137} distribution resembling that of the green foliage food chain.

11. Clinch River and Related Aquatic Studies

Aquatic studies continue to emphasize the fate and effects of radionuclides released to the Clinch River via White Oak Creek. Analyses of stable strontium in the flesh and bone of white crappie were continued to test the relation of the distribution of stable strontium and Sr^{90} between the environment and the fish. If the distribution of stable strontium and Sr^{90} between fish tissue and water are the same, it should be possible to predict Sr^{90} concentrations in tissue for continuous environmental releases. Samples have been taken

at monthly intervals to determine whether there are seasonal changes in the strontium concentrations in fish tissue. The average stable-strontium concentration in bone is 271 ± 6.34 ppm (± one standard error) based on 105 samples. This quantity of strontium in bone is a concentration factor of 4.0×10^3 over that in Clinch River water. Strontium concentrations in flesh average 0.0813 ± 0.0118 ppm (27 samples), which is a concentration factor of 1.2 over that of river water.

The biological half-life of strontium in white crappie has been determined by tagging fish with Sr^{85} and then counting the same fish at 1-min intervals in a small-animal whole-body counter. In experiments completed, the biological half-life of strontium in the flesh of different individuals has ranged from 12 to 48 min, somewhat shorter than anticipated previously. Measurement of the turnover of strontium in flesh was complicated by the rapid deposition and high concentration of strontium in fish bone, which literally masked the strontium in soft tissues. This difficulty was circumvented by constructing a fish-holding assembly and inserting it in the detector chamber of the counter. Water was pumped through the assembly during the experiments to remove excreted Sr^{85} and to provide a supply of oxygenated water.

The transport of Sr^{90} from the Clinch River by emerging aquatic midges (Chironomidae) was compared with the accrual of Sr^{90} to the river from weapons-testing fallout. Larval development of the midges occurs in the contaminated river-bottom sediments. Emerging adults were caught in insect light traps operated on the river bank at dusk. Adults in one large, composite sample contained 8.76 times as much Sr^{90} [$(3.55 \pm 1.13) \times 10^{-6}$ μc per gram of dry weight] as did an equal quantity of river-bottom sediment from the same location. Studies elsewhere have shown that 10 g m^{-2} yr^{-1} may be contained in the emergent insect biomass. These emergent insects would transport $(3.55 \pm 1.13) \times 10^{-5}$ μc of Sr^{90} per square meter per year from the river bottom. The average increment of Sr^{90} from fallout in the United States between 1959 and 1960 was 4.2×10^{-3} curie/square mile (1.62×10^{-3} $\mu c/m^2$). Thus, fallout entering the river directly would add 45 times as much Sr^{90} as removed by emerging chironomids.

Studies of the relative influence of stable strontium and stable calcium on strontium are in progress using the snail *Physa heterostropha* and highly purified and assayed calcium carbonate. Preliminary results suggest that strontium uptake is dependent primarily on stable strontium in the environment.

A study of the age distribution, growth rates, and dispersion of smallmouth buffalo, *Ictiobus bubalus* (Rafinesque), in Watts Bar Reservoir, and of their importance as an accumulator of radionuclides, was completed. The ages of 1271 commercially caught fish ranged from 4 to 15 yr; the largest number were from year class 6, the youngest year class which was completely vulnerable to commercial fishing gear. Total survival rates were found to be 49% for year class 6, 35% for year class 7, 26% for year class 8, and 19% for year class 9.

A high concentration of radionuclides in the environment was found to be necessary for smallmouth buffalo to accumulate measurable quantities in their scales. White Oak Creek is the only area of Watts Bar with sufficient radionuclide contamination for such accumulation to occur. If surface area is considered a measure of available fish habitat, White Oak Creek comprises less than 0.02% of Watts Bar Reservoir at full pool. Only a small percentage of the population would be expected to be resident in the contaminated area. However, with mobile populations contamination could be expected in larger numbers of fish because of movement into and out of White Oak Creek. This contamination could be detected in tissues such as bone or scales having a long biological half-life for the several radionuclides released. Radiometric surveys of scales revealed the smallmouth buffalo population of Watts Bar Reservoir to be a relatively minor accumulator of radionuclides, with only 0.08% having a detectable accumulation in their scales. Approximately 6% of the Clinch River fish and 77% of the White Oak Creek fish had measurable radionuclide accumulations.

The salivary gland chromosomes of *Chironomus tentans* larvae collected from White Oak Creek, an area contaminated by radioactive waste from ORNL, and from six uncontaminated areas were examined for chromosomal aberrations. White Oak Creek populations were exposed to a dose rate calculated as 230 rads/yr, or about 1000 times background. Fifteen different chromosomal aberrations were found in 365 larvae taken from the irradiated population as compared with five different aberrations observed in 356 larvae from six

control populations, but the mean number of aberrations per larva did not differ in any of the populations. The quantitative amount of heterozygosity was essentially the same in the irradiated and the control population, but there was three times the variety of chromosomal aberrations found in the irradiated area. From this evidence it was concluded that chronic low-level irradiation from radioactive waste was increasing the variability of chromosomal aberrations without significantly increasing the frequency.

PART III. RADIATION PHYSICS AND DOSIMETRY

12. Theoretical Radiation Physics

Calculations of rad and rem doses in a tissue slab from protons with energies up to 400 Mev have been completed. A code has also been developed for calculating dose in a finite geometry phantom (parallelepiped), and results for this case are nearing completion. Preliminary studies at proton energies greater than 400 Mev are in progress.

A code has been written to compute the distribution of dose with LET, in order to analyze the biological response of animals exposed to neutron irradiation. An investigation of shell corrections in atomic stopping-power theory has been made. The low-energy end of the slowing-down spectrum of electrons in a free-electron gas has been computed using a numerical solution of the appropriate integral equation and numerical values of the requisite interaction cross sections. The dispersion relation for surface plasmons has been investigated in a semiclassical approximation. An analytic solution for the distribution of transition radiation from a two-layered foil has been obtained. A semiclassical derivation has been given of the cross section for photon absorption in metals due to the presence of impurity scattering centers. A formulation of the constitutive equations for a moving medium has been given. The interaction of an electron or an ion beam moving through a stationary plasma has been investigated.

13. Experimental Physics of Dosimetry

Recent work on the interaction of alpha particles with water molecules reveals that the interaction is a physical process in which the cross section for momentum transfer is a factor of 2 larger than that obtained from theory. The cross section for the dissociative electron capture process in D_2O has been measured and compared with that obtained in H_2O.

The recently developed time-of-flight technique for investigation of electron transport in gases has been applied to the measurement of drift velocities and diffusion coefficients in several gases and, in particular, in mixtures of water vapor and ethylene. A newer version of the electron time-of-flight machine is under construction and will permit measurements to be made for a wider range of gases. A combination of spectroscopic and ionization experiments on the effect of alpha particles on atomic argon has led to a rather complete description of the ways in which alpha particles interact with atomic argon.

The angular and spectral distribution of photons emitted by silver foils, 660 and 1980 A thick, when bombarded by 40-kev electrons has been determined experimentally in the wavelength region 2500 to 5600 A. The spectral distribution of light polarized in the plane of incidence showed a sharp peak at 3300 ± 12 A, this value being an average over photon directions 10 to 50° from the foil normal. In addition to the peak, the spectrum showed a continuum which decreased slowly with increasing wavelength and a deep minimum at 3200 A with a rise in the shorter wavelengths. The angular distribution of photons emitted at the peak wavelength showed a maximum at 30° from the foil normal with zero intensity at 0° and near 90°, whereas the photons emitted at other wavelengths in the continuum, for example, at 2700 and 4500 A, were most intense at 50° from the foil normal.

An operational analyzer has been designed and built for generalized dosimetry applications.

The transmission, resolution, and energy calibration of the Keplertron, a spherical electrostatic analyzer, have been further checked with the Sm^{152} Auger line at 32.8 kev and the Ni^{64} Auger line at 6 kev from relatively thin sources of Eu^{152} and Cu^{64}, respectively, and found to be in good agreement with the values previously determined at lower energies by means of an electron gun. The electron slowing-down spectrum in copper of negatrons from Cu^{64} has been measured with the Keplertron and found to be in absolute agreement from 37 kev to 1 kev with the Spencer-Fano theory. Difficulties in experimental techniques used in

making the above measurement have either been corrected or are under study. Programs have been written for the CDC 1604 computer to calculate theoretical spectra and to correct experimental data.

14. Physics of Tissue Damage

The intensity of thermoluminescence has been shown to depend strongly upon the presence of a gas both during the irradiation of the sample and during the subsequent warmup. Experiments have been conducted in an effort to understand the mechanisms involved in this gas effect. One experiment was an attempt to observe whether the ions or electrons formed in the gas during irradiation influenced the thermoluminescent intensity. This experiment gave negative results. An attempt was also made to detect by gas chromatography gaseous emissions from the samples, particularly as these might correlate with the optical emissions. A more sensitive experiment along these lines is now being conducted. A third experiment involved the technique of electron spin resonance. Correlations between the numbers of radiation-induced spins and integrated thermoluminescent intensity for varying sample crystallinities and gaseous conditions were sought. No gaseous dependence of spin resonance signals was found.

An electron gun is under development which will permit studies of electronic energy levels excited in solids and gases by the passage of fast electrons. A time-of-flight energy selection will be used to obtain an electron beam homogeneous in energy to 0.01 ev, thus enabling studies of energy levels of this or higher energies. The gun, drift tube, and electronics have been assembled, and bursts of electrons having energies between 2 ev and 15 ev have been obtained. The square of the reciprocal arrival time was found to be a linear function of the electron energy as expected from elementary kinematics. A new gun, ultrahigh vacuum system, and open-window electron multiplier are being installed so that studies of beam gating by electrostatic and magnetic methods may be made.

15. Radiation Dosimetry

The major effort of the Radiation Dosimetry Group was directed to the Ichiban Dosimetry Program, dosimetry research, and installation of the Health Physics Research Reactor. Analysis of most of the data from Operation BREN was completed, and the HPRR commenced routine operation on May 31, 1963. A study was completed on the long-term buildup and fading in metaphosphate glass.

PART IV. INTERNAL DOSIMETRY

16. Estimation of Internal Dose

The program of the Internal Dose Estimation Section is directed toward radioactive materials which enter the body. In particular the maximum concentrations are estimated for radioactive materials in air, $(MPC)_a$, or in water, $(MPC)_w$, that would limit the burden to a prescribed amount over a working life.

A retention function has been defined which represents the retention of strontium in the body over extended periods of adult life. The function consists of three exponential terms, two of which are obtained by simultaneously adjusting the parameters so that retention and excretion data during the period of about 100 to 200 days following injection of strontium are represented. The third exponential is obtained by selecting parameters to make the function consistent with data on levels of stable strontium in diet and in bone of Western man and to be in fair agreement with data on the rate of remodeling of bone. Thus the function is in reasonably good agreement with the data now available on chronic retention of strontium in normal adults. Using this model, $(MPC)_w$ values for Sr^{90}, Sr^{89}, and Sr^{85} are obtained and compared with values derived on the basis of other models. On the basis of the general agreement of these models, it is suggested that an $(MPC)_w$ of 4×10^{-6} $\mu c/cm^3$ is acceptable for occupational exposure (168 hr/week) to Sr^{90}.

17. Stable-Element Metabolism by Man

The elemental composition of bodies of grossly normal adults provides one of the best sources of information concerning the distributions of various isotopes within the body that are to be expected following chronic exposure to the materials. In the search to determine the elemental composition of standard man, 415 bone samples were analyzed from long-term residents of 11 major cities in the

United States and 13 cities in foreign countries. Each sample was examined for 20 elements. These data are perhaps the most extensive source of information on the concentrations of many trace elements in bone.

The accuracy of the Quantometer values was checked for several elements using atomic absorption, flame spectrophotometry, and colorimetry. In each case the agreement was generally good.

The influence of age, race, and geographical location on the trace-element content in tissue has been studied. On the whole the concentrations of trace elements were not different from those in adults, but certain elements showed significant variations. Except for the higher lead ($p \leq 0.05$) in kidney, liver, and lungs of males, there were no sex differences in the American group. There appeared to be no significant differences due to race *per se*.

PART V. HEALTH PHYSICS TECHNOLOGY

18. Aerosol Physics

Fundamental and engineering studies of radioactive surface contamination are continuing. Major emphasis is on the development of reproducible sampling techniques for evaluating the extent of particulate contamination on surfaces and the application of redispersion test results to the establishment of contamination control criteria. Studies of contamination sampling indicate that the smear and adhesive paper methods are strongly affected by the characteristics of the surface, the concentration of the contaminant, and variations in technique among monitoring personnel. A new sampling method, employing air dispersion, is essentially independent of surface roughness and dustiness, and results in minimal monitoring variation among different personnel; redispersion efficiency varies with particle size of the contaminant and with velocity of the air impinging on the surface.

The adsorption of radioactive iodine vapor onto condensation nuclei has been investigated by use of aerosols produced by exploding silver and platinum wires. In the absence of aerosol particulates, the iodine vapor diffuses to the container walls with a half-life of 49 min. When the metallic aerosols are mixed with the iodine vapor, iodine concentration in the container is lost at a much slower rate. In the case of platinum aerosol, 17% of the iodine is associated with a particulate phase which is lost to the container walls with a half-life of 6.9 hr; the remainder is lost with a half-life of 41 min. The silver aerosol adsorbs and retains the iodine much more effectively than does the platinum aerosol.

The high-volume annular impactor is an air sampling device which employs inertial forces to deposit airborne particulates on a collecting surface. Dust deposition patterns usually include a central circular deposit and one or more annuli of deposited dust with definite minima or clear areas separating the deposition sites. Study of the design and operating parameters of the device has shown that deposition of dust at the center and at the primary impaction annulus begins as soon as the sampler is started; all parts of the pattern develop concurrently. Investigation of the airflow patterns near the collecting surface indicates the presence of at least two stable, toroidal vortices contiguous to the surface. To a considerable degree, the patterns of static pressure distribution and dust deposition appear to be correlated.

Tests have continued to explore the capabilities of the exploding wire aerosol generator to produce and disperse a wide variety of submicron aerosols. Aerosols can be produced which differ greatly in chemical composition, density, electrical and thermal conductivity, permittivity, and other physical properties which may be of interest in testing instruments or simulating health physics field problems in the laboratory. Wires or foils of 18 different metals have been exploded in a nitrogen atmosphere. The pertinent data regarding yield and composition of the resultant aerosols are tabulated. It was found that aerosol yield increases with increasing gas pressure in the explosion chamber at all operating voltages, but the primary particle size is not affected dramatically by either pressure or voltage. These and other findings of the study may indicate that particle formation in the exploding wire phenomenon occurs in the shock wave.

19. Applied Internal Dosimetry

Continuing improvements of instrumentation and operating program at the ORNL In Vivo Gamma-Ray Spectrometry Facility (IVGS) have made it possible to increase the rate of routine in vivo counts for monitoring purposes and, at the same time, initiate

a limited research program. A thin-crystal assembly [three NaI(Tl) crystals 5 in. in diam by $\frac{1}{16}$ in. thick] is now available for use in the spectral analysis of electromagnetic radiation in the energy region below 150 kev. Thin crystals are particularly important in the study of lung burdens of plutonium. At present, the assembly can detect slightly less than 40 nanocuries of Pu^{238} in the chest region, provided a background count is made on the individual prior to the plutonium exposure (four standard deviations). If no such prior count is available, the limit of detection is increased to slightly less than 80 nanocuries of Pu^{238} in the lungs. The routine monitoring program, previously confined to examination of known or suspected exposure cases, has been expanded in scope. Increased emphasis is being placed on counting of potentially exposed persons and obtaining baseline counts for individuals prior to their entering new work involving potential internal radiation exposure. All routine human counts are now made in a scanning bed geometry in which the subject, lying prone on a rolling bed, is moved under an 8- by 4-in. NaI(Tl) crystal. This counting mode replaces the chair geometry formerly used for most routine counting. Gamma detection efficiency for scan counts is approximately equal to chair count efficiency and may be less sensitive to changes in geometry occasioned by nonuniform distribution of radioisotopes in the subject being counted. The computer program for processing in vivo counting data can now be used in evaluating a majority of the routine counts. As a result, less analyzer time is required for obtaining and evaluating net spectra. During the past year a total of 492 human counts were made. The present rate of counting is about 110 persons per month, excluding instrumentation downtime.

Members of the Health Physics Technology and the Internal Dose Estimation Sections cooperated in a special study of the uptake and retention of I^{131} by human thyroid gland. The work was undertaken to provide human data with which to evaluate the ICRP-NCRP parameters, assumptions, and predictions regarding the uptake and retention of radioiodine. Five male volunteers ingested cow's milk containing I^{131} bound to the milk protein. Uptake of I^{131} by the thyroid was measured by gamma counting at the IVGS facility. A 3- by 3-in. lead-collimated NaI(Tl) crystal was positioned over the thyroid gland of the supine subject, in contact with his throat. Three of the subjects also submitted total voiding urine during the study. The amounts of I^{131} ingested were small in comparison with permissible levels but provided adequate counting rates. Two cases of single ingestion and three cases of repeated daily ingestion were compared. Best-fitting curve plots of the data were obtained by the least-squares method using two different weighting factors. The data, presented in tables and graphs, show that extrapolations from single intake data and the application of ICRP-NCRP parameters provided slight overestimates of the thyroid and whole-body burdens observed in the cases of chronic intake. Data from the two single ingestion cases were helpful in evaluating a case of accidental inhalation of I^{131} vapor. The ingestion and inhalation cases are compared.

Phosphoric acid, obtained through normal laboratory supply sources, was found to contain minute quantities of radium D (Pb^{210}) and its daughters. When 10 ml of H_3PO_4 is added to urine in the $BiPO_4$ precipitation procedure for determining plutonium in urine, the alpha count background is increased by 0.4 dis/min. This is probably due to the alpha of Po^{210}, one of the radium D daughters. Quantitative removal of these contaminants from the H_3PO_4 by means of cation exchange resin treatment can reduce the reagent contamination of the urine specimen analysis from about 0.4 dis/min to 0.08 dis/min per sample.

Analysis of cattle thyroids and of milk for fallout I^{131} continued. Data from the period of highest I^{131} activity indicate that the concentration of radioiodine in a liter of milk averages only about 8% of the concentration per gram of cattle thyroid. Milk must be reduced in volume by a factor of about 8000 to 1 to achieve a detection sensitivity equal to the sensitivity for thyroids; while the thyroids require no laboratory preparation other than interim refrigeration. Cattle thyroids, therefore, are a valuable biological monitor of fallout I^{131}; they provide a sensitive detection limit with a minimum of laboratory equipment and preparation.

PART VI. EDUCATION, TRAINING, AND CONSULTATION

20. Education, Training, and Consultation

The need for trained health physicists, both in this country and abroad, continues. The AEC Fellowship students and several foreign students

completed the program at Vanderbilt University and Oak Ridge, and the Fellowship group for the 1963–64 program has been selected. Lectures and laboratory courses were provided for laboratory, division, and civic programs.

It is anticipated that in the future more training in health physics will be provided for ORNL personnel and for foreign students on an individual basis.

Contents

SUMMARY iii

PART I. RADIOACTIVE WASTE DISPOSAL

1. LIQUID INJECTION INTO DEEP PERMEABLE FORMATIONS 3
   - Strontium Exchange by Sandstones 3
   - Fission Product Dispersion in the Ground 6
   - Radionuclide Migration and Dispersion in Sandstone 7
2. DISPOSAL BY HYDRAULIC FRACTURING 13
   - Mix Development 13
   - Well Drilling 15
   - Plant Design 16
3. DISPOSAL IN NATURAL SALT FORMATIONS 19
   - Heated Model Room 19
   - Demonstration of High-Level Waste Solids Disposal in Salt 22
   - High-Temperature Experiments 29
   - Chlorine Release from Gamma-Irradiated Salt 32
   - Creep Measurements in Mines 34
   - Floor and Ceiling Cores 35
4. CLINCH RIVER STUDY 37
   - Water Sampling and Analysis 37
   - Bottom Sediment Studies 38
   - Hydrology 44
   - Safety Analysis 45
5. STUDY OF WHITE OAK CREEK DRAINAGE BASIN 51
   - Quantity, Distribution, and Transport of Radionuclides in the Bed of Former White Oak Lake 51
   - Movement of Radionuclides in White Oak Creek 57
   - Time of Water Travel in White Oak Creek 60
   - Ground-Water Levels in White Oak Creek Basin 60
6. MINERAL EXCHANGE STUDIES 62
   - Strontium Removals by Hydrous and Anhydrous Sesquioxides 62
   - Strontium and Cesium Removal by Vermiculite 67

7. ENGINEERING, ECONOMIC, AND SAFETY EVALUATIONS 70
Engineering and Economic Evaluations 70
Interim Storage of Solidified Wastes 71
Effects of Fission Product Removal 72
Tank Hazard Study 73
Activity Distribution 73
Atmospheric Dispersion 74

8. RELATED COOPERATIVE PROJECTS 76
Geologic and Hydrologic Studies by U.S. Geological Survey 76
Cooperation of Other Agencies in ORNL Studies 77
Visiting Investigators from Abroad 77
Nuclear Safety Review 77
Committee Work 78
Participation in Educational Programs 78

PART II. RADIATION ECOLOGY

9. RADIOACTIVE WASTE AREA AND RADIATION EFFECTS STUDIES 81
Glass-Rod Dosimetry in Environmental Studies 81
Penned-Mammal Study 81
Hematology of Native Mammals 88
Use of Radioactive Tags to Evaluate Movements of Wild Mammals 88
Distribution of Gamma-Emitting Nuclides in Trees Bordering Radioactive Waste Pit No. 5 89
Vegetation Studies Around the HPRR 92
Neutron Dosimetry and Seed Irradiation 92
Gamma-Ray Dosimetry in Cs^{137}-Tagged Tulip Poplar 93
Use of Radioactive Tracers for Analysis of Food Chains 94

10. FOREST STUDIES 95
Computer Feedback Models 95
Components of Forest Litter Fall 96
Rates of Litter Breakdown in Contrasting Climates 97
Transfer of Co^{60} and Ru^{106} from Oak and Ash Leaves to Several Forest Soils 97
Microbiology of Forest Litter 98
Gross Effects of Arthropods and Microflora on Rates of Leaf Litter Breakdown 98
Leaf Litter Consumption by Millipedes 100
First-Season Redistribution of Cs^{137} in Canopy of a Tagged *Liriodendron* Forest 100
Determination of Potential Cesium-Organic Binding Sites in *Liriodendron* and Other Woody Species 102
Entry of Cs^{137} into Litter and Soil of a Tagged *Liriodendron* Forest 104
Microbial Immobilization of Radionuclides in Forest Litter 105
Mobility of Cs^{137} in Forest Food Chains 106

11. CLINCH RIVER AND RELATED AQUATIC STUDIES 107
Strontium in White Crappie (*Pomoxis annularis*) Flesh and Bone 107
Biological Movement and Reservoirs of Sr^{90} 109
Uptake and Accumulation of Strontium by Algae and Snails 109
Smallmouth Buffalo Population Studies and Fish Marking 110
Population Genetics and Radiation Effects Studies on *Chironomus tentans* 112
Safety Evaluation of Clinch River Fisheries 114
Related Activities 115

PART III. RADIATION PHYSICS AND DOSIMETRY

12. THEORETICAL RADIATION PHYSICS 119
Dosimetry of High-Energy Protons 119
Studies Concerning the Relation of RBE and LET 123
Shell Corrections to Atomic Stopping Power 124
Low-Energy End of the Secondary Electron Cascade in Metals 125
Surface Plasmon Dispersion Relation 127
Transition Radiation from a Two-Layered Foil 128
Photon Absorption in Metals Due to Impurity Scattering Centers 129
Constitutive Equations for a Moving Medium 130
Instabilities in a Plasma-Beam System Immersed in a Magnetic Field 131

13. EXPERIMENTAL PHYSICS OF DOSIMETRY 134
Electron Interactions with Water Molecules 134
Time-of-Flight Investigations of Electron Transport in Gases 135
Interaction of Energetic Charged Particles with Atomic Argon 137
Measurement of Transition Radiation and Optical Bremsstrahlung from Electron-Bombarded Metal Foils 137
Spherical Electrostatic Analyzer and Electron Slowing-Down Spectra in Copper 141
An Operational Analyzer for Generalized Dosimetry 142

14. PHYSICS OF TISSUE DAMAGE 143
Effects of Adsorbed Gas on Optical Emissions of Irradiated Biochemicals 143
Time-of-Flight Electron Beam Monochromator 144

15. RADIATION DOSIMETRY 146
Gamma-Ray Spectrometry 146
Fast-Neutron Spectrometry 146
Gamma-Ray and Fast-Neutron Dose as a Function of Incidence Angle 147
Energy Response of BREN Normalizing Counter 150
Spatial Dose Distribution in Air-over-Ground Geometry 151
Radiation Measurements over Simulated Plane Sources 152
Metaphosphate Glass Microdosimeters 153
Health Physics Research Reactor (HPRR) 154

PART IV. INTERNAL DOSIMETRY

16. ESTIMATION OF INTERNAL DOSE 157
$(MPC)_w$ Values for Occupational Exposure to Sr^{90}, Sr^{89}, and Sr^{85} 157
Maximum Permissible Body Burdens and Maximum Permissible Concentrations Estimated by an Equivalence Relation Between External Dose and Internal Dose 163
$(MPC)_w$ for Rn^{222} 166
Maximum Permissible Concentration and Body Burden Values for Various Transuranic Radionuclides 169
Related Projects 175
17. STABLE-ELEMENT METABOLISM BY MAN 176
Influence of Age, Race, and Geographical Location on the Trace Element Concentration in Human Tissue 176
Tissue Analysis Laboratory Progress Report 178

PART V. HEALTH PHYSICS TECHNOLOGY

18. AEROSOL PHYSICS 185
Studies of Surface Contamination 185
Study of the Adsorption of Iodine Vapor onto Aerosols 187
Deposition of Dust in an Annular Impactor 189
Production of Submicron Aerosols 191
19. APPLIED INTERNAL DOSIMETRY 194
ORNL in Vivo Gamma-Ray Spectrometry Facility 194
Human Uptake and Excretion of I^{131}: Accidental Inhalation and Chronic and Single Ingestion of Iodine in Milk 194
Computer Program for in Vivo Counting Data 202
Developments in the ORNL in Vivo Gamma Ray Spectrometry Facility 204
Method for Removal of Alpha Contaminants in Phosphoric Acid 205
Iodine-131 in Milk and in Cattle Thyroids 206

PART VI. EDUCATION, TRAINING, AND CONSULTATION

20. EDUCATION, TRAINING, AND CONSULTATION 209

PAPERS, PUBLICATIONS, AND LECTURES

PAPERS 213
PUBLICATIONS 218
LECTURES 223

Part I. Radioactive Waste Disposal

F. L. Parker

1. Liquid Injection into Deep Permeable Formations

D. G. Jacobs O. M. Sealand O. H. Myers

STRONTIUM EXCHANGE BY SANDSTONES

Previous exchange studies were made of Na-Ca-Sr exchange by Richfield sand. These "exercised" columns were used to study the effect of pH on the exchange of calcium and trace concentrations of strontium from 0.01 *N* $CaCl_2$. The influent solution was tagged with Sr^{85} and brought to the desired pH with HCl in series A or with NaOH in series B. The results in Table 1.1 show that the sorption of both calcium and strontium is reduced by the same relative amounts as the pH of the influent solution is lowered. At an influent pH of 2, dissolution of minerals in the exchange column caused interference with the EDTA titration of calcium. Redetermination of the exchange capacity at pH 7 indicated that a substantial portion of the exchange capacity had been lost due to the action of the acid. Dissolution of minerals in the column continued during a second operation at pH 2.

Table 1.1. Calcium-Hydrogen-Strontium Exchange by Richfield Sand from 0.01 *N* $CaCl_2$

Run	Influent pH	Calcium K_d (ml/g)	Strontium K_d (ml/g)	K_{Ca}^{Sr}
1A	7	6.21	6.51	1.05
2A	6	5.09	5.33	1.05
3A	5	4.58	4.85	1.06
4A	4	3.70	4.30	1.16
5A	3	3.11	3.22	1.04
6A	2		0.71	
7A	7	2.67	3.65	1.37
8A	2		0.38	
1B	7	5.04	6.80	1.35
2B	8	5.58	7.18	1.29
3B	9	5.43	7.72	1.42
4B	10	6.01	11.26	1.87
5B	11	8.42	21.11	2.51

As the solution is made more basic, strontium is more selectively removed from solution than calcium. The increased removal of both calcium and strontium above pH 10 suggests the precipitation of slightly soluble salts, with the strontium salt being less soluble than the calcium salt.

Attempts were made to develop a standard procedure for exchange analysis of calcareous sandstones without alteration of the sample. Five grams of Richfield sand and varying amounts of reagent grade $CaCO_3$ were weighed into 40-ml centrifuge tubes. Ten saturation steps were performed with 25 ml of 0.005 *M* Ca^{2+} (chloride solution saturated with $CaCO_3$ at pH 7) tagged with Ca^{45}. After saturation the samples were washed twice with 95% ethanol, and the Ca^{45} was isotopically replaced by untagged $CaCl_2 \cdot CaCO_3$ solution of the same concentration as the saturating solution. Each of the ten successive desorbing increments of solution was sampled for Ca^{45} counting, and the exchangeable calcium was determined. Essentially all of the Ca^{45} was removed by this exchange process. Strontium-85 exchange was then determined for the samples, employing solution having the same composition of stable chemicals. In the final step the samples were leached five times with 1 *N* $NaC_2H_3O_2$, and the calcium was titrated with EDTA.

Because of dissolution of the slightly soluble $CaCO_3$, the $NaC_2H_3O_2$ determination does not give an accurate representation of the calcium exchange capacity of the Richfield sand (Table 1.2). The results obtained using Ca^{45} sorption from a $CaCO_3$-saturated solution are much more meaningful, although the $CaCO_3$ did exchange approximately

Table 1.2. Calcium-Strontium Exchange by Mixtures of Richfield Sand and Calcium Carbonate

	Run							
	1	2	3	4	5	6	7	8
Weight of Richfield sand (g)	5.00	5.00	5.00	5.00	5.00	5.00	5.00	
Weight of $CaCO_3$ (g)		0.0010	0.010	0.10	0.50	1.00	2.00	2.00
Ca^{45} exchanged (meq)	0.1415	0.1370	0.1575	0.1500	0.1580	0.1670	0.1770	0.0382
Ca^{2+} titrated by EDTA in $NaC_2H_3O_2$ leaches (meq)	0.2530	0.2525	0.2790	0.4120	0.5845	0.5810	0.6280	0.1846
Sr^{85} exchanged (% of total in 100 ml)	18.0	16.4	18.5	18.4	18.4	19.0	18.1	1.2
Ca^{45} exchanged by Richfield Sand[a] (ml/g)	2.83	2.74	3.15	2.96	2.97	2.96	2.78	
Sr^{85} exchanged by Richfield Sand[a] (ml/g)	4.38	3.92	4.54	4.49	4.46	4.58	4.18	
K_{Ca}^{Sr}[b]	1.55	1.43	1.44	1.52	1.50	1.55	1.51	0.31

[a]Corrected for amount exchanged by the added $CaCO_3$.
[b]The corrected values for Ca^{45} and Sr^{85} exchange were used in calculation for runs 1 through 7.

1.9 meq of Ca^{2+} per 100 g and remove relatively less Sr^{85} from solution. (The strontium-to-calcium selectivity coefficient of the $CaCO_3$ was found to be 0.31.) This results in a decreasing apparent strontium-to-calcium selectivity coefficient with increasing amounts of calcium carbonate in the sample. When the exchangeable calcium and strontium values for the Richfield sand are corrected for the amounts held by the calcium carbonate, the resulting strontium-to-calcium selectivity coefficient for Richfield sand is quite constant.

The exchange capacity of the Richfield sand determined in this series of measurements averaged 2.91 ± 0.11 meq/100 g, and the strontium-to-calcium selectivity coefficient was 1.50 ± 0.04. This exchange capacity agrees very well with the value of 2.96 meq/100 g obtained previously in nonexercised columns of Richfield sand, and the strontium exchange was about the same as obtained during the first column determination after the column had been exercised once.

The Ca-Sr exchange properties of numerous sandstone and clay samples were determined, by use of columns and the slurry technique described above with calcium carbonate–saturated solution (Table 1.3). The exchange capacities obtained for the clay minerals generally agreed quite well with those determined by Jackson's EDTA method.[1] In the case of the phosphatic, calcareous, or dolomitic samples, the exchange capacity determined by Ca^{45} sorption is much lower than that determined by EDTA titration, because there is less dissolution of the slightly soluble calcium salts. The samples taken from a Reagan sandstone type locality in Oklahoma by J. B. F. Champlin, U.S. Bureau of Mines, showed very low capacities for sorbing calcium and strontium (series Q, Table 1.3). In general, the sorption of strontium is directly related to the calcium sorption properties of the mineral.

[1]M. L. Jackson, *Soil Chemical Analysis*, p 64, Prentice-Hall, Englewood Cliffs, N. J., 1958.

Table 1.3. Strontium-Calcium Exchange by Various Sands and Minerals

Sample	Exchange Determined by				
	Slurry			Column	
	EDTA (meq/100 g)	Ca^{45} (meq/100 g)	Strontium K_d (ml/g)	Ca^{45} (meq/100 g)	Strontium K_d (ml/g)
Bentonite B	103	80.1	76.5		
Nontronite, H-33	97.8	114	94.8		
Wyoming bentonite	84.2	71.1	36.1		
Vermiculite, BO-A	74.9	56.6	35.5		
Panther Creek bentonite	64.1	69.2	67.3		
Montmorillonite, H-31	62.8	51.9	60.3		
Texas bentonite	57.5	59.6	66.4		
Metabentonite, H-41	47.4	27.0	25.7		
Fithian illite	35.7	14.6	23.7		
Metabentonite, H-42	30.4	28.3	33.1		
Attapulgite	30.1	25.9	36.8		
Glauconite	28.1	25.5	42.2		
Halloysite, No. 12	13.8	13.2	16.6		
Georgia kaolinite	6.72	6.79	7.29		
North Carolina kaolinite	4.42	4.12	4.76		
Kaolinite, H-9	3.75	2.06	9.6		
Variscite	16.5	9.70	32.5		
Crandallite	3.44	1.41	4.40		
Superphosphate	9.05	2.98	16.7		
Florida pebble phosphate	7.45	8.59	14.9		
Tennessee rock phosphate	11.4	9.46	16.4		
Pennington sand	3.75	2.16	8.12	1.27	3.08
Noxie sand	1.75	1.87	4.09		
Gilliland sand	2.30	1.71	6.34		
Fowler sand	2.28	1.53	4.14		
Crab Orchard sand No. 1	1.43	1.01	2.57	0.48	0.77
Crab Orchard sand No. 2	1.31	1.10	2.97		
Berea sand	1.12	0.52	3.06		
Bartlesville sand	2.73	0.49	1.50		
Q-0, Honey Creek dolomite	7.75	1.53	2.19	0.11	0.21
Q-1, Honey Creek dolomite	1.94	1.38	3.82	0.89	1.25
Q-3, weathered quartzitic sandstone with feldspar	0.86	0.42	1.13	0.30	0.35

Table 1.3 (continued)

Sample	Exchange Determined by				
	Slurry			Column	
	EDTA (meq/100 g)	Ca^{45} (meq/100 g)	Strontium K_d (ml/g)	Ca^{45} (meq/100 g)	Strontium K_d (ml/g)
Q-5, conglomerate sandstone	0.82	0.27	1.05		
Q-6, conglomerate with feldspar and quartz	0.77	0.42	1.02		
Q-7, conglomerate with feldspar, fine quartz, and arkosic sand	1.46	0.59	1.22	0.50	0.53
Q-8, conglomerate with quartz, feldspar, and arkosic sand	1.00	0.67	1.32	0.14	0.42
Black Royer dolomite	2.86	1.12	2.23		
Speckled Royer dolomite	1.49	0.79	1.78		
Gray Royer dolomite	1.80	0.79	2.36		
White Royer dolomite	8.70	0.33	0.15	0.54	0.36

FISSION PRODUCT DISPERSION IN THE GROUND

When a liquid waste of different composition than the native water is discharged into an aquifer, there are numerous changes that occur which lead to a spreading of the radionuclide front. When diffusion of the radionuclide through a film of water to the surface exchange sites is the rate-controlling step of the exchange reaction, leakage of the radionuclide will be observed prior to the major concentration breakthrough. When the migration of the exchangeable ion from the surface to interior exchange sites (particle diffusion) is the rate-controlling step for the exchange reaction, a "tailing off" of the breakthrough curve at somewhat less than 100% breakthrough will result. In the case of a nonlinear adsorption isotherm, the sorption front will be self-sharpening, because the selectivity of the sorbent for the radionuclide is greater as the concentration of the sorbed species is reduced due to the sorption process. Changes in the sorptive characteristics of the exchanger may also result from the exchange of macrocomponents of the solution. At the leading edge of the waste solution invasion, the solution composition is altered until it comes to equilibrium with the ions on the exchanger, while near the point of injection the ionic composition of the exchanger surface is altered until it comes to equilibrium with the waste solution. The effects of macrocomponent exchange are especially pronounced if the exchange alters the crystal structure and the reversible exchange capacity of the sorbing minerals.

At very low flow rates, spreading due to longitudinal and lateral ionic diffusion may be quite pronounced, although, fortunately, the absolute rates of movement will be quite low. At moderate flow rates eddy dispersion is of consequence; at higher flow rates turbulent flow causes longitudinal mixing of the interstitial liquids.

Flow maldistribution, or channeling, due to the discontinuity of individual receiving beds and the interspersion of lenticular beds of greatly different permeabilities within the general disposal

formation, may cause dispersion orders of magnitude above that predicted on the basis of laboratory column tests.[2] If the total electrolyte concentration of the influent solution is greatly different from that of the formation solution, there may be a change in the zeta potential of the charged clay surface. Peptization of the clays may result when the zeta potential is raised by injection of a solution with a lower electrolyte concentration, or flocculation may occur when the injected solution has a higher electrolyte concentration. These physical changes will affect the flow maldistribution of the system by the closure of existing channels as a result of swelling or by the formation of new channels as a result of shrinkage. Large differences in total electrolyte concentrations will also give rise to density and viscosity gradients at the invasion front which may lead to instability and fingering of the solution.

In addition to exchange reactions, other chemical phenomena may be important in altering the chemical and physical environment of the formation. Precipitation reactions, changes in oxidation-reduction potentials, and changes in pH may cause significant variations. In fact, these changes may be more important than simple ion exchange in affecting the movement of some of the radionuclides.

It would be quite impossible to develop a mathematical model that would take into account all of the factors affecting ion migration in the environment. In fact, drastic idealizations are required even to derive the simple equations used to describe the behavior of the well-packed, linear-flow exchange columns.[3] However, extension of the simplified equations developed by Glueckauf[4–6] to describe ion exchange in linear columns provides a framework for depicting radionuclide migration in the environment. In Glueckauf's treatment, based on the concept of the "theoretical plate," four perturbances to column operation are considered, each of which is due to either finite particle size, slow particle diffusion, slow film diffusion, or longitudinal ionic diffusion. In the case of a linear adsorption isotherm, these disturbances have been shown to be additive when correction terms of higher order are neglected.[3]

In uniformly packed laboratory columns, the perturbances outlined by Glueckauf must be considered. However, since the dispersion of solution in nonhomogeneous natural formations is likely to be a few orders of magnitude higher than that in well-packed laboratory columns,[2] it seems quite reasonable to neglect the ion exchange contributions to dispersion in environmental analysis. It should be remembered that extrapolation of laboratory measurements of radionuclide sorption must reflect the increased time of travel as well as the increased distances in the environment as compared with those in the laboratory. Fortunately, neglect of slow exchange kinetics would lead to conservative estimates for the rate of radionuclide movement in the ground.

RADIONUCLIDE MIGRATION AND DISPERSION IN SANDSTONE

A slab of Berea sandstone 6 ft × 6 ft × 6 in. was obtained from the Cleveland Quarries Company, Amherst, Ohio. The slab is sawed smoothly on all six sides and weighs approximately 2500 lb. It is supported by a sturdy frame over a drip pan, which will be used to collect any accidental spillage of solution (Fig. 1.1). A sheet of Lucite ½ in. thick is bonded with epoxy to the top of the slab, and a ½-in. layer of epoxy serves as an impermeable boundary at the bottom of the slab. The metal fittings for the injection and relief wells, as well as for the pressure and sampling grid ports, are fitted into epoxy. The epoxy seems to penetrate the sandstone to a depth of about 1/16 to ⅛ in., which should be sufficient to prevent solution leakage along the boundary between the sandstone and the Lucite sheet without materially affecting the properties of the sandstone.

Individual pans are installed at the four open edges of the sandstone to provide a boundary of constant potential. The water level in these pans is adjustable, should it be desirable to impose a cross-bed gradient. Overflow from these pans goes into a hot drain.

---

[2] C. V. Theis, *Ground Disposal of Radioactive Wastes, Second Conference Proceedings Held at AECL, Chalk River, Canada, September 26–29, 1961*, TID-7628, pp 166–78 (March 1962).

[3] F. Helfferich, *Ion Exchange*, pp 421–506, McGraw-Hill, New York, 1962.

[4] E. Glueckauf, *Trans. Faraday Soc.* 51, 34 (1955).

[5] *Ibid.*, p 1540.

[6] E. Glueckauf, *Ion Exchange and Its Applications*, p 34, Society of Chemical Industry, London, 1955.

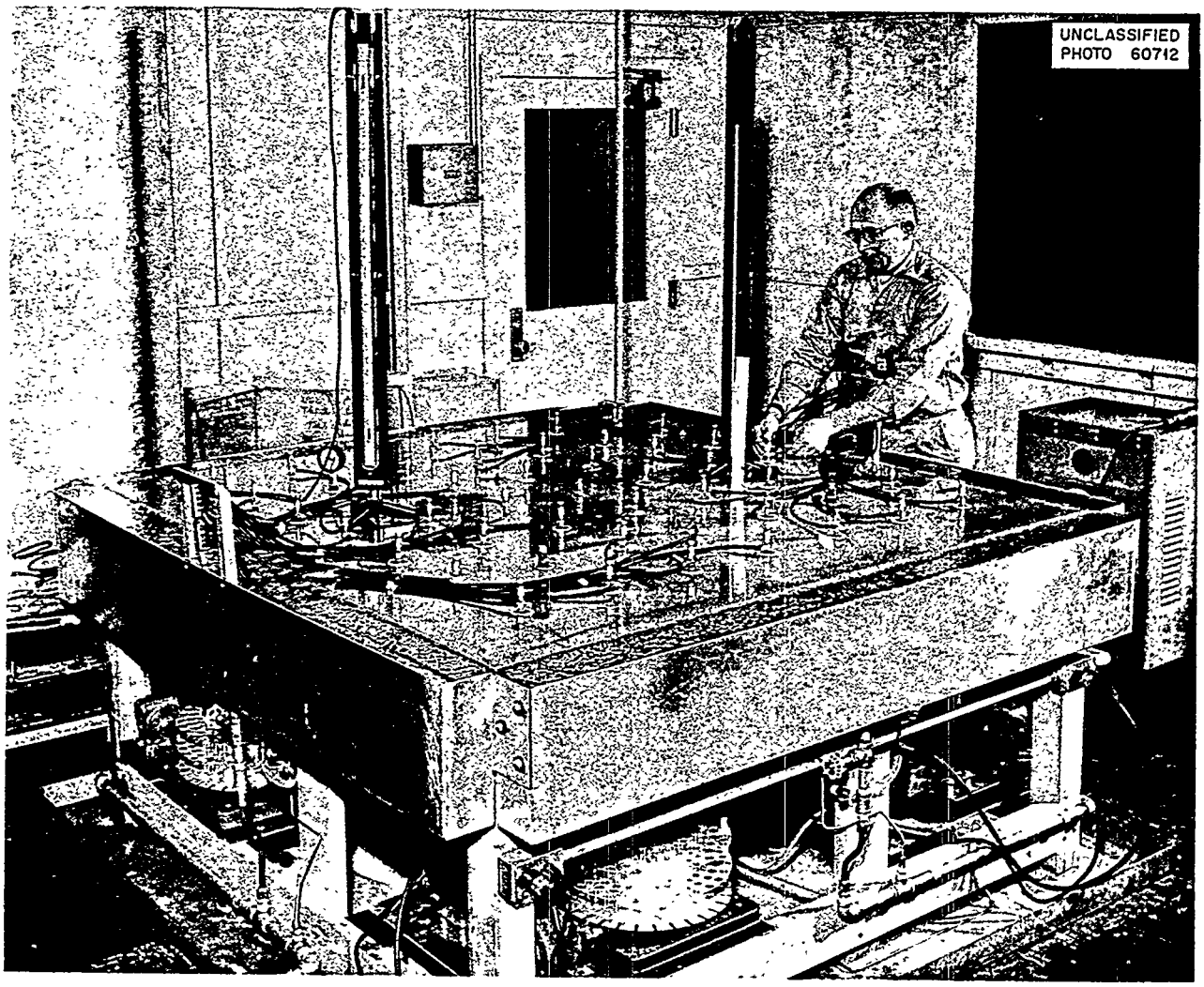

Fig. 1.1. Sandstone Model for Experimental Studies of Radionuclide Movement Through Porous Exchange Media.

An inverted five-spot system will be used with the injection well located at the center of the sandstone slab and the four relief wells at each corner of a 3-ft square oriented in the same direction as the edges of the slab. The injection and relief wells are $^{33}/_{64}$ in. in diameter and are threaded into place in the epoxy. Solution is pumped into the injection well at 50 ml/min by a $^{1}/_{20}$-hp American Metering duplex positive-displacement pump. If plugging occurs, a safety relief valve has been installed to prevent buildup of excessive pressure in the system. A pressure gage, installed on the influent well, provides direct observation of the pumping pressures required. American Metering simplex pumps are used to provide a uniform flow rate (12.5 ml/min) at the relief wells. Fraction collectors and a flow diversion valve are used to intermittently collect samples at the relief wells. Most of the time the effluent flows into a hot drain line. An electronic timing device actuates a valve to divert the flow into the fraction collector for 1 or 2 min every $^{1}/_{2}$ hr.

Pressure and sampling ports $^{1}/_{8}$ in. in diameter have been drilled $4^{1}/_{2}$ in. deep into the sandstone on a 9-in. grid. A duplex fitting (Clippard Instrument Laboratories, Inc.) mounted into the epoxy permits sampling of solution. Pressure can be measured through a sidearm port which leads to a manifold. Two pressure-measuring manifolds have

been installed; each is connected to one-half of the sampling ports. The lines leading to the manifold have valves so that the pressure at individual ports can be measured independently by either a pressure gage, a mercury manometer, or a CCl_4 manometer. An exhaust port allows the pressure in the manifold to be relieved after each measurement.

Properties of the Berea Sandstone

A similar sample of Berea sandstone was sent to Core Laboratories, Inc., Dallas, Texas, for physical testing. The results (Table 1.4) show that the average permeability along the bedding planes (samples 1A, 1B, 2A, and 2B) is substantially higher than the permeability perpendicular to the bedding planes (samples 1C and 2C). The average porosity was 18.3%, the grain density 2.67 g/cm^3, and the bulk density 2.18 g/cm^3. Particle size analysis (Table 1.5) indicates an effective particle size of 0.003 cm diameter with a uniformity coefficient of 5.1.

The Ca-Sr exchange properties of a Berea sandstone core were also measured, yielding a value of 0.55 ± 0.02 meq/100 g for the exchange capacity and a strontium-to-calcium selectivity coefficient of 1.82 ± 0.16.

Table 1.4. Physical Properties of Gray Berea Sandstone[a]

Sample No.	Permeability (millidarcys)	Porosity (%)	Grain Density (g/cm^3)	Bulk Density (g/cm^3)
1A	142	18.4	2.67	2.18
1B	112	18.1	2.67	2.19
1C	78	19.2	2.66	2.15
2A	123	18.1	2.66	2.18
2B	119	18.0	2.66	2.17
2C	38	18.0	2.68	2.19

[a]Measurements made by Core Laboratories, Inc., Dallas, Texas.

Table 1.5. Particle Size Analysis of Gray Berea Sandstone[a]

Diameter of Sieve Opening (cm)	Amount Passing Sieve (%)	
	A	B
0.0043	12.0	12.8
0.0074	19.2	21.0
0.0104	27.3	31.1
0.0150	52.5	60.7
0.0178	84.6	89.9
0.0249	99.8	99.4
0.0419	100.0	100.0

[a]Measurements made by Core Laboratories, Inc., Dallas, Texas.

Pressure Distribution and Net Flow of Fluid in the Sandstone Slab

Equipotential lines and streamlines for the sandstone slab for operation under an inverted five-spot system or for central well injection were determined, under the supervision of W. B. Drescher, United States Geological Survey (USGS), Madison, Wisconsin, with a USGS analog model analyzer. These equipotential lines and streamlines for the five-spot and central-well-injection systems, with a water boundary at the four sides, are shown in Figs. 1.2 and 1.3. The pressures obtained by use of the analog compare quite closely with the values measured at the grid ports when CO_2 was injected into the center well (Table 1.6). No serious heterogeneities were found in the sandstone. The results also agree quite well with water flow rates measured at each of the sampling ports and with pressure measurements obtained with a CCl_4 manometer during constant water injection.

The sandstone model will be used for evaluating the usefulness of equilibrium and kinetic data from linear flow systems to accurately predict radionuclide movement in nonlinear flow systems. In addition, the model will be used to test the effectiveness of various barriers to radionuclide movement.

UNCLASSIFIED
ORNL-DWG 63-3912

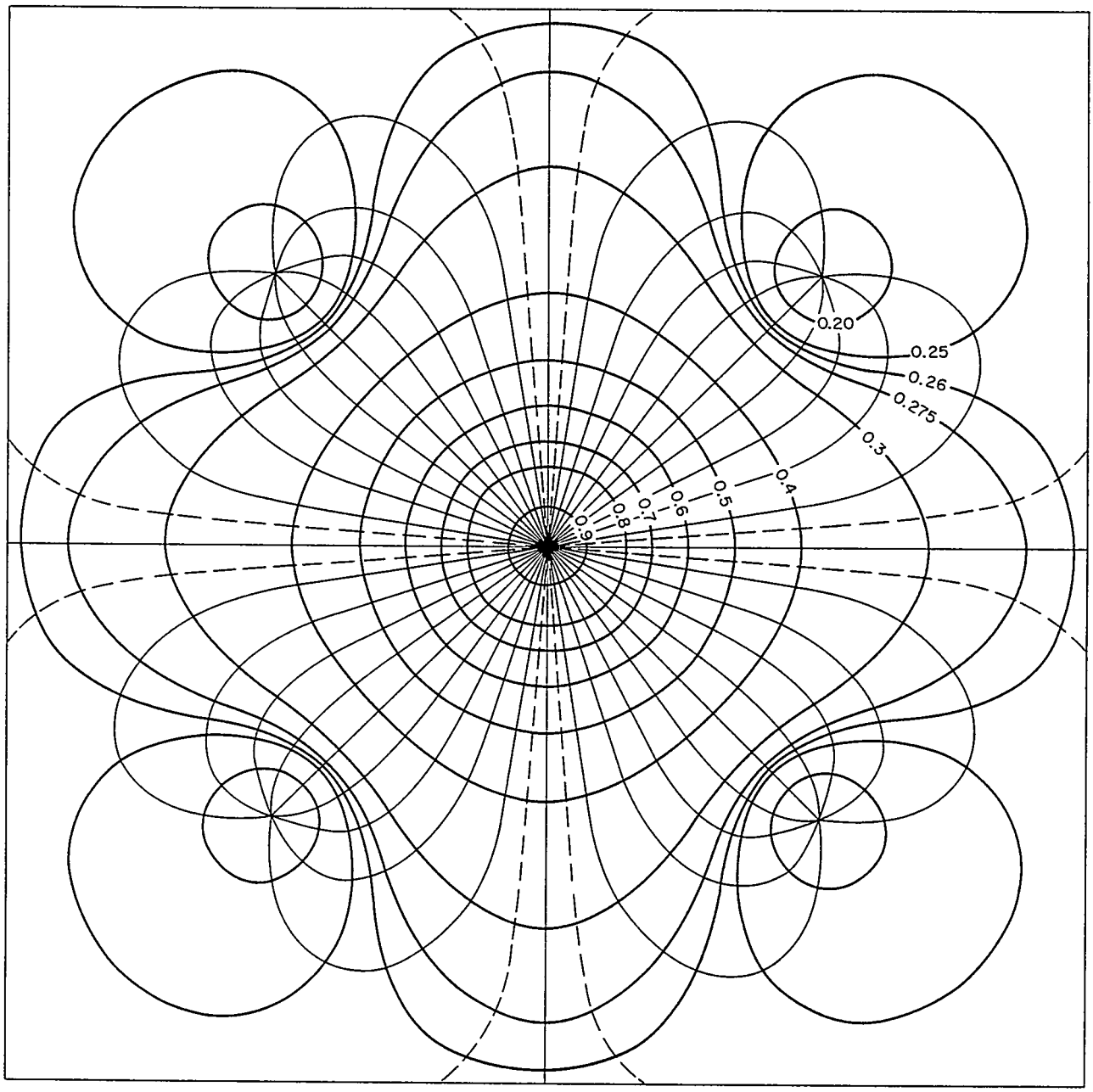

Fig. 1.2. Equipotential Contours and Streamlines for an Inverted Five-Spot System with an Injection Well at the Center, Four Relief Wells, and Water Boundaries. Two and one-half percent of the total flow is conducted between any two adjacent solid streamlines.

UNCLASSIFIED
ORNL-DWG 63-3913

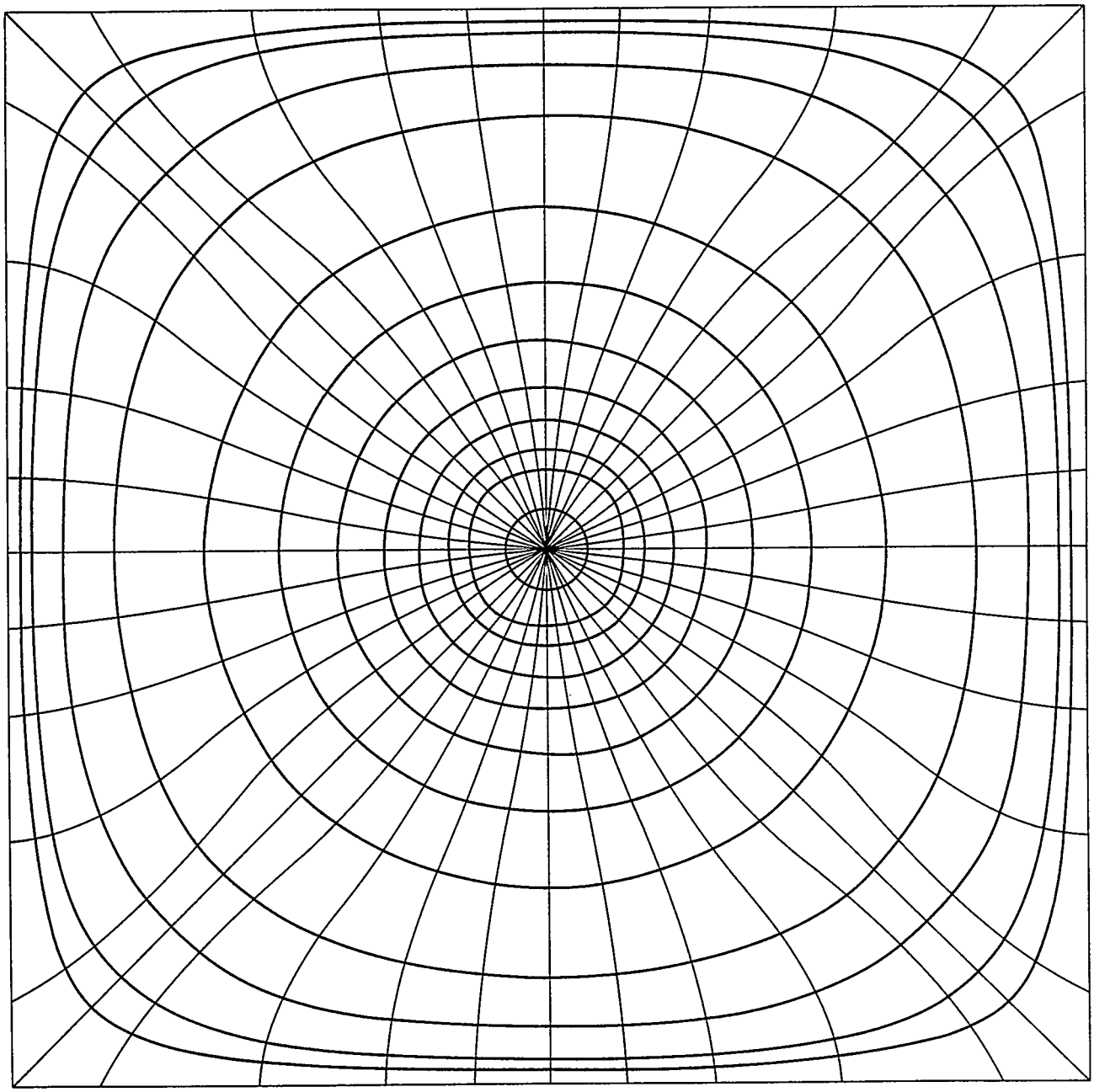

Fig. 1.3. Equipotential Contours and Streamlines for a Central Injection Well Operated in a Square Sandstone Slab with Water Boundaries. Two and one-half percent of the total flow is conducted between any two adjacent streamlines.

Table 1.6. Comparison of Grid Pressures Measured During CO_2 Injection with Those Obtained Using an Electric Analog

Well No.	Position from Center (in.) X	Position from Center (in.) Y	Pressure, Electric Analog (cm of Hg)	Pressure, CO_2 (cm of Hg)	Well No.	Position from Center (in.) X	Position from Center (in.) Y	Pressure, Electric Analog (cm of Hg)	Pressure, CO_2 (cm of Hg)
1	−27	27	3.6	3.6	26	0	−9	53.3	52.2
2	−27	18	7.7	7.1	27	0	−18	29.4	29.2
3	−27	9	11.4	11.7	28	0	−27	12.8	13.0
4	−27	0	12.8	12.2	29	9	27	11.4	11.3
5	−27	−9	11.4	12.4	30	9	18	25.2	25.1
6	−27	−18	7.7	6.9	31	9	9	43.6	42.4
7	−27	−27	3.6	3.7	32	9	0	53.3	53.6
8	−18	27	7.7	6.7	33	9	−9	43.6	42.0
9	−18	18	16.9	19.1	34	9	−18	25.2	25.2
10	−18	9	25.2	24.2	35	9	−27	11.4	12.2
11	−18	0	29.4	29.1	36	18	27	7.7	7.6
12	−18	−9	25.2	25.7	37	18	18	16.9	20.7
13	−18	−18	16.9	16.5	38	18	9	25.2	31.6
14	−18	−27	7.7	6.5	39	18	0	29.4	30.2
15	−9	27	11.4	12.0	40	18	−9	25.2	25.6
16	−9	18	25.2	24.7	41	18	−18	16.9	14.5
17	−9	9	43.6	41.2	42	18	−27	7.7	8.8
18	−9	0	53.3	53.3	43	27	27	3.6	3.8
19	−9	−9	43.6	43.4	44	27	18	7.7	7.7
20	−9	−18	25.2	25.2	45	27	9	11.4	11.6
21	−9	−27	11.4	12.5	46	27	0	12.8	13.7
22	0	27	12.8	12.2	47	27	−9	11.4	12.6
23	0	18	29.4	26.8	48	27	−18	7.7	8.0
24	0	9	53.3	51.7	49	27	−27	3.6	3.8
25	0	0							

2. Disposal by Hydraulic Fracturing

Wallace de Laguna
Tsuneo Tamura
R. C. Sexton[1]
H. O. Weeren[2]
E. G. Struxness
F. S. Brinkley
B. L. Houser

In experiments on disposal by hydraulic fracturing several 40,000-gal batches of intermediate-level waste solution will be mixed with cement and then injected into a shale formation at an approximate depth of 900 ft. Here, the waste-cement mix is expected to set up in thin, parallel, approximately horizontal grout sheets several hundred feet across. Injections will take place over an interval of several months with a minimum of two weeks between injections. Each injection is expected to require one day or less. At some time after the completion of the third injection, the formation will be core drilled to verify the location of the grout sheets and evaluate the various mixes.

MIX DEVELOPMENT

A formulation for an acceptable waste mix has been developed under subcontract by Westco Research of Dallas, Texas. This mix is usable with normal waste solution, with waste solutions whose chemical composition differs considerably from normal, and with waste solutions concentrated by a factor of 10. The composition of this waste mix is 454 g of portland cement, 265 cm^3 of waste solution,[3] 6% (27.2 g) bentonite, 0.8% (3.63 g) CMHEC (carboxymethylhydroxyethylcellulose), and 0.8% calcium lignosulfonate.

For normal waste this mix has a fluid loss of 16 cm^3/30 min at 100 psi and 56 cm^3/30 min at 1000 psi. Its pumping time is about 50 hr. The term "fluid loss" is a measure of the amount of liquid that would be lost from a slurry to a permeable formation; it is measured by a standard test in which the quantity of fluid lost in 30 min across 3.5 in.^{2} through a 325-mesh screen is determined at various pressures. Pumping time is defined as the time required for the slurry to develop a nominal viscosity of 100 poises.

Tests on the proposed waste mix have indicated that considerable variations in pumping time result when the concentration of NaOH in the waste solution is changed. The maximum pumping time, 50 hr, was observed when the NaOH concentration was 0.22 *M* (the assumed normal waste composition); a reduction in pumping time resulted whenever the NaOH concentration was either decreased (40 hr at 0.11 *M*) or increased (19½ hr at 2.2 *M*). The addition of Na_2CO_3 (0.038 *M*) reduced the pumping time to 30 hr. The presence of materials in the concentrations to be expected in ORNL waste solution had little effect on slurry properties.

In the proposed waste mix, CMHEC acts to reduce the fluid loss. It has been found that calcium lignosulfonate (CLS) also acts to reduce fluid loss, and CLS is much cheaper than CMHEC (about a factor of 10). It is desirable to substitute CLS for CMHEC to the greatest possible extent. To obtain information on the limits of this substitution, the fluid loss of mixes containing different amounts of CLS and CMHEC was measured. The results of these tests are shown in Fig. 2.1 for mixes with simulated ORNL intermediate-level

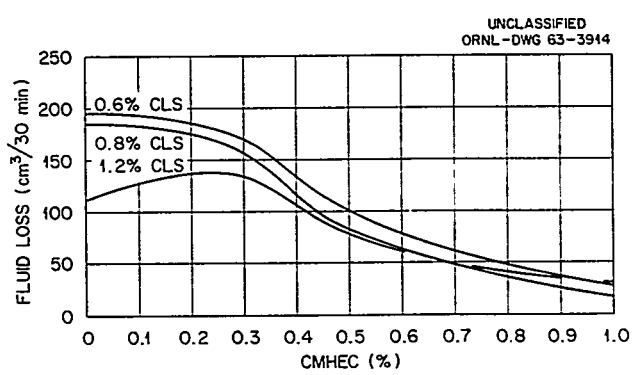

Fig. 2.1. Fluid Loss of Slurries with Normal ORNL Wastes.

[1]Engineering and Mechanical Division.

[2]Chemical Technology Division.

[3]The assumed composition of normal waste solution is 0.317 *M* $NaNO_3$, 0.219 *M* NaOH, 0.037 *M* Na_2SO_4, 0.025 *M* NH_4NO_3, 0.022 *M* $Al(NO_3)_3$, 0.006 *M* NaCl.

waste and in Fig. 2.2 for mixes with simulated ORNL waste concentrated by a factor of 10. Concentrations of CLS greater than 1.2% were not considered because of the long setting times of such mixes. These figures indicate that if a low fluid loss is desired, CMHEC must be used; if a fairly high fluid loss is acceptable, CLS is an effective substitute for CMHEC; and, whatever the desired fluid loss, some substitution of CLS for CMHEC is probably justified. More specific conclusions are not justified at this time since variation of other components of the mix also affects the fluid loss to an undetermined extent. The above tests were run with a bentonite concentration of 6%. Tests made with a 12% bentonite concentration gave similar results with unconcentrated waste; with concentrated waste a low fluid loss (100 cm^3/30 min) was noted in the tests with no CMHEC, and the effect of different CLS concentrations was slight. Obviously, bentonite concentration is also a significant variable.

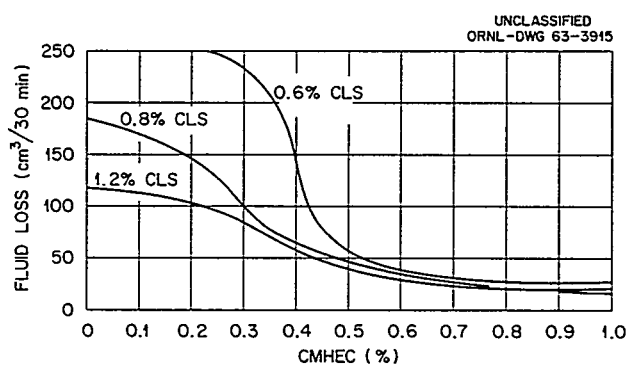

Fig. 2.2. Fluid Loss of Slurries with ORNL Wastes Concentrated by a Factor of 10.

Several samples of ORNL's intermediate-level waste have been analyzed. A typical analysis is shown in Table 2.1. The stable-element analysis shows that the waste has a much lower $NaNO_3$ and NaOH content (by a factor of 5 to 10) than the synthetic waste which has been formulated for preparing mixes. Obviously, the composition of ORNL's intermediate-level waste changes considerably over a period of time.

A slurry was prepared with the proposed waste mix and a sample of actual waste with the composition shown in Table 2.1. The fluid loss was 30 cm^3/30 min at 100 psi as compared with 48 cm^3/30 min when synthetic waste with the previously accepted standard $NaNO_3$ and NaOH concentrations was used. The filtrate from the fluid-loss test of the actual waste was analyzed for its radionuclide content. The results are also shown in Table 2.1. Gross gamma activity per milliliter in the filtrate is reduced by 89%. The concentrations of Sr^{90}, Cs^{137}, and Ce^{144} in the fluid that separated from the grout were less than 10% of those in the original waste.

After the fluid-loss test, the slurry was placed in a 2-in. by 2-in. by 2-in. mold and cured for 5 days at 80°F. After curing, the cement specimen was placed on a stand in a bottle and immersed in 500 cm^3 of demineralized water. The water was stirred with a magnetic stirrer, and a 1-ml aliquot was periodically sampled and counted. The activity buildup in the water is shown in Fig. 2.3. After 17 days of leaching, the solution was scanned with a 512-channel analyzer, and the radionuclides identified were Cs^{137} and Co^{60}. The highest count rate recorded corresponds to a loss of about 7% of the Cs^{137} from the original waste solution. The test was repeated with a specimen cured for 28 days; the Cs^{137} loss was lower by a factor of 2.

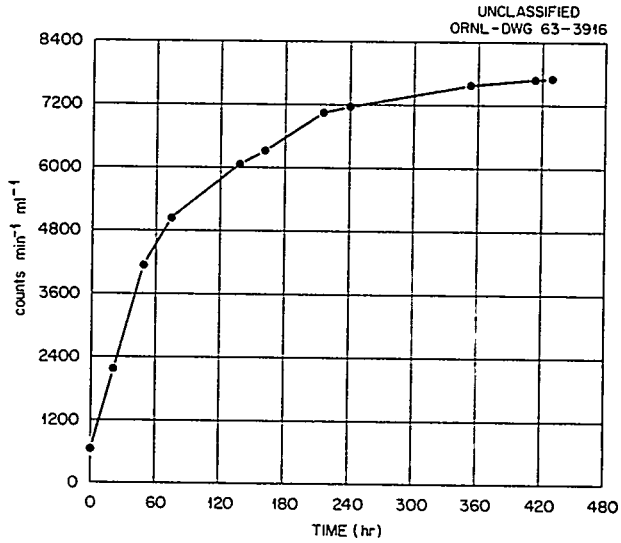

Fig. 2.3. Activity Buildup in Water by Leaching Grout Cured for Five Days.

Table 2.1. Composition of ORNL Waste and of the Filtrate from Fluid-Loss Test

Stable-Chemical Analysis of Waste		Radiochemical Analysis		
Ion	Concentration (*M*)	Radionuclide	Waste Concentration (dis min^{-1} ml^{-1})	Fluid Lost from Slurry (dis min^{-1} ml^{-1})
Na^+	0.1	Sr^{90}	6.34×10^3	440
OH^-	0.04	Cs^{137}	1.44×10^6	5.55×10^4
NO_3^-	0.029	Ru^{106}	1.84×10^6	4.04×10^5
CO_3^{2-}	<0.0005	Ce^{144}	6.54×10^3	180
SO_4^{2-}	0.0005	Co^{60}	1.3×10^3	1.0×10^3
SO_3^{2-}	0.00025	$Zr-Nb^{95}$	780	206
Cl^-	<0.001	Gross beta	3.0×10^5 [a]	2.06×10^4
Al^{3+}	0.001	Gross gamma	4.4×10^5 [a]	25.01×10^4
K^+	0.0004			
Mg^{2+}	0.0004			

[a]Counts min^{-1} ml^{-1}.

Ruthenium was the major nuclide detected in the filtrate from the fluid-loss test, but it was not detected in the water used to leach the set grout. Cobalt appears to be difficult to tie up in this system, as evidenced by its presence in both the fluid-loss filtrate and the leaching solution.

The mix that has been developed adequately fulfills the requirements that were originally proposed – low fluid loss, complete water retention, and an 8-hr pumping time. Subsequent developments have indicated, however, that some of these original requirements could be modified and the mix cost considerably lowered without losing the desirable features of the mix. In particular, the need for the use of a fluid-loss additive, the single most expensive constituent of the mix, is in question. Work is now being directed toward developing lower-cost mixes and evaluating their properties.

Slurry Pumping Test

The mixing and pumping characteristics of 1000 gal of slurry of the Westco mix were determined by the Halliburton Company by pumping continuously through a closed loop of 2-in. tubing for 8 hr 35 min at an approximate rate of 105 gal/min and at an average pressure of 3200 psi. A synthetic waste mixture was used with a concentration about 6.5 times that of so-called normal laboratory waste. There was no pump packing leakage during this entire period and no maintenance of any type made on any of the pumping equipment throughout the entire test. After the completion of the test, the pump valves and inserts were inspected and found to be in satisfactory condition.

WELL DRILLING

An injection, an observation, and a monitoring well are being used in the fracturing experiment (Fig. 2.4). The injection well is 1080 ft deep with a $5\frac{1}{2}$-in.-OD main casing string and has 150 ft of $9\frac{5}{8}$-in. surface casing to isolate it from the surface water. It is cemented to the well hole throughout its entire length. The observation well, 150 ft north of the injection well, is 1080 ft deep with a $2\frac{7}{8}$-in.-OD main casing string and has about 230 ft

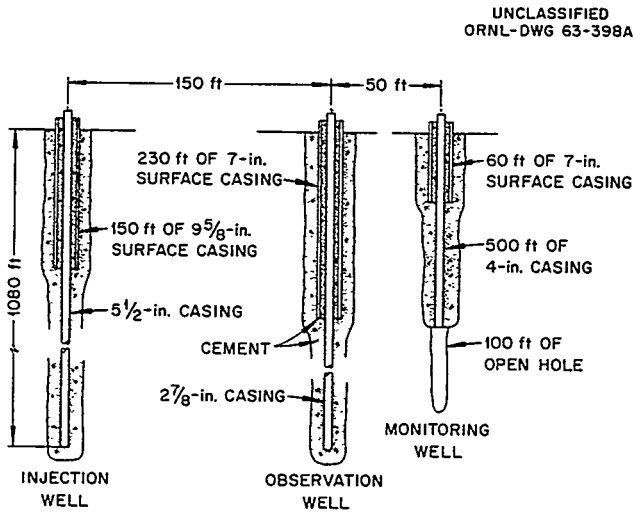

Fig. 2.4. Sketch of Wells for Shale Fracturing Experiment.

of 7-in. surface casing. It too is cemented to the well hole throughout its entire length. The monitoring well, 50 ft east of the observation well, has a 7-in. surface casing 60 ft long and a 4-in. casing 500 ft long cemented to the well hole. Below this will be about 100 ft of open hole.

All waste injections will be made through slots cut in the casing and surrounding cement of the injection well.

The observation well will be logged after each waste injection, to determine where and if the grout sheet from the injection well intersected the casing of the observation well. If the information obtained from these logs is verified by subsequent core hole drilling, it may be possible in the future to rely on readings from observation wells and eliminate or reduce core hole drilling.

When grout is injected into the shale the entire overburden is lifted a distance approximately equal to the thickness of the grout sheet. Repeated injections will eventually provide stresses in the rocks in the disposal area, which may eventually result in movement along bedding planes and the formation of new joint patterns or the opening up of old joints. The monitoring well will be used to detect any increase in the permeability of the formation which may occur as the result of this uplift and deformation of the rock cover overlying the grout sheets. This will be done by noting at intervals at what rate water can be injected into the formation above the injection zone under fairly low pressures. Any marked increase in this rate will be a danger signal.

The injection well and the observation well have been drilled, logged, cased, and cemented. The monitoring well is being drilled. The logs of the injection and observation wells show that the injection well is inclined about 29 ft southeast and the observation well is virtually straight. The logs also show that the identifiable geologic formations occur at about the same depth in each well; the expected 20° upward slope toward the observation well was not found.

The injection well was slotted at 985 ft, and the formation fractured at a wellhead pressure of 3700 psi. Approximately 2000 gal of water was pumped into the fracture and allowed to flow back slowly; 950 gal had been recovered at the end of 70 hr. The flow at this time was down to 1½ gal/hr. An injection of 50,000 gal of water was then made into the same fracture. This water will be allowed to flow back over a period of several weeks, and a careful record of the volume that flows back will be kept. This figure will be compared with a similar figure obtained from a later injection of 50,000 gal of a mixture of water and a fluid-loss additive. This comparison will provide some information as to whether and by what mechanism water is taken up by the shale formation.

PLANT DESIGN

The site of the shale fracturing experiment is about ½ mile west of the site of the previous series of experiments. The waste solution that is to be used in the injections will be pumped to the site through the existing waste transfer system and a new waste transfer line that will cross White Oak Creek. The waste solution will be stored at the site in three underground waste storage tanks that have a total capacity of 45,000 gal. A sketch of the proposed site layout is shown in Fig. 2.5.

Prior to each injection the waste tanks will be agitated and sampled. The sample will be mixed with a cement mix such as will be used in the injection so that the pumping time and other pertinent characteristics of the waste-cement mix can be verified and adjusted if necessary. Agitation will be by means of air-lift spargers – four each in two of the tanks and two in the third tank, which is shorter.

UNCLASSIFIED
ORNL-LR-DWG 78665

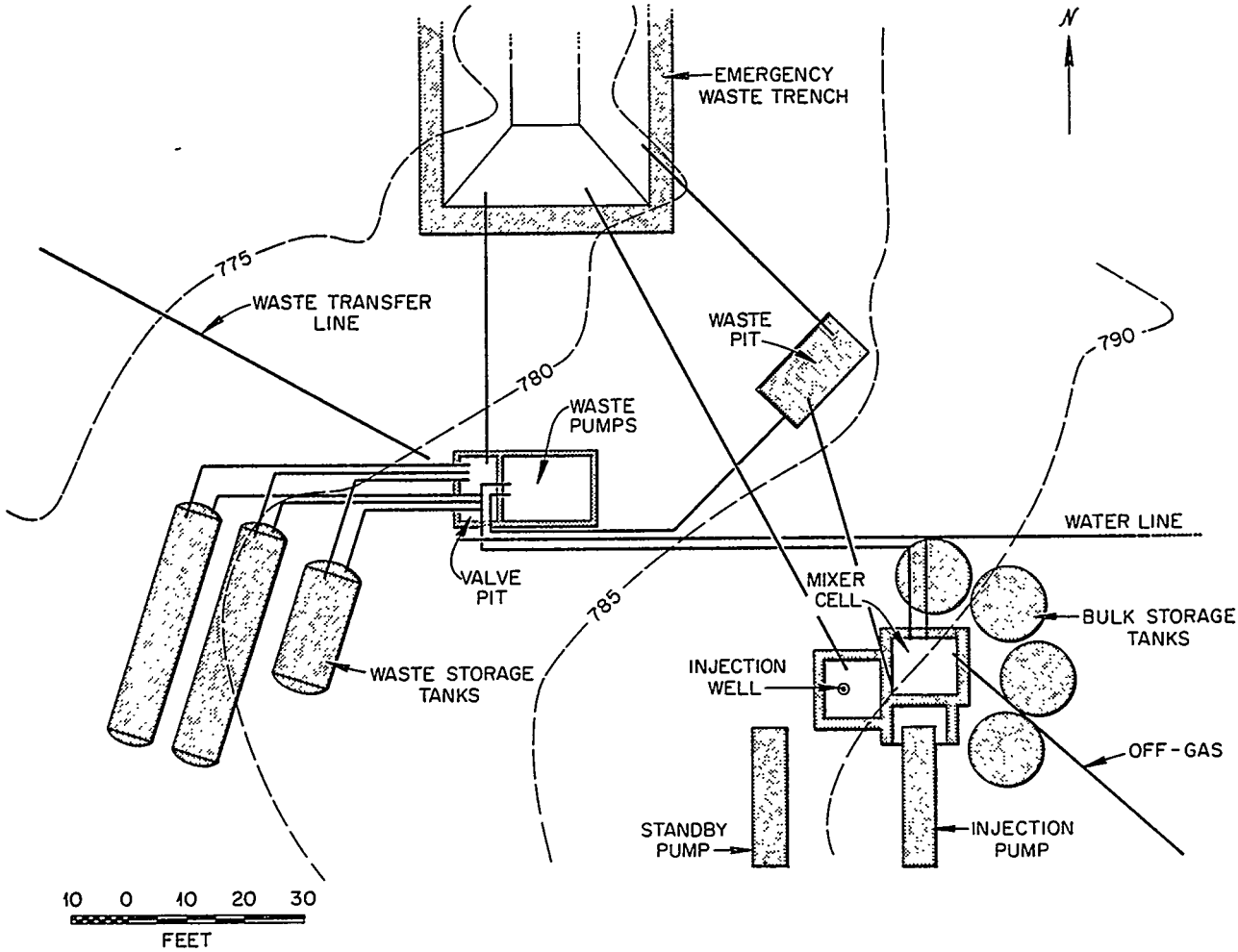

Fig. 2.5. Layout of Shale Fracturing Experiment.

The equipment used for the injection of each batch of waste consists of a waste transfer pump and spare, four bulk storage tanks to store the cement and other solid constituents of the mix, a jet mixer, a surge tank, a high-pressure injection pump, a standby injection pump and mixer, and assorted valving and special equipment. The arrangement of this equipment is shown in Fig. 2.6. The mixer, surge tank, injection pump, and wellhead valving will be installed in cells to reduce the radiation exposure of the operators and to limit the area that would become contaminated in the event of a leak in the equipment or piping. The cells will be made of a 12-in. thickness of concrete block and roofed with sheet metal. The cells will be painted, but unlined. All necessary control operations will be carried out from the outside of the cell during an injection. The calculated radiation exposure at the wall of the mixer cell during an injection is 11 mr/hr. This calculation is based on the assumptions that the specific activity of the waste solution is 0.5 curie/gal and that a 200-gal batch of grout is in the sump tub 5 ft away. It is not expected that the specific activity of the waste solution will, in fact, be this high for the first series of injections. Activities in the past have ranged between 0.01 and 0.1 curie/gal; in the absence of any clear basis for predicting what the waste activity will be in the future, it has been assumed that the

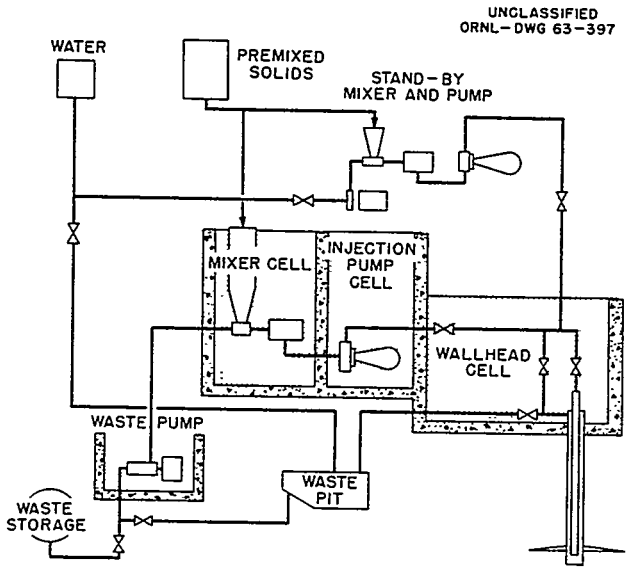

Fig. 2.6. Schematic Flow Diagram of Shale Fracturing Experiment.

waste solution that will be used in the first series of injections will have an activity of 0.05 curie/gal, and that concentrated waste injected at a later date will have an activity of 0.5 curie/gal.

There are two phases to each waste injection. In the first phase a slurry of sand and water will be pumped down a 2½-in. tube hanging in the injection well and out a jet at the bottom of the tubing string to impinge on the casing at that point. The erosive action of the sand will cut the casing and the surrounding shale formation to a sufficient depth to make subsequent initiation of the desired fracture a relatively easy job. The spent slurry will be brought to the surface through the annulus between the tubing and the casing; the sand will be allowed to settle out; and the water will be recirculated. The hatch in the roof of the wellhead cell will be open during this phase, and the tubing string will be slowly rotated by hand. This phase of the operation is expected to require about 30 min. At the end of this phase the jet at the bottom of the tubing string will be dislodged and brought to the surface. The hatch in the roof in the wellhead cell will be closed for the next phase of the injection.

In the second phase of the injection, water will be pumped down the injection well and pressure will be allowed to increase until the formation fractures. The water will then be shut off, and waste solution will be pumped to the mixer and mixed with solids from the bulk storage tanks. The resulting slurry will be pumped down the 2½-in. tube hung in the injection well and out into the fracture; injection of waste will continue in this fashion until the end of the run. A waste pumping rate of about 180 gal/min is planned; the injection will require about 4 hr if uninterrupted. At the end of the run a plug of cement will be pumped down the well and allowed to set to seal the injection. Control of the system during the injection of the waste will be largely manual; very little automatic instrumentation will be used. One operator will control the rate of addition of solids to the system by adjustment of a butterfly valve according to visual observation of the solids level in the mixer hopper. Another operator will control the rate at which waste is fed to the mixer and the rate at which grout is pumped down the well. He will adjust one or the other of these flow rates as the slurry level in the mixer tub varies. The proper ratio between liquid and solids feed rates will be adjusted automatically from slurry density measurements. A health physicist will be available with portable survey equipment. The operators will be employees of the Halliburton Company.

The 100,000-gal emergency waste trench shown on the layout (Fig. 2.5) is being dug to serve as a place to dump large quantities of waste or grout that may be spilled during an injection. It is approximately 100 ft long, 20 ft wide, and 6 ft deep. The sides are sloped and are stabilized with an asphalt emulsion to reduce erosion.

The waste storage tanks, the waste pumps, the waste transfer line, and the emergency waste trench were completed. The construction and installation of the rest of the facility will be completed in fiscal year 1964.

3. Disposal in Natural Salt Formations

J. O. Blomeke[1]
W. J. Boegly, Jr.
R. L. Bradshaw
F. M. Empson
T. W. Hodge
Hisashi Kubota[2]
T. F. Lomenick
F. L. Parker
J. J. Perona[1]
W. F. Schaffer, Jr.[1]
E. G. Struxness

HEATED MODEL ROOM

It is expected that holes in the floors of mined openings will be used for ultimate disposal of high-level radioactive solids in salt. Therefore the effect of elevated temperatures on rectangular rooms is important.

Under certain limited conditions, theoretical solutions exist for stress distributions around cylindrical openings in an elastic medium and for plastic closure of cylindrical openings at elevated temperatures. However, for rectangular openings, the only theoretical solutions known to exist are those for the stress distributions in an elastic medium around openings with rounded corners.

Even in the case of cylindrical openings, it is not known how well the theoretical solutions will predict thermal flows in an actual salt formation where some of the assumptions made in the theoretical solutions may not be valid. Thus, to obtain empirical data, both cylindrical and rectangular openings must be heated. Since the electrical energy requirements for heating an actual mine room are extremely high, studies of this nature are best carried out on scale-model openings.

To study the effect of temperature on a rectangular room of proportions similar to a mine room, an opening 8 ft wide by 9½ ft deep by 2 ft high was created in the face of a very large pillar in the Carey Salt Company mine in Hutchinson, Kansas. Immediately after the opening was created, electrical transducer-type strain gages, capable of operating at 200°C, were installed to measure floor-to-ceiling convergence, movement of the floor, and convergence of the side walls.

After the gages were installed (June 15, 1962), background creep-closure data were collected for a period of 214 days. The gages were then temporarily removed (February 11, 1963) to permit the installation of heaters, which were turned on March 18, 1963, and which are still in operation.

The heating system consists of ten tubular heaters, with diameters of 0.44 in. and active lengths of 7 ft, located inside the cavity. Heater power is controlled by a thermostat (exposed to the cavity air but shielded from radiant heat) set for 170°C.

Two radiant-heat-shielded thermocouples monitor the cavity air temperature. Six thermocouples are installed in the cavity surfaces with the junctions recessed ½ in. into the salt. A total of 24 thermocouples are installed in the salt structure around the room at distances of 6 in. to 8 ft from the cavity. Six thermocouples, in two series, are located 1½, 5, and 8½ ft from the front of the room; all the other thermocouples are in the plane 5 ft from the front of the room.

Background Data

Figure 3.1 shows the floor-to-ceiling movement which took place in the cavity at the various gage locations, after it was excavated and before the heating system was installed. To excavate the cavity, an undercutter was used to slice into the wall; the resulting salt slab was then broken off and removed. (The undercutter was turned on its side to make the vertical cuts.) As soon as the slab was removed, the strain gages were installed; the total elapsed time was three days from the first cut to the first set of gage readings (zero time on Fig. 3.1).

The initial deformation (flow) rates were high, but they decreased rapidly as the salt flowed to relieve the stress concentrations produced by the creation of the cavity. During the period of rapidly decreasing flow rates (about 50 days), the gages near the wall (Nos. 8 and 9) indicated

[1]Member of Chemical Technology Division.
[2]Member of Analytical Chemistry Division.

slower floor-to-ceiling convergence than those in the middle of the room (Nos. 2, 5, and 6). This might be interpreted as a beam deflection of the ceiling, except for the fact that the floor-only gage in the center of the room (No. 7) indicated that floor movement accounted for about three-fourths of the total deformation (see Fig. 3.2). The floor-only gage apparently had a tendency to stick, as indicated by the flat portion in the middle of the curve (Fig. 3.2).

After the initial transients, all of the gages indicated steady flow rates, decreasing only slightly with time. The rates of movement for the final 114 days of the background period are shown in Table 3.1. The unit deformation rates (in. in.$^{-1}$ day^{-1}) were obtained by dividing total rates by the height of the room.

As may be noted from Table 3.1, the floor-to-ceiling flow rates near the walls (gages 8 and 9) were nearly as large as those in the center of

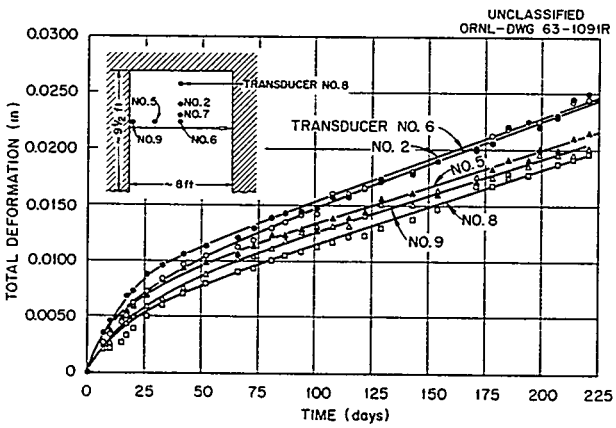

Fig. 3.1. Floor-to-Ceiling Movement at Ambient Temperature and Plan View of Model Room Containing Strain Transducers.

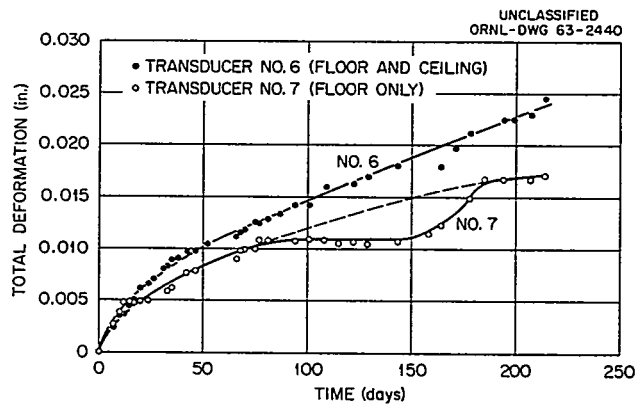

Fig. 3.2. Deformation at Ambient Temperature.

Table 3.1. Heated-Room Transducers – Background Closure Data

Gage Number	Cumulative Deformation (in.)		Rate of Movement, Final 114 Days	
	100 Days	214 Days	in./day	in. in.$^{-1}$ day^{-1}
			$\times 10^{-5}$	$\times 10^{-6}$
2	0.0153	0.0239	7.5	3.1
5	0.0132	0.0209	6.8	2.8
6	0.0146	0.0236	7.9	3.3
8	0.0113	0.0192	6.9	2.9
9	0.0124	0.0201	6.8	2.8
7[a]	0.0120	0.0173	4.6	1.9

[a]Based on idealized curve in Fig. 3.1.

the room. It has also been observed in the measurements made in various locations in the mine that after the initial transient period in the first few months after the opening was created, the floor-to-ceiling convergence rate near the pillars was almost as large as that in the center of the openings. In comparison, the deformation rates in Hutchinson mine openings, ranging from about 2 to 30 yr in age and from 6 to 12 ft in height, fall within the range of 2×10^{-6} to 7×10^{-6} in. in.$^{-1}$ day^{-1}.

The floor-only gage (No. 7) indicated that the floor was rising a little faster than the ceiling was falling. The wall-to-wall gage (No. 3) was inadvertently connected so that it measured wall-to-wall movement, plus floor movement near the wall. Since there was no floor-only gage near the wall, the readings cannot be readily interpreted; thus the data from this gage are not shown.

Heating Data

The heating phase began at 12:15 on March 18, 1963, with a power input of 11 kw. The average power input has now decreased to about 9 kw.

Temperature-rise isotherms around the center of the cavity after 32 days of operation are shown in Fig. 3.3. As shown by the temperature increases ½ in. into the salt around the perimeter of the cavity, the heating was reasonably uniform, although the floor and walls were somewhat cooler than the ceiling. Temperatures were beginning to approach equilibrium, and thus the cavity deformation due to thermal expansion also should have been approaching equilibrium.

Figure 3.4 shows the cavity deformations which took place during the first 40 days of heating. The cumulative deformation from wall to wall (~1 in.), gage No. 3, was about the same as that from floor to ceiling near the wall, gage No. 9, and only about two-thirds as great as the floor-to-ceiling movement in the center of the room (~1½ in.), gage No. 6. Gage No. 6 is typical of the other floor-to-ceiling gages, which are not shown.

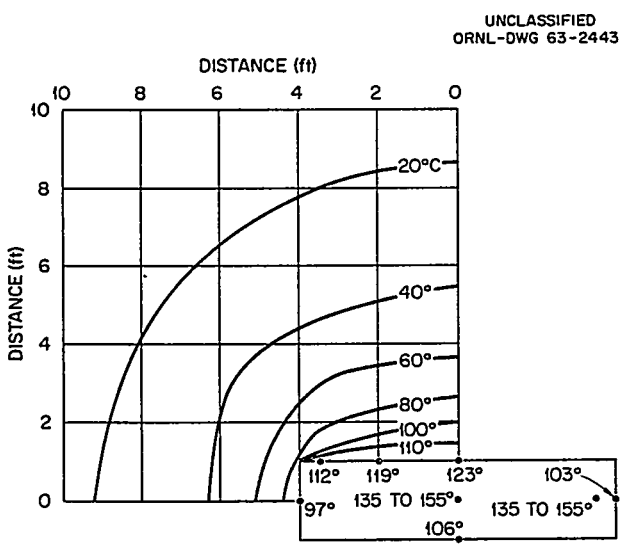

Fig. 3.3. Heated-Room Temperature-Rise Isotherms After 32 Days of Operation.

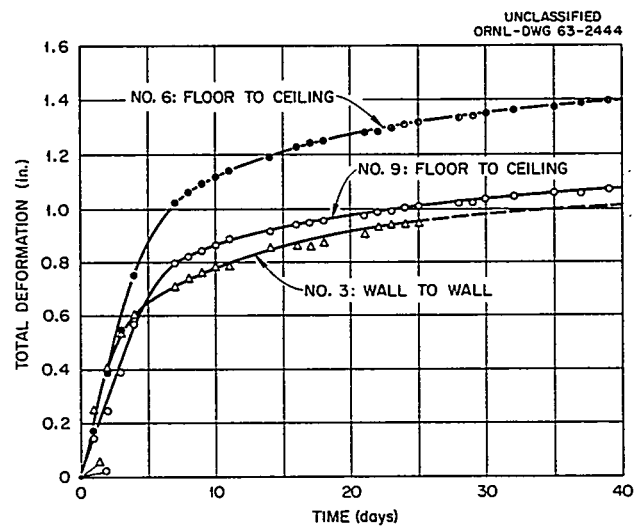

Fig. 3.4. Deformation During Heating – Heated-Room Experiment.

Deformation rates for the period from 30 days to 40 days are shown in Table 3.2. The floor-to-ceiling rates appear to be about the same throughout the cavity, although the accuracy in measuring the flow rates over such short portions of the curves is probably not very good. Comparing the deformation rates with those of the background period (Table 3.1), it is seen that the cavity is closing at a rate two orders of magnitude greater than before heating. Even at this accelerated rate, it would take 12 yr for the cavity to close completely. However, it must be remembered that this is, in effect, an isolated cavity and does not represent the behavior expected with a series of adjacent openings, as in a mine operation.

Table 3.2. Cavity Closure During Heating

Gage Number	Cumulative Deformation (in.)		Rate of Movement, 30 to 40 Days	
	30 Days	40 Days	in./day	in. in.$^{-1}$ day^{-1}
			$\times 10^{-3}$	$\times 10^{-4}$
2	1.31	1.36	5	2.1
5	1.38	1.43	5	2.1
6	1.35	1.40	5	2.1
8	1.19	1.24	5	2.1
9	1.04	1.08	4	1.7
3	>0.94			
7	>0.35			

DEMONSTRATION OF HIGH-LEVEL WASTE SOLIDS DISPOSAL IN SALT

A demonstration of the disposal of high-level radioactive waste solids is being designed for the Carey Salt Company mine in Lyons, Kansas. Fourteen irradiated Engineering Test Reactor (ETR) fuel assemblies, contained in seven cans, will supply radiation in lieu of actual solidified wastes. The assemblies will be placed in a circular array of holes in the floor, with one can in the center and the other six cans located peripherally, spaced 5 ft on centers. The test will last 2 yr; at the end of this time, all fuel assemblies will be returned to the Idaho Chemical Processing Plant (ICPP) for recovery of the unfissioned fuel.

An identical array with electrical heaters only will be operated as a control to determine the effect of radiation and heat on the salt characteristics.

The engineering and scientific objectives of the demonstration are: (1) demonstration of handling equipment and techniques; (2) determination of possible gross effects of radiation on hole closure, floor uplift, salt-shattering temperature, etc., in an area where salt temperatures are in the range 100 to 200°C; (3) determination of possible radiolytic production of chlorine; and (4) collection of information on creep and plastic flow of salt at elevated temperatures which can be used later to design an actual disposal facility.

A schematic cross section of the demonstration is shown in Fig. 3.5. The plot plan of the demonstration site is shown in Fig. 3.6. As presently conceived, the assemblies, after canning in Idaho, will be shipped by rail in a specially modified cask. At Lyons, the cask will be removed from a rail car standing on a spur and upended over a cased, vertical shaft extending to the mine working area, approximately 1000 ft below. The assemblies are to be lowered, one at a time, through the shaft and into a shielded cask mounted on a fuel assembly transporter which will permit vertical, as well as horizontal, movement of the cask. The transporter is to move to the experimental area where the cask will be positioned and lowered over the designated hole in the floor of the mine. Then the can will be lowered through the bottom of the cask into place; and the holes, approximately 10 in. in diameter by 12 ft deep, will have suitable liners and thus permit removal of the cans at the conclusion of the experiment. Lead or uranium shields placed in the top of each can will serve as biological shielding while the cans are in place.

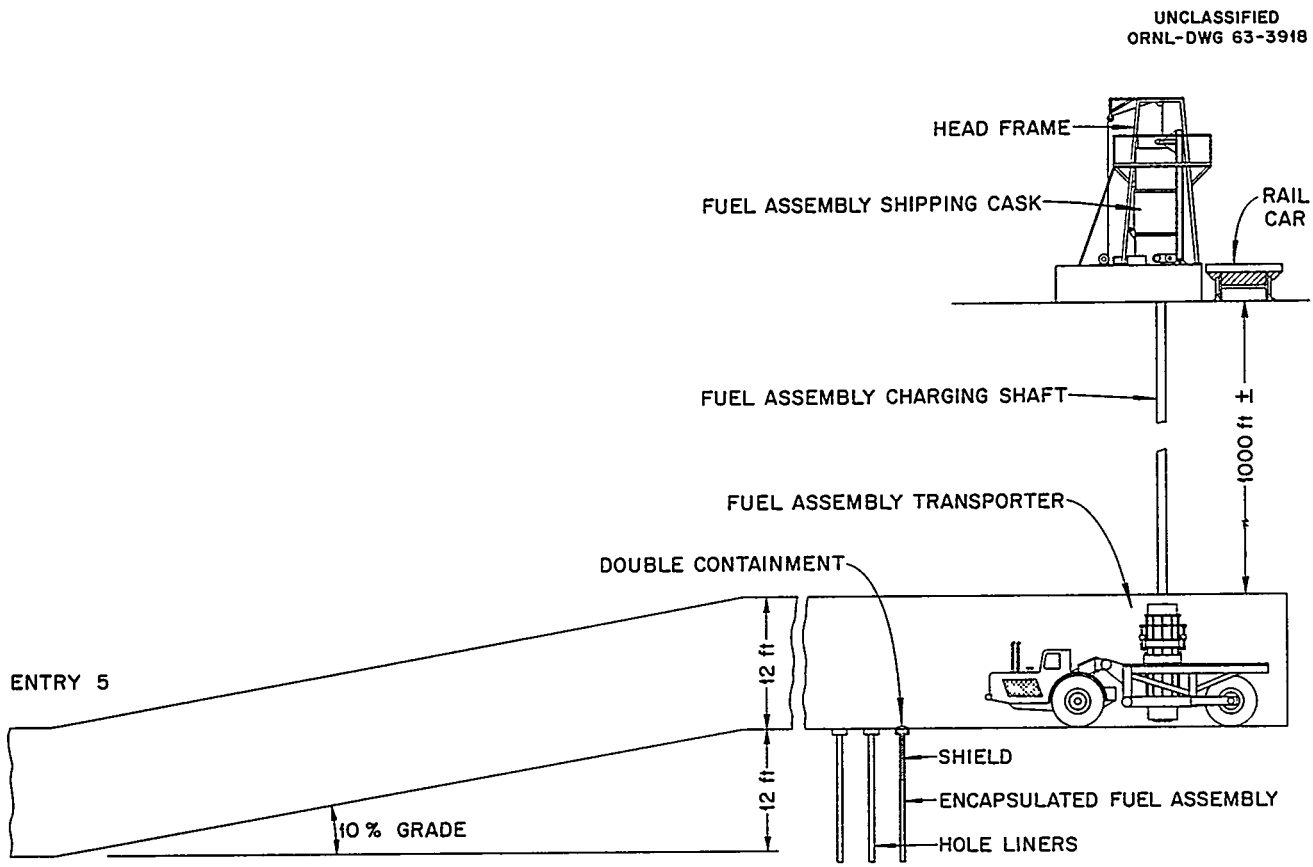

Fig. 3.5. Schematic Cross Section of Demonstration.

Fuel Element Selection

The decision to use irradiated reactor fuel elements in this experiment, rather than actual calcined wastes or separated fission product sources, was based on considerations of availability, cost, and radiation characteristics. The ETR fuel was selected after the operating cycle of the reactor and the number and dimensions of elements required to charge seven holes in the demonstration were considered. From the standpoint of thermal stability, power reactor elements were preferable; but uncertainties in availability led to the selection of the ETR fuel assembly as the best overall choice.

The ETR has an average thermal flux of about 2×10^{14} and a cycle time of about six weeks. A typical reactor cycle might average about 20 full-power days out of 23 operating days.

The aluminum cladding (mp, 660°C) sets the minimum decay time at which the assembly can be canned for use in the hot demonstration. If the assembly temperature is to be kept below 475°C, it can be canned in about 60 days at the earliest, resulting in a 90-day-decayed assembly before it is placed in the salt mine.

The final salt-dose calculations have not yet been made; but, based on preliminary calculations, it appears that the peak salt dose with two 90-day-decayed ETR assemblies in a can will be about 3×10^8 rads. Since laboratory tests have indicated little change in physical properties at 10^8 rads, but a significant (about 10%) drop in compressive strength at 5×10^8 rads, it is desirable to achieve, if practical, doses near 10^9 rads in this experiment. Changing the assemblies three times during the 2-yr test (four sets of assemblies, total) should increase the

UNCLASSIFIED
ORNL-DWG 63-3919

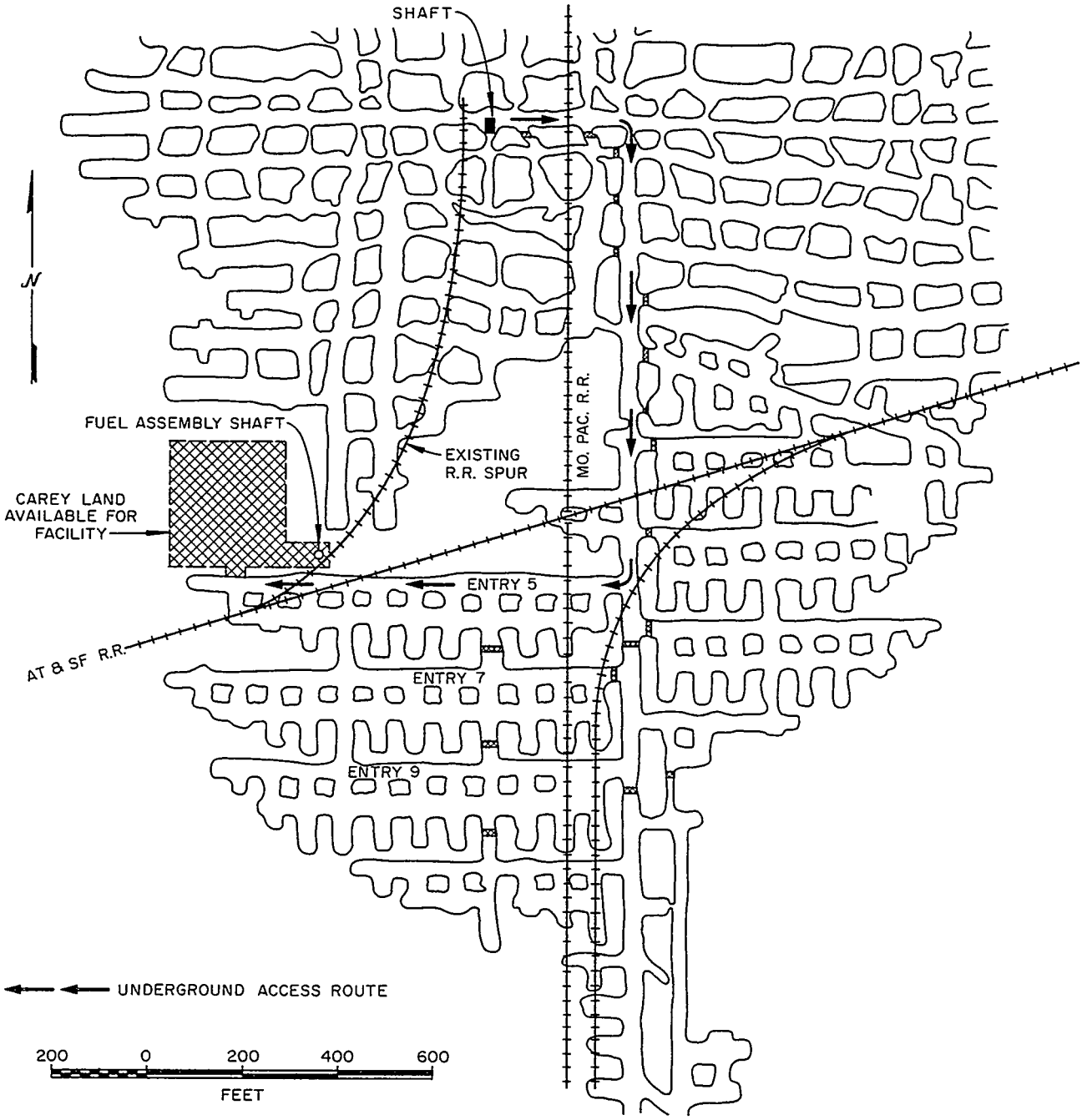

Fig. 3.6. Demonstration Site in Newly Mined Area, Lyons, Kan.

peak dose to about 8×10^8 rads. At the same time, this will give additional experience with the operation of the handling equipment.

Experimental Layout in Mine

From the standpoint of the economics of an actual disposal operation in an abandoned mine, it would probably be cheaper to use existing mine space for the disposal of the waste, rather than using it to store excess salt, *provided it could be shown that the use of existing space for disposal did not significantly reduce the safety of the operation.* At this time it is not possible to predict the structural safety of a mine in general, or the Lyons mine in particular, under temperature conditions which would prevail in a disposal operation. In the Lyons mine, and in practically all existing bedded salt mines, there is considerable water-bearing shale in the floor. Available corrosion data indicate that stainless steel waste containers will corrode rapidly in the presence of salt and water.

The major portion of the mined area in the Lyons mine, while generally similar to the modified checkerboard pattern in current use, really fits no repeating pattern; and, thus, it would be difficult to extrapolate from a test run in the existing mine.

Therefore it was concluded that the hot demonstration should be run in the periphery of the mine, with the fuel cans located in the relatively pure salt strata originally mined, thus reducing the corrosion problem and also allowing the choice of a desirable experimental layout.

The chosen experimental pattern, which simulates an operating disposal facility, is shown in Fig. 3.7. If the 30-ft rooms and pillars were a repeating pattern, the extraction ratio would be 50%; if the 40-ft rooms and 20-ft pillars were repeating, the extraction ratio would be 67%. With these extraction ratios at ambient temperature, the end rooms should show negligible salt flow; and the center rooms should not show enough flow to produce roof falls or noticeable floor heaves.

The radioactive and duplicate arrays are contained in the end rooms. The center pillar is heated by 22 heaters with an input of 1546 w each. The temperature-rise pattern in the floor at the

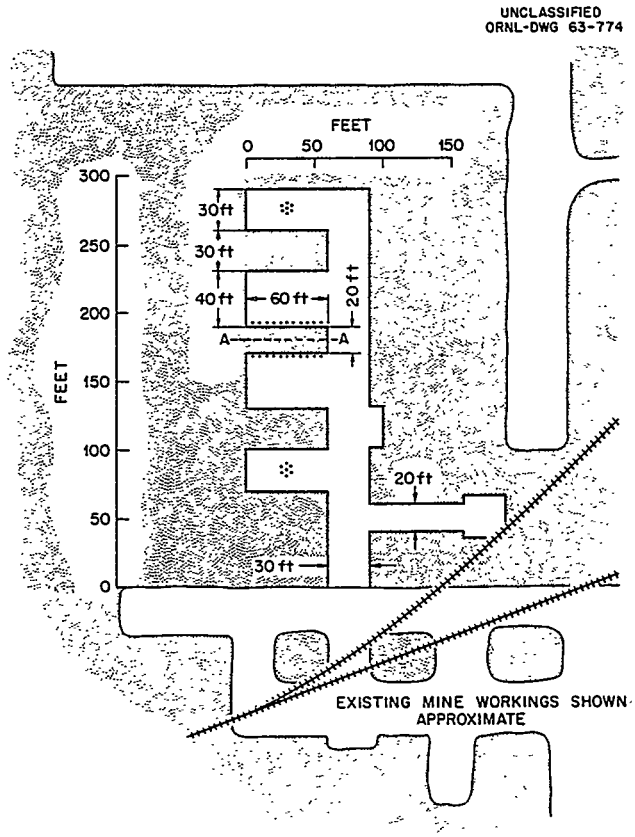

Fig. 3.7. Proposed Layout for Hot Demonstration Area Room and Pillar Pattern.

heater center plane after $1\frac{1}{2}$ yr operation (12,800 hr) of the 22 heaters is shown in Fig. 3.8. The major portion of the pillar base will have temperature rises in excess of 70°C. Also, the temperature rise in the center of the floor in the end rooms will be negligible; and, thus, heating of the center pillars should not have any thermal effect on the radioactive and duplicate arrays. These arrays, however, will contribute to heating of the two end pillars. (This contribution is not shown in Fig. 3.8.)

Renovation of Lyons Mine for Experiment

The shaft at the Lyons mine of the Carey Salt Company was excavated in 1890 by the Bevis Salt Company; mining was continued by a number of companies until 1949, when mining operations were suspended. The main shaft is timber lined and consists of two hoisting compartments and

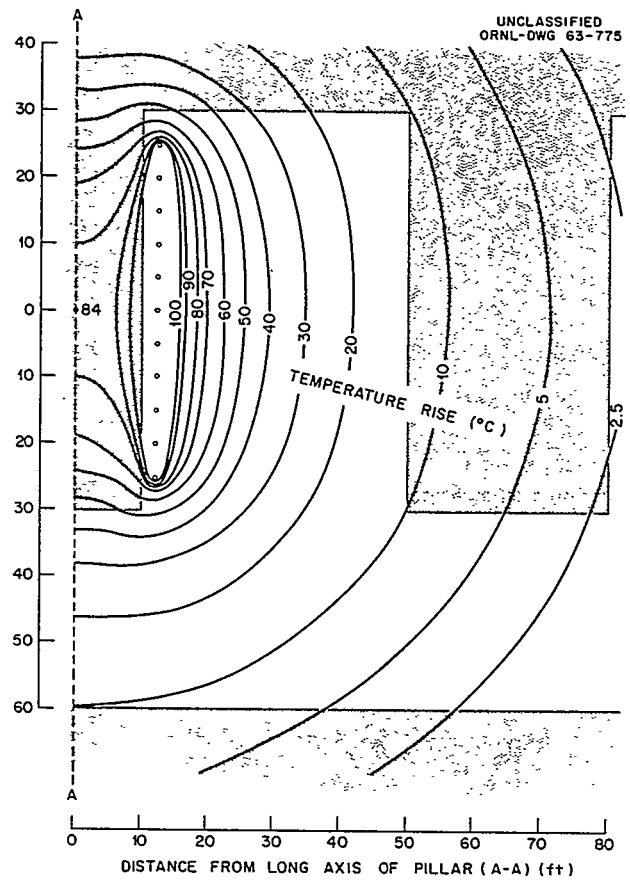

Fig. 3.8. Nine Feet Below Floor Level and Temperature-Rise Isotherms After 12,800 hr Operation of 22 Heaters at Base of Pillar, with a Power Input of 1546 w per Heater.

one airway. The present headframe was installed in 1955 when the old timber headframe and salt-processing equipment were removed. The headframe is equipped with one sheave wheel, permitting hoisting in only one compartment. At the present time, the headframe, man cage, and hoist combination will handle about a 3000-lb load. The hoist is a converted steam hoist with two cable drums, each 8 ft in diameter by 2 ft 9 in. wide.

Since the proposed experiment will necessitate lowering larger loads than can be handled by the existing facilities, the hoisting system will be renovated to handle 7-ton loads.

The shaft timbering is in remarkably good shape, considering the age of the mine; and only routine repairs to the timbers, guides, and water-collecting rings will be required. Some replacement of timbers at the shaft bottom may be necessary.

Underground, the Lyons mine shows considerable evidence of earth-pressure-produced floor heaves and ceiling sags. The major portion of the below-ground renovation will be the removal of these heaves and sags in order to provide safe access to the experimental site and to provide the necessary headroom for the mine transporter carrier. Since the experiment will be located above the mine floor, in the perimeter of the mine, it will be necessary to excavate a ramp to reach the higher elevation. The grade on this ramp has been set at 10%, and the new mine floor will be about 12 ft above the existing floor.

A new shaft from the surface to the mine will be drilled near the experimental area in order to lower the fuel element cans from the topside carrier to the mine carrier. Figure 3.6 shows the approximate location of the experimental area and the waste shaft.

Engineering Design of Demonstration

The engineering design of the demonstration for handling the radioactive materials requires major effort in the following categories.

Encapsulation of the Fuel Assemblies. – Sixty-day-cooled ETR fuel assemblies will be transferred, after removal of the end boxes, to the Multi-Cell Facility in Idaho [National Reactor Testing Station (NRTS)] for encapsulation. The fuel assembly capsule is being designed as a cylindrical container, ~5 in. in diameter and $7\frac{1}{2}$ ft long, for two ETR assemblies in tandem; at the upper end the present design incorporates a uranium shield plug, necessary for certain handling requirements, and four thermocouples and connectors for monitoring the temperatures in the central regions of the fuel assemblies.

The capsule will be pressure tested for leakage before shipment. Final design of the capsule is contingent upon mechanical strength, procedural mockup, and irradiation tests at ORNL and NRTS.

Shipment of Fuel Assembly Capsules from NRTS, Idaho, to Lyons, Kansas. – The carrier proposed for shipping seven fuel assembly capsules is a modified version of an available carrier at ORNL. The carrier modifications include a new water-cooled rotating magazine for holding the fuel capsules; addition of a sleeve in the rear section

for the grapple; addition of 2 in. of lead shielding to the body to bring the total shield thickness to 10 in. of lead, or equivalent; and an auxiliary operating door in the front section of the carrier.

Transfer of the Capsule from the Ground Surface to the Mine. – A vertical charging hole from the ground surface to the mine receiving area is planned adjacent to an existing railroad spur. The carrier will be elevated to a vertical position over the charging hole; a railroad crane will be used to move the carrier from the gondola to the charging station. Work platforms will be required at the top and ground level of the carrier, and a cable hoist for lowering the fuel capsules from the carrier to the mine is planned. A specially designed grapple, connected to the hoist cable, will be inserted in the upper end of the carrier and operated to lock the grapple and fuel capsule into one unit. The shield door in the lower section of the carrier will be opened to allow passage of the fuel element to the mine, and a shield on a specially designed diesel-powered transporter (described in the next paragraph) will be in a position to receive the fuel capsule. After the fuel capsule enters the shield, the cable is to be disconnected, and the grapple will remain with the shield.

Transfer of the Capsule to the Demonstration Area. – The HLS (High-Level Solid) Waste Disposal Carrier will be used to receive the fuel capsule, move it within the mine, and then discharge it into an experimental disposal hole in the floor. This carrier is to be a standard diesel-powered two-wheel rubber-tired tractor and a special trailer equipped with a lead shield; it must be highly maneuverable because of the limiting confines of a salt mine. To receive the radioactive waste, the shield will have to be positioned under the charging hole from the ground surface and elevated to engage with the shadow shields in the roof to protect personnel. Doors on the upper end of the shield will then be opened to receive the capsule. After the capsule is received in the shield, the doors will be closed and the shield lowered to transport position and secured. At this point the cable will be disconnected from the grapple; then the carrier will be driven to the demonstration area and positioned over the disposal hole. The shield is to be lowered to the floor, ready for the transfer of the capsule to the salt environment. After the lower shield doors are opened, a trailer-mounted cable hoist, connected to the grapple cable outside the shield, will be used to lower the capsule into the hole. The shield doors will be closed and the shield raised and moved adjacent to the hole for removal of the grapple. At the upper end of the capsule the uranium shield should minimize radiation from the disposal hole for limited access during removal of the grapple. A cover plate and supplementary shielding, if required, will then be put in place to close the hole and permit start of the demonstration.

Floor Hole Liner and Associated Components. – The disposal hole for the demonstration with fuel elements differs from the plans for actual waste disposal in salt, in that a metal hole liner is used to prevent contact of the fuel capsule with the salt. This liner should minimize corrosion problems and prevent hole closure by salt flow, so that the fuel capsule may be recovered. In order to measure salt movement and sample the gases released from the salt, as a result of the radiation and heat emitted from the fuel capsule, an annulus approximately 2 in. wide is allowed in the region surrounding the hole liner adjacent to the fuel elements. Supplemental shielding in the form of steel shot is provided in the annular space above the fuel elements to protect personnel at the surface from radiation. Additional shielding above the fuel capsule will probably be necessary. The liner with the top cover and seal in place provides a secondary containment vessel to avoid release of radioactive material into the salt mine. Tubes for sampling gas are brought out to a junction box which connects them to gas samplers. Heaters in the annulus will supplement the heat emitted from the fuel elements and provide closer approximation to the heat generated by solid radioactive waste. The liner and junction boxes will be set in concrete to hold the assembly in place, provide an inexpensive method of sealing the annular space, and permit sampling of the gases.

Materials Problems

A sodium chloride–moist air atmosphere or sodium chloride in the presence of moisture at a high temperature is very severe service for most construction materials. Type 304 stainless steel thermocouple sheaths used in the single-heater and array experiments (described later) showed severe scaling and stress corrosion in areas where the

temperature reached ~175°C. The relatively thin-wall (0.018 in.) sheath of the thermocouples was completely penetrated in a number of cases. Heavy scaling and intergranular attack up to 0.045 in. (ref 3) were observed in the wall and floor heater cans which operated at temperatures greater than 500°C. Carbide precipitation was also observed in these cans. The array heater which reached a maximum temperature of ~425°C showed slight scaling and no carbide precipitation. The difference in carbide precipitation (which promotes corrosion) appears to be due to operation of the array heater at the lower end of the precipitation range and operation of the wall and floor heaters near the middle of the range.

Construction materials being tested include stainless steel (types 304L, 310, and 347), Hastelloy C, Haynes alloy No. 25, titanium, carbon steel, aluminum, nickel, Monel, Inconel, Ni-o-nel, and protective coatings designed to allow use of a cheaper material, such as carbon steel, as the base metal. Corrosion testing is being performed by the corrosion group of the Reactor Chemistry Division.

The test environment consists of ground natural salt (or reagent salt plus contaminants present in Kansas rock salt) in air and contained in sealed quartz tubes. These quartz tubes, containing the welded coupons and ground reagents in air, are placed in a furnace maintained at the test temperature. Some tests have already been performed under these conditions; they covered a period of 30 days (720 hr).

Tables 3.3 and 3.4 present the results of corrosion tests at 300 and 500°C. Titanium and carbon steel were eliminated from the 500°C tests and 1100 aluminum from both 300 and 500°C tests because rapid attack was observed in earlier, aborted tests.

The data presented in these tables show that in natural salt all the materials (types 304L and 310 stainless steel, Hastelloy C, and Haynes alloy No. 25) exhibit satisfactorily low corrosion rates at 500°C. At 300°C the type 310 stainless steel and the carbon steel have low corrosion rates but show pitting. On the basis of these data, type 304L stainless steel will be the most economical and satisfactory material for use in natural salt at both 300 and 500°C. Hastelloy C, Haynes alloy No. 25, and titanium would also be satisfactory at 300°C, but undesirable, because they are more expensive and more difficult to fabricate. Because of the unpredictable nature of pitting corrosion, any material which develops pits is considered unsuitable.

The materials discussed above are now being tested at 200°C. Tests of the additional materials (type 347 stainless steel, nickel, Monel, Inconel, Ni-o-nel, and protective coatings) and a test of the

[3]R. S. Crouse, *Metallography Report No. 449*, Metals and Ceramics Division (Dec. 28, 1962).

Table 3.3. Corrosion in Salt

Medium	Penetration (mils/yr)[a]					
	Type 304L Stainless Steel	Type 310 Stainless Steel	Hastelloy C	Haynes Alloy No. 25	Ti-45A	Carbon Steel
Natural NaCl	0.4	0.2[b]	0.1	0.1	0	2.0[b]
Reagent-grade NaCl	0.2	0.1	<0.1	0.1	0	1.6[b]
99.5% NaCl–0.5% H_2O	0.5[b]	0.3[b]	0.1	0.1[b]	0.1	1.5[b]
99.75% NaCl–0.25% $MgCl_2$	0.8	0.4[b]	0.1	0.2	0.1	3.5[b]
95% NaCl–5% $CaSO_4$	0.6[b]	0.2[b]	0.1	0.1[b]	0	1.9[b]
94.25% NaCl–0.5% H_2O–0.25% $MgCl_2$–5% $CaSO_4$	0.4	0.3	0.1	0.1[b]	0.1	3.8[b]

[a]Exposure at 300°C for 720 hr.
[b]Pitting attack.

Table 3.4. Corrosion in Salt

Medium	Penetration (mils/yr)[a]			
	Type 304L Stainless Steel	Type 310 Stainless Steel	Hastelloy C	Haynes Alloy No. 25
Natural NaCl	0.5	0.1	0.1	0.2
Reagent-grade NaCl	0.3	0.5[b]	0.1	0.1
99.5% NaCl–0.5% H_2O	0.6	0.4	0	0.1
99.75% NaCl–0.25% $MgCl_2$	0.5	0.4[b]	0.5	0.3
95% NaCl–5% $CaSO_4$	0.4[b]	0.3[b]	<0.1	0.1
94.25% NaCl–0.5% H_2O–0.25% $MgCl_2$–5% $CaSO_4$	0.7	0.2	0.1	0.1

[a]Exposure at 500°C for 720 hr.
[b]Pitting attack.

corrosion of type 304L stainless steel in a cobalt gamma-radiation field are being prepared.

HIGH-TEMPERATURE EXPERIMENTS

Single-Heater Experiments

Cylindrical heaters, 6 in. in diameter by 4 ft long, were used in 10-in.-diam holes in the floor and in a column of the mine to investigate the physical properties of salt *in situ* at temperatures above 300°C. Instrumentation was provided to measure floor rise around the heater in the floor and column expansion about the wall installation and to collect water vapor from the holes.

Both the floor- and wall-cylinder tests began on July 18, 1962, with a power input of 3500 w each. Salt-temperature rises in the plane perpendicular to the center of the heater are shown in Fig. 3.9, along with theoretical curves based on the 100°C salt thermal properties. After 45 and 49 hr operation of the wall test and the floor test, respectively, the power was turned off for 3 hr, during which time the heater was removed from the hole and the hole diameter was calipered at 1-ft intervals. Both heaters were restarted at 5000 w; and the power remained constant, with the exception of a 5- to 10-min daily period (to record heater temperatures) and one period of about 45 min (to inspect the wall heater hole).

No thermocouples were installed at the periphery of the heater holes (0.42 ft from the center of the heater), but the theoretical salt temperature was ~210°C when the caliper measurements were

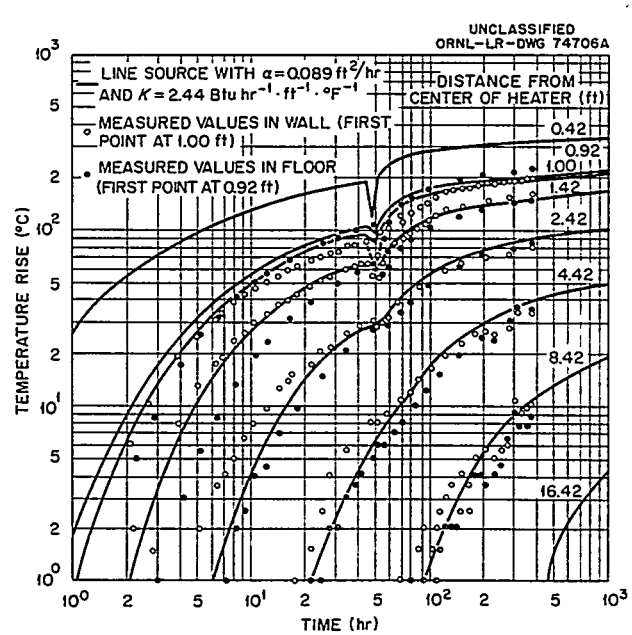

Fig. 3.9. Comparison of Temperature Rise in High-Temperature Cylinders with Theoretical for Line Source.

begun. Maximum closure of the holes (after 45 hr) was about 0.4 to 0.5 in. at the center of the heater, a depth of 8 ft (Fig. 3.10). Data on the floor hole were more variable, and fewer points were measured than on the wall hole; but there was little difference in the amount of closure of the two holes down to a depth of about 6 ft. Also, the amount of vertical closure and horizontal closure of the wall hole did not seem to differ significantly, indicating that the closure was primarily due to thermal expansion.

Tests both in the laboratory and in the mine have established that massive salt from the Carey Salt Company's Hutchinson mine will shatter when heated above 260 to 290°C. This fracturing has been attributed to the buildup of water pressure generated by the heating of the water trapped within the salt framework. Salt samples from other mines have been tested in the laboratory, and their stabilities are given in Table 3.5.

Micrographic examination of salt from the Hutchinson mine reveals inclusions of water, or negative crystals. Figure 3.11 shows a microphotograph of a negative crystal with an air bubble floating in liquid. Similar examination of a sample from the Grand Saline mine failed to show any negative crystals.

Although the salt shattered at an estimated 280°C, it did not seem to have significantly affected heat transfer (see Fig. 3.9).

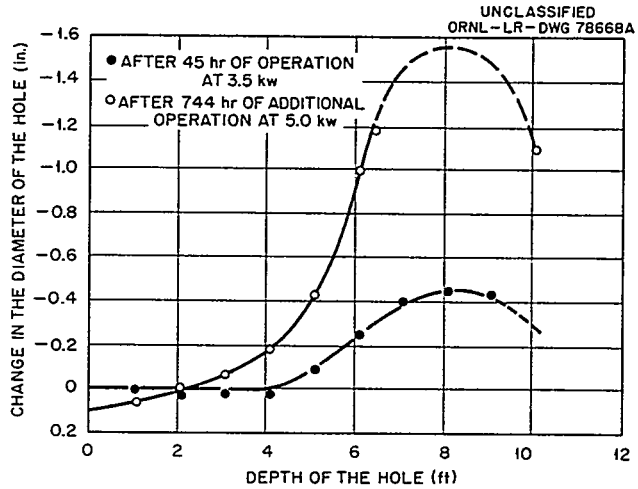

Fig. 3.10. Thermal Closure of Wall Hole.

Water evaporated from shale partings or released by salt shattering was condensed at mine temperature in air-cooled condensers. About 15.5 liters from the floor heater hole and 250 ml from the wall heater hole were recovered. One-gallon samples of the water from the floor hole, together with a reference sample of known recent water, were submitted to the laboratory of the U. S. Geological Survey for tritium dating.

Table 3.5. Thermal Stability of Salt

Mine	Number of Samples Tested	Fracturing Temperature (°C)	Salt Type
Hutchinson, Kan.	30	260–320	Bedded
Lyons, Kan.	8	285–320	Bedded
Fairport Harbor, Ohio	2	380	Bedded
Retsof, N. Y.	2	*a*	Bedded
Winnfield, La.	2	*a*	Dome
Grand Saline, Tex.	2	*a*	Dome
Weeks Island, La.	2	*a*	Dome

[a]Indicates that the salt did not fracture up to 400°C.

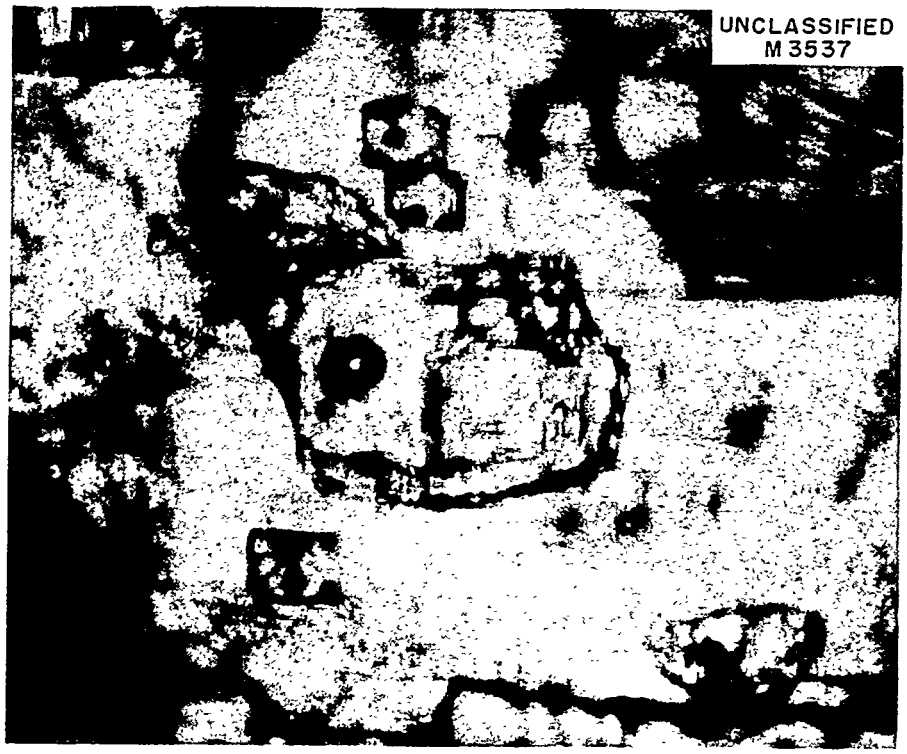

Fig. 3.11. Negative Crystal in Rock Salt.

The floor- and wall-cylinder tests were terminated after 792 hr of operation, and the salt temperatures were allowed to decrease to ambient temperature prior to heater removal. The floor heater was removed without difficulty; however, the wall heater was encased in the salt shattered from the sides of the hole where the temperatures were greater than 280°C; consequently, removal was difficult.

When the hole closures which were measured after 45 hr of operation are plotted against the theoretical temperature rise at the points of closure measurement, a straight line results. It was found that the measured closures after 792 hr of operation also plot a straight line, but one with greater slope than the 45-hr line. By extrapolating the 792-hr line to the peak salt-temperature rise (330°C) at the midpoint of the heater, it was possible to estimate the closure that would have occurred in the shattered zone if the salt had not shattered. On this basis the maximum permanent hole closure (Fig. 3.10) would have been 1.55 in. (15% diameter decrease) at the center of the heater where the peak salt temperature at the original hole radius was about 350°C.

Column expansion around the wall heater is shown in Fig. 3.12. The maximum expansion, about 0.5 in., occurred 2 ft from the center of the heater. Expansion 2 ft from the hole was greater than that 1 ft from the hole, presumably because the salt near the hole could flow plastically into it and thereby reduce expansion in the other direction. As the temperatures in the salt decreased

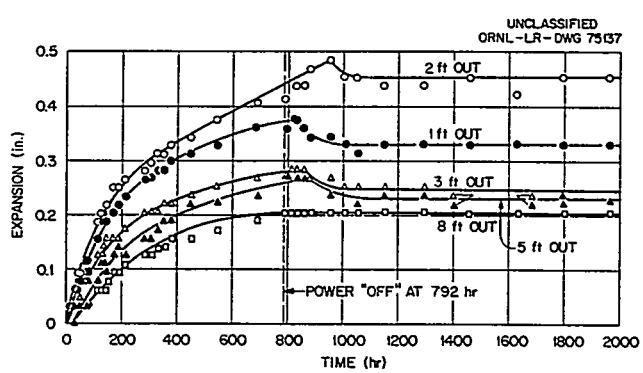

Fig. 3.12. Expansion of Column at Various Distances on Horizontal Line from Center of Heater Hole — Wall-Cylinder Test.

upon completion of the experiment, only a small fraction of the expansion was recovered, indicating that the expansion was inelastic. Similar observations were made around the floor heater; however, the expansions were greater – at 2 ft from the heater, the expansion was 0.8 in.

With the salt-temperature profile at 620 hr, and assuming unrestrained expansion in the axial direction, calculation of the thermal expansion around the wall heater hole indicates that a thermal expansion of 1.14 in. could have been produced. This value, as expected, is higher than that observed, since the salt was restrained and some salt had moved radially into the hole.

The volume of salt contained in the zone to the 290°C contour, including that expanded into the hole, is 1.8 ft^3. The moisture released from samples of Hutchinson salt shattered in the laboratory averages about 0.19% by volume. The actual water collected in the wall test after shattering had begun was 189 ml, or 0.37% by volume.

Three possible explanations for this apparent water volume discrepancy are: (1) the extra water came from the radial cracks extending away from the hole; (2) the shattered zone is larger than estimated; or (3) more moisture was released under the test conditions than is released when the explosions take place in the laboratory. That all of the moisture is not released in the laboratory tests was confirmed by microscopic examination of small pieces of a sample which had exploded violently in a laboratory test. Several brine-filled negative crystals (cavities), containing small vapor bubbles, were observed.

High-Temperature Array

An array of seven heaters is necessary to heat a large section of the floor above 100°C. Probably the minimum space between cylinders of calcined waste in an actual disposal operation will be about 5 ft. The central heater, which simulated a calciner pot, was a 5-ft length of 6-in. sched-40 stainless steel pipe, with 4 ft of heaters inside. The six peripheral heaters consisted of 4 ft of furnace elements in a 2.5-in. tube. The central heater hole was 10 in. in diameter, giving a 1.5-in. annulus for observing possible salt shattering and/or flow into the hole.

The array was started at 2:30 pm on July 23, 1962, and the peripheral heaters began to fail after about 8 hr of operation. Inspection of the first heaters to fail showed that the nickel connecting wires had broken for reasons not readily apparent. (Later studies indicated that the failure was due to sulfide embrittlement.) Operation of the experiment was continued as a single-heater experiment, with the central heater operating at 3700 w.

Hole closures and floor expansions followed the same general trend as in the floor- and wall-cylinder tests, but the magnitude was smaller due to the lower power input. About $8\frac{3}{4}$ liters of water was collected from the central heater hole.

CHLORINE RELEASE FROM GAMMA-IRRADIATED SALT

The storage of high-level wastes in salt formations will expose the surrounding salt to radiation, and the dose in the immediate proximity of the packaged wastes is expected to be as high as 10^{10} rads. While it is known that radiation will cause some damage to alkali halides, there has been no definitive work to prove or disprove the release of free halogen from sodium chloride. The only work found in the literature that seems to be related to this problem is that of Epstein,[4] who gives quantitative data on the amount of oxidizing substance (presumably chlorine) formed in solid potassium chloride upon exposure to high levels of gamma or beta radiation. Epstein could not detect any chlorine in the gas phase with certainty; thus he placed an upper limit of 0.5% of the total oxidizing power generated within the solids which escapes to the gas phase. The oxidizing power stored within the crystalline solid was determined by dissolving the solid in water and determining the oxidizing equivalent against potassium iodide or *o*-tolidine. Values of *G* (number of molecules produced per 100 ev of energy absorbed) are given which decrease with dose – from 1.47×10^{-2} at 2×10^7 rads to 5.1×10^{-4} at 3.27×10^9 rads.

[4] L. M. Epstein, *Formation of Chemically Free Halogen by Radiolysis of Solid Potassium Chloride*, Westinghouse Electrical Corp. Research Laboratories, Pittsburgh, Pa., WERL-0100 (June 1962).

Sodium chloride has been gamma irradiated at the steady-state temperature (35 to 60°C) of a 10,000-curie Co^{60} source, as well as at temperatures up to 250°C. No release of chlorine to the vapor phase has been detected by gas chromatography or by chemical methods in the irradiations performed at 35 to 60°C with doses up to 8×10^9 rads and at 250°C with 3×10^8 rads. The G values for the production of oxidizing power generated in the solid decreased with dose. These values for sodium chloride at 35 to 60°C are nearly an order of magnitude less than those given by Epstein for potassium chloride at equivalent doses.

White, crystalline sodium chloride changes color with increased doses of irradiation. At 10^6 rads it is light tan; it progressively deepens to brown and finally to a dark blue-black at about 5×10^8 rads. Color produced by irradiation can be annealed out. The annealing process is temperature dependent; it is essentially complete in a few hours at 250°C, but it requires nearly a week at 190°C. When salt is irradiated at elevated temperatures, the resultant color depends on which process is faster — the accumulation or the annealing of the color centers. For example, at 160°C accumulation predominates, and the salt becomes colored; but at 250°C the annealing process predominates, and the salt remains white. As a result, the salt irradiated at 250°C still retains oxidizing power even though it shows no apparent change in color.

The G values obtained by the irradiation at the lower temperatures were used to calculate the oxidizing power that would be produced in the surrounding salt during a storage period. These values are given in Table 3.6. The G values used for the higher dose rates were obtained by extrapolating the values obtained at 35 to 60°C. The temperature of the zones receiving doses of 10^9 rads and more is expected to hover above 200°C, and the G values for these zones are expected to be lower than those used in the table.

The time rate of production is shown in Table 3.7. This table was based on a Purex-type waste that had been cooled 2 yr before burial.

Table 3.7. Probable Rate of Formation of Chlorine in Solid NaCl

Time After Burial	Dose	Percent of Total Chlorine Produced
20 days	8.6×10^6	8.5
40 days	1.7×10^7	11.0
80 days	3.4×10^7	14.0
160 days	6.9×10^7	17.0
320 days	1.4×10^8	21.0
1.75 yr	3.8×10^8	30.0
3.5 yr	7.5×10^8	38.0
7 yr	1.5×10^9	49.0
14 yr	3×10^9	63.0
28 yr	6×10^9	80.0

Table 3.6. Yield of Oxidizing Agent with Dose

Dose (rads)	G	Moles of Oxidizing Substance (per gram of salt)	Mass of Salt Radiated (g)	Total Moles of Oxidizing Agent Produced
10^6	9×10^{-3}	9×10^{-9}	1.4×10^7	0.2
10^7	3.7×10^{-3}	3.7×10^{-8}	6.8×10^6	0.4
10^8	1.4×10^{-3}	1.4×10^{-7}	3.6×10^6	0.3
10^9	7×10^{-4}	7×10^{-7}	1.5×10^6	1.0
1.2×10^{10}	2×10^{-4}	4×10^{-6}	2.9×10^5	0.7

The studies indicate that the release of chlorine from irradiated salt is negligible from the standpoint of a short-term storage. It is not known whether long-term storage and irradiation will result in an accumulation of up to 2 moles of free chlorine in the gas phase surrounding the irradiated salt.

CREEP MEASUREMENTS IN MINES

Ten measuring stations were installed in the Hutchinson mine and four in the Lyons mine to obtain information on the effects of percent salt extraction, depth, and age on the flow occurring at ambient mine temperatures. During the year, one of the Hutchinson gages was discontinued, since the area occupied by the gage interfered with the current mining operation. In addition, three of the Hutchinson gages were installed around heat experiments; as a result, they are not representative of flow under normal mine conditions. The results of the measurements of room closure for the remaining six gages and the discontinued gage are shown in Table 3.8. The Reid wires to measure floor and roof movement are not included, since present data are insufficient for accurately predicting percentage of movement in the floor and roof.

The plots of weekly readings from all gages show a rate of movement which decreases with time. In Table 3.8 the effect of age can be seen by comparing stations 1, 8, 2, and 3, in that order, although stations 3 and 8 do not seem to follow the pattern. Station 8 rates are too low for reasons explained later. The reason for the higher rate of movement at station 3 has not been determined; however, it may be due to a local increase in percent of extraction or to the relative location of the gage and the mined-out workings. In the case of stations 6 and 7 (located in areas of higher extraction), the oldest working has the highest rate; however, station 6 is near the center of the mining pattern, and, as a result, the pillar loading should be higher than that at station 7, which is four entries from the extreme end of the mine.

One observation which can be made from the results obtained to date is that, for openings older than ~1 yr, the observed rate of closure next to the column is about equal to that observed in the center of the room; whereas, in openings less than 1 yr old, the rate of movement in the center of the room is greater than that near the column.

Station 8, installed near the periphery of an area mined in January 1959, had a closure rate at the edge of the room of 0.0003 in./day in March 1962 and showed a sudden increase in rate of movement when mining was resumed in the area. Rates of movement as high as 0.0021 in./day were observed as the mining progressed. This increase in rate

Table 3.8. Rate of Movement at Various Gaging Stations in the Hutchinson Mine

Gaging Station	Rate of Movement (in./day)		Age of Room (yr)	Salt Extraction (%)
	Center of Room	Edge of Room		
1	0.0008	0.0007	1.3	75
2	0.0003	0.0003	7	75
3	0.0005	0.0005	10	75
4	0.0001	0.0001	27.5	70
6	0.0007	0.0006	15.5	80
7	0.0004	0.0004	11	80
8[a]	0.0003	0.0003	3.3	75

[a]Rates as of March 1962.

of movement was produced by increased pillar and roof stresses as a result of the retreat of the periphery and subsequent load transferal to existing pillars.

FLOOR AND CEILING CORES

The location of the experimental plot for the best placement of canned fuel elements within the mine is governed to a large extent by the quantity of shale interbedded with the salt. Therefore rock conditions above and below the mine floor were investigated.

At the Lyons mine, the Hutchinson salt member consists of about 300 ft of nearly flat-lying beds of salt, shale, and anhydrite, with salt comprising about 60% of the sequence. The mine is operated in the lower part of the member. Within the mined unit, 1- to 6-in. layers of relatively pure NaCl are separated by clay and shale laminae usually less than 1 mm thick. These laminae are the major impurity in the salt and are characteristic of most bedded salt deposits. Shale beds, several inches in thickness and separated by about 15 to 18 ft of salt, lie above and below the mined unit and thus limit the vertical extent of mining. The mine floor is generally within a few inches of the underlying shale bed, while the roof is normally several feet below the overlying shale bed. The least-contaminated salt, and thus the source of most of the production in the mine, lies in a 9-ft-thick section that extends from the top of the shale below the floor upward to a thin shale parting, $\sim 1/16$ in. thick. Another prominent shale parting lies about $3\frac{1}{2}$ ft above the 9-ft roof; and, in some parts of the mine, this section was also mined. However, the additional excavation has resulted in a weak roof that buckles and fractures and frequently allows a 3-ft section of overlying impure, or "dirty," salt ($12\frac{1}{2}$ to $15\frac{1}{2}$ ft above the mine floor) that extends to a relatively thick shale bed above the mined area to fall.

At the time of the investigation, the canned-fuel experiment was to be located in the extreme southwest end of entry 9 in the mine (see Fig. 3.6). However, due to the nature of the experiment, it would be more convenient to place the fuel elements in an excavated portion of the present floor of the mine. An alternate plan specified that the tests be conducted in an unused part of the salt section from which salt had been mined. This latter plan would have required the excavation of a considerable amount of salt lying in the section above the present mine roof and, of course, would have increased operating costs. Therefore, prior to the selection of the actual test site, it was necessary to define in detail the rock conditions existing both below the floor and above the roof of the mine.

Two 2-in.-diam by 30-ft-deep core holes were drilled in the floor of the mine in entry 9, while two cores approximately 20 ft in length were obtained from the roof of the mine at the same locations. These cores, along with the log of a hole drilled previously in entry 7 (ref 5), were used to construct a geologic cross section of a portion of the salt section from the northwest end of entry 7 to the southwest end of entry 9 (see Fig. 3.13).

Considerable quantities of shale and some anhydrite are included in the salt section from the floor down to a depth of about 115 in. in entry 9 and to a depth of approximately 135 in. in entry 7. The shale, which is noncalcareous and greenish gray to black, commonly occurs in beds <1 in. to 16 in. thick that usually contain a few crystals of clear-to-orange halite and some stringers of fine-grained anhydrite. As seen in Fig. 3.13, these beds vary considerably in thickness over relatively short distances. Frequently, the beds grade, both laterally and vertically, into salt that contains many pods and irregularly shaped lenses of shale. This unit of the section is underlain by about 80 to 125 in. of relatively pure salt. The salt consists essentially of medium-to-coarsely crystalline, clear-to-brownish halite containing disseminated blebs and inclusions of dark-colored clay that gives the salt a dark, smoky appearance in places.

A second zone of interbedded salt, shale, and anhydrite, about 40 to 50 in. thick, lies beneath the relatively pure salt sequence. The shale and anhydrite are similar to those described higher in the section, but the shale beds are thinner, and a larger amount of anhydrite is present in the form of lenses. For the remaining part of the section in entry 9, which was cored to a depth of about 360 in. below the mine floor, the cores show a relatively pure salt sequence like that described above. In

[5] W. B. Heroy, *Lithology of the Salt Section in the Mine of The Carey Salt Company, Lyons, Kansas, Technical Report No. 62-9*, The Geotechnical Corp., June 1962.

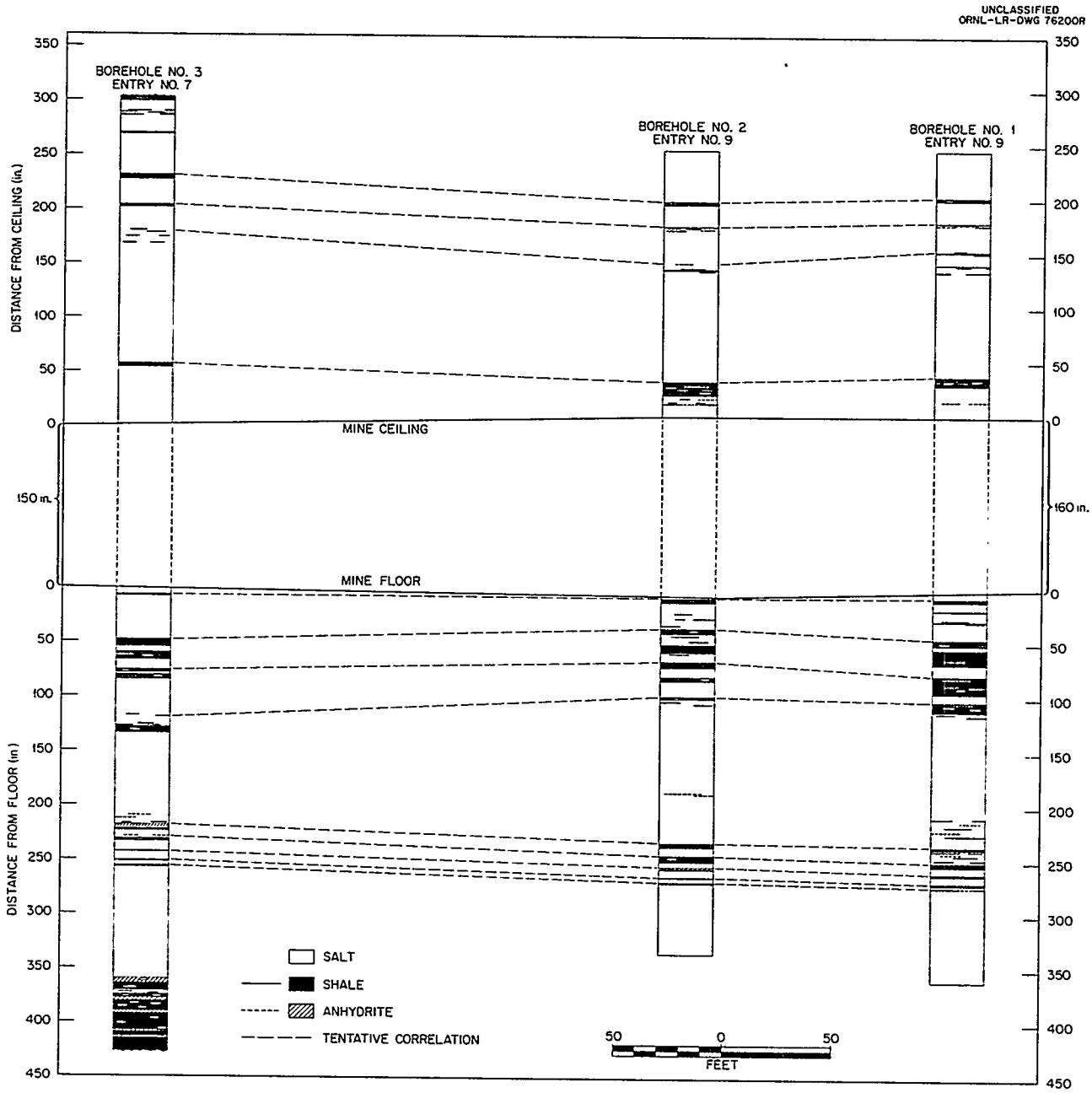

Fig. 3.13. Generalized Geologic Cross Section of a Portion of the Hutchinson Salt Member of the Wellington Formation in the Carey Salt Company Mine, Lyons, Kan.

entry 7 the salt is interrupted by thick shale and anhydrite beds at a depth of about 360 in. This same thick shale and anhydrite unit would probably have been intercepted in entry 9 if the drilling had proceeded a few feet deeper.

Up to about 250 in., the ceiling of the mine consists of a relatively pure salt sequence interrupted by four separate shale zones. These zones, like those below the mine floor, are greenish gray to black and frequently contain lenses and crystals of clear-to-orange halite along with stringers and lenses of anhydrite. The thickest shale bed lies at a minimum of ~20 in. above the present roof of the mine. The bed was observed to

2 copies

be about 12 in. thick in borehole 2, entry 9, but only about 3 in. in the core from entry 7. The other shale zones (shown in Fig. 3.13) lie ~130 to 230 in. above the roof. The salt from the ceiling cores is composed mainly of medium- to coarse-grained, clear-to-brownish halite crystals that contain many blebs and irregularly shaped masses of clay, which give the material a smoky appearance. In addition, from about 70 in. above the mine roof to the end of the cored section, the salt contains many scattered blebs of an orange-to-red microcrystalline mineral tentatively identified as polyhalite.

---

4. Clinch River Study

N. J. Ackermann, Jr.[1]
W. P. Bonner
P. H. Carrigan, Jr.[2]
K. E. Cowser
E. E. Eastwood
J. S. Forrest[1]
B. J. Frederick[2]
R. J. Morton[3]
F. L. Parker
W. E. Parker[1]
R. J. Pickering[2]
E. G. Struxness
Tsuneo Tamura

WATER SAMPLING AND ANALYSIS

Results for the first year's collection and analyses indicate that mass curves (cumulative transport obtained from the product of the flow and the radionuclide constituents) of each of the four major isotopes (Ru^{106}, Cs^{137}, Co^{60}, and Sr^{90}) passing through the Clinch River show that essentially all of the radioactive material discharged over White Oak Dam eventually passes by the Centers Ferry sampling station. Adjusted results for radioactive material discharged by White Oak Creek and for that already present in the Clinch River at the mouth of White Oak Creek show that 107% of the ruthenium (see Fig. 4.1), 110% of the cesium, 89% of the cobalt, and 95% of the strontium passed Centers Ferry. It is obvious that amounts greater than those discharged could not pass the downstream station, but these values do give some measure of the order of magnitude of the errors.

Results from the second year of sampling, while following the same general trend, have some anomalous results which have to be investigated and adjusted, if necessary, by use of a correlation of the concentrations at the various sampling points on the river.

Because of anomalous results, and in order to evaluate the possibility of radioactive waste entering the Clinch River at points other than the monitored release point at the White Oak Dam gate structure, the following factors were investigated: leakage through White Oak Dam, waste disposal practices at the Tower Shielding Facility, and surface drainage entering the Clinch River from other possible sources of contamination.

The data collected in the investigations indicate little possibility of introduction of radioactive contamination, other than fallout, through surface drainage into the Clinch River at any point in the Oak Ridge Reservation except White Oak Dam and the ORGDP area. Drainage from ORGDP is either within the security fence or is affected by Clinch River waters and thus could not be readily checked.

---

[1]Temporary summer employee.

[2]U.S. Geological Survey.

[3]U.S. Atomic Energy Commission.

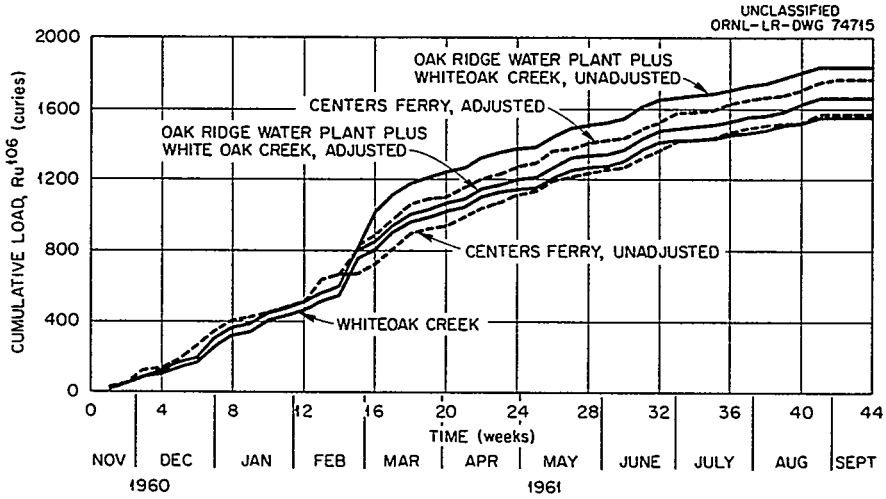

Fig. 4.1. Cumulative Load of Ru^{106} in Clinch River System.

However, it is known that gross quantities of fission products are not handled at ORGDP.

Network water sampling, described in the 1961 annual progress report,[4] was discontinued on November 30, 1962, after approximately two years' data had been accumulated. Some of these sampling stations are being modified for use in measuring changes in dilution and flow characteristics of the Clinch River due to the impending operation of Melton Hill Dam for electric power production.

Statistical analysis of the stable-chemical data of Clinch and Tennessee River waters is in progress. Variations in the concentration of each chemical constituent, and correlation and regression coefficients for constituent pairs are being obtained by use of a computer program. Preliminary results indicate that iron, manganese, and much of the silica present in the river waters occur as solids, rather than in solution.

BOTTOM SEDIMENT STUDIES

Core Sampling

Undisturbed cores of bottom sediments at 15 cross sections on the Clinch River, two cross sections on the Emory River, and two cross sections on Poplar Creek (Fig. 4.2) were obtained during June, July, and August 1962 by the use of the Swedish foil sampler. The sampler utilizes a piston and thin steel strips (foils) to prevent friction between the sample tube and the sediment while coring is proceeding, and to prevent loss of core while the core tube is being raised to the surface.

Core recovery was between 80 and 100% at sampling points where radioactivity is believed to be present throughout the full thickness of the penetrated sediment. Recovery of fine sediment was aided by the on-the-job development of a sampling shoe containing a basket core retainer. Coarse gravel was sampled with dredge samplers, and small pockets of very fine sediment were sampled by hand with the aid of SCUBA equipment.

Variation in gross radioactivity with depth in each core is being measured with a special core scanner. The core scanner consists of a 3 × 3 in. NaI scintillation crystal and matched phototube enclosed in a 4-in.-thick lead shield with a 2 × 2 × 2 in. collimator slit, and a hoist which automatically moves the core vertically past the collimator in 2-in. increments (Fig. 4.3). By putting the phototube output through various associated instruments, either the gross gamma activity or a gamma-ray spectrum of the core segment being examined can be obtained. The slit height of the collimator and the incremental movement of the hoist can be adjusted.

[4]E. G. Struxness *et al.*, *Health Phys. Div. Ann. Progr. Rept. July 31, 1961*, ORNL-3189, p 15.

UNCLASSIFIED
ORNL-LR-DWG 31563A

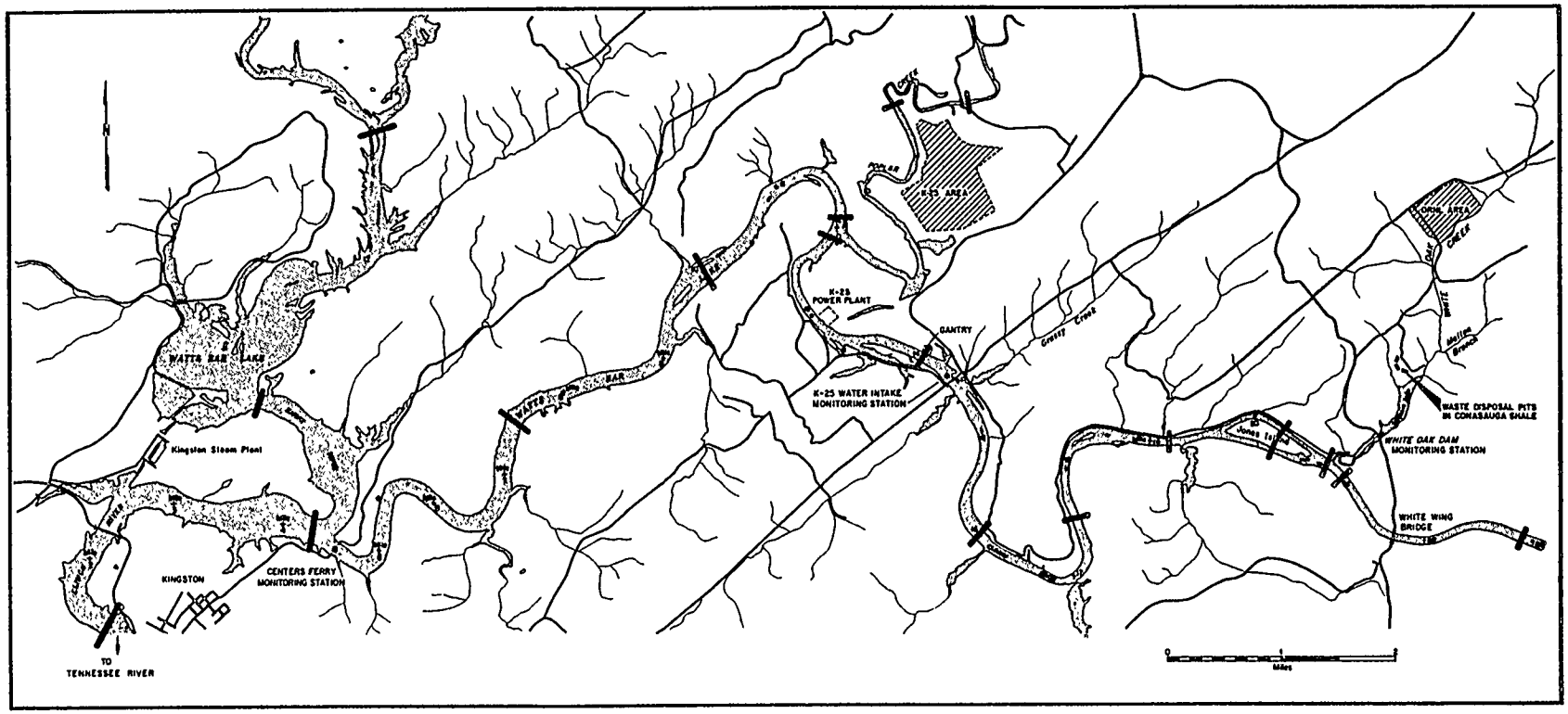

Fig. 4.2. Sediment Core Sampling Stations.

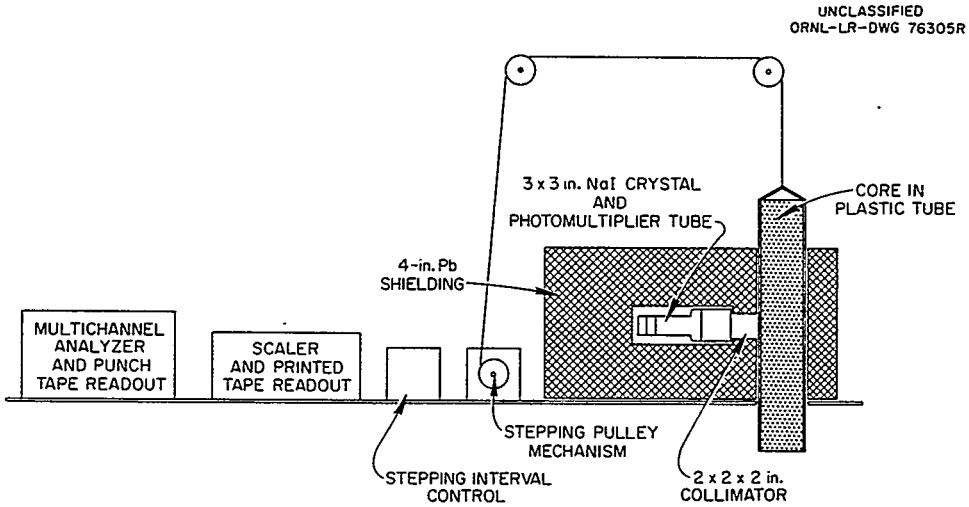

Fig. 4.3. Schematic of Core Counting Equipment.

Calibration of the core scanner was accomplished by determining the gross gamma count rate produced by a plane source of radioactivity at various distances below the center line of the collimator slit. The core scanner measures a segment of core longer than the desired 2 in. A computer program was developed which corrects each "observed" incremental gross gamma activity count for collimation angle. Figure 4.4 shows uncorrected and corrected gross radioactivity graphs for hole 5, CRM 1.3 (Clinch River Mile). The graphs demonstrate the vertical variations in gross radioactivity within the core and indicate that the segment sampled included the entire thickness of the zone of radioactivity. Figure 4.5 shows the results of coring and gross gamma radioactivity determinations for the section at CRM 1.3.

After gross gamma scanning of the cores has been completed, the vertical distribution of specific radionuclides in selected cores will be determined by routing the output of the core scanner through a 512-channel analyzer. All cores will then be dissected, and the radionuclide content of composites of the cores in each cross section will be determined in order to calculate the total radionuclide content of Clinch River bottom sediments. Various physical and chemical tests will be performed on the composite samples and on selected cores or core segments in order to better understand the processes by which the radionuclides become incorporated with the bottom sediments.

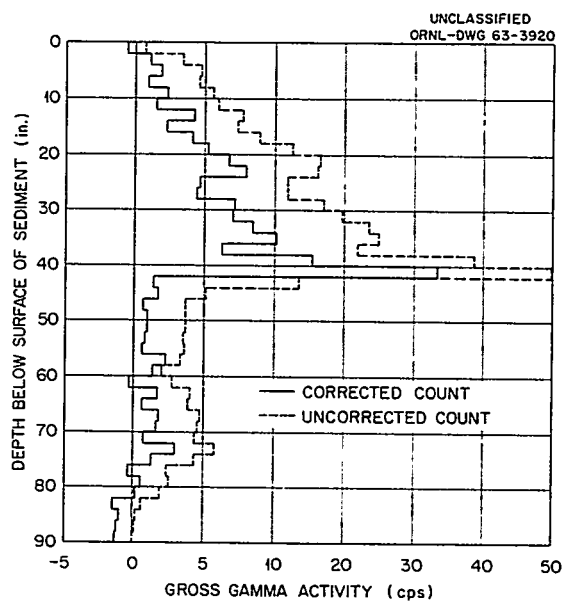

Fig. 4.4. Distribution of Radioactivity in Core 5, CRM 1.3.

Distribution of Radionuclides in Bottom Sediments

In a study of the distribution of radionuclides in bottom sediments in the Clinch and Tennessee Rivers, the longitudinal distribution patterns for several radionuclides were found to be similar. The longitudinal distributions of seven radionuclides were compared by means of regression

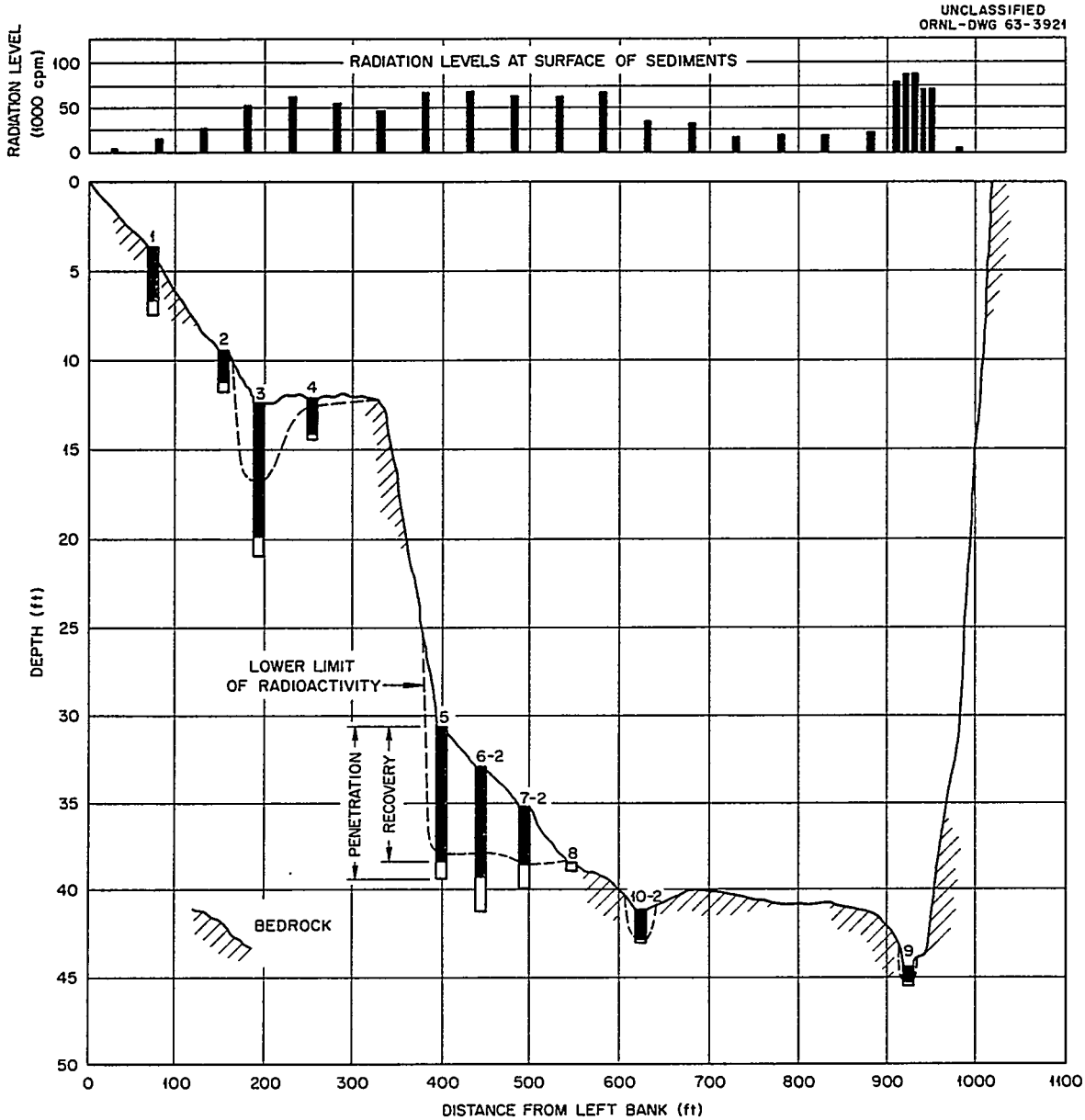

Fig. 4.5. Shape of Section and Radiation Levels at CRM 1.3.

analysis techniques; the results are illustrated in Fig. 4.6. Data used for the regression analysis were obtained by personnel of the ORNL Applied Health Physics Section during the 1961 annual survey of radioactivity in bottom sediments from White Oak Creek to Kentucky Dam.

The slope of the curves is nearly the same for the logarithmic correlation of Cs^{137} to Ru^{106}, the trivalent rare earths (excluding Ce^{144} and including Y^{90}), and Co^{60}; and the indices of correlations for these curves are extremely good also. Thus the results shown in the figure suggest that similar mechanisms control the longitudinal distribution of these particular radionuclides.

The observed rates of decrease in concentration of cesium, ruthenium, cobalt, and the rare earths

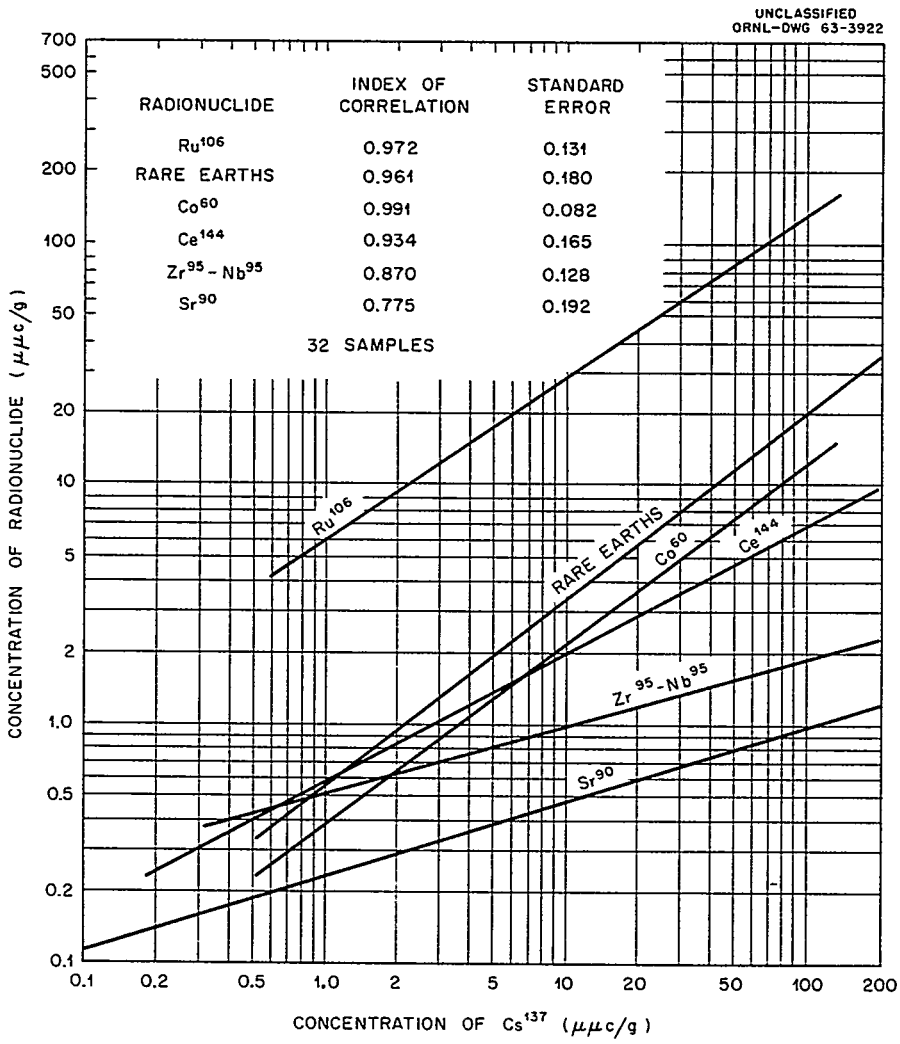

Fig. 4.6. Correlations Showing Similarity in the Longitudinal Distribution of Radionuclides in the Bottom Sediments of the Clinch and Tennessee Rivers.

with distance downstream from White Oak Creek are much greater than rates calculated on the basis of flow dilution alone. This lack of relationship between concentration and flow dilution and the similar longitudinal distribution pattern of the radionuclides suggest that the mechanism controlling their longitudinal distribution pattern may be a sedimentation process, rather than a chemical process such as equilibration between radionuclide concentrations in the sediments and radionuclide concentrations in the water.

The slope of the curves for Zr^{95}-Nb^{95} and for Sr^{90} in Fig. 4.6 is less than that for cobalt, ruthenium, or the rare earths, indicating that somewhat different mechanisms may be controlling the longitudinal distribution of zirconium-niobium and strontium in the bottom sediments.

The good correlations indicate that the longitudinal distribution in the bottom sediments of several radionuclides may be determined on the basis of the distribution of one or two of those radionuclides.

Calcite Precipitation in the Clinch River

The formation of calcite coating on metal objects submerged in the Clinch River for periods of several months has led to the assumption that precipitation of calcite from the river water may

be a common phenomenon. The presence of fine-grained calcium carbonate in Clinch River bottom sediments has been inferred from the results of determinations of the exchangeable cation content of five samples of bottom sediment. The amount of "exchangeable" calcium in all five samples was greater than the total cation exchange capacities of the sediment samples. These anomalous results, together with high pH values reported for the same sediment samples, appear to indicate that calcium carbonate in the sediment was dissolved during the removal of the "exchangeable" cations from the sediment and that this factor produced the unreasonably high values for "exchangeable" calcium in the sediment.

A calcite coating on a metal current meter which was recovered after being submerged 14 months at CRM 19.1 contained 124 $\mu\mu c$ of $Ru^{103-106}$ and 10 $\mu\mu c$ of Sr^{89-90} per gram (dry weight). Such material, if present in Clinch River bottom sediments, would add materially to the Ru^{106} and Sr^{90} content of the sediment. Additional tests for calcite precipitation in the Clinch River have been planned.

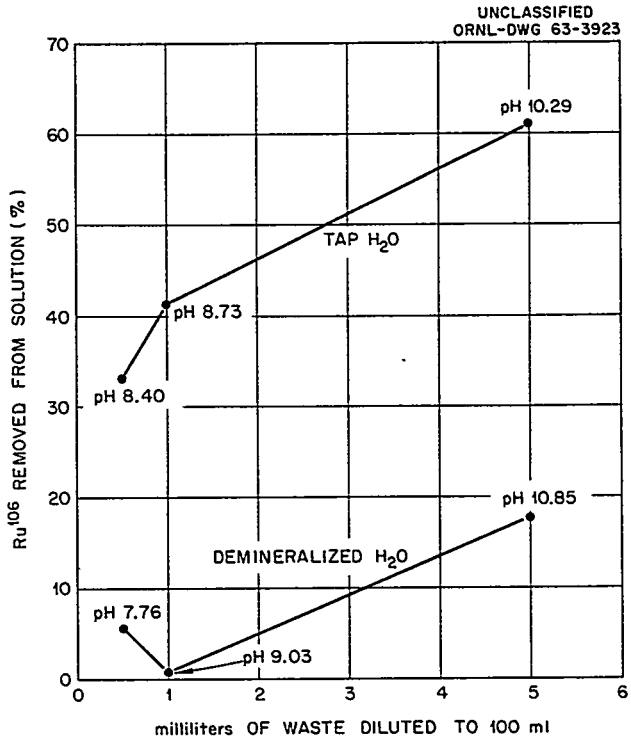

Fig. 4.7. Removal of Waste Ruthenium in Tap and Demineralized Water with Different Dilution Ratios.

Behavior of Waste Ruthenium in Water

When radioactive waste solution from the ORNL waste-tank farm is diluted 1:19 with tap water, approximately 60% of the ruthenium is removed from solution (Fig. 4.7). Further dilutions of 1:99 and 1:199 show a reduction in the percentage of ruthenium removed. Diluting the waste solution with demineralized water resulted in less than 20% removal of ruthenium. Dilution of the waste resulted in a decrease in pH as expected; with 1:19 dilution the pH was 10.3 in tap water and 10.8 in demineralized water. With 1:199 dilution the pH was 8.4 in tap water and 7.8 in demineralized water.

Observations revealed that a fine colloidal precipitate was formed in the solution containing tap water. From the known analysis of tap water, it was concluded that the precipitate was $CaCO_3$. Studies are in progress to identify and characterize the precipitate.

The addition of Clinch River sediment to the diluted waste (1:19) with tap water made no difference in the percentage removal of ruthenium; but when sediment was added to waste identically diluted with demineralized water, approximately 25% was removed. The sediment in contact with the waste solution diluted with tap water was washed free of excess solution and kept in contact with fresh tap water. After 144 hr, approximately 20% of the ruthenium was found in the liquid phase; the pH of the suspension was 8.3. When the pH was increased to 12, the liquid phase contained 28% within 16 hr; but 100% of the ruthenium was in the liquid phase when the pH was reduced to 2. This observation does not confirm earlier tests performed on Clinch River sediments. In the earlier leaching tests, approximately 45% of the ruthenium was removed at pH 12 and less than 5% at pH 2. Further tests are being carried out on these systems including length of sediment-ruthenium contact time as a variable in order to understand the nature of the reaction in natural systems.

HYDROLOGY

Melton Hill Dam Construction

Construction of Melton Hill Dam is essentially complete except for the installation of the two turbines in the powerhouse. The installation of turbines has been delayed, and the first generating unit is scheduled to begin operation late in 1963. Flow over the spillway at the dam was discontinued in May 1963, during which time the reservoir was filled. Water from Melton Hill Reservoir is presently being released through appurtenances of the navigation lock.

As a result of power generation at Melton Hill Dam, the flow duration in the Clinch River at White Oak Creek may vary from 0 to 24 hr each day, and flows in the Clinch River below the dam will almost instantaneously change from zero to several thousand cubic feet per second.

Some of the radioactivity released from White Oak Lake will accumulate in Clinch River waters in the vicinity of White Oak Creek during no-flow periods. During periods of power releases from Melton Hill Reservoir, this radioactive reservoir will be swept downstream in a cloud.

Dispersion Studies

A laboratory study of the dispersion in the lower Clinch River of the radioactive cloud due to power waves is being conducted in order to acquire immediate qualitative information on the effects of power waves on dispersion of radionuclides and to develop numerical methods of describing the diffusion process. Salt-tracer tests were made in a flume operated by the U.S. Geological Survey at the Hydraulics Laboratory, National Bureau of Standards, Washington, D.C.

The discharge, bed slope of the flume, water depth for no-flow conditions, and bed roughness were adjusted to conform, at distorted scales, to anticipated conditions in the Clinch River. Horizontal distortions were on the order of 250:1, and vertical distortions were on the order of 20:1. A power wave was created by suddenly diverting the established discharge from a by-pass channel to the test channel. The variation of salt-tracer concentration with time was measured continuously at several points in the flume, using recording conductivity bridges.

The variation of concentration with time for one complete test is shown in Fig. 4.8. Results from

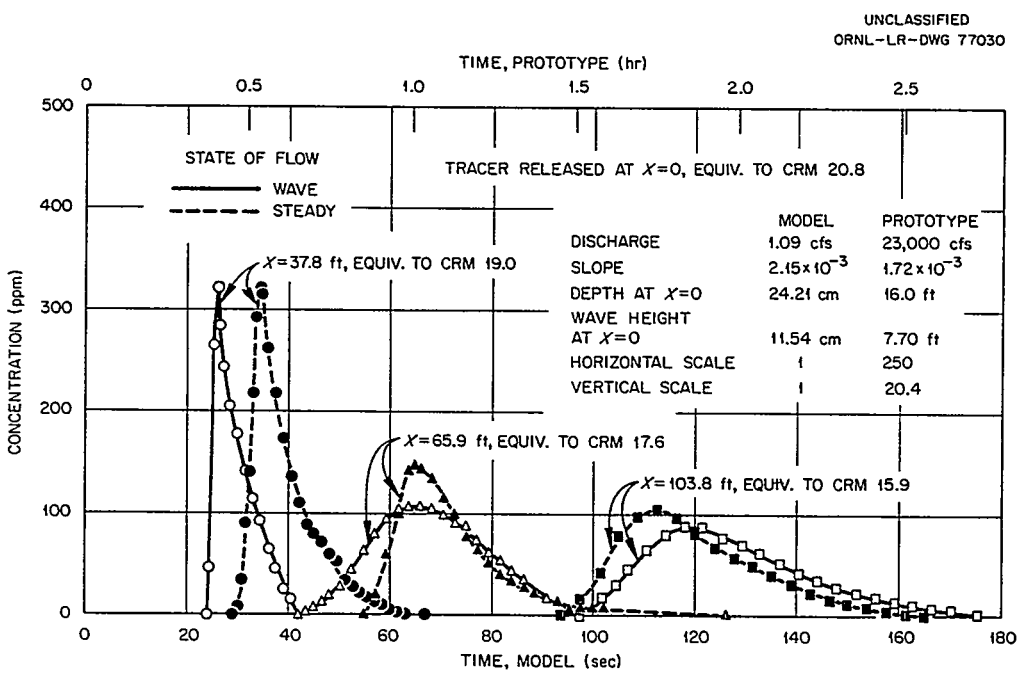

Fig. 4.8. Variation of Tracer Concentration with Time and Distance.

this test indicate that the dispersion process due to power releases is not greatly different from that for steady flow, especially at sections sufficiently removed from the tracer injection section. At equivalent CRM 15.9, about 1½ miles upstream from the water plant intake for ORGDP, the peak concentrations and the durations of the tracer cloud for the wave and steady-flow conditions were about the same.

As a check on model similitude, wave height and travel time for the model were compared with height and times predicted by TVA for the Clinch River. For flow conditions tested, the equivalent wave height was 7.72 ft, as compared with the predicted height in the river of 7.70 ft. The equivalent travel time for the model was about 3% greater than the time interpolated from information furnished by TVA.

In further work the general diffusion equation will be solved by use of numerical techniques. Analytical solutions of the diffusion equation are available if the flow is uniform and steady. However, for the case of power waves in the Clinch River, flow is not steady or uniform.

By determining diffusion coefficients for steady flow, the variation of contaminant concentration, with time and in space, during periods of power releases may be calculated by applying numerical methods to the general diffusion equation.

SAFETY ANALYSIS

Knowledge of water utilization downstream on the Clinch River indicated that the important avenues of exposure resulting from discharge of radioactive wastes may include: (1) consumption of contaminated water and fish, (2) exposure to contaminated water and bottom sediments during recreational and industrial use of the water, (3) consumption of agricultural produce that may be irrigated with river water, and (4) exposure to buildup of radionuclides in sludge and deposits in water systems utilizing river water.

Radionuclides Released and Concentrations in the Rivers

Virtually all the radioactivity emanating from the Laboratory and reaching the Clinch River passes through White Oak Creek. Total curies per year were calculated (Table 4.1) for each radionuclide present in measurable amounts and released through

Table 4.1. Yearly Discharges of Radionuclides to Clinch River (Curies)[a]

Year	Gross Beta	Cs^{137}	Ru^{106}	Sr^{90}	Total Rare Earth Less Ce	Ce^{144}	Zr^{95}	Nb^{95}	I^{131}	Co^{60}
1949	718	77	110	150	77	18	180	22	77	
1950	191	19	23	38	30		15	42	19	
1951	101	20	18	29	11		4.5	2.2	18	
1952	214	9.9	15	72	26	23	19	18	20	
1953	304	6.4	26	130	110	6.7	7.6	3.6	2.1	
1954	384	22	11	140	160	24	14	9.2	3.5	
1955	437	63	31	93	150	85	5.2	5.7	7.0	6.6
1956	582	170	29	100	140	59	12	15	3.5	46
1957	397	89	60	83	110	13	23	7.1	1.2	4.8
1958	544	55	42	150	240	30	6.0	6.0	8.2	8.7
1959	937	76	520	60	94	48	27	30	0.5	77
1960	2190	31	1900	28	48	27	38	45	5.3	72
1961	2230	15	2000	22	24	4.2	20	70	3.7	31

[a]Values calculated from data supplied by Applied Health Physics Section.

White Oak Creek. Estimates of the mean annual concentrations of radionuclides in the Clinch and Tennessee Rivers are based on dilution ratios and the fact that the effluent of White Oak Creek is completely mixed with the river after about 3 to 5 miles of flow downstream from the mouth of the creek. The concentration values derived in this way are conservative, since no allowance is made for decreases of the radioactivity in the water, for example, by removal and deposit in bottom sediments.

The following were selected for the evaluation analyses: CRM 14.5 (6.3 miles downstream from the White Oak Creek discharge at CRM 20.8), CRM 2.6 (downstream from mouth of Emory River and near Kingston Steam Plant), TRM (Tennessee River Mile) 529.9 (Watts Bar Dam), and TRM 465.5 (at Chattanooga water supply intake and 5.5 miles downstream from Chickamauga Dam). At CRM 14.5 and in the vicinity of CRM 2.6, water supplies taken from the river are used by ORGDP and the Kingston Steam Plant for sanitary and industrial purposes. There are downstream recreational areas at the Kingston waterfront, at Watts Bar Dam, and at numerous places along Watts Bar Reservoir. There are large recreational areas along Chickamauga Reservoir, notably just above Chickamauga Dam (TRM 471.0). The first large population center (Chattanooga, Tennessee) is located a few miles downstream from Chickamauga Dam (TRM 471.0) and is served by a public water supply taken from the Tennessee River at TRM 465.3. The quantity of water passing each location annually was calculated from average flow values (Table 4.2). The average concentration of radionuclides at each location was determined from the curies released and the total water flow for each year.

Table 4.2. Mean Annual Flow in Clinch and Tennessee Rivers[a]

Year	CRM 14.5[b]	CRM 2.6[b]	TRM 529.9[c]	TRM 471.0[c]
1943	5,310	6,620	26,130	32,330
1944	4,800	6,870	25,690	32,290
1945	4,940	7,020	26,490	32,270
1946	5,150	6,880	29,100	38,540
1947	4,420	5,720	24,040	31,190
1948	4,290	6,480	26,370	34,360
1949	5,460	7,560	33,300	43,630
1950	6,630	9,360	34,240	44,030
1951	6,170	8,760	28,070	36,560
1952	4,570	5,770	22,470	29,770
1953	4,340	5,710	22,160	28,130
1954	2,990	4,730	20,480	26,050
1955	4,850	6,610	23,790	30,530
1956	5,040	7,340	24,750	30,990
1957	6,350	9,300	36,310	45,250
1958	5,560	6,880	27,780	34,330
1959	3,490	5,260	23,760	29,000
1960	4,460	6,200	25,150	31,010
1961	4,780	7,110	29,520	37,430

[a]In cubic feet per second.

[b]Estimated on the basis of discharge records of the Clinch River at Scarboro, Tenn., and Emory River at Oakdale, Tenn.

[c]According to Tennessee Valley Authority records.

Critical Organs Considered

Based on the type and concentration of radionuclides released, the maximum permissible concentration in water, $(MPC)_w$, for these radionuclides, the potentially significant avenues of exposures, and the type of individual under consideration, the radiation dose was computed for bone, gastrointestinal tract (GI), thyroid, gonads, and total body.

Dose from Drinking Water

The fraction of $(MPC)_w$ attained for the case of internal dose was calculated according to the recommendation of the ICRP.[5] All $(MPC)_w$ values used for data relating to the Clinch River are taken as $\frac{1}{10}$ the occupational $(MPC)_w$ values for continuous exposure. To obtain $(MPC)_w$ values relating to the Tennessee River, the $(MPC)_w$ for continuous occupational exposure has been reduced by a factor of $\frac{1}{100}$ for whole body as the critical organ and by $\frac{1}{30}$ with thyroid, bone, and GI tract as the critical organs.

The fraction of the $(MPC)_w$ attained by drinking water at CRM 14.5 and TRM 465.5 is shown in Table 4.3. For the particular mixture of radionuclides in the river water, estimated exposure to the bone constitutes a greater fraction of the maximum permissible limit than the calculated exposure to the other body organs. This is attributable to the Sr^{90} released. The largest fraction of the $(MPC)_w$ attained was 0.51, in 1954. The increase in internal dose to the GI tract in 1960 and 1961 is due to the increased release of Ru^{106}.

Because the MPC's which enter into the calculations have been estimated on the basis of "standard man," the dose really represents only that which would be received by a person of physical characteristics and habits resembling standard man. Very little is known at present about differences in metabolic rates or processes of children and adults as they relate to important radionuclides. However, dose correction factors can be estimated which take into account differences due to intake and organ size. With data

[5]Report of Committee II on Permissible Dose for Internal Radiation, *International Commission on Radiological Protection, Publication 2*, Pergamon, London, 1959.

Table 4.3. Fraction of $(MPC)_w$ from Clinch and Tennessee Rivers

Year	CRM 14.5				TRM 465.5			
	Bone	GI Tract	Total Body	Thyroid	Bone	GI Tract	Total Body	Thyroid
1949	0.30	0.0043	0.076	0.021	0.11	0.0016	0.094	0.0077
1950	0.065	0.0022	0.016	0.0043	0.029	0.0010	0.025	0.0021
1951	0.052	0.0017	0.013	0.0038	0.026	0.00087	0.022	0.0019
1952	0.18	0.0015	0.044	0.0098	0.081	0.00069	0.068	0.0045
1953	0.35	0.0018	0.087	0.015	0.16	0.00053	0.13	0.0053
1954	0.51	0.0032	0.13	0.022	0.17	0.0011	0.15	0.0074
1955	0.22	0.0037	0.055	0.0099	0.10	0.0019	0.086	0.0047
1956	0.23	0.0042	0.060	0.010	0.11	0.0020	0.097	0.0051
1957	0.15	0.0024	0.037	0.0063	0.062	0.00099	0.052	0.0027
1958	0.30	0.0031	0.075	0.013	0.14	0.0015	0.12	0.0077
1959	0.20	0.021	0.050	0.0084	0.070	0.0075	0.060	0.0030
1960	0.070	0.050	0.018	0.0037	0.030	0.021	0.026	0.0016
1961	0.053	0.048	0.014	0.0027	0.020	0.019	0.017	0.0010

taken from Blackfair, Straub, and others,[6–10] Fig. 4.9 shows the dose correction factors for the skeleton of the male and female. The base line represents the ratio of intake to organ weight for standard man. It is apparent that there is a significant correction to be made for infants and young children when dose to the skeleton is in question.

A code was developed for Data Control 1604 that permits machine computation of critical organ burdens and dose received. A final dose evaluation, taking account of all known factors that might affect the result, is not available at this time. The code was run under the following assumptions:

1. Individuals of ages 1 through 18 and standard man drink untreated water from the Clinch River at CRM 14.5 (the neighborhood of the controlled area of ORNL). They continue to drink water from this source through 1961, after which time water is obtained from an uncontaminated source.
2. Intake and skeleton may vary with age according to data in Fig. 4.9. Thus all water taken into the body in food or other form is assumed equally contaminated.
3. The percent of total activity due to Sr^{90} in 1944–48 is the same as that for the period of 1949–58.
4. All other factors that might affect the results are negligible.

The relative annual dose rates were computed and are shown in Fig. 4.10, normalized to the maximum individual dose found; that is, the dose to the 14-yr-old. The differences among dose rates are attributed to differences in intake and size of the skeleton. Unquestionably, refinement of these preliminary calculations is necessary before a dose evaluation can be made.

Immersion in Contaminated Water

Due to the presence of radionuclides, the river will act as a source of radiation to persons engaged in swimming, boating, fishing, and water skiing. Since direct measurements of immersion dose rate are unavailable, it is necessary to calculate the dose rate by considering the radionuclide composition of the water.

The immersion dose calculation assumes the body is at the center of a sphere and receives equal quantities of radiation from all directions.

[6]K. D. Blackfair, *Report of the Committee on Growth and Development of the Child, Part II, Anatomy and Physiology, White House Conference on Child Health and Protection Called by President Hoover*, The Century Co., New York, 1933.

[7]C. P. Straub, *U.S. Public Health Service, Robert A. Taft Sanitary Engineering Center, Cincinnati, Ohio*, unpublished correspondence.

[8]E. C. Albritton, *Standard Values in Nutrition and Metabolism*, W. B. Saunders Co., 1954.

[9]Department de la Protection Sanitaire Contrat de L'association CEA/Euratom, "Données Biologiques de Base pour l'étude des Niveaux de Contamination Applicables aux Enfants" (February 1962), supplied to the ICRP by Dr. Jammet.

[10]W. S. Spector (ed.), *Handbook of Biological Data*, Wright Air Development Center, October 1956.

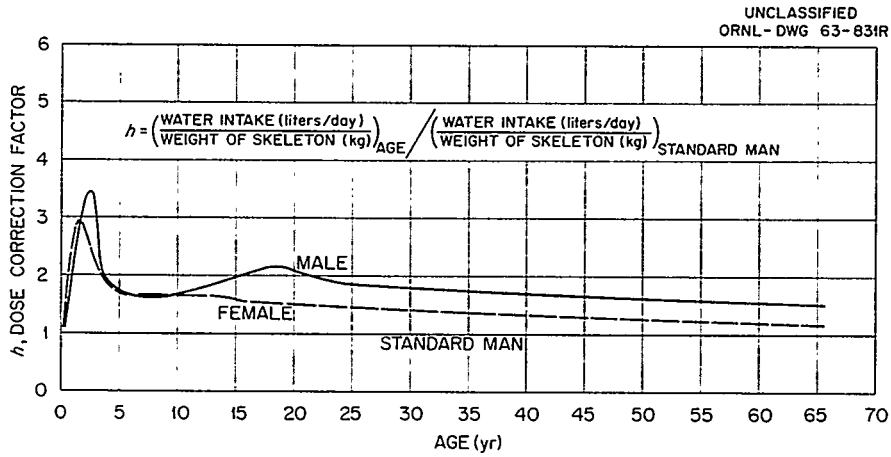

Fig. 4.9. Dose Correction Factor for Skeleton.

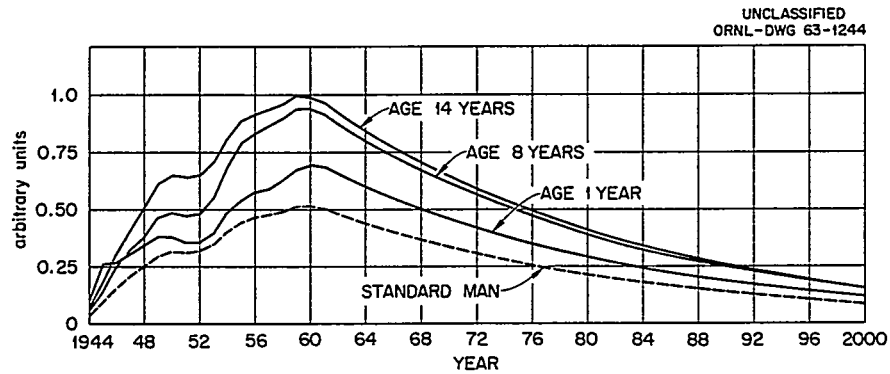

Fig. 4.10. Dose to Skeleton of Males.

The external exposure from beta radiation may be calculated by means of an equation recommended by Morgan.[11]

With certain reasonable assumptions, this expression in rads per day is simplified to

$$\text{beta dose rate} = 51.2\ QE_i\ , \qquad (1)$$

where

$Q = \mu c/g$ of water,

E_i = effective absorbed energy per disintegration.

An empirical formula was used to estimate the average effective absorbed energy of a beta disintegration:[5]

$$E_i = 0.33\ E_m\ f\left(1 - \frac{\sqrt{z}}{50}\right)\left(1 + \frac{\sqrt{E_m}}{4}\right), \qquad (2)$$

where

E_m = maximum energy of type considered,

f = fraction of disintegrations at a particular energy,

z = atomic number.

The penetration distance in water is about 1 cm for the most energetic beta particles from the radionuclides involved. Therefore the beta radiation at the surface of a body immersed in the contaminated water is effectively one-half of that calculated by Eq. (1). The external exposure from gamma radiation may be calculated by means of a similar formula,[11] for which the simplified expression in units of rads per day is

$$\text{gamma dose rate} = 51.2\ Q\ E_m\ f\ , \qquad (3)$$

in which the terms Q, E_m, and f are the same as in Eqs. (1) and (2). In each instance where some latitude is allowed in the assumptions, a conservative approach is taken; therefore the computed dose rates would be expected to be overestimated.

Where the water contains a mixture of radionuclides, it is necessary to calculate the dose rate associated with each radionuclide. The total dose rate is simply the sum of the individual dose rates. Decay schemes presented by Blomeke and Todd[12] are used in the calculations. The dose-rate values for beta and gamma, respectively, are one-half the beta dose rate [Eq. (1)] and the total gamma dose rate [Eq. (3)].

A maximum dose rate of 0.027 millirad per day of exposure at CRM 14.5 (1960) is calculated. The dose rate is a function of nuclide type and concentration. Until 1958, the largest fraction of beta dose was associated with Sr^{90}, and the largest gamma dose was generally due to Cs^{137}. In recent years, Ru^{106} has accounted for about 79% of the total immersion dose.

[11] K. Z. Morgan, *Health Control and Nuclear Research, External Exposure*, unpublished.

[12] J. O. Blomeke and M. F. Todd, *Uranium-235 Fission-Product Production as a Function of Thermal Neutron Flux, Irradiation Time, and Decay Time: 1. Atomic Concentrations and Gross Totals*, ORNL-2127 (Aug. 19, 1957).

Contaminated Bottom Sediments

Radionuclides associated with solids that have settled to the river bottom can be expected to contribute to the total radiation dose received by man. Although earlier calculations assumed complete dilution of fission products in the river, annual surveys made by the ORNL Applied Health Physics Section have shown that some of the radionuclides are retained by the bottom sediments.[13] Average concentrations of specific radionuclides in bottom sediments were calculated by averaging all values for the entire study reach of the Clinch River and of the Tennessee River. The principal radionuclides associated with these sediments were found to be Cs^{137}, Ce^{144}, Co^{60}, and, more recently, Ru^{106}. Major changes in the radioactivity of the bottom deposits were found, but the details of sediment transport must be delineated before conclusions can be drawn about observed changes in radionuclide concentrations.

The Flounder is used principally to furnish qualitative information on the buildup of gamma-emitting radionuclides in sediments. Construction of the device makes it insensitive to beta radiation. Although the Flounder is calibrated routinely with a sealed radium source (as a stability or sensitivity check), the complex spectrum of gamma rays from both the contaminated sediments and the radium source prevents a direct determination of exposure dose by use of this instrument. Exposure dose can be estimated, but the limitations of such data must be recognized.

In a general way the measurements in the Clinch River reflect the quantity of Cs^{137} and Co^{60} released each year. Maximum readings in the Clinch River (usually at CRM 8.3) were larger than the average readings by a factor of 1.9 ± 0.09; similarly, the ratio in the Tennessee River was 1.8 ± 0.2. For the purpose of estimating the radiation dose to man, calculations of dose were made by using the average radionuclide composition of the sediments. It was assumed that this average composition of the sediments was distributed uniformly in an infinite source. To assume an infinite source containing the maximum concentration of radionuclides observed seems overly conservative. Further, it was assumed that the individual would be exposed to one-half the submersion dose of beta particles and to one-half the submersion dose of gamma emission (i.e., from one-half a sphere). Such an assumption is reasonable, since the individual receiving the dose is likely to be standing on or floating above the contaminated sediments. Normally, only the feet would be subjected to the total beta and gamma dose rate.

Calculated dose rates from bottom sediments in the Clinch River and Tennessee River are determined by assuming one-half the beta dose rate calculated from Eq. (1) and one-half the gamma dose rate calculated from Eq. (3). Since the source is not infinite in extent, the calculated values give a larger estimated dose rate than that actually available. Accordingly, the largest bottom sediment dose rate of 12 millirads per day of exposure would have occurred in 1959, and would have been divided as 0.4 beta and 0.6 gamma radiation. The percentage contribution of specific radionuclides to the beta and gamma dose rates shows that the total rare earths, Cs^{137}, and, more recently, Ru^{106} are the principal contributors to beta dose rates and that Co^{60} and Cs^{137} account for the largest fraction of gamma dose rates.

Since bottom sediments are usually underwater, the gamma dose rate to the gonads of an individual standing on the river bottom would be reduced by attenuation. An average attenuation coefficient for water was calculated by weighing both the fraction of time a photon of a given energy was emitted by a particular radionuclide and the fraction each radionuclide contributed to the total loading of the bottom sediments. The estimated maximum gamma dose rate, after attenuation through 3 ft of water, was 0.39 millirad per day of exposure.

The other avenues of potential exposure previously mentioned are being investigated. Although irrigation is not practiced along the Clinch River and is of almost negligible extent along the Tennessee River, calculations have been made of radionuclide transfer from soil to crop to man for hypothetical situations. Laboratory and field experiments are being planned in order to elucidate this potential vector of contamination. No apparent difference exists in external radiation in water treatment plants using Clinch River water from plants above and below the confluence of White Oak Creek and the Clinch River. A large fish-sampling program continues and, accompanied by results of a survey of fish consumption, will allow estimates to be made of dose due to contaminated fish. Whenever opportunity permits, direct measurements of dose received or of dose rate will be made.

[13] W. D. Cottrell, *Radioactivity in Silt of the Clinch and Tennessee Rivers*, ORNL-2847 (Nov. 18, 1959).

5. Study of White Oak Creek Drainage Basin

T. F. Lomenick W. M. McMaster[1]
H. J. Wyrick R. M. Richardson[1]
D. A. Gardiner[2]

QUANTITY, DISTRIBUTION, AND TRANSPORT OF RADIONUCLIDES IN THE BED OF FORMER WHITE OAK LAKE

From 1943 to 1955, White Oak Lake served as a final settling basin for low-level radioactive wastes discharged from the Laboratory. The temporary holdup provided by the impoundment afforded some dilution and a period for the decay of short-lived radionuclides before release to the Clinch River. It also allowed the deposition and accumulation of contaminated sediments. In 1955 the lake was drained, leaving behind approximately 1,000,000 ft^3 of contaminated lacustrine deposits.[3]

In order to determine the quantity, type, and distribution of radionuclides presently in the lake bed and to aid in defining the migration of these products, a series of 250 core samples were taken within the area. A map of White Oak Lake bed showing the sample locations is presented in Fig. 5.1. The lake bed was laid out in a 50-ft-square grid, with sample locations being chosen by use of a table of random numbers. The method of allocating these points is optimum with respect to the area of sections of similar radioactivity (as determined by data collected previously) and with respect to the variability of the previously collected data. Owing to the high cost of strontium and total-rare-earth analyses as compared to gamma identification, only a limited number of the cores and their segmented sections were analyzed for these nuclides.

A 2-in.-diam thin-walled Shelby tube sampler was used to obtain core samples in the lake bed. The instrument was driven into the earth and recovered manually. Since previous work indicated that practically all the contamination was associated with the upper few feet of soil,[4] all cores were taken to a depth of 2 ft. The samples were sliced and segmented into increments of 0 to 6, 6 to 12, 12 to 18, and 18 to 24 in. Approximately 10 g from each increment was oven dried, weighed, and scanned using a Packard automatic gamma counting system which consists of a spectrometer with well-type scintillation detector, automatic sample changer and control unit, digital printer, and tape punch. Concentrations of Ru^{106}, Cs^{137}, and Co^{60} were determined by use of an IBM 7090 computer program for stripping the gamma spectrum. Standard radiochemical procedures were used for strontium and total-rare-earth analyses.

By visual inspection of the recovered cores, a generalized depth of lacustrine sediment in the bed was determined (Fig. 5.2). The sediment is as thick as 19 in. in the lower part of the lake bed near the dam; however, there is a gradual thinning of the layer upstream and, in general, toward the shoreline of the lake.

In general, most of the Cs^{137} is associated with the relatively thin layer of recent lacustrine sediment that covers the lake bed. Thus, in areas near the shoreline, where the sediment is thinnest, the smallest quantities of activity are found. For the first 6 in. of soil (Fig. 5.3), the concentrations of Cs^{137} vary from $<1 \times 10^{-3}$ to 77×10^{-3} μc per gram of dry weight, and the areas of maximum concentrations lie roughly adjacent to the course of White Oak Creek through the bed and in the present impoundment area behind the dam. As shown in Fig. 5.2, the greatest depth of lacustrine sediment in the lake bed is also found in these areas. In the soil section 6 to 12 in. below the surface, Fig. 5.4, the concentrations of Cs^{137} at most of the sample points are much less than those observed in the upper layer of soil. The higher values are restricted to sites where the lake sediment is more than 6 in. deep.

With the exception of a few narrow zones parallel to the creek in the upper part of the bed, the highest concentrations of Sr^{90} are found within the inundated area behind the dam (Fig. 5.5). This would indicate that strontium is presently being removed from the lake water and is accumulating in the bottom sediments. The concentrations of Sr^{90}

[1]U.S. Geological Survey.

[2]Mathematics Division, ORNL.

[3]A. S. Fry, ORNL, memorandum to M. A. Churchill, "Sediment Investigations, White Oak Lake," June 30, 1953.

[4]R. E. Blanco and E. G. Struxness, *Waste Treatment and Disposal Progress Report for June and July 1961*, ORNL TM-15.

UNCLASSIFIED
ORNL-LR-DWG 78674

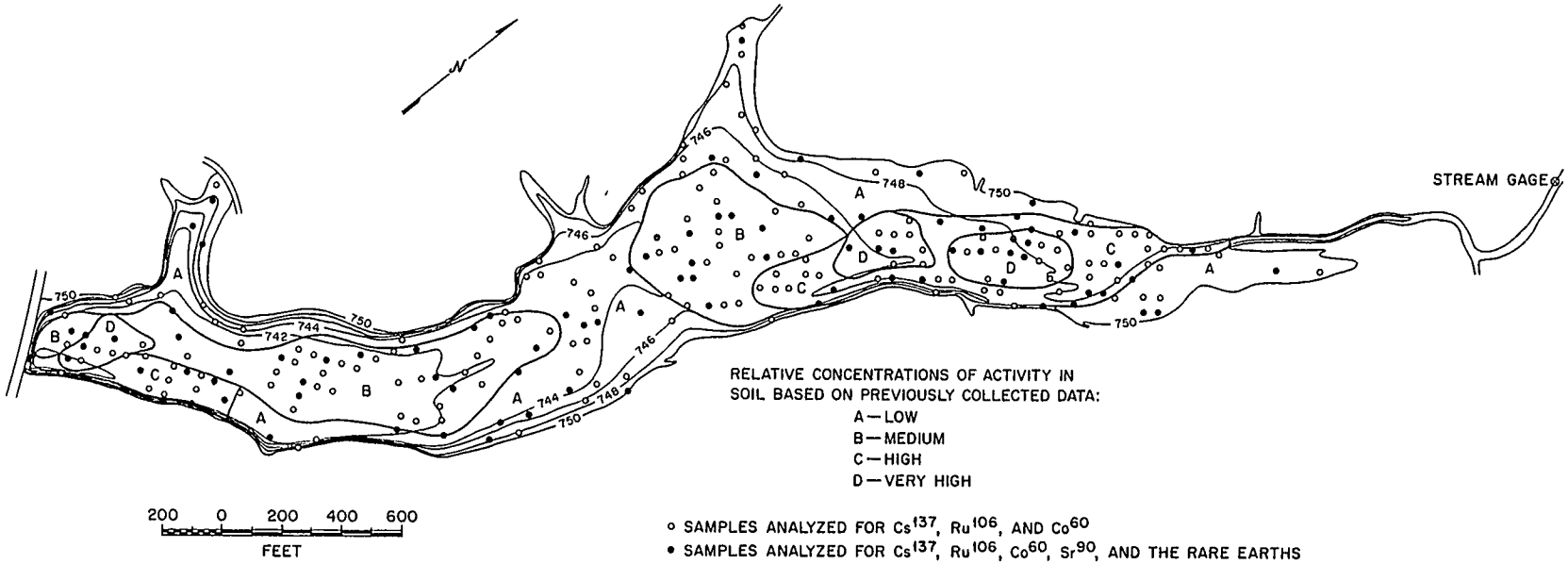

Fig. 5.1. Location of 2-ft Core Samples in the Bed of Former White Oak Lake.

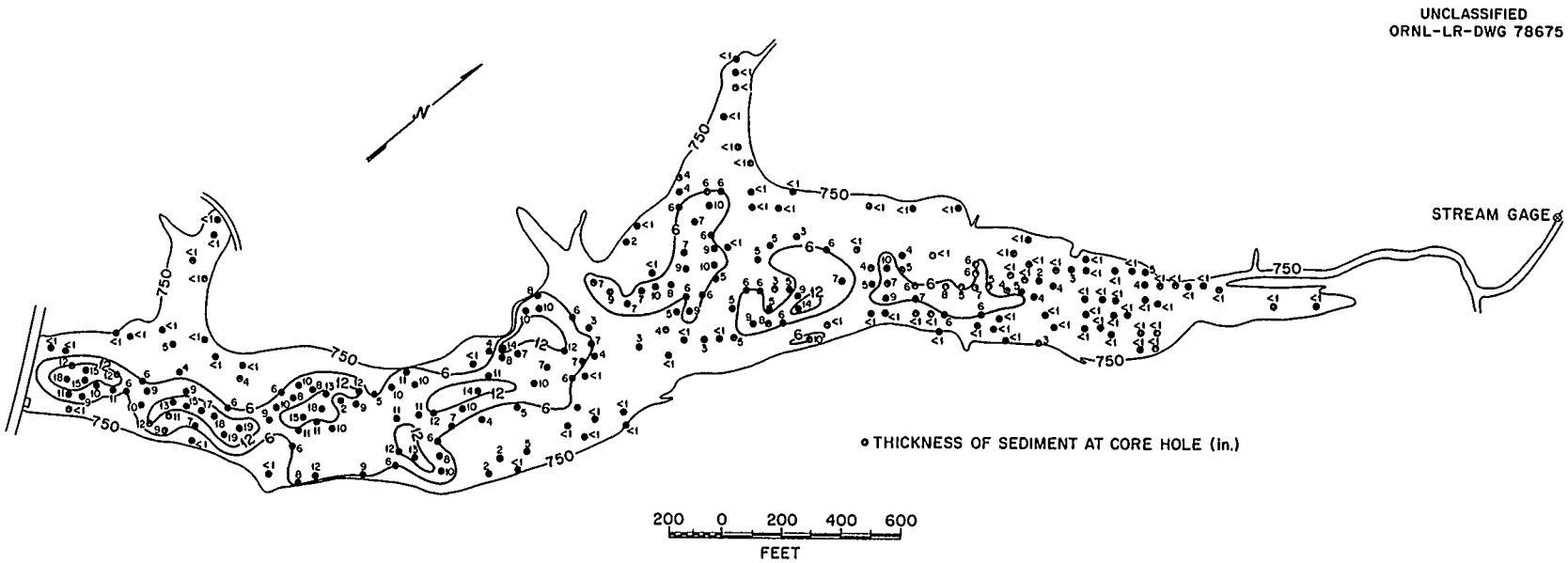

Fig. 5.2. Map of Former White Oak Lake Bed, Showing Thickness of Contaminated Sediment.

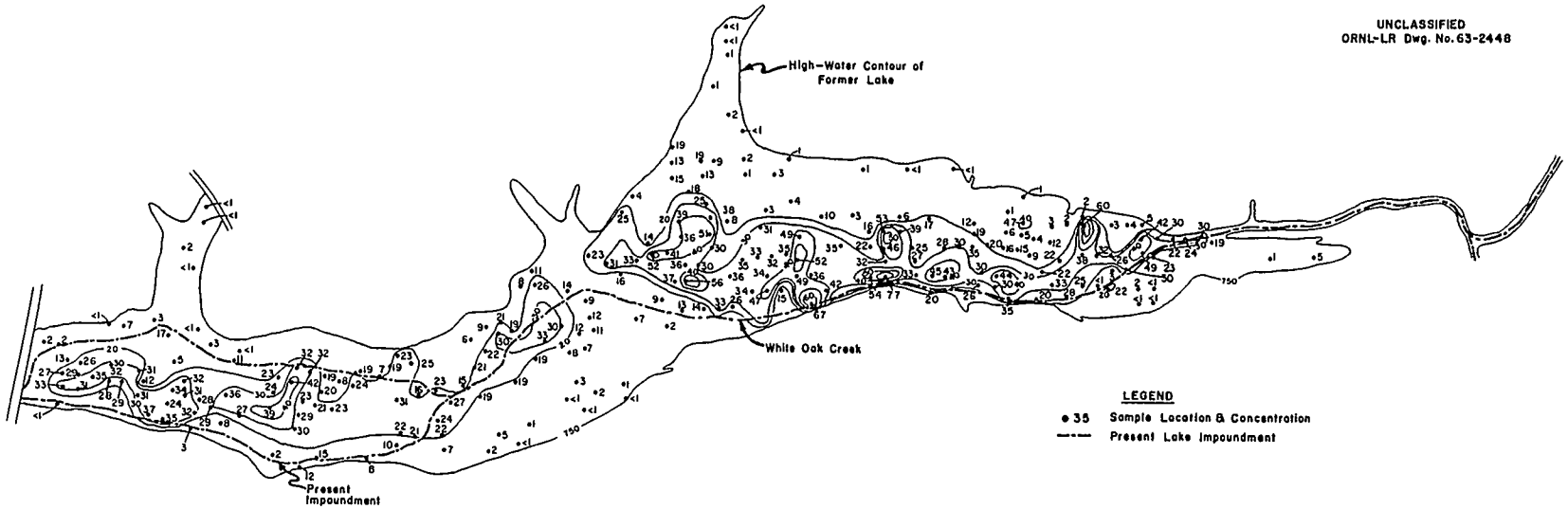

Fig. 5.3. Map of White Oak Lake Bed, Showing Cs^{137} Concentrations in 10^{-3} μc per Gram of Dry Weight for 0-to-6-in. Soil Layer.

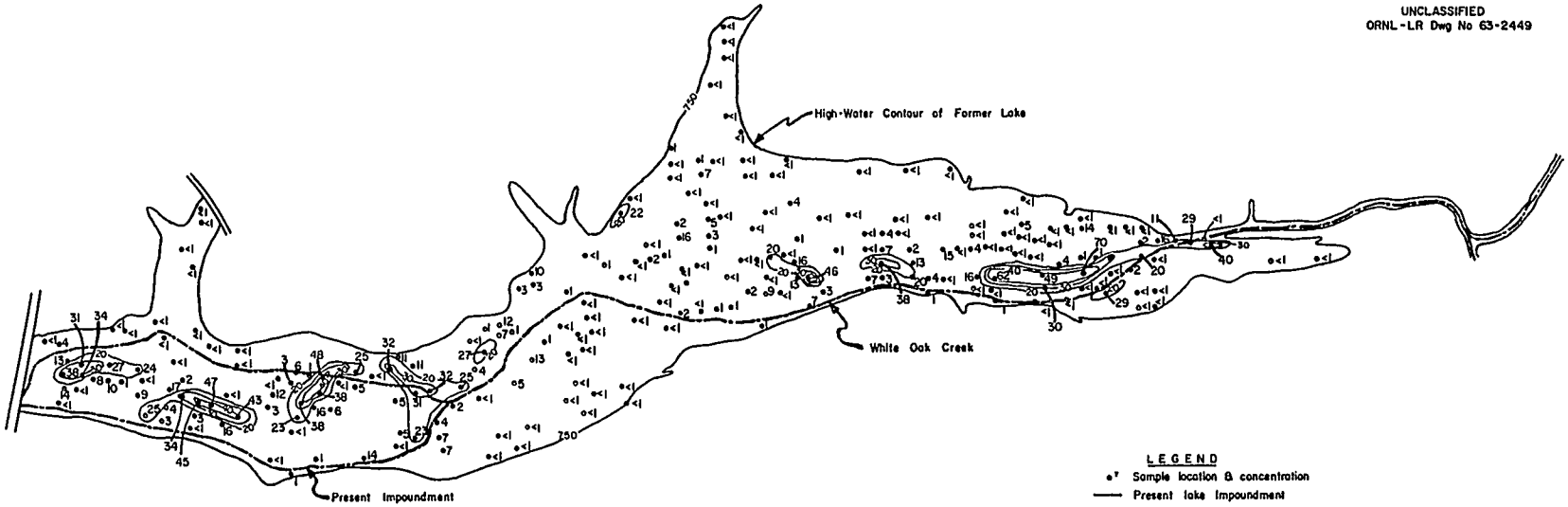

Fig. 5.4. Map of White Oak Lake Bed, Showing Cs^{137} Concentrations in 10^{-3} μc per Gram of Dry Weight for 6-to-12-in. Soil Layer.

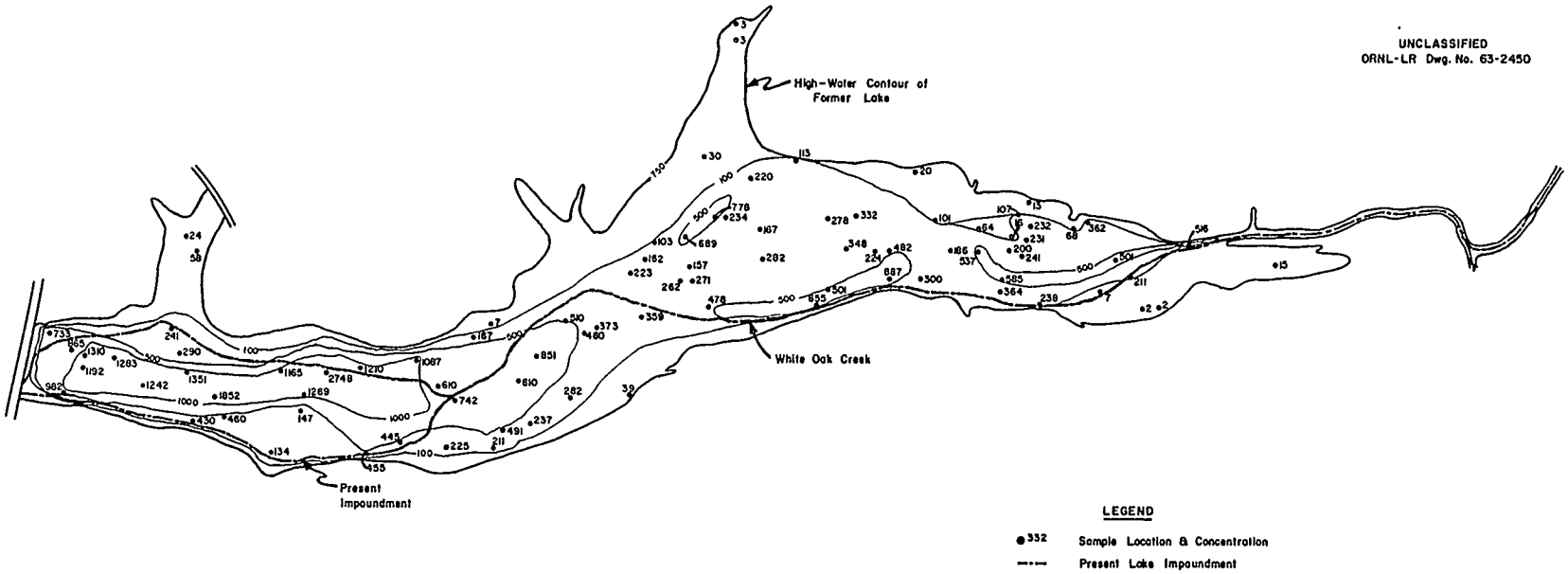

Fig. 5.5. Map of White Oak Lake Bed, Showing Sr^{90} Concentrations in $\mu\mu c$ per Gram of Dry Weight for 0-to-6-in. Soil Layer.

Table 5.1. Quantity and Distribution of Radionuclides in White Oak Lake Bed – December 1962

Radionuclides	Depth from Surface (in.)									
	0–6		6–12		12–18		18–24		Total	
	Curies	Standard Error	Curies	Standard Error	Curies	Standard Error	Curies	Standard Error	Curies	Standard Error
Ru^{106}	594	76	276	38	112	19	56	10	1038	88
Cs^{137}	468	20	204	25	29	12	3	1	704	35
Co^{60}	119	9	22	2	8	1	3	0.5	152	9
TRE[a]	13	3	2.5	0.1	1.0	0.1	0.1	0.1	16.7	3.3
Sr^{90}	10	0.9	3.5	0.5	1.0	0.3	0.1	0.1	14.6	1.1

[a]Trivalent rare earths less Y^{90}.

in the soil were found to be roughly 100 times less than those of Cs^{137}.

The quantities of the various radionuclides in the lake bed are summarized in Table 5.1. Ruthenium-106 (1038 curies) and Cs^{137} (704 curies) account for more than 90% of the total activity present; and Co^{60} (153 curies), the rare earths exclusive of Y^{90} (17 curies), and Sr^{90} (15 curies) comprise the remainder. The largest amounts of activity occur in the upper 6 in. of soil, whereas the 18-to-24-in. layer contains only a small fraction of the total radionuclides.

MOVEMENT OF RADIONUCLIDES IN WHITE OAK CREEK

A sampling train that separates suspended solids directly from creek water is being used to study the transport of suspended solids and their associated activity in White Oak Creek. The unit consists of a strainer and four separate hydroclones. The median diameters of the solids removed from the hydroclones are 29, 19, 12, and 9 μ respectively.

To date, eight operating runs, ranging from 1 to 4 hr duration, have been made in White Oak Creek at mile 1.8. The flow rate of the creek for the sample periods varied from 5 cfs (one-half the average rate) to 57 cfs, and the concentration of suspended solids in the water varied from 0.004 to 3.261 g/liter. Construction work in and around the creek, which resulted in the removal of soil cover, may account, in part, for the extremely high concentrations of suspended solids in some of the runs.

The percentages of cesium and strontium in creek water associated with the liquid phase and with several particle-size ranges of suspended solids for the eight runs are presented in Tables 5.2 and 5.3. The highest values of sorbed cesium and strontium occur in runs 2, 7, and 8; these are the runs made during high suspended-solids load and/or high stream flow. The maximum strontium sorbed was approximately 25% (run 7), while more than 95% of the cesium in the creek water was found to be associated with suspended solids in runs 7 and 8. It appears that during low flow rates and/or low suspended-solids loads, most of the strontium and cesium in White Oak Creek is associated with the liquid phase; but for high stream flows and/or heavy suspended-solids loads, practically all the cesium and a significant part of the strontium are transported downstream by suspended solids. It was also found that, although more activity is transported downstream by suspended solids during periods of high stream flow and/or high sediment load, the concentration of activity sorbed on the solids during these periods is less than that sorbed when the stream flow and/or the

Table 5.2. Percentage of Cs^{137} in the Liquid and the Solid Phases of White Oak Creek Water

Run No.	Creek Flow Rate (cfs)	Suspended-Solids Concentration (g/liter)	Percentage of Cs^{137}						
			Liquid Phase	Solid Phase — Median Diameter Particle Size (μ)					
				<9	9	12	18	29	>250
1	14.4	0.011	71.3	25.7	0.2	1.0	1.3	0.5	<0.1
2	57.2	0.044	50.7	39.9	0.5	1.8	3.5	2.6	1.0
3	5.5	0.004	58.7	37.7	0.9	1.2	0.3	1.2	<0.1
4	6.1	0.012	79.5	19.3	0.4	0.4	0.1	0.3	<0.1
5	5.0	0.010	79.6	18.8	0.5	0.5	0.5	0.1	<0.1
6	5.3	0.006	77.1	15.9	2.2	1.9	2.2	0.6	0.1
7	7.8	3.261	4.3	85.3	4.0	2.4	2.9	1.1	<0.1
8	43.5	0.692	3.9	65.4	7.8	5.6	8.7	8.3	0.3

Table 5.3. Percentage of Sr^{90} in the Liquid and the Solid Phases of White Oak Creek Water

Run No.	Creek Flow Rate (cfs)	Suspended-Solids Concentration (g/liter)	Percentage of Sr^{90}						
			Liquid Phase	Solid Phase — Median Diameter Particle Size (μ)					
				<9	9	12	19	29	>250
1	14.4	0.011	99.26	0.61	0.03	0.03	0.04	0.03	<0.01
2	57.2	0.044	98.09	1.01	0.08	0.17	0.47	0.17	0.01
3	5.5	0.004	99.30	0.55	0.04	0.06	0.01	0.04	<0.01
4	6.1	0.012	99.63	0.33	0.02	0.01	<0.01	0.01	<0.01
5	5.0	0.010	99.43	0.52	0.02	0.02	0.01	<0.01	<0.01
6	5.3	0.006	99.50	0.40	0.04	0.03	0.02	0.01	<0.01
7	7.8	3.261	75.52	18.07	3.36	1.68	1.10	0.27	<0.01
8	43.5	0.692	92.92	3.94	0.87	0.69	1.06	0.50	0.02

suspended solids are low.[5] Finally, there is considerably more activity associated with suspended solids of particles less than 9 μ than with the larger sizes.

[5]R. E. Blanco and E. G. Struxness, *Waste Treatment and Disposal Progress Report for June and July 1962*, ORNL TM-396 (Dec. 19, 1962).

To further define the transport of activity in the creek with high discharge and sediment load, a series of samples was taken during the rise and subsequent fall of the creek due to a light rainfall. Stream discharge, suspended-solids concentration, and strontium and cesium transport during the cycle are shown in Fig. 5.6. It appears that the

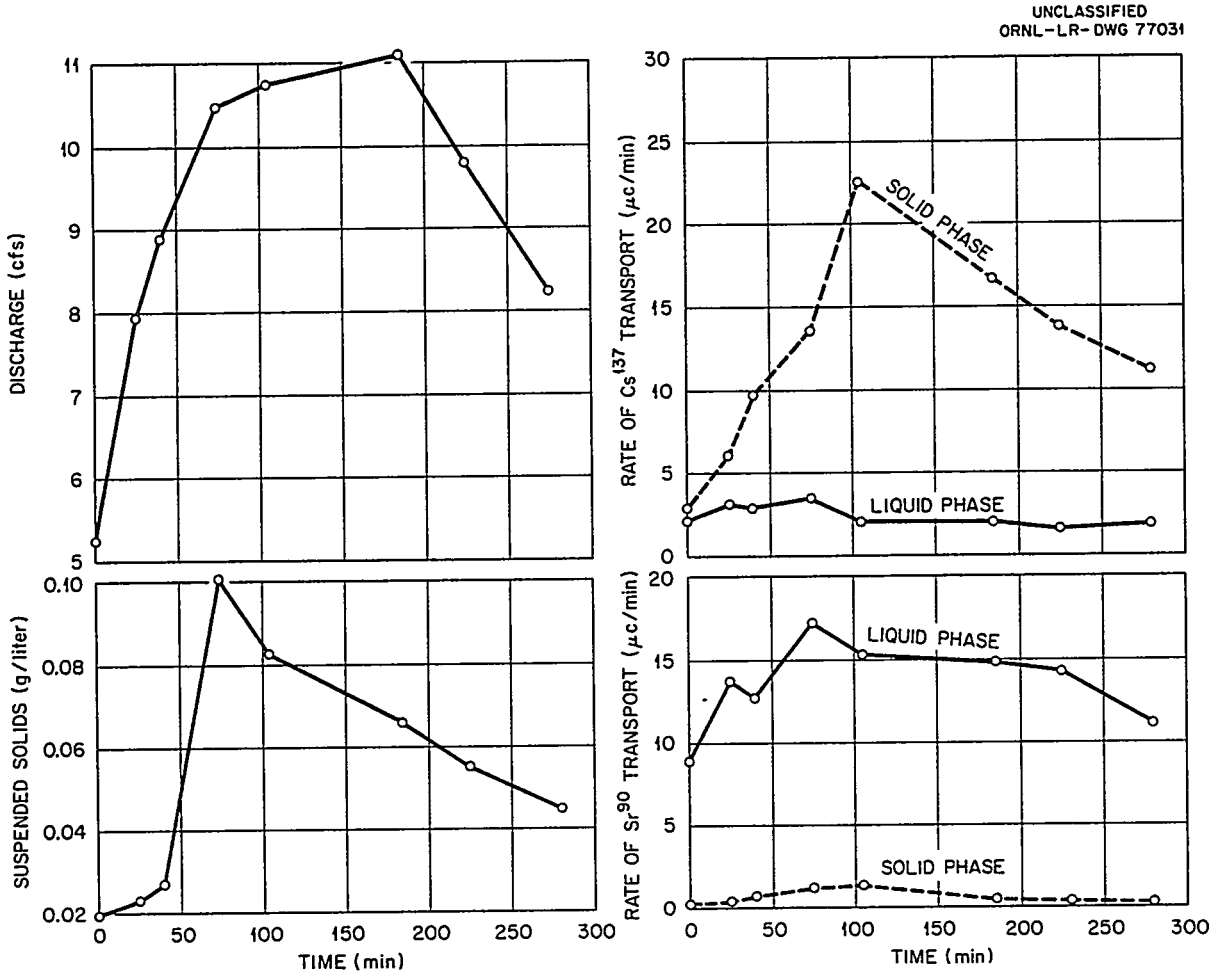

Fig. 5.6. Stream Flow, Concentration of Suspended Solids, and Sr^{90} and Cs^{137} Transport in White Oak Creek Resulting from Light Rainfall.

sediment load in the stream does not vary directly with stream discharge. The suspended-solids concentration rises quite abruptly to a peak concentration well before the crest of the stream flow is reached. Also, the quantity of cesium and strontium transported downstream is greatest when the sediment load is highest, which is prior to the peak stream discharge. Finally, there is little variation in the quantity of cesium transported downstream that is associated with the liquid phase of creek water, but the amount associated with suspended solids increases considerably with an increase in stream flow and/or suspended-solids concentration. For strontium, however, there is little variation in the quantity sorbed on sediments, whereas significant increases occur in the quantity of that associated with the liquid fraction of creek water.

The exact source is not known of the additional cesium and strontium accompanying a rise in stream flow and/or suspended-solids concentration. It is likely that much of the increase is due to scouring of the stream bed. However, some may be due to surface- and ground-water leaching.

A preliminary survey of the bed of White Oak Creek and its flood plain has revealed that bottom sediments to a depth of 18 in. at mile 2.3 contain Sr^{90}, Cs^{137}, Co^{60}, and the rare earths (exclusive of Y^{90}) in concentrations from 100 to 3450, 4000 to 76,900, 290 to 2200, and 0 to 14,100 $\mu\mu c$ per gram of dry weight respectively. In general, for Sr^{90} and the rare earths the highest concentrations

occur in the uppermost few inches of the sediment, whereas for Cs^{137} and Co^{60} the higher concentrations were found at depths of 6 to 12 in. The concentrations of radionuclides found in the flood plain along the bank of the creek are roughly the same as those observed in the creek bed.

TIME OF WATER TRAVEL IN WHITE OAK CREEK

Studies on the time of water travel in White Oak Creek have been made at discharges ranging from 4.5 to 200 cfs. The reach used for comparison of results (shown in Table 5.4) is the segment of channel between the gaging station at White Oak Creek miles 2.6 and 1.8. Tracers used for the studies were the organic dyes fluorescein, rhodamine B, and Pontacyl Pink and Au^{198}.

Table 5.4. Results of Time-of-Travel Studies for White Oak Creek, 1962–63

Discharge (cfs)	Mean Velocity (fps)	Velocity of Peak Concentration (fps)	Maximum Velocity (fps)
4.5	0.40	0.43	0.48
4.7	0.45	0.50	0.65
5.5			0.66
200	2.30	2.30	2.60

GROUND-WATER LEVELS IN WHITE OAK CREEK BASIN

Water levels were measured in the permanent wells in White Oak Creek Basin in March 1963 during the period of highest ground-water surfaces for the 1963 water year. Figure 5.7 is a very generalized map of part of White Oak Creek Basin. It is based on measurements taken during that period, showing areal distribution of depths to water by ranges.

In and near the valley floors the water surface is generally less than 20 ft below land surface, the depth decreasing with proximity to stream channels. Depth to water increases with elevation above the valley floors, the known maximum depth in March being 283 ft in the well near the crest of Melton Hill (shown in the lower left corner of Fig. 5.7).

Annual variations in water level are generally greater in the higher elevations than in the lower, as shown in Fig. 5.8. Ground surface at well CR-1 is about 861 ft, and at well CR-2 about 965 ft. Both wells are developed in the Knox dolomite of Chestnut Ridge and are located about 900 ft apart. The increase in magnitude of water-level variation with elevation is due primarily to the movement of ground water toward points of discharge at lower elevations. Thus, water moving from higher elevations serves to recharge lower elevations as water moves through and out of the system.

Where the depth to water is extreme, however, water levels appear to be only slightly affected by rainfall and show no immediate response. For example, the water level in the well located near the crest of Melton Hill has varied between 283 and 287 ft below land surface during the one-year period of record of water level. These characteristics are apparently due to a combination of factors, the most important being the time required for recharge by precipitation to move down to the water table, and the lack of any large discharge of ground water from Melton Hill.

Fig. 5.7. Generalized Depth-to-Water Map of White Oak Creek Basin, March 1963.

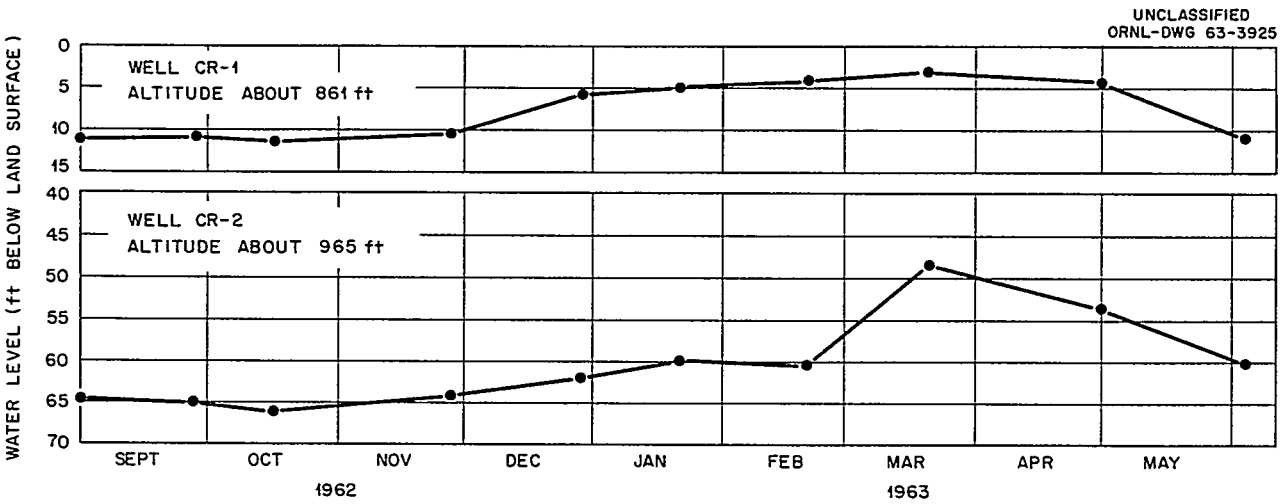

Fig. 5.8. Water-Level Variations in Wells CR-1 and CR-2, August 1962 to June 1963.

6. Mineral Exchange Studies

Tsuneo Tamura
W. P. Bonner
F. S. Brinkley
D. G. Jacobs
O. H. Myers
Tohru Murano[1]

STRONTIUM REMOVALS BY HYDROUS AND ANHYDROUS SESQUIOXIDES

When gibbsite, an aluminum hydroxide, is decomposed by heating, the product is a highly selective sorbent for strontium in neutral and alkaline media. Measurements showed that the surface area had increased from about 0.3 m^2/g for the unheated gibbsite to over 200 m^2/g for the heat-treated material. For further characterization of the heat-treated material, its maximum (saturation) capacity to sorb cesium and strontium without any interfering ions was determined.

Other materials were also investigated to determine the effect of heating on their ability to sorb strontium. Several promising minerals have been found to show improved sorbing qualities for strontium following heating at 500°C.

Capacity of Heat-Treated Gibbsite for Cesium and Strontium

The amounts of cesium and strontium sorbed by the heat-treated gibbsite, in a column, are shown in Table 6.1. The amount of sorbed cesium remained relatively constant over the pH range from 6 to 10. The material shows much higher affinity for strontium; it sorbed approximately $2\frac{1}{2}$ times as much strontium as cesium.

The saturated material was leached by solutions of $NaNO_3$ of the same pH. When the solution became ineffective as a desorbing solution, the

[1]Visiting scientist from Atomic Fuel Corporation, Tokai-mura, Japan.

$NaNO_3$ concentration was increased to hasten the reaction. The results of the leaching tests are shown in Table 6.2. Leaching with 23 meq of Na^+ per meq of sorbed Cs^+ desorbed 96% of the cesium. The removal of cesium was accomplished quite easily; 1.7 meq of Na^+ per meq of Cs^+ desorbed 57% of the cesium, and 3.3 meq/meq removed 83%.

Strontium removal was more difficult. After passage of sodium equivalent to over a hundred times the amount of strontium on the sorbent, only 50% of the strontium was desorbed. Over 730 meq of Na^+ per meq of Sr^+ desorbed 77%. Over 95% removal was not achieved until about 7000 meq/meq was used.

The difficulty with which strontium is desorbed is evidence of a strong bond between the sorbent and strontium. However, the strontium is desorbed quite readily if the pH is dropped below neutral. This rapid release with decrease in pH would indicate that the reaction is taking place on the surface of the sorbent, rather than with discrete particles.

Table 6.1. Capacity of Heat-Treated Gibbsite for Cesium and Strontium

	Run No.	pH	Saturation Capacity (meq/100 g)
Cesium	1	6	4.33
	2	8	4.06
	3	8	4.44
	4	10	4.83
Strontium	5	6	9.77
	6	6	11.2
	7	8	14.3
	8	8	11.8
	9	8	11.9

New Heat-Treated Materials as Strontium Sorbents

Several hydrous oxide minerals of iron and aluminum were heated to test whether they would show properties favorable for the sorption of strontium. Diaspore ($HAlO_2$), geothite ($HFeO_2$), and limonite ($Fe_2O_3 \cdot xH_2O$) were used.

In Table 6.3 the results of surface area measurements and the strontium sorption tests are given for materials which had been heated at 500°C for 3 hr. In addition, the results for reagent-grade ferric oxide powder are given. In every case the heated materials showed a higher surface area than the unheated mineral. The heat-treated materials were also superior to the unheated for removing strontium. The reaction reached equilibrium in about 4 hr or less. Limonite showed a relatively high affinity for strontium even prior to heating, but the heat treatment produced a superior sorbent. The high reactivity of limonite

Table 6.2. Desorption of Cesium and Strontium from Heat-Treated Gibbsite by $NaNO_3$

Cation Sorbed	Normality of $NaNO_3$	pH of Solution	Total Na^+ Used (meq)	Na^+/Ca^+ or $Na^+/\frac{1}{2}Sr^{2+}$	Percentage Removed
Cesium	0.01	8	0.25	1.7	57
	0.01	8	0.50	3.3	83
	0.01	8	3.5	23	96
Strontium	0.01	8	3.5	7	22
	0.1	8	50	103	50
	1.0	8	352	733	77
	5.0	8	3540	7375	95

Table 6.3. Percentage Sorption of Strontium by Several Natural Materials from 0.1 *M* $NaNO_3$ Containing 1×10^{-5} *M* Sr^{2+}

0.25 g of sorbent per 50 ml of solution

	Surface Area (m^2/g)	Sorption and pH for Specified Contact Time									
		1 hr		4 hr		24 hr		48 hr		96 hr	
		% Sorbed	pH	% Sorbed	pH	% Sorbed	pH	% Sorbed	pH	% Sorbed	pH
Diaspore (<325 mesh)											
Unheated	6.6	16.3	9.85	17.3	9.90	18.6	9.70	17.5	10.00	17.4	9.65
Heated[a]	68.5	72.8	9.45	84.0	9.80	85.7	9.75	86.1	9.80	84.7[b]	9.20[b]
Goethite (<325 mesh)											
Unheated	3.3	15.8	9.80	18.3	9.70	17.8	9.80			17.7	9.60
Heated[a]	62.1	95.5	9.75	97.6	9.75	98.1	9.80			97.3	9.60
Limonite (<325 mesh)											
Unheated	20.8	84.2	9.70	94.4	9.80	97.8	9.60	98.3	9.90	98.2	9.60
Heated[a]	93.2	98.2	8.95	99.6	9.60	99.7	9.70	99.8	9.80	99.6[b]	9.15
Fe_2O_3											
Unheated		33.8	9.75	40.3	9.90	41.9	9.80	41.8	8.85	38.5[b]	9.10[b]

[a]500°C for 3 hr.

[b]Sample contacted 144 hr.

in the natural state was probably due to the initially high surface area.

The best material for the sorption of strontium (Table 6.3) appears to be heat-treated limonite, and a comparison of its behavior with that of the heat-treated gibbsite is shown in Fig. 6.1. Like gibbsite, the heated limonite removed strontium best from alkaline solutions. The heat-treated gibbsite sample used here did not possess a surface area as high as some of the earlier samples. Since very few investigations have been made to determine the optimal conditions for preparing these materials, it cannot now be stated which of the hydrous oxides is best for removing strontium.

The observation that unheated limonite possesses a high affinity for strontium is significant. This mineral is very common in soils and may be responsible, along with hydrous aluminum oxides, for sorbing a significant portion of the strontium present in waste streams. If the heat treatment is beneficial primarily because of the development of greater surface area, then the hydrous oxides in soils take on even greater significance since they occur as much finer particles and would possess even greater surface area. These considerations are being investigated, and preliminary evidence suggests that the hydrous oxides play a significant role in strontium sorption in soils.

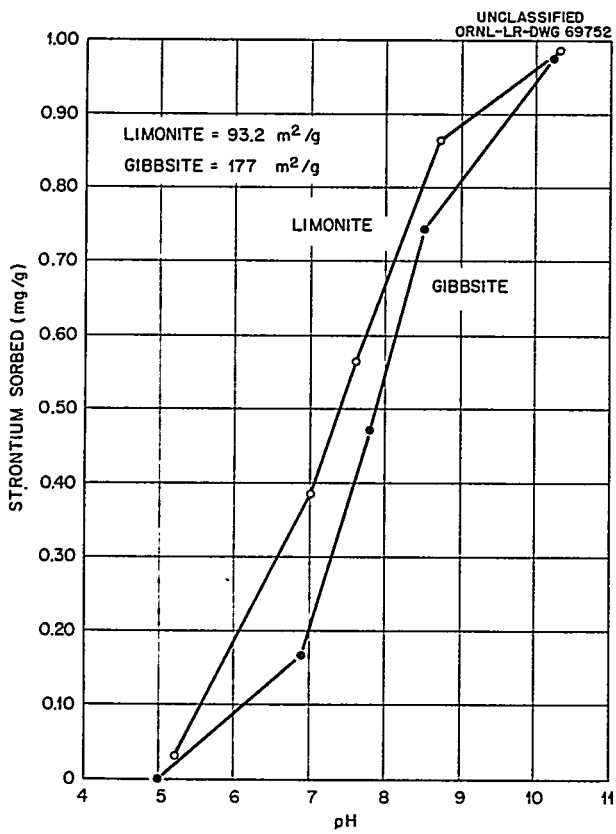

Fig. 6.1. Strontium Removed by Heat-Treated Minerals in 0.1 M $NaNO_3$.

Column Study of Several Sorbents for Strontium

In studies with columns of sorbents for removing strontium from solution, gibbsite that had been heated to 400°C showed a high selectivity for strontium in alkaline $NaNO_3$ solution. After investigation of the properties of unheated and heat-treated gibbsite, it was concluded that the heat treatment had converted the gibbsite into a product similar to that sold as activated alumina by the Aluminum Company of America. A sample of activated alumina (F-20) was obtained from Alcoa, and slurry tests showed that it was also selective for strontium. This development made it highly desirable to compare several materials in column systems in order to ascertain the potential usefulness of F-20 for waste treatment. The four materials included in the tests were Dowex 50-X12, clinoptilolite, vermiculite, and F-20 alumina. The Dowex 50 and vermiculite were pretreated with NaCl to convert them into the sodium forms. The clinoptilolite was treated with 1 M HCl to decompose the calcite impurity in the sample. Following pretreatment each sample was washed until tests with $AgNO_3$ for chloride were negative. No treatment was given to F-20 alumina prior to use in the first column test.

The tests were run with ½-in. glass tubing, containing 10 g of sorbent (weight based on the air-dried sample). The simulated waste solution was 0.5 M $NaNO_3$ adjusted to pH 10 with NaOH and containing 10^{-5} M $Sr(NO_3)_2$. The flow rate was maintained at 3 ml min^{-1} cm^{-2}.

The volume throughput and effluent activity measured in the four test runs are shown in Fig. 6.2. It appears that the flow rate was too high for both vermiculite and clinoptilolite to be efficient. The first 50-cm^3 volume showed activity breaking through in both these columns; the clinoptilolite did show improvement with

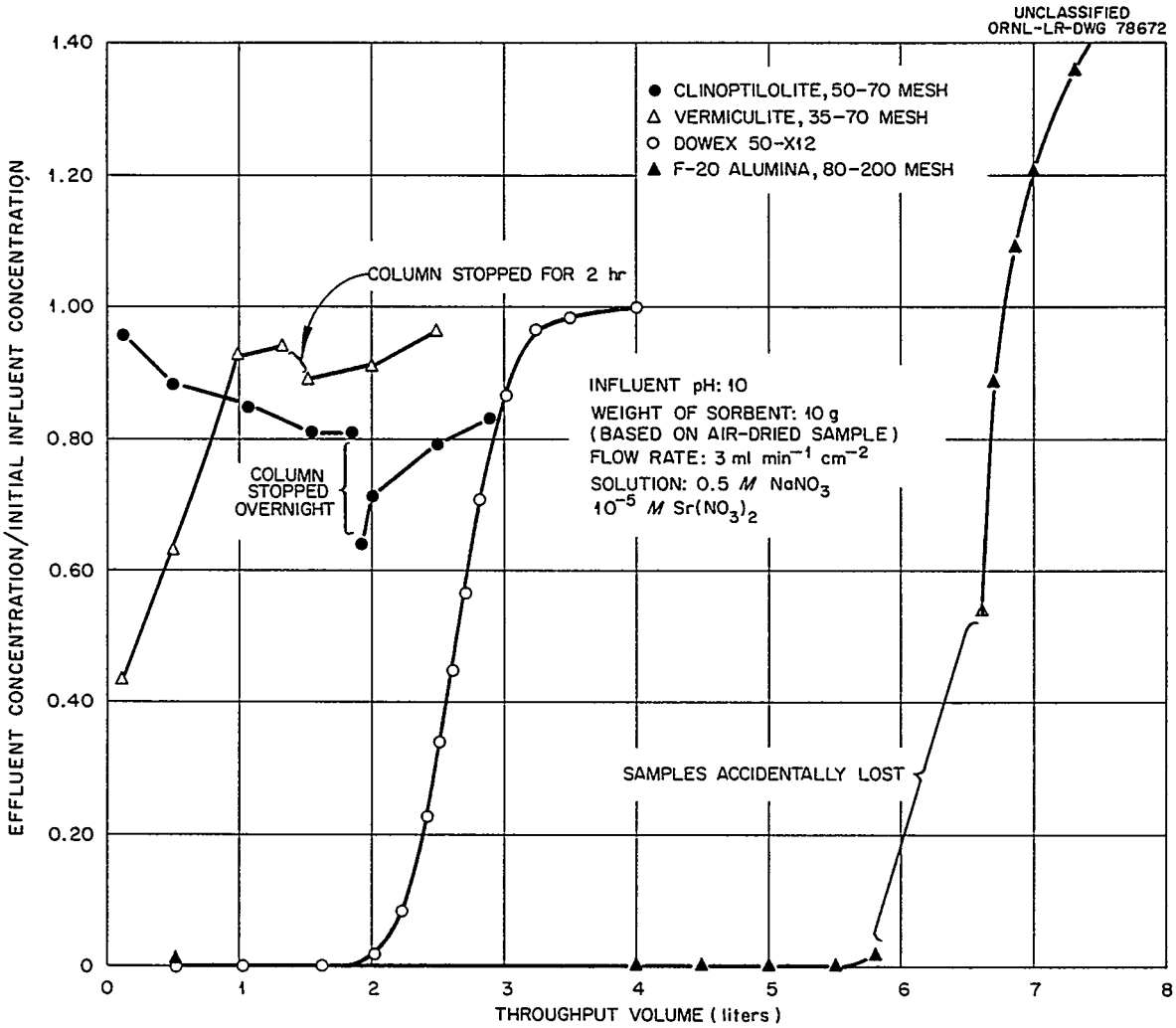

Fig. 6.2. Strontium Removal by Several Sorbents: Effluent Activity of Simulated Waste.

time. The latter behavior may be due to the change-over of clinoptilolite from the hydrogen to the sodium form. The effluent from Dowex 50 showed very little activity in the first 2 liters; with F-20 alumina, very little activity was measured in the effluent up to 5800 cm^3. Unfortunately, effluent samples from the alumina column were lost in the collection procedure, and the next reliable sample showed 54% activity. The behavior of the alumina was unusual in that the continued flow of solution, presumably after the alumina was saturated, resulted in an effluent that contained more strontium than the influent solution. This behavior suggests that the surface-layer alumina may be dissolving or "flaking off" with continued flow. (The high pH of the influent solution would facilitate this dissolution of the alumina.) After the end of the run the column was monitored along the outside wall with a G-M survey meter, and the activity distribution showed that the influent zone had a lower concentration of strontium than the effluent zone. It is also significant to note that the F-20 alumina does show sorption capacity for strontium to an extent that is competitive with other sorbents.

Since it was thought that the high effluent activity of the F-20 alumina column was caused by the high pH of the influent waste solution, another column was run to test this idea. Prior to passing the simulated waste through the column, it was decided to run 0.5 *M* $NaNO_3$ adjusted to pH 10 (without strontium) through until the

effluent pH equaled the influent pH of 10. After this treatment the pH of the system would be favorable for dissolution or "flaking," and strontium breakthrough was expected to occur after a few column volumes of waste had passed through. However, the first 20-cm^3 increment had a pH of 9.4; after passage of 1700 cm^3 of solution, the pH was 7.65. Subsequent samples showed gradual reductions in pH. It was therefore decided to start the simulated waste through the column with close attention to the pH in addition to the activity of the effluent.

The results of the second F-20 alumina run are plotted in Fig. 6.3. The results of the earlier alumina run are also plotted. The pretreated alumina showed less than 1% breakthrough up to 13,000 cm^3, compared with 5800 cm^3 for the first run. The effluent activity showed a gradual increase and after 35,000 cm^3 was about 85% of that of the influent. The pH of the effluent, which was measured periodically, did not reach the influent pH of 10 during the entire test run. The maximum observed pH of the effluent was 9.0 in the 50-cm^3 increment collected after passage of 23,700 cm^3. The minimum pH was 7.50 in the 50-cm^3 increment collected after 15,500 cm^3. The pH varied continuously over the reported range during the entire run. Although the results of this column run showed improved performance over the first test run, it should be pointed out that the cause of the improvement is not known.

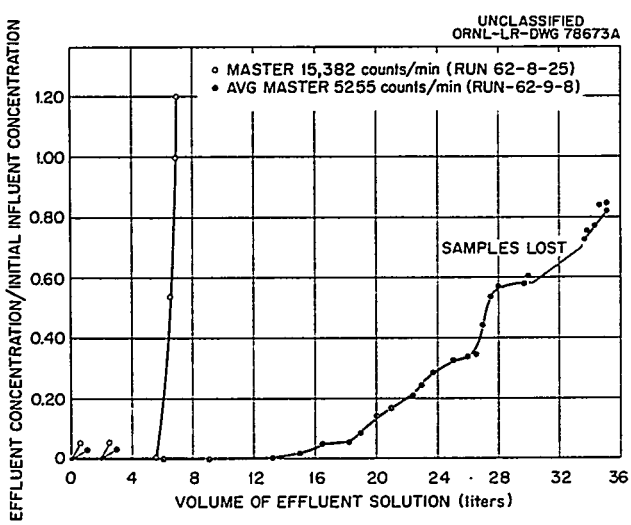

Fig. 6.3. Strontium Removal by F-20 Alumina: Effluent Activity of Simulated Waste.

These tests were run in 0.5 *M* $NaNO_3$ solutions; in different Na/Sr ratios or at different pH's the other sorbents could be more effective. Under acid conditions alumina is ineffective, whereas Dowex 50 would still function. With lower Na/Sr ratios the loading on the ion exchangers would favor strontium, whereas the loading on the alumina may be unaffected. The latter possibility appears plausible, since the removal of strontium occurs in a system that expends hydroxide ions, which suggests that ion exchange may not be the mechanism for removing strontium. Work is in progress to elucidate the nature of the alumina reaction, with particular attention being given to comparisons of reactions with known ion exchangers such as Dowex 50.

STRONTIUM AND CESIUM REMOVAL BY VERMICULITE

Factors Optimizing Cesium Removal by Vermiculite

Previous studies have shown that potassium treatment of Zonolite BO-4 (hydrobiotite obtained from American Zonolite Company, Travelers' Rest, South Carolina, an interlayered hydrobiotite of approximately 40% biotite and 60% vermiculite lattices with a particle-size range of −20 +65 mesh) results in an increase of the distribution coefficient for trace cesium exchange from high sodium salt systems by a factor of 2.7 when determined by slurry techniques. This increased sorption is attributed to the increased number of collapsed (10-A) lattices which provide exchange sites at the edges of the basal spacings which are sterically favorable for cesium compared to sodium. However, when column techniques are employed to measure sorption of trace quantities of cesium from 0.5 *M* $NaNO_3$, the continued leaching action of the sodium nitrate is effective in removing the interlayer potassium. As a result the lattices collapsed to 10 A by potassium treatment rehydrate upon sodium saturation and expand to 14 A; thus, the exchange sites at the edges of the basal spacing lose their specific attractiveness for cesium, and the full beneficial effects of potassium treatment are negated.

Cesium Exchange by Potassium-Treated Vermiculite

Zonolite BO-4 was treated with 1 *M* KCl to induce lattice collapse. The excess salt was removed by elutriation with ethanol (95%). The treated Zonolite had a sharp x-ray diffraction maximum at 10 A and an exchange capacity of 5.9 meq/100 g. Eight liters of 0.5 *M* $NaNO_3$ containing traces of cesium (1.7×10^{-7} *M*) was passed through columns filled with 10 g of the treated vermiculite. Various amounts of potassium were added to the influent to maintain the collapsed lattice structure. The results (Table 6.4) show that optimum cesium removal was obtained with an influent potassium concentration of 0.0005 *M* which gave a cesium K_d of 366 ml/g and a final exchange capacity of 46.8 meq/100 g. Higher concentrations of potassium were more effective in maintaining collapsed lattices, as indicated by a lower final exchange capacity; but the increased numbers of favorable exchange sites were not sufficient to counteract the increased competition caused by the greater concentration of potassium.

Table 6.4. Effect of Addition of Potassium to the Influent on the Sorption of Cesium by Potassium-Treated Vermiculite from 0.5 *M* $NaNO_3$ Containing the Mass Equivalent of 2 μc of Cs^{137} per ml

Potassium Concentration (*M*)	Cesium K_d (ml/g)	Cesium Leached (%)	Final CEC[a] (meq/100 g)
0.0000	252	15.0	67.0
0.0001	311	16.2	63.7
0.0002	352	10.5	56.2
0.0005	366	9.8	46.8
0.001	358	10.8	37.9
0.002	262	9.5	16.7
0.005	180	10.2	9.1
0.01	147	9.6	10.0
0.05	65	10.2	9.0

[a]Cation exchange capacity.

Strontium Exchange by Vermiculite with Potassium Added to the Influent

Addition of potassium to 0.5 *M* $NaNO_3$ influent to raise the potassium concentration above 0.01 *M* results in collapse of vermiculite lattices and the interlayer fixation of trace concentrations of cesium by physical entrapment of the cesium held at exchange sites on the basal surface of the vermiculite. However, no appreciable quantities of strontium could be fixed in this manner (Table 6.5). The uptake of strontium was reduced by increased concentrations of potassium, although the reduction was not proportional to the reduction in final exchange capacity. In addition, the major portion of the strontium remained in an exchangeable form.

Table 6.5. Effect of Addition of Potassium to the Influent on the Sorption of Trace Quantities of Strontium by Vermiculite from 0.5 *M* $NaNO_3$

Potassium Concentration (*M*)	Strontium K_d (ml/g)	Strontium Leached (%)	Final CEC[a] (meq/100 g)
0.00	43.8	84.1	86.0
0.01	46.9	76.2	65.5
0.02	36.0	86.1	44.6
0.04	24.1	70.7	22.8

[a]Cation exchange capacity.

Influence of Temperature and Time on Cesium Loading on Vermiculite

Increased temperatures resulted in faster rates of exchange by vermiculite-biotite systems, but the effect on sorption of trace quantities of cesium was influenced primarily by the effects on the sodium-potassium exchange in the system. When 0.5 *M* $NaNO_3$ tagged with Cs^{137} was passed through columns of sodium- or potassium-treated vermiculite, a more rapid release of potassium from the collapsed vermiculite or biotite layers was favored at higher temperatures and resulted in a greater degree of lattice expansion. This

resulted in a higher exchange capacity but a lower cesium loading due to the decreased number of cesium fixation sites (Table 6.6).

When the 0.5 *M* $NaNO_3$ influent solution was brought to 0.04 *M* with respect to KNO_3, the reverse reaction was favored. As a result, a more complete lattice collapse and a reduced exchange capacity were favored by higher temperatures. However, at 81°C the potassium of the influent provided too much competition for cesium and resulted in lower cesium sorption than at room temperature. Either the lattices were collapsed to 10 A before the cesium could arrive at the exchange sites within the basal spacing or the elevated temperature reduced the hydration of the potassium ion, resulting in a higher relative affinity of the vermiculite surface for potassium. In the cold system (0°C), collapse of the vermiculite was not sufficiently complete to obtain optimum cesium removal. This was evident from the high final exchange capacity.

Several 4-g columns of vermiculite were run at a constant flow rate of 0.80 ml cm^{-2} min^{-1} at room temperature. The runs were terminated after various lengths of time. The columns were quartered for determination of the exchange capacity and the cesium loading of each segment. The results show that, when the influent solution is deficient in collapse-inducing cations, the exchange capacity increases slowly with continued leaching (Table 6.7). The increase in exchange capacity was directly proportional to the square root of time, suggesting that the release of potassium from collapsed lattices is a diffusion-controlled process.

When the influent solution was potassium-rich, the exchange capacity decreased with time, indicating continued conversion of vermiculite to biotite (collapsed lattice). Continued lattice collapse was accompanied by increased interlayer fixation of cesium. In the columns filled with sodium-treated vermiculite, the cesium loading increased slowly with time, presumably due to slow penetration of the collapsed biotite layers by the cesium ions. As time passed, more of the cesium migrated to the interlayer fixation sites of the closed lattices and was, therefore, less subject to leaching than when it occupied fixation sites near the edges of the basal spacing.

In the case where columns filled with potassium-treated vermiculite were saturated with a potassium-deficient solution of 0.5 *M* $NaNO_3$, the advantage of increased time was counterbalanced by re-expansion of the closed lattices after 24 hr, and after 48 hr there was a slight decrease in the net cesium loading.

Table 6.6. Influence of Temperature on the Sorption of Cesium by Vermiculite

Material	Temperature (°C)	Solution	Cesium K_d (ml/g)	CEC[a] (meq/100 g)	Cesium Leached (%)
Na-treated vermiculite	81	6 liters of 0.5 *M* $NaNO_3$	95	84.7	22.0
	25		109	67.3	23.0
	0		115	63.4	22.4
Na-treated vermiculite	81	8 liters of (0.5 *M* $NaNO_3$ + 0.04 *M* KNO_3)	140	8.0	3.42
	25		610	14.9	5.82
	0		379	28.0	7.06
K-treated vermiculite	81	8 liters of 0.5 *M* $NaNO_3$	106	74.8	15.6
	25		218	62.9	13.7
	0		301	52.2	9.8

[a]Cation exchange capacity.

Table 6.7. Influence of Time on the Sorption of Cesium by Vermiculite

Time (hr)	0.5 *M* $NaNO_3$ + 0.04 *M* KNO_3			0.5 *M* $NaNO_3$			0.5 *M* $NaNO_3$		
	Na-Treated Vermiculite			Na-Treated Vermiculite			K-Treated Vermiculite		
	Cs K_d (ml/g)	CEC[a] (meq/100 g)	Cs Leached (%)	Cs K_d (ml/g)	CEC[a] (meq/100 g)	Cs Leached (%)	Cs K_d (ml/g)	CEC[a] (meq/100 g)	Cs Leached (%)
1	54	62.0	3.75	39	75.4	48.2	59	18.0	29.2
2	93	56.7	2.74	52	75.3	42.0	80	20.4	27.9
4	183	49.6	2.23	66	76.9	40.6	149	24.8	21.7
8	334	43.7	1.92	82	76.5	35.6	205	31.0	18.8
24	513	34.4	1.17	116	80.0	36.9	247	48.3	11.7
48	857	29.0	1.04	134	80.2	35.5	249	59.8	13.0
72	903	26.5	0.83	141	79.9	29.8	243	62.9	23.0
96	1240	23.8	0.78	145	81.1	27.4	225	68.4	24.1
120	1290	22.6	0.79						
144				160	83.4	33.6	226	73.8	17.6
168	1360	20.7	0.77	166	83.3	30.4	218	74.6	18.3
240	1540	20.1	0.78						
336				162	83.3	29.6	221	82.1	20.9
435				166	85.3	28.2			

[a]Cation exchange capacity.

7. Engineering, Economic, and Safety Evaluations

R. L. Bradshaw
J. J. Perona[1]
L. C. Emerson
J. O. Blomeke[1]

ENGINEERING AND ECONOMIC EVALUATIONS

This study, undertaken in cooperation with the ORNL Chemical Technology Division, has as its objective the evaluation of the economics and safety associated with alternative methods for the ultimate disposal of highly radioactive liquid and solid wastes. All steps between fuel processing and ultimate storage are being considered, and the study should define an optimum combination of operations for each disposal method and indicate the most promising methods for experimental study.

[1]Chemical Technology Division.

A plant that can process 6 metric tons of fuel per day is assumed – processing 1500 metric tons of uranium converter fuel per year at a burnup of 10,000 Mwd/metric ton and 270 metric tons of thorium converter fuel per year at a burnup of 20,000 Mwd/metric ton. This hypothetical plant would process all the fuel from a 15,000-Mw (electrical) nuclear economy, which may be in existence by 1975. The preliminary operations to be evaluated are interim liquid storage, conversion to solids by pot calcination, interim storage of solids, and shipment of calcined solids. The ultimate disposal methods to be evaluated include the storage of calcined solids in salt deposits, in vaults, and in vertical shafts and the storage of liquids in salt deposits, in porous geologic formations by deep-well injection, and in tanks. Cost studies of the preliminary operations which have been completed and reported previously were devoted to interim liquid storage,[2] conversion to solids by pot calcination,[3] and shipment of calcined solids.[4] Studies of interim storage of solidified wastes[5] and the effects of fission product removal on waste-management costs[6] have recently been completed.

INTERIM STORAGE OF SOLIDIFIED WASTES

Interim storage facilities were designed to handle cylinders of solidified wastes produced by the pot calcination plant described previously.[3] It was assumed that Purex and Thorex wastes were converted to solids and calcined in cylinders 6, 12, and 24 in. in diameter by 11 ft high. Calcination after storage of the wastes as both acid and neutralized solutions was considered, as was the production of glass from acid Thorex waste.

Interim solids storage periods of 1, 3, 10, and 30 yr in water-filled canals were considered for cylinders with contents aged 120 days, 1 yr, 3 yr, and 10 yr by interim liquid storage. Although the wide range of conditions resulted in facilities of different sizes and configurations, they consisted, in essence, of a central-facility canal for receiving and removing cylinders, canals for storing cylinders, a service area containing the equipment for cooling and purifying the water, a personnel office, and a change room.

It was assumed that a masonry building would enclose the central facility, service area, offices, and change rooms and that the storage canals would be housed in a frame building of lighter construction.

Capital costs expressed on an annual basis were computed as the sum of the costs for the various components, allowing 4% interest. Excavation, concrete, and buildings were amortized over 50 yr; aluminum partitions and cranes, over 25 yr; cooling system, over 20 yr; and demineralizer system, epoxy lining, and radiation monitors, over 10 yr. The total capital costs ranged from about $35,000/yr for 1 yr storage of 10-yr-old acid Purex waste to $521,000/yr for 30 yr storage of 120-day-decayed reacidified Thorex waste.

Labor costs were assumed to be $113,000/yr for all cases considered. This allowed for 9 man-years (4 shift operators, 1 supervisor, 1 health physicist, and 3 maintenance craftsmen).

Total costs, expressed in terms of mills per electrical kilowatt-hour, were computed, as a function of age, for handling each waste type separately and for the combination of acid Purex–acid Thorex and reacidified Purex–reacidified Thorex wastes. Although costs did decrease with age of waste at time of storage, this effect was not very pronounced, usually amounting to less than a 15% reduction in costs for storage of 10-yr-decayed wastes compared to equivalent length storage of the same wastes aged only 120 days.

The costs of storing Purex and Thorex wastes together in the same facility ranged from 0.0015 mill/kwhr (electrical) for 1 yr of storage to 0.0048 mill/kwhr (electrical) for 30 yr of storage for the

---

[2] R. L. Bradshaw, J. J. Perona, J. T. Roberts, and J. O. Blomeke, *Evaluation of Ultimate Disposal Methods for Liquid and Solid Radioactive Wastes. I. Interim Liquid Storage*, ORNL-3128 (Aug. 7, 1961).

[3] J. J. Perona, R. L. Bradshaw, J. T. Roberts, and J. O. Blomeke, *Evaluation of Ultimate Disposal Methods for Liquid and Solid Radioactive Wastes. II. Conversion to Solid by Pot Calcination*, ORNL-3192 (Sept. 27, 1961).

[4] J. J. Perona, R. L. Bradshaw, J. O. Blomeke, and J. T. Roberts, *Evaluation of Ultimate Disposal Methods for Liquid and Solid Radioactive Wastes. IV. Shipment of Calcined Solids*, ORNL-3356 (Oct. 4, 1962).

[5] J. O. Blomeke, J. J. Perona, H. O. Weeren, and R. L. Bradshaw, *Evaluation of Ultimate Disposal Methods for Liquid and Solid Radioactive Wastes. III. Interim Storage of Calcined Solid Wastes*, ORNL-3355 (in press).

[6] J. J. Perona, J. O. Blomeke, R. L. Bradshaw, and J. T. Roberts, *Evaluation of Ultimate Disposal Methods for Liquid and Solid Radioactive Wastes. V. Effects of Fission Product Removal on Costs of Waste Management*, ORNL-3357 (June 12, 1963).

calcined acid wastes and from 0.0018 to 0.0063 mill/kwhr (electrical) for the calcined reacidified wastes. The storage of acid wastes as solids was cheaper by factors of from 2 to 2.7 than the storage of the same wastes as liquids.[2] However, for most storage times, the storage of neutralized wastes as liquids was slightly cheaper than that of reacidified Purex and Thorex calcined solids.

EFFECTS OF FISSION PRODUCT REMOVAL

The object of this study was to compare two costs: (1) management costs for wastes from which large fractions of fission products have been removed by improved processes representative of the best future technology and (2) the costs for managing the original wastes with all fission products present. Three cases were studied, each representing a different degree of uniform removal of all fission products: 0, 90, and 99%. The waste from which fission products were removed was assumed to be acid Purex.

Although removal of 90 and 99% of the fission products simplifies the subsequent handling of the wastes because of decreased heat generation and decreased shielding requirements, the remaining isotopes represent a hazard requiring management under essentially the same conditions of safety as those demanded for the original waste. Costs were estimated in each case, therefore, for the interim storage of liquid waste, pot calcination of waste, interim storage of calcined waste, shipment of the calcined solids, and disposal of the solids in a salt mine. Treatment and disposal schemes were then worked out to minimize the total costs.

No attempt was made to estimate the costs of fission product removal or subsequent disposal of used fission product sources, because there is not yet sufficient information about the separations processes or source characteristics to permit accurate cost estimates.

The compositions and volumes of the waste (in liquid and solid forms) from the fission product separation plant were assumed to be the same as for the neutralized Purex waste previously treated in this study;[2,3] that is to say, the processes for the removal of the fission products did not greatly increase the volume or solids content of the waste produced per ton of uranium processed. With these assumptions, adjustments in the costs of waste management are attributable to the reduced heat load and the reduced shielding requirements caused by fission product removal.

Costs of interim liquid storage were less for fission-product-depleted wastes because of the reduced amount of heat to be dissipated and because mild steel tanks could be used rather than stainless steel. These costs were about the same for 90%- and 99%-depleted wastes, ranging from 0.0011 to 0.0025 mill/kwhr (electrical); whereas, costs for acid Purex waste ranged from 0.0018 to 0.0069 mill/kwhr (electrical) for storage periods of 1 to 30 yr.

Pot calcination costs were the same for depleted wastes as for neutralized Purex waste, because these costs were not affected by heat removal considerations and the variations in shielding requirements had negligible effect on the costs. They varied from 0.0215 to 0.0113 mill/kwhr (electrical) for depleted wastes and from 0.0123 to 0.0081 mill/kwhr (electrical) for acid Purex from which no fission products had been removed.

Interim solids storage costs were less for depleted wastes than for calcined acid Purex for short storage periods (up to 3 yr), where cooling system costs were important; however, these costs were higher for depleted wastes for longer storage periods as their greater volume, resulting in more cylinders to be stored, became the predominating effect.

Both 90%- and 99%-depleted wastes could be shipped immediately after discharge from the calcination plant in the largest feasible shipping casks, which hold four 24-in.-diam cylinders. Acid Purex must be aged at least 11 yr before it can be shipped in this manner. Shipping costs were generally lower for acid Purex than for depleted wastes when 6- or 12-in.-diam cylinders were used; they were about the same when 24-in.-diam cylinders were used.[1] These costs fell in the range of 0.0005 to 0.005 mill/kwhr (electrical) for 1000-mile shipments.

Ultimate disposal costs of calcined wastes in a salt mine were roughly half as much for depleted wastes as for acid Purex: 3.7×10^{-3} to 5.6×10^{-3} mill/kwhr (electrical) for depleted wastes vs 6.7×10^{-3} to 13.2×10^{-3} mill/kwhr (electrical) for acid Purex. Removal of fission products would decrease the heat generation rate of the waste and thus allow closer spacing of the cylinders in the floor of the room. Spacing was controlled by the limiting salt temperature of 400°F,

rather than the limiting calcination temperature of 1650°F at the axis of the waste cylinder. Mine space requirements range from 2 to 6 acres/yr for acid Purex waste, 0.2 to 1.3 acres/yr for 90%-depleted waste, and 0.04 to 0.17 acre/yr for 99%-depleted waste. Minimum center-to-center spacings were assumed to be 2, 5.3, and 8 ft for 6-, 12-, and 24-in.-diam cylinders. Acid Purex waste in 24-in.-diam cylinders must age about 30 yr (minimum) before it can be placed in the salt formation; however, 6- and 12-in. cylinders filled with waste depleted of 99% of the fission products would be stored at the minimum spacing for all ages.

The term "total waste-management costs" is used here to mean the cost of disposal in a salt formation plus the costs of all necessary preliminary steps. The disposal cost is a function of the age at burial, diameter of the cylindrical container, and degree of fission product removal. Thus, total waste-management costs reflect these functions. In computing total costs, consideration was given to the minimum ages for calcination, shipment, and disposal in vessels of a given diameter, as determined by fission product heat-generation rates. In obtaining the total waste-management costs, the minimum cost of each step was used, subject to the various minimum age requirements.

Total waste-management cost for acid Purex decreased as age at burial increased; and at 30 yr, the upper limit used in the study, it was about 0.025 mill/kwhr (electrical) with both 12- and 24-in.-diam cylinders. Costs for depleted wastes were cheaper with 24-in.-diam vessels and not so strongly affected by age, falling in the range of 0.017 to 0.019 mill/kwhr (electrical) for both 90%- and 99%-depleted wastes aged 0.33 to 30 yr. Relatively little cost reduction (about 7%) is achieved by increasing the fraction of fission products removed from 90% to 99%.

A rather optimistic estimate of the amount to be gained in waste-management costs with removal of 90 to 99% of the fission products is about 0.006 mill/kwhr (electrical), which is equivalent to about $400 per metric ton of uranium processed. Thus the cost of managing wastes that contain only 1% of the fission products is 70% as much as the cost for wastes containing all the fission products, representing a saving of 30%. Because this saving is not nearly enough to pay for fission product separation, packaging, and disposal, such practices would not be carried out as part of a waste-management scheme, but would necessarily depend on a large and diverse market for fission products to pay the major portion of these costs.

TANK HAZARD STUDY

The previously reported hazard-evaluation study[7,8] of the storage of high-level radioactive waste in tanks has been resumed under a slightly different set of postulates. The primary difference between the present study and the earlier, incomplete study lies in the location of the hypothetical storage tanks. The site for the earlier investigation was dictated by a concomitant study of the economic aspects of tank storage and was specified to lie along the Ohio River between Cincinnati and Louisville. During the course of the study, the meager knowledge of the underlying geologic formations became a severe deterrent to the study of the underground movement of waste streams. The site for the present study is located in the ORNL area, as selected by the Project Hope Study Committee.[9] In addition to having the advantage of site specificity, the ORNL location permits a more thorough investigation of the atmospheric and hydrospheric contamination problems because detailed knowledge of the local environment has developed during years of extensive study. Other than its relative inaccessibility, the ORNL location presents no obvious characteristic which would eliminate its selection for such a facility; conversely, because of its favorable soil structure, ORNL would be rather well suited for a tank-farm site.

ACTIVITY DISTRIBUTION

Essentially the same basis as that used previously has been assumed in this study: that is, a facility that can process 6 metric tons of fuel

[7] L. C. Emerson, *Health Phys. Div. Ann. Progr. Rept. July 31, 1959*, ORNL-2806, pp 106–17.

[8] L. C. Emerson, *Health Phys. Div. Ann. Progr. Rept. July 31, 1961*, ORNL-3189, pp 72–76.

[9] *Project Hope, A Chemical Reprocessing Plant for a Nuclear Power Economy*, ORNL-1638 (Jan. 21, 1954).

per day – 1500 metric tons of uranium converter fuel per year at a burnup of 10^4 Mwd/metric ton and 270 metric tons of thorium converter fuel per year at a burnup of 2×10^4 Mwd/metric ton.

The method for determining activity concentrations has already been described.[7] Although the size of the tanks cannot be determined until the correlative engineering and economic evaluation is complete, it was necessary to select a specific tank size in order to establish a definite filling time (5.33 yr). For this purpose the previously used tank capacity of 400,000 gal was chosen. Actually, this capacity is in the range of tank capacities being considered in this evaluation of the interim storage of liquid waste.

Figure 7.1 shows the initial activity levels (at the time of filling) of fission products and transuranics and how these activity levels change with time. These calculations show the following: Of the 4×10^9 curies in the tank at the time of filling, about 14% is due to the strontium and its daughter products and 13% is due to the Cs^{137} chain. It is expected that these fission products will largely determine the extent of hazard for the first several hundred years. Fifty percent of the activity is due to the Ce^{144}-Pr^{144} combination, while the only other major contributor, Pm^{147}, accounts for 14% of the activity. The initial transuranic content is 1.2×10^6 curies, with the isotopes of americium contributing 52% of the transuranic activity. As found earlier, the combined activity of the transuranics is less than that due to the fission products, except for the interval between 400 and 20,000 yr in the storage period. For this study it was assumed that 99% of the plutonium is recovered from the spent fuel elements and therefore does not contribute materially to the waste tank activity.

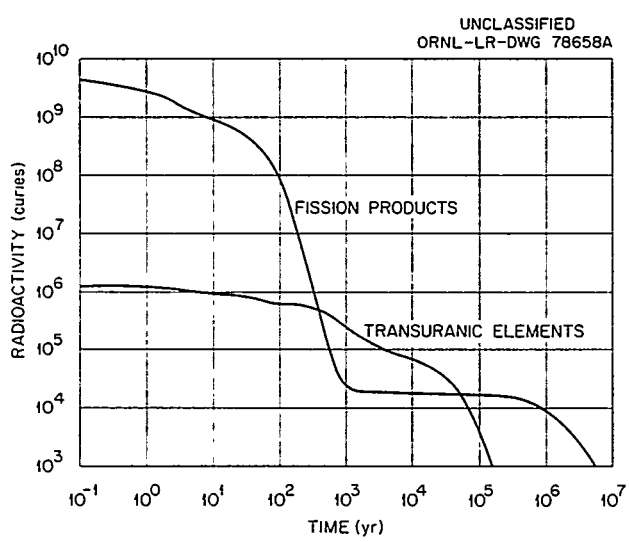

Fig. 7.1. Amounts of Radioactivity in Storage Tank as a Function of Time.

ATMOSPHERIC DISPERSION

The atmospheric contamination problem resulting from an assumed accidental release of fission products from the hypothetical tank storage facility has been analyzed with local meteorological parameters developed from a comprehensive study[10] of atmospheric conditions within the Oak Ridge area. The results of this study are to be used to estimate radiation doses to neighboring populations in a separate phase of this program. The events leading to the release, as well as the type and magnitude of the release, are still to be considered.

The results are incorporated in computer programs which accept as input the meteorological parameters and the coordinates of the downwind positions of interest and produce, from this, the downwind ground concentrations. The programs are flexible in that they allow for a wide range of input parameters. A continuous release and an instantaneous release are the two general cases that have been studied.

Although the radiation dose values cannot be obtained until some data are available regarding the magnitude and conditions of the assumed release, some features of the study may be seen by assuming a release of a unit amount of activity. For the continuous-release accident, 1 curie/sec was assumed to be released to the atmosphere. The resulting downwind concentrations in microcuries per cubic centimeter at ground level are shown in Fig. 7.2. For this case, typical daytime meteorological conditions were assumed. The wind direction chosen corresponds to the most frequent daytime direction for surface winds within

[10] *A Meteorological Survey of the Oak Ridge Area*, ORO-99, November 1953.

UNCLASSIFIED
ORNL—DWG 63—3926

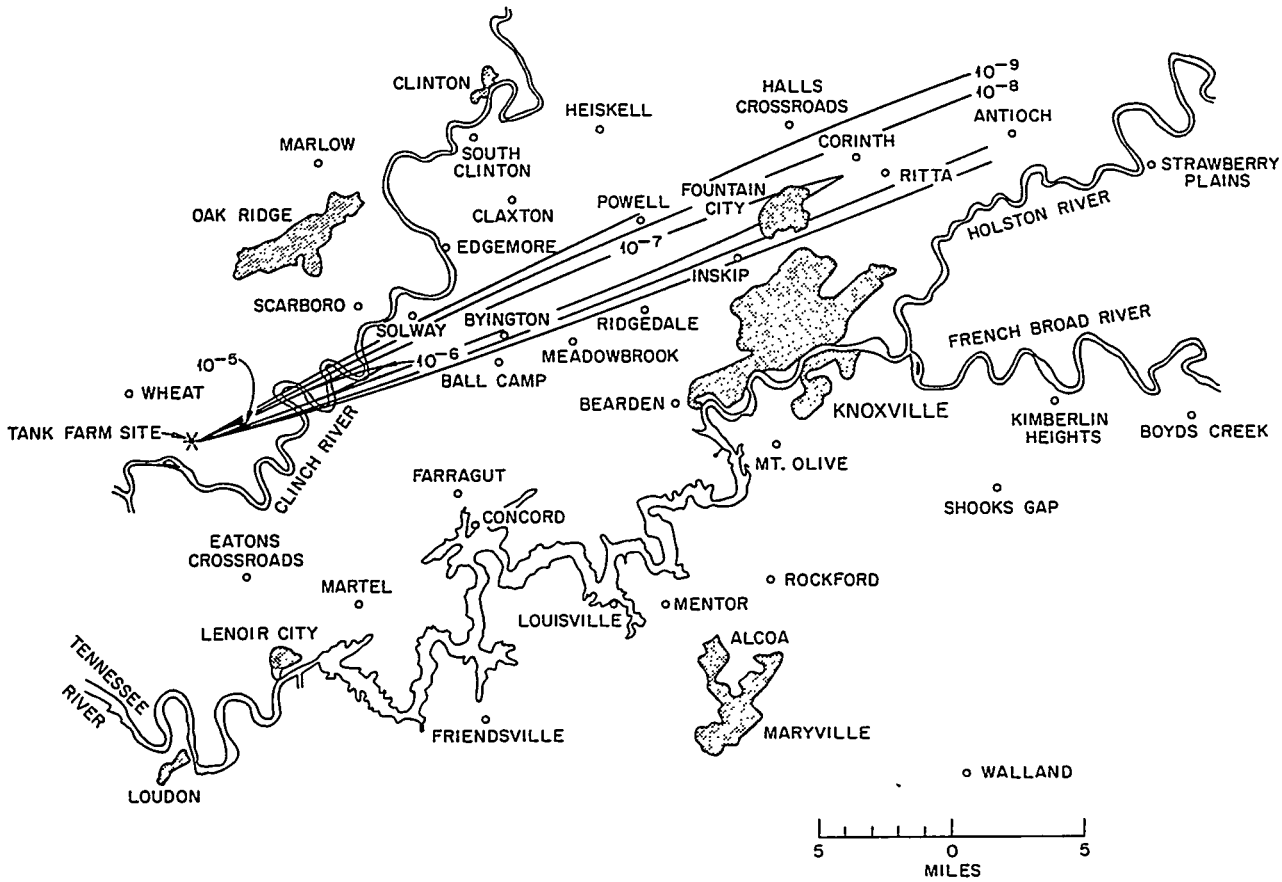

Fig. 7.2. Downwind Ground Concentration, Assuming a Continuous Unit Release per Unit of Time Under Typical Daytime Conditions.

the Southern Appalachian area. These concentrations do not take into account the removal of activity from the cloud by fallout or surface impaction. The patterns, in any real release, undoubtedly would be modified by the presence of the hill-and-valley type of terrain in the general vicinity of the hypothetical tank-farm site.

In Figs. 7.3 and 7.4, typical results are presented for the instantaneous release of 1 curie of activity at two downwind positions under daytime and nighttime weather conditions respectively. The effects of a relatively stable atmosphere are seen in Fig. 7.4 in the form of a small, but more highly concentrated, radioactive cloud.

The next phase of the study will be a consideration of the modifying effects of fallout and removal by rainfall and the radiation exposure doses resulting from this ground deposition.

Two other phases of this general problem are also being studied. The first of these is the hydrospheric contamination problem which would result from failure of the storage tank. Subsurface travel paths are being studied to determine expected rates and directions of activity movements. Of prime concern here are the possible high concentrations in the Clinch River system. The second phase is a study of the possible events leading to a release of activity from the storage facility. The principal aim is to determine the possible type and extent of tank failure and to describe the actual release in something more than qualitative terms.

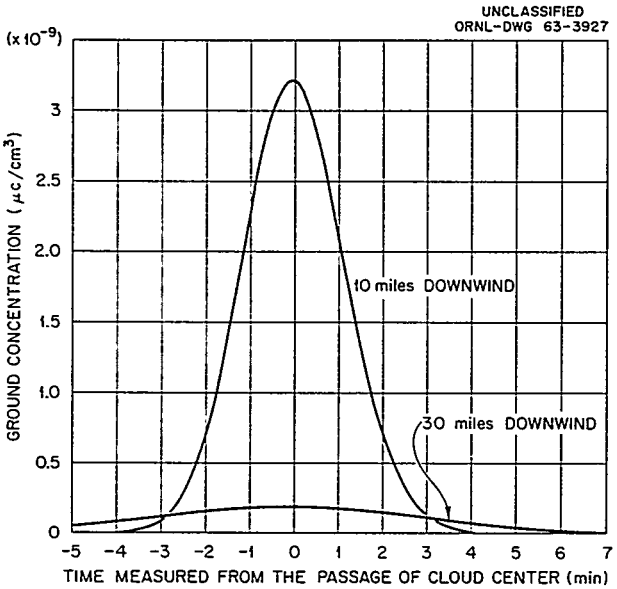

Fig. 7.3. Downwind Ground Concentration, Assuming an Instantaneous Release of Unit Amount Under Typical Daytime Conditions.

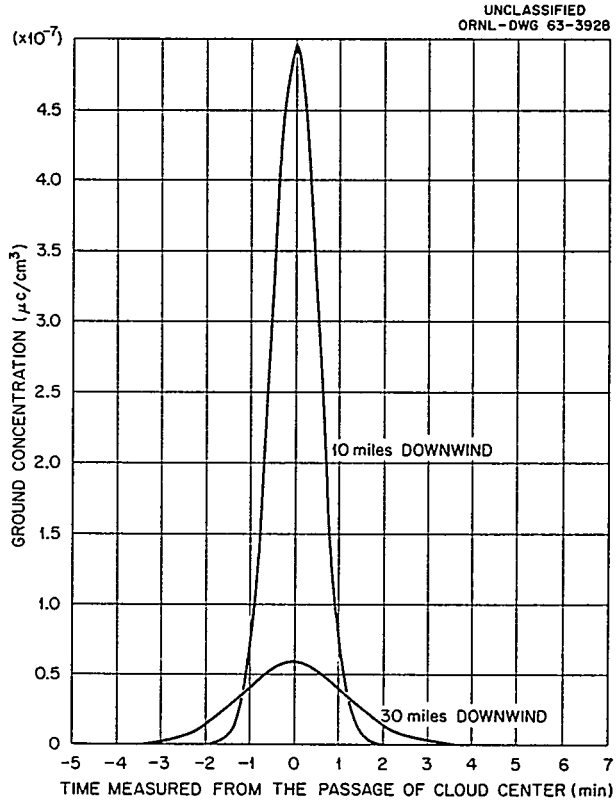

Fig. 7.4. Downwind Ground Concentration, Assuming an Instantaneous Release of Unit Amount Under Typical Nighttime Conditions.

8. Related Cooperative Projects

GEOLOGIC AND HYDROLOGIC STUDIES BY U.S. GEOLOGICAL SURVEY

The U.S. Geological Survey continued to operate 13 continuous-record gaging stations and a network of 24 partial-record base-flow and crest-stage gages. The partial-record stations are being used to obtain information on base-flow and flood characteristics in the area and for quality-of-water sampling.

Geologic mapping of White Oak Creek Basin for the purpose of relating the basin geology to the hydrology of the basin was completed in fiscal year 1963. The resulting map and an explanatory text are to be issued early in fiscal year 1964 as an interim report on the hydrology of White Oak Creek Basin. The geologic map will be accompanied by a generalized soils map of the White Oak Creek Basin and an explanatory text in which the locations of the general soil types will be shown

and the general soils characteristics and associations with geologic units will be described.

COOPERATION OF OTHER AGENCIES IN ORNL STUDIES

The research and development program of the Radioactive Waste Disposal Section of this Division is of special interest to various public and private agencies. Several study projects provide an opportunity for others to participate, both to supplement the Laboratory's research effort and to gain information and experience of value to the other agency. The ways in which another agency may cooperate include assignment of on-loan personnel as temporary additions to the ORNL staff, performance of specific work under cooperative agreements to augment ORNL programs, work authorized under ORNL subcontracts and performed by the contracting agency, or coordination of related work projects with ORNL projects for mutual benefit.

Clinch River Study

The Clinch River Study is a cooperative study under the guidance of the Clinch River Study Steering Committee, which coordinates arrangements for participation of the agencies represented by membership on the Committee. In addition to ORNL, these include the U.S. Geological Survey, the U.S. Public Health Service, the Tennessee Valley Authority, the Tennessee Department of Public Health and Stream Pollution Control Board, the Tennessee Game and Fish Commission, the Divisions of Reactor Development and Biology and Medicine of the U.S. Atomic Energy Commission, Washington, D.C., and the Biology Division of the U.S. Atomic Energy Commission, Oak Ridge Operations. The activities of the Steering Committee participation by the several agencies and the results during the past year are presented in a preceding section (see "Clinch River Study," Chap. 4, this report).

Disposal in Salt Formations

Agencies participating in this program during the past year have included the U.S. Bureau of Mines and the Carey Salt Company of Hutchinson, Kansas, an ORNL subcontractor. The results of this cooperative program are given in a preceding section (see "Disposal in Natural Salt Formations," Chap. 3, this report).

Disposal in Deep Wells

The subcommittee of the Committee on Research of the American Association of Petroleum Geologists continued its study of the deep sedimentary basins of the United States to identify those best suited for radioactive waste disposal. Cooperation between this group, the U.S. Geological Survey, and the Oak Ridge National Laboratory has been active but informal. Somewhat more formal collaboration has been developed between the Laboratory, the U.S. Geological Survey, the U.S. Bureau of Mines, and the University of California for the planning and eventual operation of certain field experiments and demonstrations in the disposal of liquid wastes into permeable formations. The U.S. Geological Survey and the U.S. Bureau of Mines are currently evaluating a site near Bartlesville, Oklahoma, for certain small-scale experiments on the injectivity of these wastes and on ion exchange phenomena under field conditions.

VISITING INVESTIGATORS FROM ABROAD

During the year, three "noncitizen guests" were on assignment as temporary members of the research staff of the Radioactive Waste Disposal Section. Pietro Giuliani of Italy determined the effects of the flow from Melton Hill Dam on the safety of operations at White Oak Creek Dam. Young Wook Kim of Korea worked on the effects of chelating agents on calcium-strontium exchange. Tohru Murano of Japan is continuing his studies of mechanisms of alumina sorption of strontium.

NUCLEAR SAFETY REVIEW

One member of the Section served on the staff of *Nuclear Safety* as assistant editor. During the year, several individuals in the Section contributed review articles which were published under the category "Consequences of Activity Release."

COMMITTEE WORK

American Standards Association

Several members of the staff of the Radioactive Waste Disposal Section have continued to serve on working groups of ASA Sectional Committee N5, "Nuclear Fuel Cycle Engineering," its Subcommittee N5.2, "Radioactive Waste Disposal," and Working Group N5.2.2, "Site Selection Criteria."

AEC Advisory Committee on Deep-Well Disposal

One staff member has served on the AEC Advisory Committee on Deep-Well Disposal. This committee is advising the AEC in the coordination of effort in the Deep-Well Disposal Program and is reviewing plans for engineering-scale field tests.

ASCE – Committee on Sanitary Engineering Aspects of Nuclear Energy

The Section leader served as a member of the Committee on Sanitary Engineering Aspects of Nuclear Energy of the American Society of Civil Engineers.

ORNL Committees and Special Working Groups

Two sanitary engineers of the staff have been designated to provide advisory service to engineering design groups regarding protection of the potable water supply of the Laboratory against "cross-over" contamination where it is necessary to lay water mains and waste pipes across one another or in close proximity. Upon request of the design engineers during the year, a number of designs have been reviewed and discussed in the preliminary stages, and final plans have been checked for approval of the methods of protection provided.

PARTICIPATION IN EDUCATIONAL PROGRAMS

The Section leader gave two 2-hr lectures in the AEC Fellowship Course in Applied Radiation Physics, conducted by the Education and Training Section of the Division at Vanderbilt University in Nashville, Tennessee. Also during the ten weeks of field training in this course at ORNL, two students were assigned to work five weeks in the Radioactive Waste Disposal Section under the supervision of two staff members.

In the Health Physics Course primarily for foreign students conducted by the Health Physics Division in the Oak Ridge School of Reactor Technology (ORSORT), four members of the Section gave six lectures and a field tour on radioactive waste problems and waste disposal studies at ORNL. Also, the course in physical geology conducted by ORSORT, given again by one member of the Radioactive Waste Disposal staff, comprised approximately 30 lectures to the class of about 40 students, some American and some from other countries.

Four lectures and a field tour of the Laboratory's waste disposal facilities and ecological research activities were provided at ORNL by the staff of the Section as part of the course conducted by the U.S. Public Health Service on "Reactor Safety and Environmental Health Problems," in September 1962 and May 1963.

Part II. Radiation Ecology

S. I. Auerbach

9. Radioactive Waste Area and Radiation Effects Studies

S. I. Auerbach
D. A. Crossley, Jr.
P. B. Dunaway
Margaret B. Heaslip[1]
S. V. Kaye
J. P. Witherspoon, Jr.
Regina M. Anderson
Cynthia L. Corley
Gladys J. Dodson
B. E. Jacobs
T. P. O'Farrell[2]
R. J. Pryor
J. C. Ritchie[2]
Lovell Lawrence
F. G. Taylor
W. L. Tietjen[2]

GLASS-ROD DOSIMETRY IN ENVIRONMENTAL STUDIES

J. P. Witherspoon, Jr. S. V. Kaye

In new dosimetry studies, miniature metaphosphate glass rods are being used to estimate absorbed dose in air and in the plants and soils of White Oak Lake bed. Combined beta and gamma doses in the top inch of mineral soil ranged from 20 to 25 rads/day on the northwest edge of the lake bed where Ru^{106} seepage from higher ground is appreciable. Absorbed doses in air at the surface of marsh plants (*Typha latifolia* L.) in this area ranged vertically from 6.2 rads/day at ground level to 2.8 rads/day at 5 ft above the ground. Absorbed doses in stem tissue of these plants were 23% higher due to absorbed radionuclides, principally Ru^{106}. The dose to root systems was three to seven times higher than the dose to shoot components.

These soil dose rates may be high enough to prohibit germination or seedling establishment of radiosensitive plants such as conifers. To test this hypothesis, potted scrub pine seedlings (three years of age) have been placed in this radiation field. These plants, placed on racks to prevent uptake of radionuclides from soil, are absorbing about 3 to 4 rads/day as measured by glass-rod dosimeters. Apical meristem tissue will be examined microscopically at intervals to determine initial indications of terminal growth retardation. Growth rates of these plants will then be compared with those of controls located off of White Oak Lake bed where radiation levels approach background.

[1]Visiting investigator, Morehead State College.
[2]Temporary summer employee.

PENNED-MAMMAL STUDY

P. B. Dunaway
S. V. Kaye
Lovell Lawrence
B. E. Jacobs
R. J. Pryor
Regina M. Anderson
F. G. Taylor
T. P. O'Farrell

The penned-mammal study is testing for effects of continuous low-level environmental radiation on the blood of wild small mammals that live in 100-m^2 pens on the upper White Oak Lake bed. The first phase of this study began in June 1962, when pairs of cotton rats (*Sigmodon hispidus*) were introduced into the pens on the lake bed and on an uncontaminated area, and was terminated in December 1962, when floods inundated the pens. Hematological procedures, radiation dosimetric techniques, and field techniques were described previously.[3]

Radioanalyses of Soil

Analyses of two composited soil samples (each composite made from nine cores) from each of the seven lake-bed pens show that the concentrations of Ru^{106} are greater than the concentrations of Cs^{137}, Co^{60}, and Sr^{90} combined (Table 9.1). The concentrations of Ru^{106} are greater, without exception, in the top inch of the soil than in the next 3 in. below the surface, whereas the concentrations of Cs^{137}, Co^{60}, and Sr^{90} in the top inch are usually about the same or less than the respective concentrations in the next 3 in. The greater overall concentration of Ru^{106} (relative to Cs^{137},

[3]S. I. Auerbach *et al.*, *Health Phys. Div. Ann. Progr. Rept. July 31, 1962*, ORNL-3347, p 47.

Table 9.1. Burden of Radionuclides in Soils of Pens on Upper White Oak Lake Bed

Each sample is a composite of nine cores from the intersects of a grid, June 1962.

Pen No.	Soil Layer (in.)	μμc per g of Oven-Dry Weight			
		Ru^{106}	Cs^{137}	Co^{60}	Sr^{90}
		$\times 10^2$	$\times 10^2$	$\times 10^2$	$\times 10^2$
11	0–1	1250	143	70	1.15
	1–4	818	256	95.0	2.97
12	0–1	2510	193	74.4	1.91
	1–4	957	227	43.4	1.88
13	0–1	1350	247	62.0	3.39
	1–4	670	228	86.3	2.30
14	0–1	2060	185	56.1	1.91
	1–4	1120	377	78.2	4.46
15	0–1	2470	197	76.0	2.06
	1–4	1360	348	96.6	4.59
16	0–1	2220	106	80.0	2.49
	1–4	979	283	88.1	4.54
17	0–1	600	45.4	33.2	1.51
	1–4	168	22.1	12.2	1.26

Co^{60}, and Sr^{90}) and its greater concentration in the top inch of soil are attributable to the deposition of Ru^{106} from the east seep of the intermediate-level waste pits.[4] The distribution of the other radionuclides is due mostly to original lake sediments and only in part to the intermediate-level waste seeps.

Radioanalyses of Plants

Concentrations of Ru^{106}, Cs^{137}, and Co^{60} in the plants in the pens generally were considerably less than the burdens of these radionuclides in the soil, but concentrations of Sr^{90} in the soils and plants were essentially the same (compare Tables 9.1 and 9.2). The data for Cs^{137} and Sr^{90} agree well with previous findings for soil and plants on White Oak Lake bed.[3,5]

Tussocks of fescue (*Festuca* sp.) from the lake bed were sodded into each of the lake-bed pens before the experiment was begun in order to improve the food supply and cover for the cotton rats. Observations showed that fescue stems were an important food plant for the rats. Care was exercised as much as possible to take clumps from near the pens into which the fescue was transplanted, but it was necessary to take a considerable amount of fescue from near the seep drainage to place in pen 16, which may account for the high concentration of Ru^{106} in the fescue of that pen. Smartweed (*Polygonum* spp.) and aster (*Aster* sp.) were abundant in five of the seven pens; in each case the burdens of Ru^{106} and Sr^{90} were greater in *Polygonum*, but the concentrations of Cs^{137} were consistently greater in *Aster*. The differences in concentrations of Sr^{90} and Ru^{106} between these two plant species may be a reflection of the moisture in the soil in which these plants grew. Smartweed is more hydrophytic than aster. The high values for Sr^{90} in jewelweed (*Impatiens* sp.) and goldenrod (*Solidago* sp.) may be an indication

[4] E. G. Struxness *et al.*, *Health Phys. Div. Ann. Progr. Rept. July 31, 1962*, ORNL-3347, p 30.

[5] S. I. Auerbach *et al.*, *Health Phys. Div. Ann. Progr. Rept. July 31, 1959*, ORNL-2806, p 18.

Table 9.2. Uptake of Radionuclides by Plants Growing in Pens on Upper White Oak Lake Bed, June 1962

Pen No.	Plant Genus	μμc per g of Oven-Dry Weight			
		Ru^{106}	Cs^{137}	Co^{60}	Sr^{90}
		$\times 10^2$	$\times 10^2$	$\times 10^2$	$\times 10^2$
11	*Festuca*	32.8	1.61	1.42	0.38
	Festuca (stems)	17.9	1.36	1.08	0.34
	Polygonum	81.9	2.85	6.20	1.33
	Eupatorium	40.8	1.50	1.99	0.38
	Rumex	54.4	1.83	3.42	2.05
12	*Festuca*	29.7	3.55	1.27	0.92
	Festuca (stems)	18.0	1.97	1.05	0.37
	Polygonum	113	4.52	8.64	2.20
	Eupatorium	31.6	2.70	1.88	1.31
	Aster	44.7	9.04	1.42	0.91
13	*Festuca*	24.7	2.46	1.2	1.04
	Festuca (stems)	53.9	2.35	2.25	0.48
	Polygonum	98.1	4.92	7.64	2.18
	Impatiens	34.7	2.05	2.06	5.99
	Aster	32.5	17.6	1.40	1.10
14	*Festuca*	64.8	2.99	2.57	0.99
	Festuca (stems)	33.6	1.98	1.88	0.52
	Polygonum	189	3.79	1.58	1.28
	Aster	77.8	9.56	3.26	0.76
15	*Festuca*	31.5	2.86	2.05	0.38
	Festuca (stems)	43.1	1.63	2.64	0.14
	Polygonum	230	4.67	15.2	1.55
	Aster	78.2	11.9	2.42	0.64
16	*Festuca*	855	3.00	3.05	0.52
	Festuca (stems)	131	3.99	5.07	0.30
	Polygonum	234	5.58	1.68	1.18
	Aster	94.9	7.88	3.09	0.59
17	*Festuca*	56.8	1.36	2.19	1.20
	Festuca (stems)	15.0	0.67	2.22	0.75
	Solidago	27.8	14.7	13.7	4.18
	Juncus	17.3	2.02	5.11	0.93
	Aster	148	13.4	5.76	1.35

of edaphic conditions rather than an indication that these plants are "accumulators" per se.

Radioanalyses of Cotton-Rat Tissues

Almost all of the radioanalyses of rat tissues have been completed, but the data processing is in its early stages. Even at this point, the following conclusions seem justified: (1) the concentrations of radionuclides in tissues are positively correlated with the corresponding concentrations in stomach contents and plants; (2) concentrations of radionuclides in tissues are not correlated with corresponding concentrations in soil; (3) Sr^{90} in femurs is the only radionuclide in the tissues which was in greater concentration than in food or

plants; and (4) placental and mammary barriers apparently were effective in reducing the concentration of Sr^{90} in fetuses and nursing young. Analyses of these data are continuing, and a detailed report is planned.

Glass-Rod Dosimetry

Silver-activated metaphosphate glass microdosimeters were utilized to estimate doses accumulated by the cotton rats in the 100-m^2 enclosures. Two of these dosimeters were inserted subcutaneously (one dorsally and one ventrally) in each of the adult rats placed in the pens and in each of the rats born in the pens and caught after leaving the nest. The dosimeters and implantation techniques have been described elsewhere.[6] Rods were usually removed every six to twelve weeks and new ones inserted. This exchange of rods permitted evaluation of dose during different intervals of the experiment.

Data from 38 cotton rats which had accumulated a total of 2681 dosimeter-exposure days are shown in Fig. 9.1. The straight lines were fitted to the points by the least-squares method utilizing reciprocal variance weight factors. The lines have been extrapolated from the first point (August) to the beginning date of the experiment (15 June). This extrapolation comes close to the point plotted for the beginning date of the experiment, which was obtained by exposing dosimeters in each of the pens for four days prior to the start of the experiment. Exposure conditions of the ventral dosimeters under the skin of live rats were simulated in this prerelease experiment by placing the rods 3 cm above the soil surface and using 1 mm of plastic between the rods and the soil to simulate shielding by skin. The largest source of error in this method is obviously the lack of integration over the area of the pen as occurs when the dosimeters are carried by live animals.

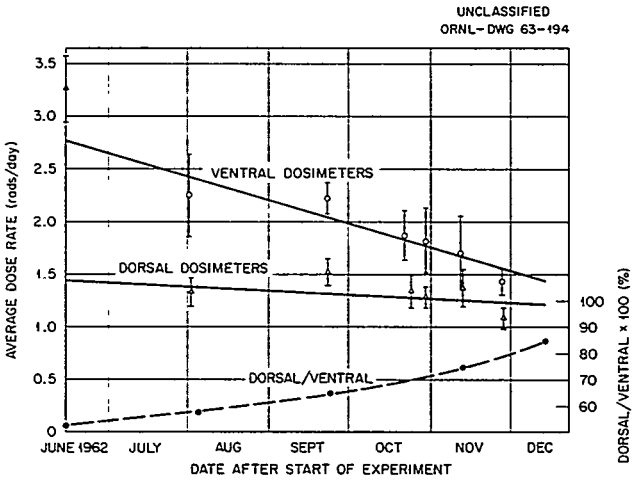

Fig. 9.1. Average Absorbed Dose Rate for 38 Cotton Rats (*Sigmodon hispidus*) on the Radioactive White Oak Lake Bed.

If the ratio of the dorsal dose rate to the ventral dose rate for any given value of the independent variable were constant, then the differences in dose rate would be due solely to tissue absorption and distance from the source. Conversely, Fig. 9.1 shows that this ratio increases from summer to winter. The phenomena of decreasing dose rate and an increasing ratio of dorsal dose rate to ventral dose rate are attributable to seasonal changes in the water table of White Oak Lake bed. A high water table reduces low-energy radiation and thus reduces the dose rate above the soil surface, whereas a low water table does not affect the energy spectrum or dose rate. During the summer months the mean water table is at its maximum depth (~3 ft) below soil surface, and it gradually rises until it reaches the soil surface in winter. This rising water table is chiefly a result of increased rainfall and reductions in evaporation and transpiration by herbaceous vegetation.

A certain fraction of the dose absorbed by the fluorods implanted in the rats was from gamma-emitting radionuclides in the tissues; however, this contribution is minute because the concentrations of radionuclides in the soil of the lake bed are usually about two orders of magnitude higher than the concentrations in the body (excepting Sr^{90}). The doses from internal beta-emitting radionuclides will be calculated, as done in the past, after the tissues have been radioassayed.[7]

Hematology of Cotton Rats

Blood samples were taken from the original cotton rats one week before release into the pens and thereafter during trapping periods about 2, 6,

[6] P. B. Dunaway and S. V. Kaye, "Effects of Radiation on Mammalian Population Dynamics," to be published in the *Proceedings of the First International Conference on Wildlife Disease.*

[7] S. V. Kaye and P. B. Dunaway, *Health Phys.* 7, 205–17 (1962).

10, and 16 weeks postrelease. Blood samples from the cotton rats born in the pens also were taken until flooding of the lake-bed pens terminated the experiment in mid-December. Hematological measurements included total counts for erythrocytes and leucocytes, leucocyte differential counts,[8] hematocrits, mean corpuscular volumes, cell-volume distributions, and total serum solids.

The numbers of erythrocytes for the original cotton rats on both the lake bed and the uncontaminated areas decreased from the prerelease sampling to the two-week postrelease sampling, after which the RBC count did not change appreciably (Fig. 9.2, plot A). The hematocrit percentages (Fig. 9.2, plot C) also reflect this initial decrease in erythrocyte numbers, because it was found that cell-size distributions did not change during the entire experiment. The numbers of RBC in the cotton rats born in the pens increased until the animals were about one month old, after which the RBC numbers were about the same as the numbers for the original animals (Fig. 9.2, plot B). The hematocrit percentages again parallel the RBC count (Fig. 9.2, plot D). The numbers of erythrocytes and hematocrits were greater in male than in female cotton rats (Fig. 9.3) in contrast to reports by others that these values are not different in the sexes of laboratory rodents.[9]

Differential counts for the original rats show that the segmented granulocytes increased by two

[8]We wish to acknowledge the help of Bobby S. Joslin, Health Division, in performing these leucocyte differential counts.

[9]M. M. Wintrobe, *Clinical Hematology*, 5th ed., p 107, Lea and Febiger, Philadelphia, 1961.

UNCLASSIFIED
ORNL-DWG 63-1986

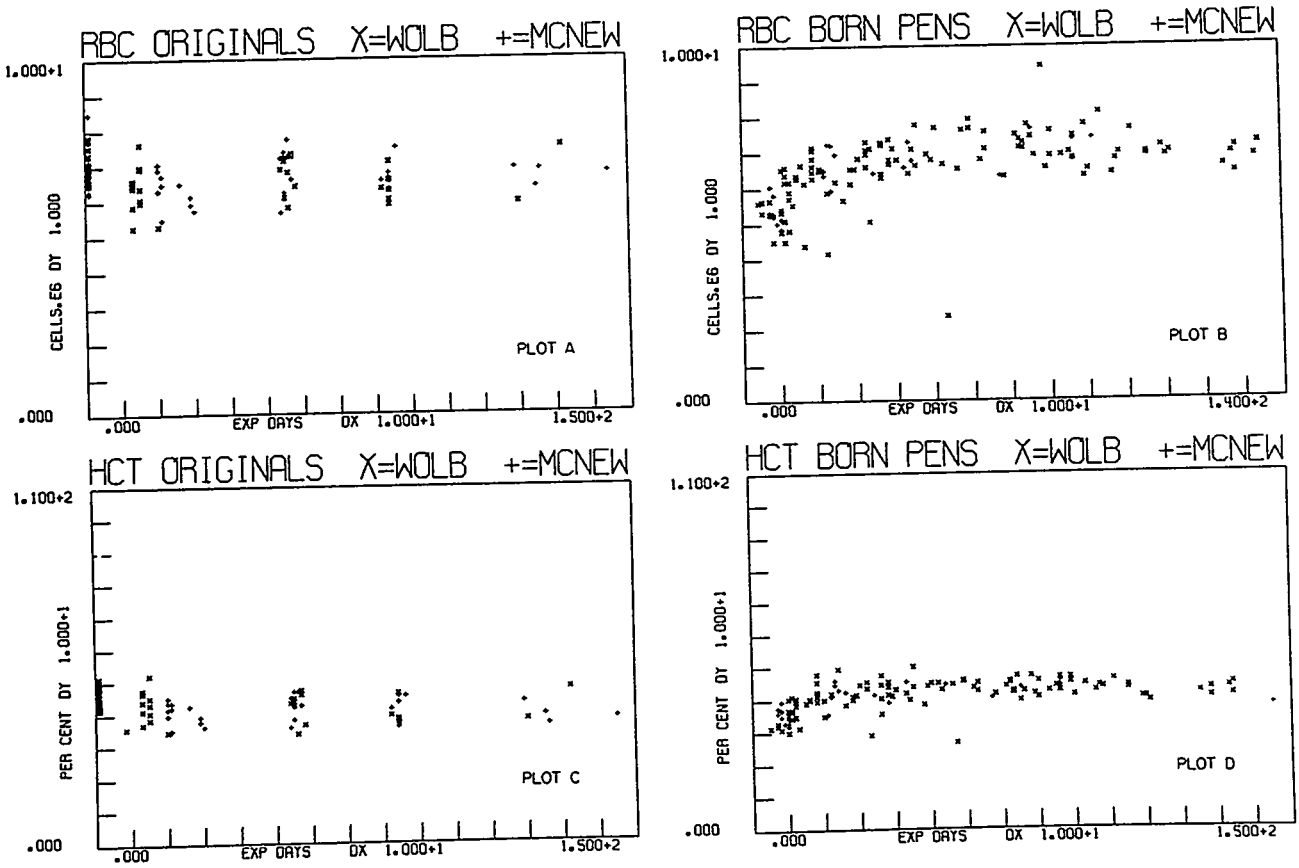

Fig. 9.2. Computer Output Plots for Erythrocyte Counts and Hematocrit Percentages for Cotton Rats in Pens. Plot A, erythrocyte counts for original animals; plot B, erythrocyte counts for offspring born in the pens; plot C, hematocrit percentages for original animals; plot D, hematocrit percentages for offspring born in the pens.

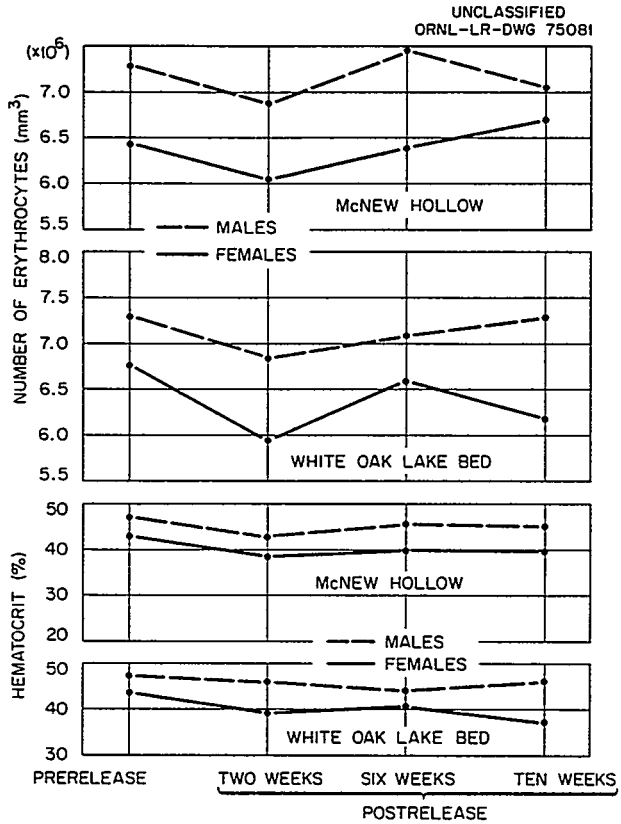

Fig. 9.3. Comparison of Erythrocyte Numbers and Hematocrits of Adult Male and Female Cotton Rats in Pens on McNew Hollow and White Oak Lake Bed Areas.

weeks but began to decrease by ten weeks (Fig. 9.4, plot C). Conversely, Fig. 9.4, plot A, shows that the lymphocytes decreased by two weeks but increased by ten weeks. The number of segmented granulocytes seemed to increase with age in the rats born in the pens (Fig. 9.4, plot D), and the number of lymphocytes seemed to decrease with age (Fig. 9.4, plot B). A decrease in granulocytes and an increase in lymphocytes appear to have occurred after approximately 130 days, but these changes may have been more related to environmental factors than to age.

Erythrocyte size distribution curves (plotted with a Coulter electronic counter) for the cotton rats placed in the pens are virtually identical regardless of sampling period. The erythrocyte-size distribution curves for the rats born in the pens have not been analyzed completely, but it appears from preliminary information that the curves for the adults are essentially the same as for the rats originally placed in the pens. The curves for the young animals differ only in that the curves are not as high because the cell count is not as high in the adults. The mean erythrocyte volume in all cotton rats was about 63 μ^3. The conclusion that can be drawn from the size-distribution data for the penned cotton rats is that cell volume is very constant regardless of animal age and environmental factors, including the low-level continuous radiation. The size distribution curves for leucocytes varied as expected in relation to the changes in numbers of the various cell types. The distribution curves for the leucocytes of these animals before release peaked in the electronic counter channels in which lymphocytes are counted, and in subsequent periods the peaks occurred in the channels in which granulocytes are counted. Thus, the electronic cell-size distribution curves for leucocytes substantiate the microscope differential counts that show segmented granulocytes to be more numerous than lymphocytes in the rats that lived in the pens, although lymphocytes were more numerous than granulocytes in these animals when confined in cages before release into the pens.

Conclusions

Effects of ionizing radiation were not apparent in the blood of the cotton rats that lived in the pens on White Oak Lake bed. Hematological effects have been reported for laboratory rodents at comparable doses.[10–12] It may be that some wild species of rodents are more radioresistant than laboratory rodents. A large amount of biological data accumulated over the past five years at ORNL strongly supports this statement. Studies on wild-mammal populations were begun on White Oak Lake bed shortly after the lake bed became inhabitable following drainage. Although these investigations lasted several years and included studies of many generations of rodents reared in a radioactive environment, no unequivocal biological effects from radiation were demonstrated.[7,13,14]

[10] P. S. Henshaw, *J. Natl. Cancer Inst.* 4, 513 (1944).

[11] P. N. Kiselev and P. A. Buzini, *Med. Radiology* 4, 36 (1959).

[12] E. N. Kapylova, *Dokl. Akad. Nauk SSSR* 124, 930 (1959).

[13] P. B. Dunaway and S. V. Kaye, *Trans. 26th N. Am. Wildlife and Natl. Res. Conf.* 167–85 (1961).

[14] P. B. Dunaway and S. V. Kaye, pp 333–38 in *Proceedings of the First National Symposium on Radioecology* (ed. by Vincent Schultz and A. W. Klement, Jr.), Reinhold, New York, 1963.

UNCLASSIFIED
ORNL-DWG 63-1069

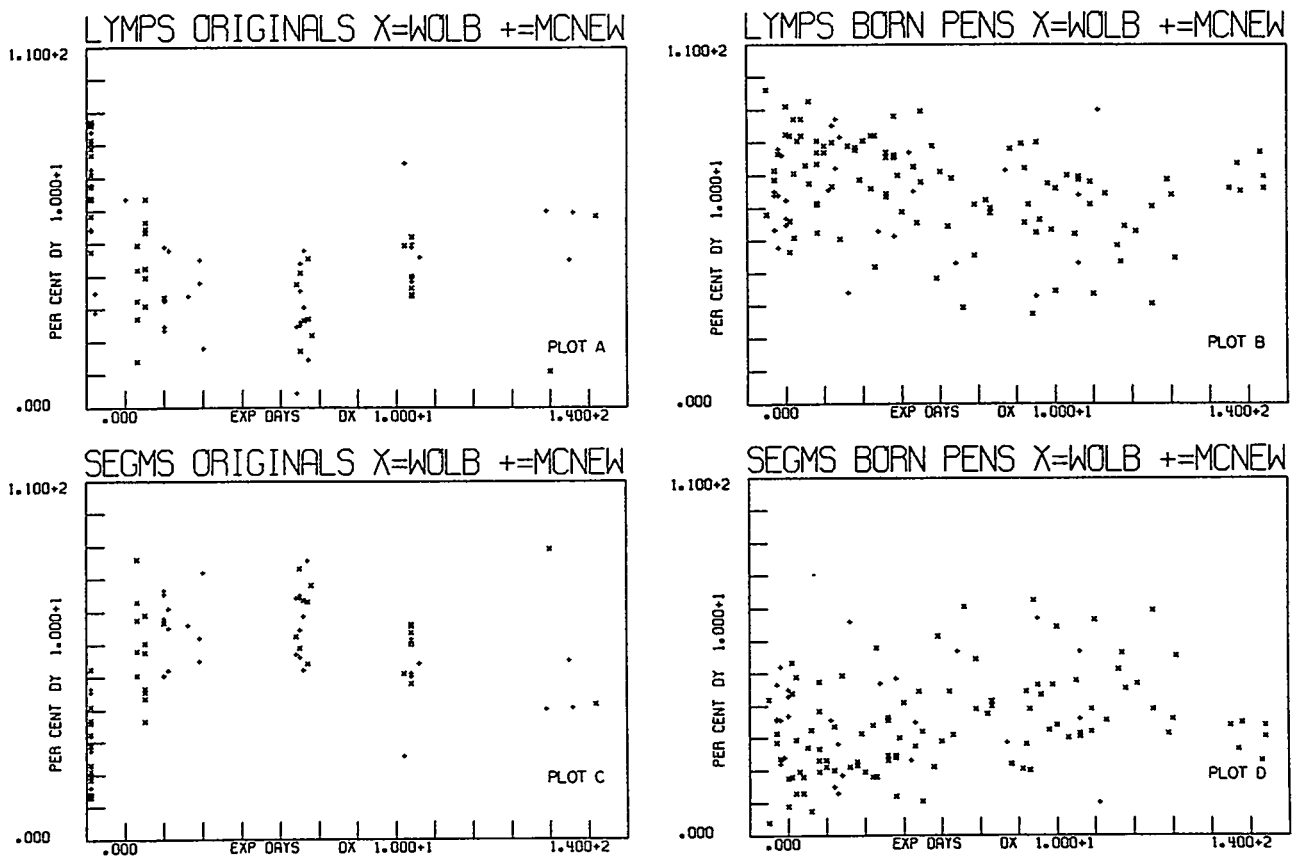

Fig. 9.4. Computer Output Plots for Lymphocyte and Segmented Granulocyte Percentages for Cotton Rats in Pens. Plot A, lymphocyte percentages for original cotton rats; plot B, lymphocyte percentages for offspring born in the pens; plot C, segmented granulocyte percentages for original cotton rats; plot D, segmented granulocyte percentages for offspring born in the pens.

In addition, a recent laboratory irradiation study with wild cotton rats failed to show any hematological effects at 5 r/day.[15] A small-scale preliminary study with acute radiation doses indicated that the $LD_{50/30}$ for the cotton rats was probably close to 1300 r.[16] The apparent radioresistance of wild rodents such as cotton rats, relative to laboratory rats, may be a result of the greater adaptability and physiological readiness of the heterogenous wild species.

On the other hand, perhaps the effects of the environmental factors in the present experiment were of sufficient magnitude to mask any radiation effects that might have been present. The changes that occurred in the erythrocyte and leucocyte numbers when the rats were placed in the pens are good examples of the hematological changes that can result because of a change in environment. It is apparent that an unequivocal answer to the question of possibly much greater radioresistance in some of the wild rodents must be forthcoming. A definitive irradiation experiment is being designed using both laboratory rats and mice and wild rats and mice.

[15] C. L. Sanders, Jr., *Diverse Physiological Effects of Gamma Irradiation Stress in the Cotton Rat (Genus* Sigmodon), Masters thesis, 1962.

[16] C. L. Sanders, Jr., personal communication.

HEMATOLOGY OF NATIVE MAMMALS

P. B. Dunaway
Lovell Lawrence
S. V. Kaye
B. E. Jacobs
Regina M. Anderson
T. P. O'Farrell
F. G. Taylor
R. J. Pryor

The hematopoetic tissues of man, laboratory mammals, and domestic mammals are affected by a multitude of innate and environmental factors. Accordingly, studies of the blood of free-ranging native mammals are being done so that the changes caused by ionizing radiation can be distinguished from the changes that result from other environmental factors. An important discovery, discussed previously, was that the number of erythrocytes is inversely related to species size and that the mean erythrocyte volume is directly related to species size in the Cricetidae, a family of native rodents.[17] Additional work completed this year has demonstrated that this relation is present also in the rodent families Muridae and Sciuridae, the shrew family Soricidae, and the primate family Cebidae, but it appears that the relation is different for each family. Erythrocyte number and hematocrit percentages are greater in the males than in the females in the species of larger body weight within a taxonomic family. However, in some species in which females are heavier than males, it may be that erythrocyte number and hematocrits are greater in the females. For instance, in previous population studies[18] it was found that only in harvest mice (*Reithrodontomys humulis*) and pine mice (*Microtus pinetorum*) were the average weights of the females consistently greater than the average weights of the respective males. Of the species examined so far these were the only two species in which average erythrocyte number and hematocrits were greater in the females than in the males. Young mammals of various species had lower erythrocyte counts than adults of the same species.

Seasonal effects on the blood of native mammals are being followed because of variations noted in cell counts and hematocrits of the blood of mammals trapped during various seasons of last year. Erythrocyte counts and hematocrits, for instance, in some species seem to be higher in the winter than during other seasons. Controversy exists as to whether season, climate, and temperature affect blood. It is important that this question of seasonal effects be resolved, since seasonal effects, if they exist, must be separated from the effects of age, sex, and other factors.

Measurements of hemoglobin concentrations are now made routinely. The standard cyanmethemoglobin test is used presently, but a technique is being tested which utilizes the same blood dilution which is used to obtain total leucocyte counts. Should this technique prove successful, more efficient utilization of small quantities of blood will be possible, and the number of manipulations can be reduced.

[17] S. I. Auerbach *et al.*, *Health Phys. Div. Ann. Progr. Rept. July 31, 1962*, ORNL-3347, p 52.

[18] P. B. Dunaway and S. V. Kaye, unpublished data.

USE OF RADIOACTIVE TAGS TO EVALUATE MOVEMENTS OF WILD MAMMALS

T. P. O'Farrell
S. V. Kaye

Pine mice (*Microtus pinetorum*) were subcutaneously tagged with Co^{60}, Ta^{182}, and Au^{198} wires and their subsequent movements traced with a Geiger counter in a field being considered for intentional contamination with radioisotopes for radiation ecology studies. The objectives of the tagging study were (1) to contribute to the knowledge of the ecology of pine mice and (2) to determine the optimum in-soil depth of sheet-metal walls which would prevent escape of burrowing pine mice.

The periods of most activity occurred between 7 to 10 PM and 2 to 6 AM, thus indicating both nocturnal and crepuscular activity periods. Diurnal hours were usually spent in underground nesting chambers (5 to 7 in. below soil surface) which were seldom vacated. The vertical stratification of movements was as follows: above ground, 2%; 0 to 2.9 in., 1%; 3 to 5.9 in., 30%; 6 to 8.9 in., 65%; and 9 to 12 in., 2%. Besides the obvious photoperiod activity relation, evidence for a soil temperature-moisture influence on vertical subterranean movements was also apparent but not intensively investigated. If this field is fenced with sheet metal that extends 12 in. into the soil, almost 100% retention of burrowing pine mice would be expected.

DISTRIBUTION OF GAMMA-EMITTING NUCLIDES IN TREES BORDERING RADIOACTIVE WASTE PIT NO. 5

S. I. Auerbach J. C. Ritchie

Earlier studies of radionuclide distribution in trees around radioactive waste pits Nos. 2, 3, and 4 demonstrated the potential feasibility of using trees as long-term monitors of radionuclide behavior.[19,20] In FY 1961, a new type of covered waste pit (No. 5) was placed in operation.[21] This pit was constructed in a stand of pine (*Pinus echinata* and *Pinus virginiana*) planted in 1938. Care was taken during construction to minimize damage to ensure that the line of trees adjacent to the pit area was uniform.

Sampling of individual trees was carried out with the aid of a truck with a 50-ft boom (Fig. 9.5). Branches were collected randomly throughout the crown of selected trees, and these branches were then composited into a single sample for each tree. Trees were sampled in four basic rows which ran parallel to waste pit No. 5. Table 9.3 indicates the location of pit No. 5 in relation to the rows and trees. A total of 77 trees were sampled. Seventy-three trees were sampled inside of the waste-pit area, and four controls were sampled in the 7565 area, which is approximately 2 miles north of the waste-pit area. Trees No. 1 through 32 were sampled on July 16, 1962. Trees No. 31 through 60 were sampled on August 20, 1962; trees No. 61 through 77 were sampled on September 29, 1962.

Significant concentrations of four gamma-emitting radionuclides were found in these pine trees. These nuclides were Ru^{106}, Zr^{95}-Nb^{95}, Cs^{137}, and Ce^{144}. Concentration of Ce^{144} was between 100 and 200 $\mu\mu c$ per g of dry weight, which is the same as fallout levels. Cesium-137 concentration was uniform in all trees at 30 to 70 $\mu\mu c$ per g of dry weight. This amount could be attributed to blowout from three open pits which are due west of waste pit No. 5. Ruthenium-106 concentration varied from 0.02 μc per g of dry weight to fallout levels, which are 40 to 70 $\mu\mu c$ per g of dry weight. Twenty-three of the seventy-three trees collected showed a concentration of Ru^{106} greater than that which could be attributed to fallout or to blowout from the open pits. This higher concentration is attributed to seepage (and subsequent uptake by the tree) from waste pit No. 5. Five trees showed a concentration of Zr^{95}-Nb^{95} which was greater than fallout levels and also greater than Ru^{106} levels. The highest concentration of Zr^{95}-Nb^{95} was 771 $\mu\mu c$ per g of dry weight. Concentration of all the isotopes except Zr^{95}-Nb^{95} tended to be greater in needle material than in twig material.

Table 9.3. Location of Trees

Row No.	Distance from Pit No. 5	Tree No.
1	50 to 75 ft east	13, 15, 16, 18, 19, 20, 23, 26, 27, 28, 46 to 58
2	0 to 10 ft east	14, 17, 21, 22, 24, 25
3	50 to 100 ft west	1 to 12, 33 to 45
4	225 to 275 ft west	31, 32, 59, 60, 67 to 73
	50 ft south	29, 30
	150 ft southeast	61, 62, 63
	200 ft southeast	64, 65, 66

The distribution of "hot" trees (Fig. 9.6) indicates that there are three fingers of seepage away from the center of pit 5. One finger extends approximately 110 ft to the southwest of well 7. Finger 2 extends approximately 75 ft to the northwest around well 6. The third finger extends 75 ft to the northeast around wells 2 and 3.

Estimates of total tree burden of Ru^{106} and Zr^{95}-Nb^{95} were made for the trees which showed high concentration of Ru^{106} and/or Zr^{95}-Nb^{95}. The highest tree burden of Ru^{106} was 72.37 μc; 18.37 μc was the highest tree burden of Zr^{95}-Nb^{95}. Most trees showed a burden of less than 1 μc.

[19] S. I. Auerbach *et al.*, *Health Phys. Div. Ann. Progr. Rept. July 31, 1957*, ORNL-2384, pp 27–37.

[20] S. I. Auerbach *et al.*, *Health Phys. Div. Ann. Progr. Rept. July 31, 1958*, ORNL-2590, pp 41–48.

[21] K. E. Cowser and W. de Laguna, *Health Phys. Div. Ann. Progr. Rept. July 31, 1960*, ORNL-2994, pp 18–21.

Fig. 9.5. Sampling Even-Aged Pine Trees Growing Adjacent to Radioactive Waste Pit No. 5. This stand, planted in 1938, is composed of *Pinus echinata* and *Pinus virginiana*.

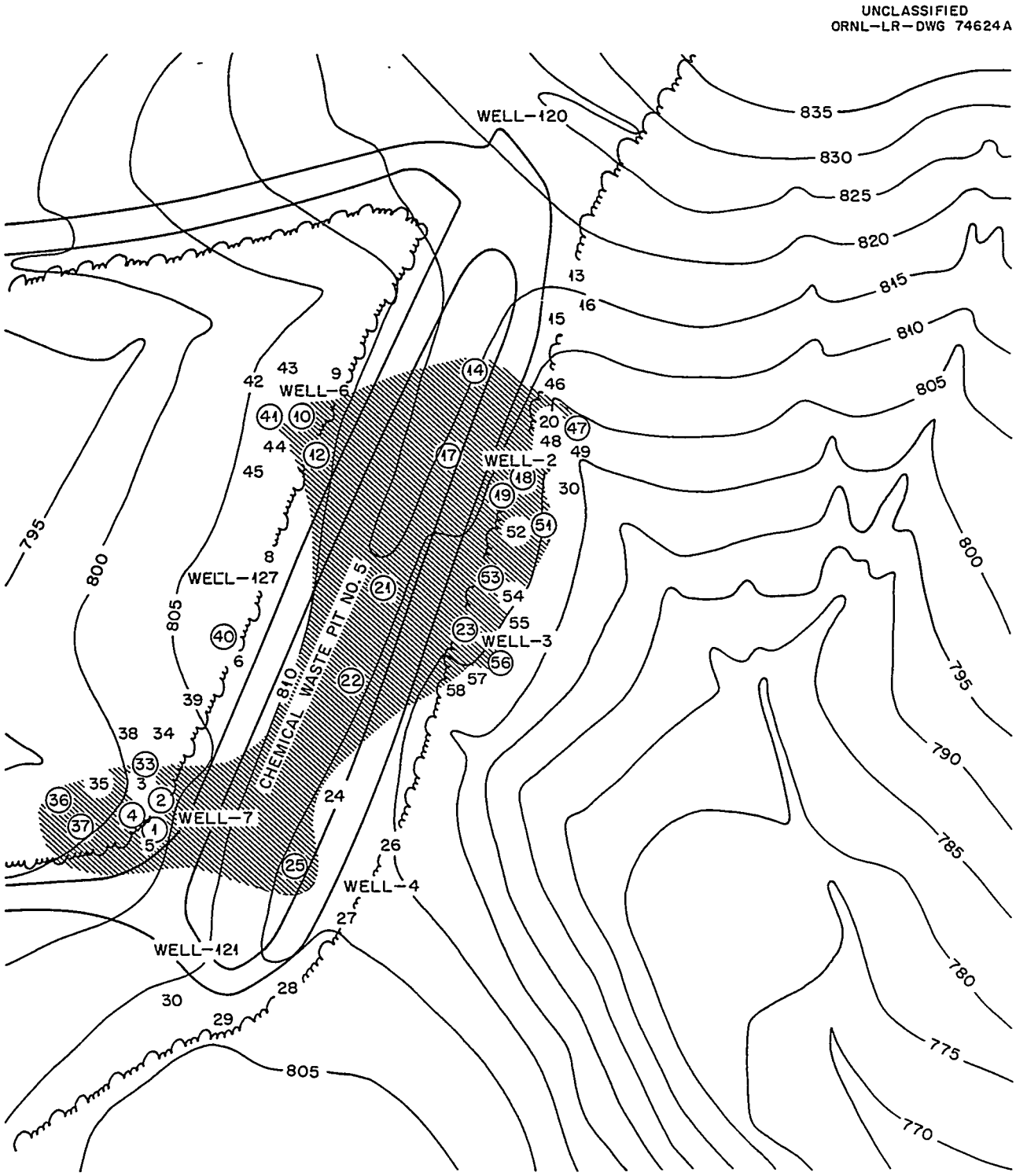

Fig. 9.6. Distribution of Ru^{106} and Zr^{95}-Nb^{95} in Pines Around Waste Pit No. 5 as of September 1962. Note three areas which indicate directional movement of wastes underground.

VEGETATION STUDIES AROUND THE HPRR

J. P. Witherspoon, Jr.

The Health Physics Research Reactor (HPRR) is surrounded by forest of the pine-hardwood type at distances varying from 30 to 300 ft. The vegetation will be subject to neutron and gamma radiation from this unshielded reactor. Doses of several thousand rads per year are anticipated for scattered saplings located within 10 m of the reactor building. Radiation-induced changes in growth rate and phenological behavior of some species are anticipated – particularly in the more radiosensitive conifers. Moreover, changes in the structure of the plant community may result from the differential radiosensitivity of species.

A grid reference system with 10- by 10-m grids has been laid out around the reactor. Woody, perennial species in these grids, 2400 m^2, have been mapped and records taken of their size and general vigor. Dominant trees in the overstory are shortleaf and scrub pine which have stem diameters up to 11 in. at breast height. The understory is composed mainly of hardwoods up to 6 in. in diameter. Pines represent 14.6% of the total number of trees; sassafras, 32.6%; dogwood, 21.0%; persimmon, 14.5%; black gum, 5.8%; red maple, 5.1%; sourwood, 3.6%; tulip poplar, 1.4%; and shrub sumac, 1.4%. Approximately 71% of the total basal area (61.5 ft^2/acre) of this forest is composed of pines.

Measurements of pine branch growth were made prior to reactor operation to establish normal growth patterns for conifers on this site. The amount of terminal growth (measured in October) was 7.0 ± 0.5 cm (mean ± standard error) for shortleaf pine and 7.9 ± 0.9 cm for scrub pine. Lateral branch growth was less, with 3.6 ± 0.2 cm for shortleaf and 3.3 ± 0.2 cm for scrub pine.

NEUTRON DOSIMETRY AND SEED IRRADIATION

J. P. Witherspoon, Jr. Margaret Heaslip

Fission foil threshold detectors were used to determine the fast-neutron dose absorbed by white oak acorns irradiated in the west animal tunnel of the ORNL Graphite Reactor. The acorns were irradiated in a 17 × 8 × 4.5 in. box of boron carbide–impregnated Lucite which absorbed thermal neutrons (over 50% of the total flux) but allowed fast neutrons to pass through the seed. Fission foils and pellets of S^{32} were placed under and on top of the sample to be irradiated – seed stacked to a depth of 4 in. After irradiation the foils and sulfur were counted immediately in the special fission foil counters of the Health Physics Division. Dose calculations were made according to the method of Hurst and Ritchie.[22] Table 9.4 gives the neutron-dose data determined in this experiment. The boron carbide–plastic box was effective in absorbing thermal neutrons as evidenced by the failure of the Au^{197} fission foil to detect energy in the thermal-neutron range. The dose, then, was primarily from fast neutrons. Some of these, however, were slowed down to thermal-neutron energy by the seed as evidenced by the detection of this energy range on top of the irradiated sample.

[22] G. S. Hurst and R. H. Ritchie (eds.), *Radiation Accidents: Dosimetric Aspects of Neutron and Gamma-Ray Exposures*, ORNL-2748A (Nov. 2, 1959).

Table 9.4. Neutron Dose to White Oak Acorns Irradiated in the ORNL Graphite Reactor

Detector	Minimum Energy Perceived (ev)	Flux (neutrons cm^{-2} sec^{-1})	Percent of Total Flux	Dose (rads/hr)	Percent of Total Dose
		Dose Under 4 in. of Acorns			
Au^{197}	2.5×10^{-2}	0	0	0	0
Pu^{239}	2.5×10^{4}	1.76×10^{8}	58.7	589.2	33.6
Np^{237}	7.5×10^{5}	8.09×10^{7}	27.0	678.6	38.7
U^{238}	1.5×10^{6}	3.08×10^{7}	10.3	331.2	18.8
S^{32}	2.5×10^{6}	1.20×10^{7}	4.0	156.8	8.9
Total		2.99×10^{8}	100.0	1755.8	100.0

Table 9.4 (continued)

Detector	Minimum Energy Perceived (ev)	Flux (neutrons cm^{-2} sec^{-1})	Percent of Total Flux	Dose (rads/hr)	Percent of Total Dose
		Dose Over 4 in. of Acorns			
Au^{197}		3.15×10^6	1.4	0.3	>0.1
Pu^{239}		1.26×10^8	58.0	423.6	33.9
Np^{237}		6.01×10^7	27.6	504.2	40.3
U^{238}		2.19×10^7	10.0	234.8	18.8
S^{32}		6.66×10^6	3.0	87.0	6.9
Total		2.17×10^8	100.0	1249.9	100.0

GAMMA-RAY DOSIMETRY IN Cs^{137}-TAGGED TULIP POPLAR

J. P. Witherspoon, Jr.

In tree-tagging experiments at ORNL, the principal objective has been to elucidate the cyclic and transfer phenomena associated with minerals in forest ecosystems. Vegetation-tagging experiments elsewhere have had various other objectives. In all these tagging experiments, the problem of internal radiation dose delivered to plants that contain radionuclides has hardly been approached. In an attempt to establish such dose information and investigate the possible use of dosimetry as a means of tracing radionuclide movement, metaphosphate glass-rod dosimeters were placed in root, trunk, and branch tissues of a Cs^{137}-inoculated tulip poplar tree. This tree, inoculated with 11.5 mc during May 1962, measures 15.5 cm in diameter at breast height and is 17 m in height. Dosimeters were placed in 2-mm-diam plastic tubes which were inserted into increment boring holes 5 mm in diameter. Two large lateral roots, four positions up the trunk, and two branches were monitored. From two to four glass rods were placed laterally in each monitoring position in holes bored to the center of each tissue. Thus, dose measurements were made in terms of lateral distribution of the radionuclide as well as vertical distribution from the roots to the crown.

Average values for gamma dose rate to tree components during part of the 1963 growing season are given in Fig. 9.7. These changes in dose rate over time reflect some of the physiological developments associated with transfers of minerals in the tree. The glass rods were inserted (March 18) before the tree leafed out. By the time of the first reading (March 29), the buds had opened and small leaves were present. The integrated dose to trunk (2.9 rads) and branches (1.7 rads) during this period was lower than the integrated dose to roots (4.9 rads), indicating the presence of larger amounts of Cs^{137} which overwintered in the root system. As the leaves developed, a net movement of Cs^{137} out of the root system into trunk and branches was evidenced by decreasing dose rate in the former and increasing dose rate in the latter. This method

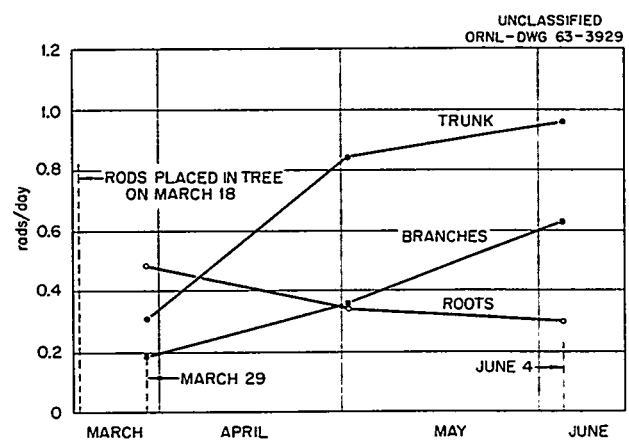

Fig. 9.7. Gamma Dose Rates in Components of a Cs^{137}-Tagged Tulip Poplar Tree.

of following radionuclide movement from one plant component to another is faster and easier than harvest-radioassay techniques. Also, it involves no destructive sampling of the material under investigation. Use of a radiosensitive tool, such as the glass-rod dosimeter, therefore appears to be a good method of establishing the time at which many transfers of radionuclides are made from one plant component to another.

Total dose delivered since March to tissues of this inoculated tree are below those believed necessary to produce visible morphological damage. The average integrated doses were 25.7 rads to roots, 59.9 rads to trunk, and 34.0 rads to branches. However, the developing seed of this species will have accumulated an appreciable gamma dose by time of maturity. Moreover, much of this total dose will have been delivered during critical, radiosensitive stages of development. Plans are in progress to compare germination and survival percentages of these inoculated tree seeds with those of control seeds collected from non-inoculated trees in the same area.

USE OF RADIOACTIVE TRACERS FOR ANALYSIS OF FOOD CHAINS

D. A. Crossley, Jr. Cynthia L. Corley
W. L. Tietjen

Radioactive tracer techniques are being developed to measure the movement of materials and energy along food chains. Previously reported work has dealt with analyses of plant-insect food chains on White Oak Lake bed.[23] The movement of Sr^{90} and Cs^{137} through food chains in that radioactive area and the total consumption of plants by insects and of herbivores by predators were estimated through application of laboratory work on biological half-lives. Current work has continued the development of techniques in which rates of accumulation and elimination of radioisotopes can be used to estimate such variables as feeding rates, metabolic rates, and productivity for the heterotrophic parts of food chains. These techniques will provide a means for assessing the movement of hazardous radionuclides in environmental systems. In addition these techniques offer new possibilities for basic ecological research on the nature and functioning of food chains.

During FY 1963, emphasis was placed on the use of biological half-lives for two different measurements, estimation of metabolic rates for arthropod populations and refinement of tracer techniques for estimation of food consumption.

For invertebrate animals, rates of metabolism are usually expressed as a function of temperature. In ecological studies the relation between respiration rate and temperature is first measured; then rates of metabolism can be inferred from temperature measurements in the environment.[24] The possibility that elimination rates for radioisotopes are a function of metabolic rates suggests the use of radioisotopes to make a more direct measure of metabolism in field situations and that laboratory measurements of metabolism might be made without confining animals in respirometers. Current research is measuring the influence of temperature on elimination rates. Figure 9.8 shows the retention of Cs^{137} by geometrid caterpillars maintained at two temperatures. The biological half-life was decreased by one-half for a 10° rise in temperature

[23] S. I. Auerbach *et al.*, *Health Phys. Div. Ann. Progr. Rept. July 31, 1962*, ORNL-3347, pp 47–48.

[24] A. L. Smalley, *Ecology* 41, 673–74 (1960).

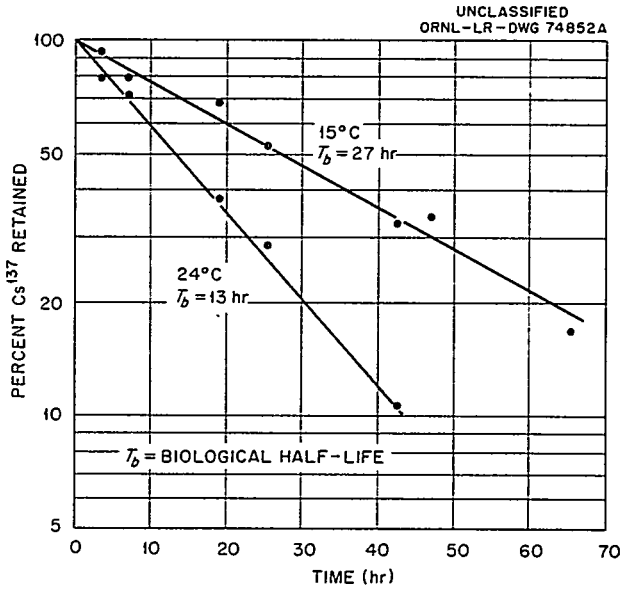

Fig. 9.8. Retention of Cs^{137} by Geometrid Larvae Maintained at Two Different Temperatures.

which suggests a Q_{10} of approximately 1 for this temperature range. Other studies of Cs^{137} elimination by third-instar larvae of *Chrysomela knabi* (a leaf beetle) maintained at 5, 15, and 25°C produced biological half-lives of 18, 9, and 7 hr respectively. Half-times for accumulation of Cs^{134} for *Chrysomela* larvae at these temperatures were estimated to be 20, 10, and 5 hr. Similar trends were found for Cs^{137}, Cs^{134}, and Co^{60} elimination by millipedes (*Dixidesmus erasus*) although multicomponent curves make evaluation more difficult. Also, estimation of elimination rates at temperatures lower than ambient was made more difficult in these experiments since arthropods were removed from controlled-environment chambers for counting. This occasional warming may have produced erroneous results in the 5 and 15° replicates, particularly for *Chrysomela*, where frequent measurements were required. These difficulties can be overcome by counting excretory products or discarded chambers rather than counting the animals themselves. An automatic frass collector now being tested will be helpful also.

These data offer abundant evidence of a relationship between elimination rate for some radioisotopes and environmental temperatures. Additional work now required includes simultaneous measurement of biological elimination and respiration, laboratory measurements under fluctuating temperatures, and field tests. The results should define the value of elimination rates for radioisotopes as a means of measuring metabolism in populations of animals.

The relation between temperature and rate of elimination for cesium evidently does not affect the validity of earlier work on White Oak Lake bed insects, although no allowances were made for temperature influences in those studies. Previous laboratory measurements on which the calculations for isotope transfer on the lake bed were based were made at temperatures between 21 and 24°C. This temperature range would include the mean environmental temperature found in studies of *Chrysomela knabi* on White Oak Lake bed, and for which excellent agreement was found between measured food consumption and estimates by radioisotope techniques. For work involving the entire insect community no correction seems indicated from present results, since laboratory studies were conducted at temperatures close to field averages.

---

10. Forest Studies

J. S. Olson
G. N. Brown
D. A. Crossley, Jr.
Martin Witkamp
H. D. Waller
J. P. Witherspoon, Jr.
Regina M. Anderson
W. C. Cate
Cynthia L. Corley
Gladys J. Dodson
Marilyn L. Frank
W. L. Tietjen[1]

COMPUTER FEEDBACK MODELS

J. S. Olson

Analog computer methodology reported in previous years has provided a useful basis for a review of the productivity parameters of ecosystems.[2] Recent models have included compartments for woody materials, as a step toward interpreting patterns of forest growth. The positive feedback representing increased photosynthetic rate with

[1] Temporary summer employee.

[2] J. S. Olson, "Gross and Net Production of Terrestrial Vegetation," paper presented at Jubilee Meeting of British Ecological Society, London, Mar. 13–Apr. 2, 1963, to be published in *Ecology*.

increased foliage mass is counteracted by opposing negative feedbacks representing not only the loss rates from respiration and other processes (litter fall, consumption, and translocation) but also a "limiting feedback" related to the capabilities of an area for producing organic matter. Diurnal and seasonal cycles of production have been combined in the same model. The brief time available for computer studies has limited the extension of earlier work simulating transfer of elements and isotopes, which depends on prior simulation of biomass changes.

A first step toward less restrictive scheduling of computers and toward larger-scale models has been the use of a digital computer program which proved adaptable to simulating ecological models in the same general way as the analog circuit, ECOS-A (Ecological Computer, Organizer, and Simulator). The program ran on the IBM 7090 monitor, reproducing numerical as well as point-graph output of simple models previously reported.[3,4]

[3]R. B. Neel and J. S. Olson, *Use of Analog Computers for Simulating the Movement of Isotopes in Ecological Systems*, ORNL-3172 (January 1962).

[4]J. S. Olson, "Analog Computer Models for Movement of Isotopes Through Ecosystems," pp 121–26 in *Radioecology*, ed. by V. Schultz and A. W. Klement, Reinhold, New York, 1963.

COMPONENTS OF FOREST LITTER FALL

J. S. Olson W. C. Cate
H. D. Waller Regina M. Anderson

In many ecosystems annual fall of needles and deciduous leaves approximately balances annual production, thereby providing one estimate of production, to complement mensurational studies of live plants. Twigs and other woody materials fall somewhat less regularly but represent a significant fraction of litter collected (in series of ten baskets) in four pine forests, three upland deciduous forests, and three lowland deciduous forests of the Oak Ridge Reservation (Table 10.1). Collected flowering parts and bud scales associated with them represent a fraction which should not be neglected, but which was only 2 to 3% of total litter fall in these forests.

Cumulative curves of litter fall over all or most of a two-year period (extended from earlier reports[5] broken down by individual forest stands) indicate surprisingly little variation between yearly averages for the three stand groups. The results thus provide an improved basis for estimating seasonal characteristics and magnitudes

[5]S. I. Auerbach *et al.*, *Health Phys. Div. Ann. Progr. Rept. July 31, 1961*, ORNL-3189, pp 109–11.

Table 10.1. Annual Fall of Forest Litter Components (g/m^2)

Material	Upland Pine 1960–61	Upland Pine 1961–62	Upland Oak-Hickory 1960–61	Upland Oak-Hickory 1961–62	Lowland Maple-Tulip-Gum 1960–61	Lowland Maple-Tulip-Gum 1961–62
Needles	280	292	11	12	27	17
Other leaves	69	101	369	327	392	407
Woody[a]	124	134	54	121	75	22
Flowering[b]	14	7	8	6	8	16
Total	487	534	442	466	502	462
Two-Year Means						
Foliage[a]	371		359		423	
Woody[b]	129		78		48.5	
Flowers[c]	10.5		7		12.5	
Total	510		444		484	

[a]Including needles and other leaves.
[b]Including nuts, cones, and other fruit.
[c]Including spring bud scales.

of loss rates from tree crowns in stands where concurrent studies[6,7] were concerned with the rates and agents of litter breakdown. These estimates start filling an important gap in data needed for models of deciduous forest systems.

Analyses of radioactive fallout of currently falling litter were made especially in the autumn of 1961; they promptly showed relatively large amounts of Zr^{95}-Nb^{95}, Ru^{106}, and Ce^{144}. Woody fractions, with smaller surface-to-volume ratios for collecting fresh fallout from Russian weapon tests, showed relatively more Cs^{137}, which had presumably been accumulating by stem flow for a much longer period.

RATES OF LITTER BREAKDOWN IN CONTRASTING CLIMATES

J. S. Olson W. C. Cate
H. D. Waller Regina M. Anderson

Further analyses of two- and three-year comparative experiments, in cooperation with the Botany Department of the University of Tennessee, showed different rates of breakdown for several kinds of deciduous leaves measured in the Oak Ridge Reservation and the Great Smoky Mountains. In all environments leaf species showed large and consistent differences in weight loss of leaves confined in bags of nylon net. Mulberry decayed rapidly to black humus, losing 0.002 to 0.0046 of its total weight per day in different environments. Beech showed the slowest visible signs of decay, with fractional weight losses of only 0.0003 to 0.0012/day. White oak, Shumard red oak, and sugar maple showed intermediate rates of weight loss and visible destruction. For any given leaf species, breakdown was more rapid in deciduous stands than in adjacent conifer stands (white oak vs shortleaf pine at 260 m above sea level, cover hardwood vs hemlock at 1040 m, and beech vs spruce at 1600 m). Differences between north and south slopes were small and inconsistent for various leaf species. Published results on first-year breakdown rates in 1959 showed a linear relation of average decomposition rate to elevations. However, 1960–61 results showed relatively slower decay at low elevations (probably due to frequent drying during the warm summers) and relatively faster decay at mid-elevations, where moisture, temperature, and organisms were favorable for decay. The fact that the years differ emphasizes the need for several-year experiments, with closely compared sets of techniques, for making generalizations about rates of ecological processes which affect the movement of nutrients or isotopes in contrasting environments.

[6]R. E. Shanks and J. S. Olson, *Science* 134(3473), 194–95 (1961).

[7]Martin Witkamp, "Microbial Populations of Leaf Litter in Relation to Environmental Conditions and Decomposition," *Ecology* 44(2), in press.

TRANSFER OF Co^{60} AND Ru^{106} FROM OAK AND ASH LEAVES TO SEVERAL FOREST SOILS

J. S. Olson H. D. Waller
W. C. Cate

Leaves of southern red oak (*Quercus falcata*) and white ash (*Fraxinus americana*), tagged with Co^{60} and Ru^{106}, were enclosed in 1-dm^2 bags of Fiberglas netting and exposed to natural weathering for two years in shortleaf pine, red maple, and white oak forests. Thin (2- to 3-cm) slabs of underlying soil (organic mor for pine forest, A_1 mull horizon for maple stand, and a combination of organic and mineral layers for oak forest) had previously been cut out of the forest floor and placed in plastic sandwich boxes with Fiberglas window-screen bottoms. Litter bags were placed on the slabs of underlying soil. Both bags and soil were dried, reweighed, and recounted at 0.5-, 1.0-, and 2.0-yr intervals.

Both leaf weight and radionuclide content decreased exponentially. The radionuclides lost by leaching were accounted for in the thin slabs of soil, indicating relatively slow leaching of both trace elements through several kinds of forest humus. Regression estimates of rates of loss from oak leaves in oak, maple, and pine forests in the first year (in percent per day) were: weight, 0.226, 0.156, and 0.197; Co^{60}, 0.350, 0.340, and 0.268; and Ru^{106}, 0.276, 0.162, and 0.246. Contrary to expectation, losses were slower for ash leaves: weight, 0.118, 0.086, and 0.103; Co^{60}, 0.201, 0.150, and 0.213; and Ru^{106}, 0.195, 0.064, and 0.131. These results and the data after two years indicate that cobalt, at least, disappeared faster than organic matter, in spite of the strong tendency for organic compounds to complex cobalt. Ruthenium-106 disappeared little faster, if at all, than did the litter. This indication of retention in dead organic materials contrasts with the rapid elimination of ruthenium from living organisms.

MICROBIOLOGY OF FOREST LITTER

Martin Witkamp Marilyn L. Frank

Microbial densities of the floor of hardwood and coniferous stands at three altitudes in the Smoky Mountains were reported last year. This year a second step was made toward a microbial inventory of the landscape by seasonal measurement of microbial populations of four leaf species and three contrasting forest types. Bacterial and fungal populations decreased on leaf species in the following order: mulberry, redbud, white oak, and pine. During decay of the litter, microbial populations of mulberry decreased, but those of pine and oak increased. Populations on redbud remained almost constant throughout the year. Growth rates of fungal mycelium increased throughout the year. In contrast to the fungal counts, mycelium growth was lowest on mulberry leaves and highest on pine needles.

Over the first year of decay, rates of microbial respiration and of loss of weight showed a highly significant correlation ($P = 0.01$) with the microbial populations, especially with bacteria. Seasonal fluctuations of microbial respiration were primarily correlated with temperature, but other significant ($P = 0.01$) correlations were found with bacterial counts, moisture content of the leaves, and age of the litter. The multiple regression for respiration as a function of these factors was

$$R = -46.50 + 3.22T + 26.86(M/D) + 11.39B - 17.92D, \quad (1)$$

where

R = respiration (μl of CO_2 per g per hr),
T = temperature (°C),
M/D = moist weight/dry weight of the litter,
B = bacterial count (10^5 bacteria per g),
D = number of days the litter has been decaying.

Measured and calculated respiration rates were well correlated ($R = 0.71$; number of samples = 198), as shown in Fig. 10.1. The positive relationship between rates of microbial respiration and turnover of radionuclides will enable prediction of turnover rates in different climates and on various substrates.

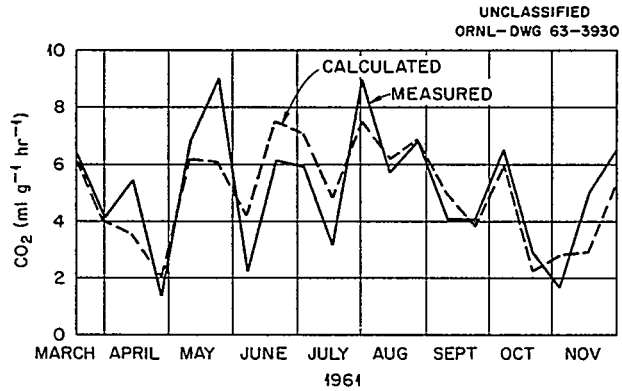

Fig. 10.1. Calculated (– –) and Measured (——) Respiration Rates of Redbud, Oak, and Pine Litter in the Three Stands for the Period March–December 1961.

In a third step in the microbiology of forest litter, microbial counts are being related to microbial mass. Knowledge of microbial mass in the forest floor is necessary to predict radionuclide contents of the microbial compartment of the forest floor. Fluorescence microscopy of soil suspensions showed that, with the exception of dark brown hyphal fragments of fungi, over 90% of the soil microbes (in direct counts) are alive. Thus it appears that permissible approximations for the measurement of microbial mass in soil can be obtained by using normal light microscopy.

GROSS EFFECTS OF ARTHROPODS AND MICROFLORA ON RATES OF LEAF LITTER BREAKDOWN

D. A. Crossley, Jr. Martin Witkamp
Gladys J. Dodson

The relationships between the minute arthropods and the microflora occurring in soils results in interactions which are responsible for the rates of breakdown and decay of fallen leaf litter. Microarthropods fragment the leaf material and mix it with soil, but bacteria and fungi are responsible for actual decay. In order that these different effects might be studied separately, an insecticide was used to reduce the arthropod populations in leaf litter, and the resulting changes in rate of weight loss and leachability of incorporated Cs^{134} were measured.

A previous report[8] gave preliminary results showing that the application of naphthalene at 100 g per m^2 of forest floor reduced the arthropod populations by approximately two orders of magnitude. Differences in rates of weight loss were reported, based on weekly measurements of litter bag weights. By the 35th week of the experiment in mid-summer, there was 15% less litter in control plots than in plots treated with 100 g naphthalene per m^2, as measured with litter bags. Also, bagged litter in treated plots retained twice as much Cs^{134} as did litter bags in control plots.

These trends were confirmed by continued measurements on the litter bags and by weights and counts taken at the completion of the experiment in mid-October 1962. Figure 10.2 compares weight loss and radiocesium loss by bagged leaf litter during the experiment. After 50 weeks about 55% of the original litter weight remained in bags in the plots treated with 100 g naphthalene, and about 40% of the litter weight remained in bags in the control plots. Percentages of Cs^{134} retained by bagged leaf litter in plots treated with 100 g naphthalene and in control plots were approximately 16% and 7.5% respectively (corrected for radioactive decay). Bags in plots receiving 35 g naphthalene per m^2 were intermediate; those in plots receiving 10 g per m^2 were not different from the controls.

In mid-October 1962, the total litter material was collected from all experimental plots and weighed in order to verify the results indicated from periodic weights of bagged litter. Newly fallen leaves were removed; and flowering parts, fruits, twigs, and pine needles were discarded. Table 10.2 shows values for remaining leaf litter in dry weight per m^2. Study areas receiving 10 g naphthalene were similar to the control areas and had mean weights of about 400 g litter per m^2. Plots receiving 35 g naphthalene had about 500 g litter per m^2, and replicates treated with 100 g naphthalene had 600 g litter per m^2. Differences in weights between 100 g replicates and controls would not be expected to correspond exactly to litter bag results since the unconfined litter consisted in part of two-year-old forest floor litter. Bags contained only year-old litter at the end of the experiment. The trends illustrated in Table 10.2 confirm the trends found in data based on bagged litter.

[8] S. I. Auerbach *et al.*, *Health Phys. Div. Ann. Progr. Rept. July 31, 1962*, ORNL-3347, pp 62–63.

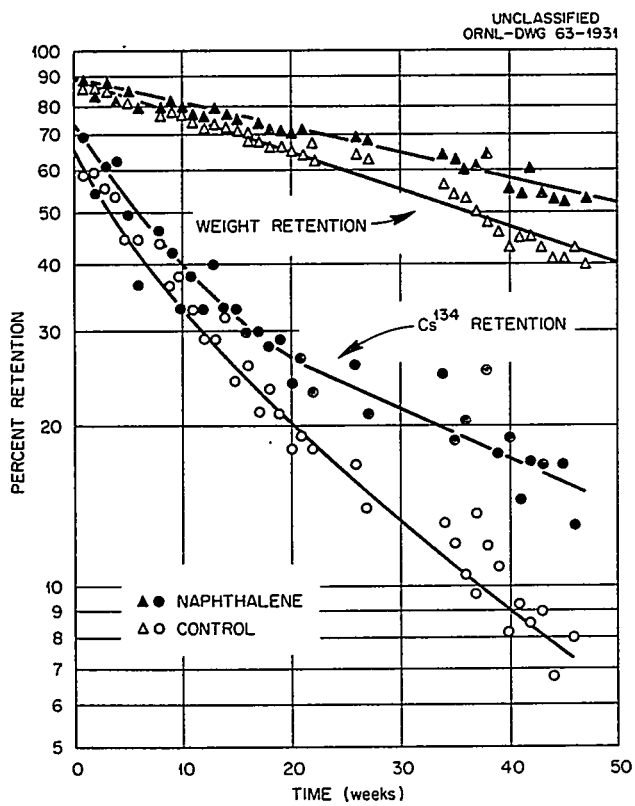

Fig. 10.2. Retention of Weight and Cs^{134} by Bagged Leaf Litter in Control Plots and in Plots Receiving 100 g of Naphthalene per m^2 of Forest Floor.

Table 10.2. Weights of Forest Floor Materials Remaining on Plots Treated with Naphthalene and on Control Plots

Values are g (ovendry weight)/m^2. Fruits, twigs, and needles are not included

Rate of Naphthalene Application	Study Area 1	Study Area 2	Study Area 3	Mean
100 g/m^2	736	441	623	600 ± 113.1
35 g/m^2	703	359	502	521 ± 99.8
10 g/m^2	559	270	316	381.7 ± 118.0
0 g/m^2[a]	655	293	284	410.7 ± 160.8

[a] Control.

LEAF LITTER CONSUMPTION BY MILLIPEDES

D. A. Crossley, Jr. Cynthia L. Corley

Work on the refinement of tracer techniques for estimating food consumption consisted primarily of laboratory work on millipedes (*Dixidesmus erasus*). Emphasis was given to (1) identification of factors influencing the shorter component in multicomponent curves of radioisotope elimination, (2) temperature influences on rates of elimination, and (3) methodology for radioisotopes with long biological half-lives.

Elimination curves for Co^{60} and Cs^{134} could be resolved into two components, the longer of the two accounting for 30 to 70% of the ingested dose of radioisotope. The shorter component appears to be due to the passage of unassimilated material from the intestines. Decreasing the temperature increased both the shorter and longer components (slower rates of elimination), but absence of food increased only the shorter component. By giving millipedes multiple feedings, the shorter component could be virtually eliminated, since the ratio of absorbed or assimilated radioisotope to unabsorbed material in the intestines became larger through repeated feedings.

Experiments measuring food consumption by these millipedes were not completely successful, due to difficulties in maintaining dead leaves in a palatable state over a period of time. Although these animals are active in richer forest situations during the colder part of the year, best laboratory results were obtained at 25°C. Results of experiments in which Sr^{85} was used to measure food consumption were encouraging. These arthropods accumulate strontium in the calcareous exoskeleton, and, consequently, rates of elimination are very slow. After 65 days, retention was 70% of initial dose at 15°C and 80% at 5°C. These data indicate that radioisotopes with long biological half-lives may have definite advantages for estimation of food consumption. For Sr^{85} accumulation by millipedes, elimination is so slight for the first 30 days or so that consumption can be estimated simply as average activity accumulated per day. This approach also obviates temperature effects on tracer elimination. Radiostrontium was not lost by millipedes during the molting process, since these arthropods ingest their cast skins. The major disadvantage of this tracer procedure is that the time of exposure to tagged food must be known.

FIRST-SEASON REDISTRIBUTION OF Cs^{137} IN CANOPY OF A TAGGED *LIRIODENDRON* FOREST

J. S. Olson W. C. Cate
H. D. Waller Regina M. Anderson

Our first large-scale tracer experiment,[9] initiated May 20–23, 1962, on a 20- by 25-m area of tulip poplar forest (*Liriodendron tulipifera*) is confirming our expectations of rapid circulation of Cs^{137} through the forest ecosystem, and is raising a number of new ecological questions involving the interpretation of this transfer. The rapid attainment of maximum foliage concentrations, averaging 1.3 μc per g of dry weight on June 6 and June 20, was followed by a decrease throughout the growing season to around 0.6 μc per g of dry weight from August 22 to early October (Fig. 10.3). Concentrations in fallen leaves decreased from only 0.25 μc per g of dry weight on September 10 to 0.13 by October 25, suggesting a marked withdrawal of Cs^{137} (and presumably total content of alkali metal elements) before leaf drop and a leaching of leaves by rain before and after leaf drop.

Rainwater that was collected in ten funnels (27.6 cm in diameter and located at random within ten subplots, 5 × 10 m each) promptly showed maximum Cs^{137} concentrations in June, when foliage radioactivity was highest (Fig. 10.4). The details

[9] S. I. Auerbach *et al.*, *Health Phys. Div. Ann. Progr. Rept. July 31, 1962*, ORNL-3347, p 66.

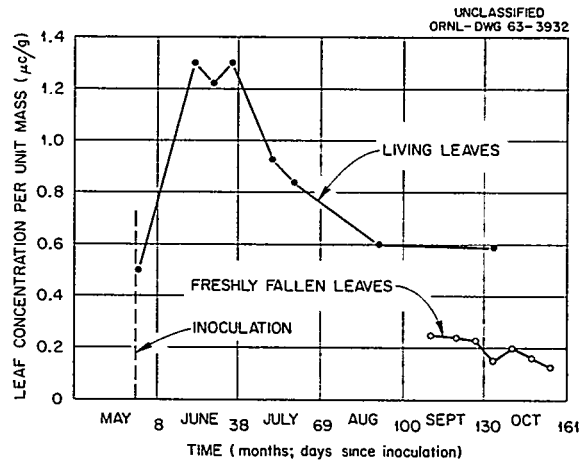

Fig. 10.3. Seasonal Distribution of Cs^{137} Into and Out of *Liriodendron* Canopy. Concentration of Cs^{137} in living leaves and freshly fallen leaves.

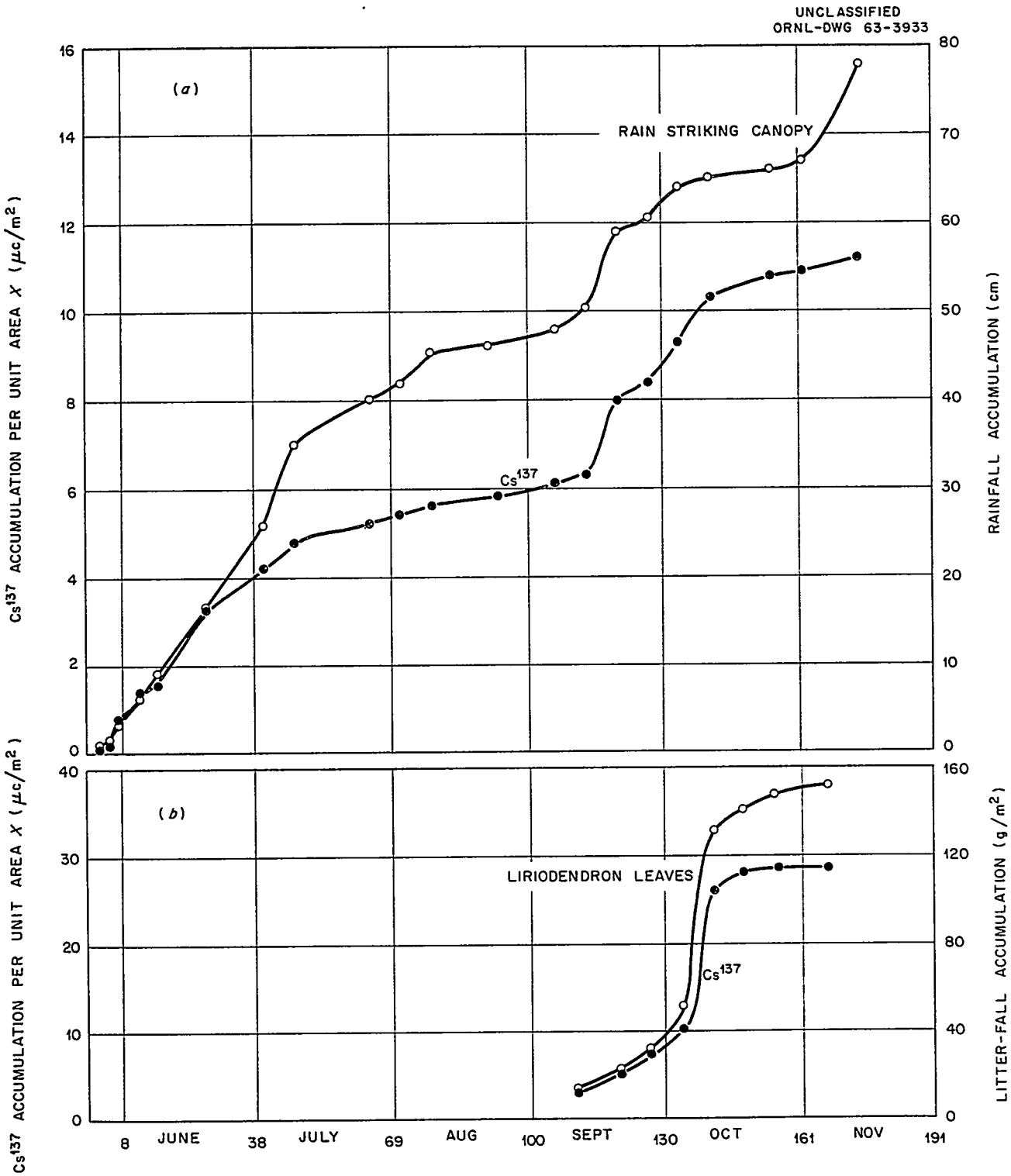

Fig. 10.4. Seasonal Distribution of Cs^{137} into and out of *Liriodendron* Canopy. (*a*) Approximate cumulative rainfall and rainout of Cs^{137}. (*b*) Cumulative litterfall and litter contribution of Cs^{137}.

of leaching in relation to time, of course, depended on the frequency and amount of rainfall. There is a suggestion of increased Cs^{137} per cm of rain late in the summer, which might conceivably reflect a period of remobilization of alkali metal reserves prior to translocation back into woody portions of the tree, but further studies now underway are needed to confirm and explain this effect.

In spite of lowered late-season concentration per unit mass (U), additions to the forest floor from falling *Liriodendron* leaves reached a maximum rate of 2.3 $\mu c\ m^{-2}\ day^{-1}$ in the week of October 4–11. Cumulative leaf contribution was 28.6 $\mu c/m^2$ (out of a total litter contribution of 31.3 $\mu c/m^2$) between September 3 and November 7. The total *Liriodendron* leaf fall of 152 g/m^2 during this period or 156 g/m^2 by January 9, 1963 (out of 233 g/m^2 total litter fall) provides a tentative basis for estimating maximum canopy content if this total approximates total mass M of foliage present in late June. If the late June average of $U = 1.27\ \mu c$ per g of dry weight is representative of the whole canopy, then foilage activity on a unit-area basis $X = UM = 1.27\ \mu c$ per g of dry weight $\times$ 156 g/m^2 = 198 $\mu c/m^2$ at a seasonal maximum. This is about one-fifth of the total introduced into tree trunks (about 1 mc/m^2). While this fraction is not as high as the maximum canopy fraction for white oak saplings,[10] it seems high for a whole stand of pole trees having an average basal area corresponding to average diameter (at a height of 4.5 ft) of 6 in. (15 cm), and with individual trees up to 12.6 and 14.3 in. in diameter at a height of 4.5 ft.

The prompt movement of cesium ions into leaves must not cease during late June, nor does the export start suddenly. The maximum presumably represents a moment when income balances opposing loss rate in dynamic steady-state. The rate of decrease of X through late summer (about 1.2% of foliage cesium per day) thus represents a minimal estimate of total turnover per day. Further data and computer simulation of simultaneous income and loss need to be combined for evaluating the general model of cesium flux[4,11] for this interesting case of a *Liriodendron* forest.

[10] J. P. Witherspoon, S. I. Auerbach, and J. S. Olson, *Cycling of Cesium-134 in White Oak Trees on Sites of Contrasting Soil Type and Moisture*, ORNL-3328 (October 1962).

[11] S. I. Auerbach *et al.*, *Health Phys. Div. Ann. Progr. Rept. July 31, 1961*, ORNL-3189, pp 124–28.

DETERMINATION OF POTENTIAL CESIUM-ORGANIC BINDING SITES IN *LIRIODENDRON* AND OTHER WOODY SPECIES

G. N. Brown

Cesium-137 introduced into living trees circulates throughout the trees over a period of time. The chemical form in which cesium is translocated in the sap stream and the degree of retention of cesium by the woody tissue probably play a major role in the rate of circulation. Therefore, a study was designed to investigate both the chemical form of cesium in sap and retention of cesium by wood.

Root and stem sections were collected from the Cs^{137}-labeled yellow poplar forest. A vacuum suction was used to extract sap from several sections of woody tissue; the sap components were then separated by paper chromatography. All separations indicated that Cs^{137} existed only in ionic form.

Other stem sections were weighed and counted for radioactivity using a small-animal whole-body scintillation counter. The sap was then removed, and the sections were again weighed and counted. One to ten percent of the fresh weight was removed with the sap, while 10 to 20% of the original radioactivity was removed. The percentages of both weight and activity loss resulting from sap extraction were inversely related to original weight. These data suggest that the bulk of the activity was retained in the woody tissue. The sections were finally oven-dried and weighed. The sap weight loss accounted for only about 10% of the total moisture weight loss, suggesting a relatively high percentage of intracellular moisture exclusive of the xylem and phloem sap.

Autoradiograms of increment cores illustrated the bulk of the activity in the phloem tissue (Fig. 10.5). Apparently, much of this activity was not in the free-flowing sap, but rather in the parenchyma and other living cells of the phloem.

The oven-dried wood was ground to a powder with a Wiley mill. This powder was placed in glass tubes to form columns of equal diameter and length. Water was run through the columns and collected in equal fractions until no more activity could be removed. The combined water fractions accounted for 60 to 80% of the total activity remaining in the wood after sap removal. The residual Cs^{137} required 1 N HCl for elution

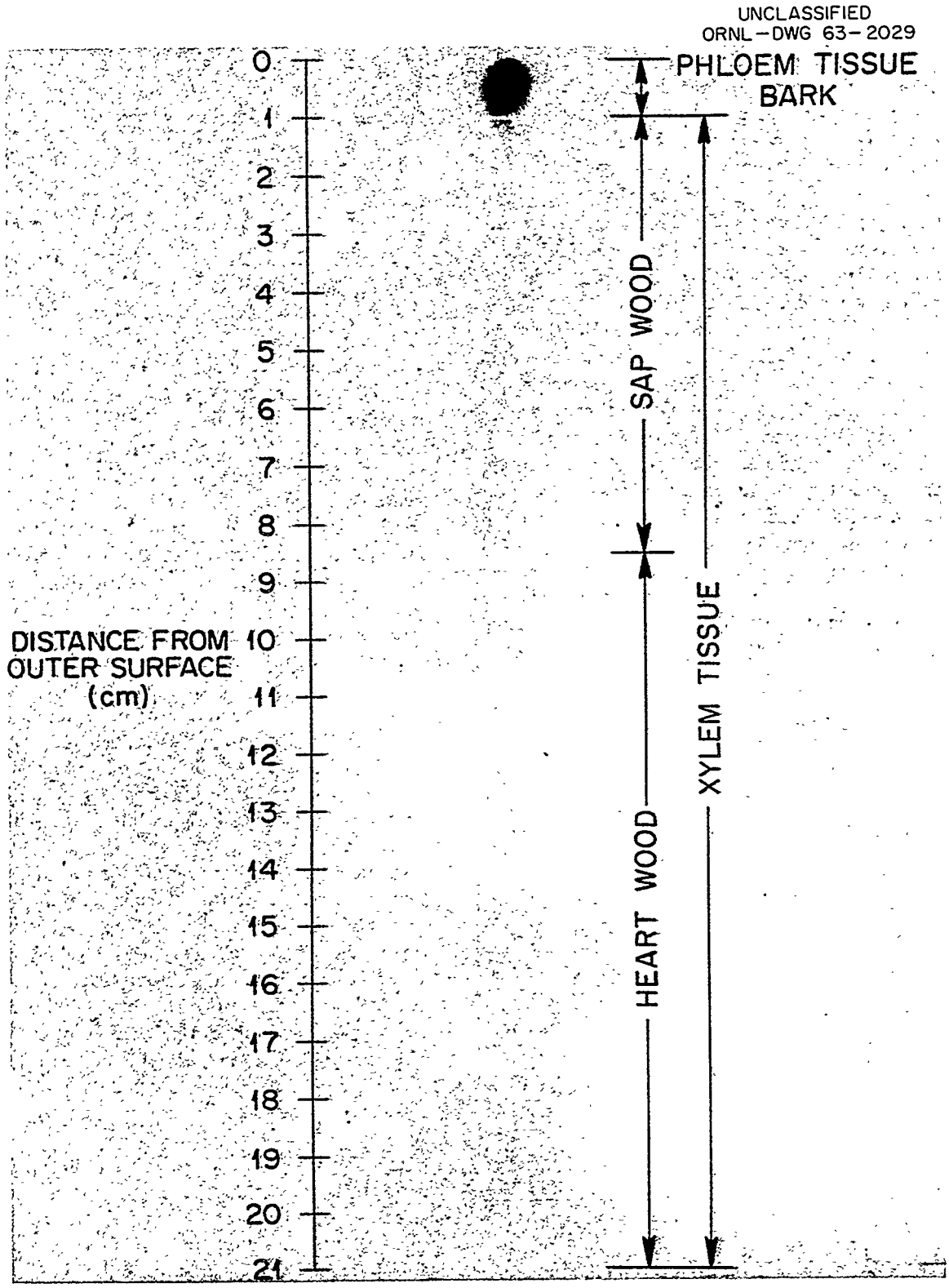

Fig. 10.5. Autoradiogram of Increment Core Illustrating Distribution of Cs^{137} Activity Transversely Across Annual Rings.

(Fig. 10.6). These observations suggest a certain degree of cesium-organic ionic bonding. Bonding of this nature seems logical since many carboxyl units, which are potentially capable of binding any of the monovalent metals, exist in various organic fractions of wood.

General retentions of monovalent metals by various species of wood were next determined. Nonradioactive tree stems were collected and powdered by use of a Wiley mill. Columns were prepared as before. All species used, both Angiosperms and Gymnosperms, retained all of the Cs^{137}, K^{42}, and Na^{24} washed through the respective columns. Washing the columns with large volumes of water eventually recovered ~90% of the activity, whereas 1 *N* HCl was required for both rapid and complete recovery of the isotopes. These data further support the observation that woody tissue, regardless of species, is capable of binding monovalent metals. It should be emphasized that ionic bonding is much more temporary, indefinite, and unstable than covalent bonding, such as the bonds between magnesium and the chlorophyll molecule. No evidence was found of this latter type of chemical bonding between cesium, potassium, or sodium and woody tissue or sap organic components.

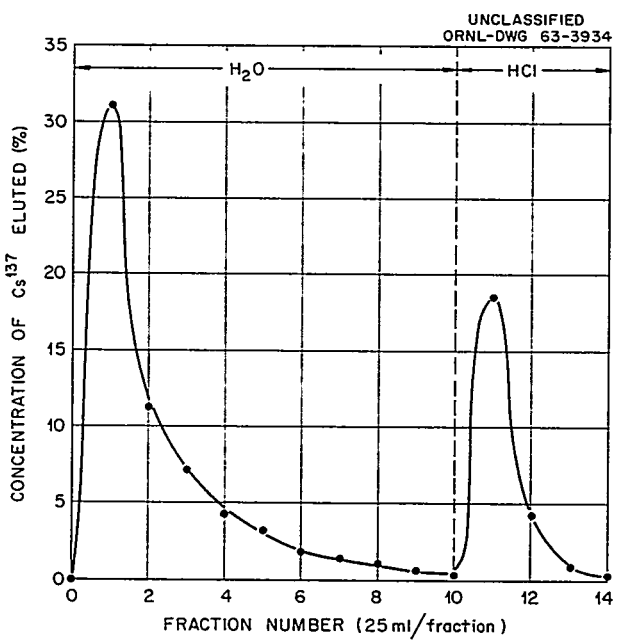

Fig. 10.6. Elution of Cs^{137} by Water and Hydrochloric Acid from Pulverized Wood of Cs^{137}-Labeled Yellow Poplar Trees.

ENTRY OF Cs^{137} INTO LITTER AND SOIL OF A TAGGED *LIRIODENDRON* FOREST

H. D. Waller J. S. Olson
Martin Witkamp W. C. Cate
Regina M. Anderson

In addition to income from rainfall and litter fall, downward movement of Cs^{137} in roots of tulip poplar apparently contributes much of this nuclide to the soil (Emory silt loam) of the tagged forest. Early litter sampling on lines on a close spacing (2 cm) showed very abrupt variation, due partly to uneven movement of rainout over the incomplete litter cover of the mull humus. The extent of variation within centimeter distances was greater than two orders of magnitude. The importance of root contribution to the highly variable initial distribution was indicated by early sampling. Root fragments which could be separated from inorganic soil particles contributed at least 90% of the total activity as of July 16, 1962. Fine rootlets that could not be separated from sieved mineral soil may already have contributed to radioactivity in this and subsequent samples.

In order to obtain a picture of average distribution, a large randomized sample system (ten cores with six layers in each of twenty 5- by 5-m plots) was included in the October sampling, and indicated a grand average forest floor concentration (including that in soil and roots) of 384 ± 29 S.E. $\mu c/m^2$ with a standard deviation of 132 $\mu c/m^2$. The mean (384 $\mu c/m^2$) is 41% of the total initial inoculum. Other data suggest that in October the total root system contains ~35% of the original inoculum.

An analysis of variance between and within 5- by 5-m plots shows that there is a significant difference between plots at the 1% level. This is to be expected since the forest floor activity is dependent upon the tagged tulip poplar trees (which are not uniformly spaced) as a source of contaminant during the early phases of the experiment. It is expected that the forest floor activity will become more uniformly distributed as each ecological compartment nears its equilibrium state.

A distribution of plot means is shown in Table 10.3.

Table 10.3. Cesium-137 Concentration in 2-in. Stratified Layers of Forest Floor

Mean of ten sample cores per 5-m square

Depth of Layer (in.)	Distribution of Cs^{137} Concentration in a 20- by 25-m Area Divided into Twenty 5- by 5-m Plots ($\mu c/m^2$)			
0–2	105.3	103.5	71.5	50.3
2–4	194.4	20.9	84.0	35.1
4–6	48.3	9.4	29.3	34.6
6–8	39.3	8.8	36.5	4.8
8–10	12.7	7.6	17.2	2.9
10–12	16.0	9.1	7.0	2.3
Total	416.0	159.3	245.5	130.0
0–2	49.5	105.9	194.1	122.6
2–4	24.0	49.0	166.4	47.2
4–6	40.0	14.6	73.9	16.8
6–8	30.8	19.0	73.0	17.1
8–10	37.8	21.7	48.5	14.4
10–12	42.7	6.5	25.4	7.3
Total	224.8	216.7	581.3	225.4
0–2	156.5	217.2	282.4	372.1
2–4	80.5	89.1	121.2	198.2
4–6	71.0	29.5	75.4	83.4
6–8	10.8	23.0	34.8	24.0
8–10	11.8	16.4	71.4	43.1
10–12	45.7	19.5	32.5	20.3
Total	376.3	394.7	617.7	741.1
0–2	234.4	192.8	211.0	128.4
2–4	86.5	179.6	113.5	181.3
4–6	52.2	58.5	65.1	38.6
6–8	10.8	10.6	33.8	30.7
8–10	11.8	27.4	27.5	44.0
10–12	45.7	6.3	38.5	19.5
Total	441.4	475.2	489.4	442.5
0–2	187.4	159.2	160.9	130.3
2–4	181.5	134.8	101.4	28.3
4–6	78.5	38.2	45.2	16.2
6–8	13.2	19.7	40.8	12.6
8–10	14.5	30.0	31.4	7.1
10–12	21.0	18.9	28.0	5.1
Total	496.1	400.8	407.7	199.6

In addition, 1-dm^2 samples were carefully separated to indicate typical patterns of vertical distribution in mineral and root fractions in the uppermost part of the forest floor. Data listed in Table 10.4 show the importance of the root contribution as sample depth increases. The results confirm the importance of roots to the early entry of Cs^{137} into the soil. It is not yet known how much of this will be released from living roots by death or excretion, or how rapidly this will occur.

Table 10.4. Vertical Distribution of Cs^{137} in Upper Part of Forest Floor in 1-dm^2 Samples Taken to a Depth of 10 cm

Each unit represents a mean of 20 samples.

Sample Depth (in.)	Percent of Cs^{137} by Sample Components					
	Soil Fraction <2 mm		Soil Fraction >2 mm		Root Fraction >1 mm	
	Mean	± S.E.	Mean	± S.E.	Mean	± S.E.
0–1	5.0	± 0.8	86.2	± 1.6	8.8	± 1.3
1–2	4.8	± 1.0	75.6	± 3.0	19.7	± 3.2
2–3	3.3	± 0.8	75.9	± 4.5	20.9	± 4.5
3–4	3.2	± 0.8	73.9	± 6.1	23.1	± 5.6

MICROBIAL IMMOBILIZATION OF RADIONUCLIDES IN FOREST LITTER

Martin Witkamp Marilyn L. Frank

Laboratory experiments on the influence of the main ecological factors on microbial immobilization of minerals were concluded, and results are being readied for publication. Microbial uptake of radionuclides from liquid media was proportional to the nuclide concentration in the liquid. On a mixture of solid and liquid substrates, uptake was proportional to the concentration of nuclides in the solids rather than that in the surrounding liquid. Consequently, in natural soil wide differences in nuclide content of a single species in a single environment may be expected, depending on nuclide concentration in the substrate.

Such wide differences were found in concentrations of Cs^{137} in mushrooms in a tagged stand

of tulip poplar. These concentrations varied at one time from 47 to 17,272 $\mu\mu c/ml$. This variability was not only the result of large differences among substrates but also the result of differences within one substrate at different locations. Concentrations of Cs^{137} in litter were 0.1 to 68 times lower than the concentrations in the underlying soil and roots. Variations of concentrations of Cs^{137} in mineral soil exceeded two orders of magnitude for surface samples taken only 10 cm apart.

Accumulation of Cs^{137} in fruiting bodies of mushrooms increased with time. The ratio of Cs^{137} concentration in the mushrooms to Cs^{137} concentration in the substrates (volume/volume) varied from 0.02 to 0.7 within one species, and from 0.02 to 9 for all species. Use of fruiting bodies as indicators of environmental contamination by radionuclides, as well as for prediction of radionuclide concentrations in the forest floor based on nuclide concentrations in mushrooms, is not yet feasible. These results illustrate the complexity of distribution patterns of radionuclides in biota and soil in space and time.

MOBILITY OF Cs^{137} IN FOREST FOOD CHAINS

D. A. Crossley, Jr. Cynthia L. Corley
Gladys J. Dodson W. L. Tietjen

New work on the transfer of radionuclides in forest food chains is being performed in the tulip poplar stand tagged with Cs^{137}. Two types of food chains are being compared: (1) the green foliage–herbivorous arthropod–predaceous arthropod type of food chain and (2) the leaf litter–herbivorous arthropod–predaceous arthropod type. Since Cs^{137} was introduced into the trunks of the trees in early spring,[12] the food chain based on green foliage received a direct tag during the first of the summer. Leaf litter received radioisotopes due to leaching of the green leaves by rainfall in the summer and leaf fall in the autumn. Objectives of these tracer studies are similar to those for the White Oak Lake bed work, namely, to understand how isotopes move through ecological systems and to use this information for further understanding of the systems themselves.

[12]S. I. Auerbach *et al.*, *Health Phys. Div. Ann. Progr. Rept. July 31, 1962*, ORNL-3347, p 66.

Samples of green leaves, herbivorous insects, and predaceous arthropods taken from the tree canopies during the summer of 1962 had relative proportions of Cs^{137} similar to that in the biota of White Oak Lake bed. Table 10.5 compares estimates of Cs^{137} content in the green foliage food chains in the tagged forest with those for the lake bed system. Distribution of isotope is similar in food chains of the two areas despite differences in the food chains themselves. The data suggest slightly lower transfer efficiencies for the forest system, but this difference may result entirely from the size of areas involved.

Table 10.5. Comparison of Cs^{137} Movement in White Oak Lake Bed and in Forest Food Chains

Values given are the mean plus or minus standard error; numbers of samples are indicated in parentheses

	White Oak Lake Bed ($\mu\mu c/g$)	Tulip Poplar Forest ($\mu c/g$)
Soil	7300	
Plant (leaves)	160 ± 32 (5)	0.47 ± 0.044 (21)
Herbivorous insects	78 ± 4.8 (5)	0.17 ± 0.033 (24)
Predaceous insects	73 (8 samples lumped)	0.14 ± 0.078 (7)

Since the forest stand is much smaller than the lake bed, there is a greater chance that samples will include untagged insects from outside the area. The general similarity in radioisotope distribution is impressive, because different types of areas, total isotope content, method of tagging, and species of organisms were involved. Forest populations were primarily geometrid caterpillars, other lepidopterous larvae, and aphids; White Oak Lake bed populations were heterogeneous but were mostly grasshoppers and leafhoppers. The similarities in Cs^{137} transfer in these two systems suggest that it may be possible to general-

ize about cesium movement in terrestrial food chains even though different insect species may be involved.

Cesium-137 concentrations were lower in the leaf litter–soil arthropod food chain than in the green foliage food chain since leaching of cesium from green leaves was the radioisotope source for the litter layers. Table 10.6 shows Cs^{137} concentrations in the food chain based on leaf litter for July through October. Radioisotope concentration in leaf litter increased gradually during the summer and abruptly during the early autumn as leaf fall progressed. Herbivores had Cs^{137} concentrations almost as high as leaf litter during the summer months. Herbivore radioactivity increased in the autumn but not as rapidly as did leaf litter radioactivity. Predators also showed an increase in Cs^{137} content during the summer and early autumn. During July and August the herbivore and predator parts of the leaf litter–soil arthropod food chain had an added input due to direct feeding on the green foliage. Phalangids (*Liobunum* sp.), for example, had Cs^{137} contents which were a factor of 2 or more higher than leaf litter concentrations. Also, some of the predators were evidently feeding in the green foliage food chain although they were trapped on the forest floor. The result was that the animal portions of the leaf litter food chain appeared abnormally high during July and August. In October the green foliage had disappeared, and the leaf litter food chain assumed a Cs^{137} distribution resembling that of the green foliage food chain.

Table 10.6. Cesium-137 Concentrations in the Leaf-Litter to Arthropod Food Chain in a Sinkhole Forest Stand

Trophic Level	Cs^{137} Concentration ($\mu\mu c$ per g of dry weight)			
	July	August	September	October
Leaf litter	3640	4910	15,600	26,400
Herbivores	3600	4700	8,100	8,300
Predators	2800	3400	3,700	4,900

11. Clinch River and Related Aquatic Studies

D. J. Nelson
S. I. Auerbach
N. R. Kevern
B. G. Blaylock[1]
R. E. Martin[1]
G. M. Rosenthal[2]
R. C. Early
N. A. Griffith

STRONTIUM IN WHITE CRAPPIE (*POMOXIS ANNULARIS*) FLESH AND BONE

D. J. Nelson N. A. Griffith
R. C. Early

The series of analyses of stable strontium in white crappie flesh and bone[3] was continued to test the relation of the distribution of stable strontium and Sr^{90} between the environment and the fish. If the distribution of stable strontium and Sr^{90} between fish tissue and water is the same, it should be possible to predict Sr^{90} concentrations in tissue for continuous environmental releases. Samples have been taken at monthly

[1]ORINS fellow.

[2]ORINS summer participant.

[3]S. I. Auerbach *et al.*, *Health Phys. Div. Ann. Progr. Rept. July 31, 1962*, ORNL-3347, p 67.

intervals to determine whether there are seasonal changes in the strontium concentrations in fish tissue.

All the samples for this study were processed and have been submitted to the Analytical Chemistry Division for the analyses. None of the series is complete, although the stable-strontium analyses of bone are essentially finished. The average stable-strontium concentration in bone, based on 105 samples, is 271 ± 6.34 ppm (±1 standard error). This quantity of strontium in bone is a concentration factor of 4.0×10^3 over that in Clinch River water. Strontium concentrations in flesh average 0.0813 ± 0.0118 ppm (27 samples), which is a concentration factor of 1.2 over that of river water.

The fish samples in this series of analyses are also being analyzed for calcium, stable cesium, and potassium. With these data it should be possible to test also strontium/calcium and cesium/potassium ratios, which are used frequently in reporting monitoring and biological uptake data for Sr^{90} and Cs^{137}.

The biological half-life of strontium in white crappie has been determined by tagging fish with Sr^{85} and then counting the same fish at 1-min intervals in a small-animal whole-body counter. In experiments completed the biological half-life of strontium in the flesh of different individuals ranged from 12 to 48 min, somewhat shorter than anticipated previously. Measurement of the turnover of strontium in flesh was complicated by the rapid deposition and high concentration of strontium in fish bone, which literally masked the strontium in soft tissues. This difficulty was circumvented by constructing a fish-holding assembly, which was inserted in the detector chamber of the counter (Fig. 11.1). Water was pumped through

Fig. 11.1. Whole-Body Counter and Fish-Holding Assembly Used in the Measurement of the Biological Half-Life of Sr^{85} in White Crappie Flesh. Water is pumped through the fish holder via the plastic tubing.

the assembly during the experiments to remove excreted Sr^{85} and to provide a supply of oxygenated water.

Experiments which show a short biological half-life for strontium in fish flesh and stable-strontium analyses which show a low strontium concentration in tissue raise a question as to whether continued Sr^{90} analyses of Clinch River white crappie are advisable. In effect the concentration of Sr^{90} in flesh will reflect quickly the Sr^{90} concentration in the water; consequently, the water may as well be sampled as the fish flesh. Furthermore, these results also suggest that the distribution of strontium and Sr^{90} should be compared in bone only and not in flesh.

BIOLOGICAL MOVEMENT AND RESERVOIRS OF Sr^{90}

D. J. Nelson R. C. Early
N. A. Griffith

The transport of Sr^{90} from the Clinch River by emerging aquatic midges (Chironomidae) was compared with the accrual of Sr^{90} to the river from weapons-testing fallout. Larval development of the midges occurs in the contaminated river-bottom sediments. Emerging adults were caught in insect light traps operated on the river bank at dusk. Adults in one large, composite sample contained 8.76 times as much Sr^{90} [$(3.55 \pm 1.13) \times 10^{-6}$ μc per gram of dry weight] as did those from an equal quantity of river-bottom sediment from the same location. Studies elsewhere[4,5] have shown that 10 g m^{-2} yr^{-1} may be contained in the emergent insect biomass. These emergent insects would transport $(3.55 \pm 1.13) \times 10^{-5}$ μc of Sr^{90} per square meter per year from the river bottom. The average increment of Sr^{90} from fallout in the United States between 1959 and 1960 was 4.2×10^{-3} curie/square mile (1.62×10^{-3} $\mu c/m^2$).[6] Thus, fallout entering the river directly would add 45 times as much Sr^{90} as removed by emerging chironomids.

Previous studies[7] showed that fresh-water clams concentrated strontium in their shells by factors of 2500 to 9000 times, and therefore are useful as indicators of Sr^{90} in the environment. Since there is a commercial clam (mussel) fishery on the Tennessee River in Tennessee and northern Alabama, calculations were made to estimate the removal of Sr^{90} from the river in clamshells. The annual harvest of shells ranges from 5000 to 10,000 tons. By using the maximum harvest and the average Sr^{90} concentration in clamshells (7.019×10^{-6} $\mu c/g$), the calculated removal of Sr^{90} was 64 mc/yr. If Sr^{90} releases were constant and if the growth of the population were in equilibrium with the harvest, a similar quantity of Sr^{90} would be incorporated into the population each year. Other studies[8] suggest there are about 4.5×10^7 clams in these populations. Assuming an average weight of 250 g each and the same Sr^{90} concentration, the reservoir of Sr^{90} in clams in the river is calculated as 79 mc. The annual removal and reservoir of Sr^{90} in clamshells is small when compared with the Laboratory releases of Sr^{90}, which have ranged from 29 to 150 curies/yr.

UPTAKE AND ACCUMULATION OF STRONTIUM BY ALGAE AND SNAILS

N. R. Kevern G. M. Rosenthal
N. A. Griffith D. J. Nelson

The uptake and accumulation of strontium by algae is being studied to determine the influence of stable-strontium and calcium concentrations in the culture medium on the accumulation process. Since algae are a major food item for many aquatic animals in the food chain leading through fish to man, it is important to understand the factors involved in the algal metabolism of the potentially dangerous radionuclides such as Sr^{90}.

The study was established according to a 3×3 factorial design with a single replication. The two variables were the concentrations of stable strontium and calcium in the algal media. As such, there were nine media combinations of strontium

[4] H. T. Odum, "Trophic Structure and Productivity of Silver Springs, Florida," *Ecol. Monographs* 27, 55 (1957).

[5] J. M. Teal, "Community Metabolism in a Temperate Cold Spring," *Ecol. Monographs* 27, 283 (1957).

[6] E. P. Hardy *et al.*, "Strontium-90 on the Earth's Surface II," TID-17090 (November 1962).

[7] D. J. Nelson, "Clams as Indicators of Strontium-90," *Science* 137, 38 (1962).

[8] G. D. Scruggs, Jr., "Status of Fresh-Water Mussel Stocks in the Tennessee River," U.S. Fish and Wildlife Service, Special Scientific Report — Fisheries No. 370 (1960).

and calcium concentrations. Other factors such as light, temperature, and other nutrients were constant. A green, single-celled alga, *Oocystis eremosphaeria*, was used to stock the culture media. A constant amount of Sr^{85} and Ca^{45} was added to each culture flask, and algal samples were taken at 1, 4, 24, 48, 72, 144, and 216 hr. The total uptake of strontium and calcium is being determined on the basis of the uptake of the radionuclides and the specific activities, for example,

$$\text{Sr in algae} = \frac{Sr^{85} \text{ in algae} \times \text{Sr in medium}}{Sr^{85} \text{ in medium}} .$$

Preliminary analyses, based only on Sr^{85} counts, suggest that both stable-strontium and calcium concentrations influenced the accumulation of Sr^{85}. The accumulation of stable strontium decreased with increasing calcium concentration and increased with increasing strontium concentration (Table 11.1). The concentration of strontium was the predominant influence. Completion of the Ca^{45} counts will provide additional data.

Table 11.1. Accumulation of Strontium by *O. eremosphaeria* in Atoms per Gram of Dry Weight of Algae[a]

Relative Ca Concentration	Relative Sr Concentration		
	1	10	100
	($\times 10^{16}$)	($\times 10^{16}$)	($\times 10^{16}$)
100	0.33	2.27	22.72
10	0.43	5.21	33.96
1	1.16	9.60	70.55

[a]Each cell is the mean of 14 samples.

Similar studies of the relative effect of stable strontium and calcium on strontium uptake are in progress using the snail *Physa heterostropha*. The preliminary results suggest that strontium uptake is dependent primarily on the stable strontium in the environment.

Both the snail and the algae studies are being conducted in media in which calcium and strontium amendments are controlled. Highly purified and assayed calcium carbonate is used to avoid significant quantities of adventitious strontium which occur normally in reagent grade calcium compounds.[9]

SMALLMOUTH BUFFALO POPULATION STUDIES AND FISH MARKING

R. E. Martin D. J. Nelson
S. I. Auerbach

A study of the age distribution, growth rates, and dispersion of the smallmouth buffalo, *Ictiobus bubalus* (Rafinesque) in Watts Bar Reservoir, and of their importance as an accumulator of radionuclides, was completed. The ages of 1271 commercially caught fish ranged from 4 to 15 yr, with the largest number being from year class 6, the youngest year class which was completely vulnerable to commercial fishing gear. Total survival rates were found to be 49% for year class 6, 35% for year class 7, 26% for year class 8, and 19% for year class 9.

The rate of change in weight as length increased was 100 g/cm for fish exceeding 31 cm in total length. Absolute growth was 422 mm at 3 yr, 441 mm at 4, 453 mm at 5, 465 mm at 6, 487 mm at 7, 522 mm at 8, and 609 mm at 9. The species characteristically exhibited the most relative growth during the second year of life. Conditions for growth evidently had improved in Watts Bar during the previous 6 yr, as was indicated by an increase in total length attained at comparable ages in succeeding years. Growth compensation was evident during the fourth and fifth years of life.

Stable-chemical analyses revealed that calcium was the most abundant element in fish scales, with at least 23 other elements present in varying quantities. Fish scales and bone were found to contain radionuclides of ruthenium, cesium, zirconium, zinc, and cobalt. Other analyses have shown the presence of Sr^{90}.

A high concentration of radionuclides in the environment was found to be necessary for smallmouth buffalo to accumulate measurable quantities in their scales. White Oak Creek is the only area

[9]S. I. Auerbach *et al.*, *Health Phys. Div. Ann. Progr. Rept. July 31, 1961*, ORNL-3189, p 137.

of Watts Bar with sufficient radionuclide contamination for such accumulation to occur. If surface area is considered a measure of available fish habitat, White Oak Creek comprises less than 0.02% of Watts Bar Reservoir at full pool. Only a small percentage of the population would be expected to be resident in the contaminated area. However, with mobile populations, contamination could be expected in larger numbers of fish because of movement into and out of White Oak Creek. This contamination could be detected in tissues such as bone or scales with a long biological half-life for the several radionuclides released. Radiometric surveys of scales revealed the smallmouth buffalo population of Watts Bar Reservoir to be a relatively minor accumulator of radionuclides, with only 0.08% having a detectable accumulation in their scales. Approximately 6% of the Clinch River fish and 77% of the White Oak Creek fish had measurable radionuclide accumulations.

Resident fish were found to have radionuclide accumulations in those portions of the scales formed while the animal was in White Oak Creek. All normal scales produced identical autoradiographic patterns of concentric circles of accumulated radionuclides associated with growth in White Oak Creek. Scales from 11 smallmouth buffalo produced autoradiographic patterns which, when compared to year marks on the sculptured surface of the scales, revealed the past movements of the individuals into and out of the contaminated area and the size of the animal when such movement occurred (Figs. 11.2 and 11.3). These dispersion data were applied only to individuals because the

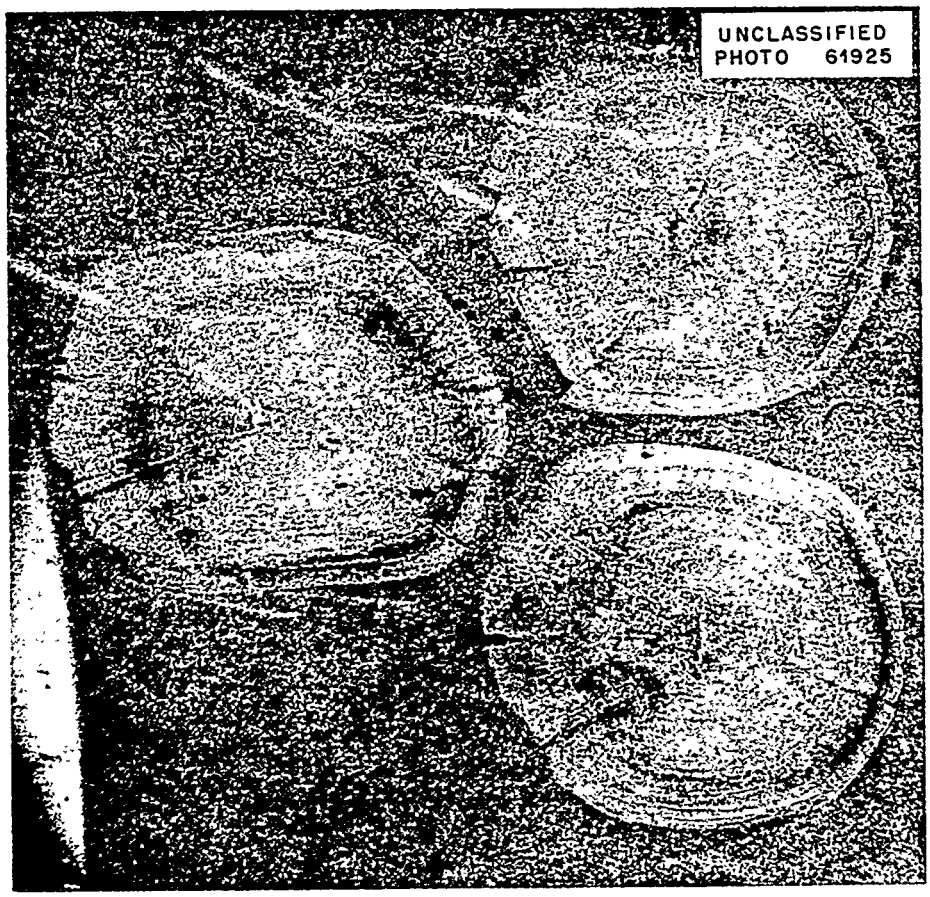

Fig. 11.2. Scale Autoradiogram Overlay of a Smallmouth Buffalo Which Hatched in the Spring of 1957 in a Noncontaminated Area. It entered White Oak Creek in the winter of 1959–60 at a total length of 294 mm. This individual remained in White Oak Creek until the spring of 1961, when it was 369 mm in total length. The specimen was caught Aug. 4, 1962, at Tennessee River mile 542, approximately 46 miles downstream from White Oak Creek.

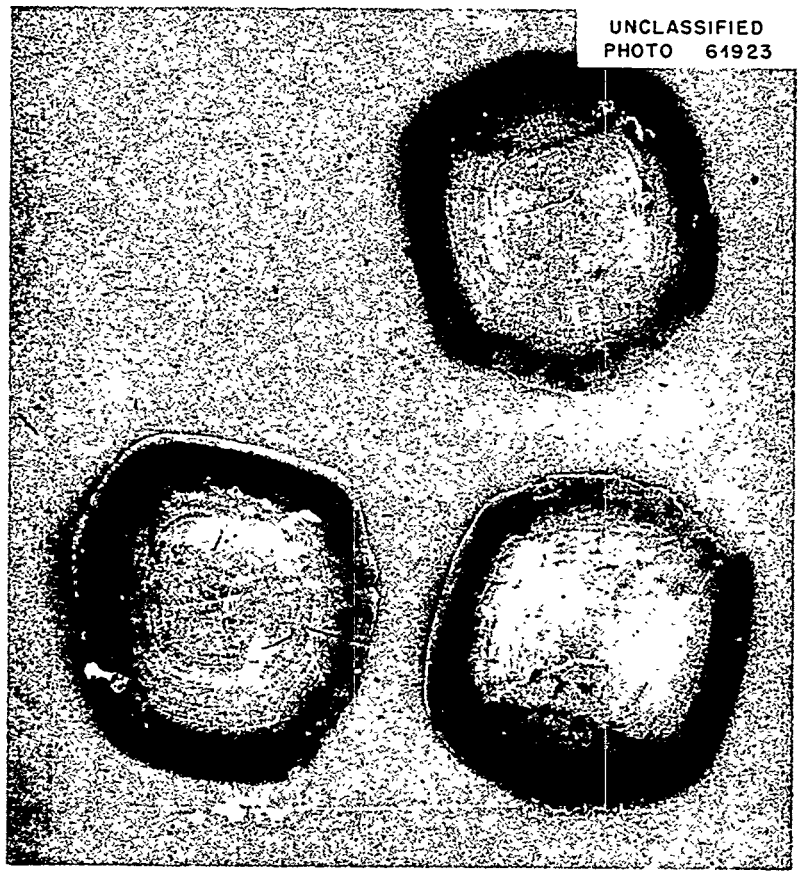

Fig. 11.3. Scale Autoradiogram Overlay of a Smallmouth Buffalo Which Hatched in the Spring of 1956 in a Noncontaminated Area. It entered White Oak Creek in the spring of 1960 at a total length of 365 mm and remained there until its capture on Nov. 6, 1961, at a total length of 440 mm and weight of 1345 g.

number was too small for generalizations on the population as a whole.

A laboratory experiment showed that scales could be tagged with Cs^{134}. This radionuclide-tagging method had an advantage over the conventional method of attaching plastic tags to the animal's body which caused a loss in length and weight of the individual. Methods were proposed for combining environmental tagging or laboratory tagging of fish with conventional capture-recapture methods for population studies.

POPULATION GENETICS AND RADIATION EFFECTS STUDIES ON *CHIRONOMUS TENTANS*

B. G. Blaylock D. J. Nelson
S. I. Auerbach N. A. Griffith

The salivary gland chromosomes of *Chironomus tentans* larvae collected from White Oak Creek, an area contaminated by radioactive waste from ORNL, and from six uncontaminated areas were examined for chromosomal aberrations.[10–12] White Oak Creek populations were exposed to a dose rate calculated as 230 rads/yr, or about 1000 times background. Fifteen different chromosomal aberrations were found in 365 larvae taken from the irradiated population, as compared with five different aberrations observed in 356 larvae from six control populations (Fig. 11.4), but the mean number of aberrations per larva did not differ in any of the populations. The quantitative amount of heterozygosity was essentially the same in the

[10] S. I. Auerbach *et al.*, *Health Phys. Div. Ann. Progr. Rept. July 31, 1961*, ORNL-3189, p 129.

[11] Clinch River Study Steering Committee, Status Report No. 2 on Clinch River Study, ORNL-3202, p 71 (Mar. 30, 1962).

[12] S. I. Auerbach *et al.*, *Health Phys. Div. Ann. Progr. Rept. July 31, 1962*, ORNL-3347, p 68.

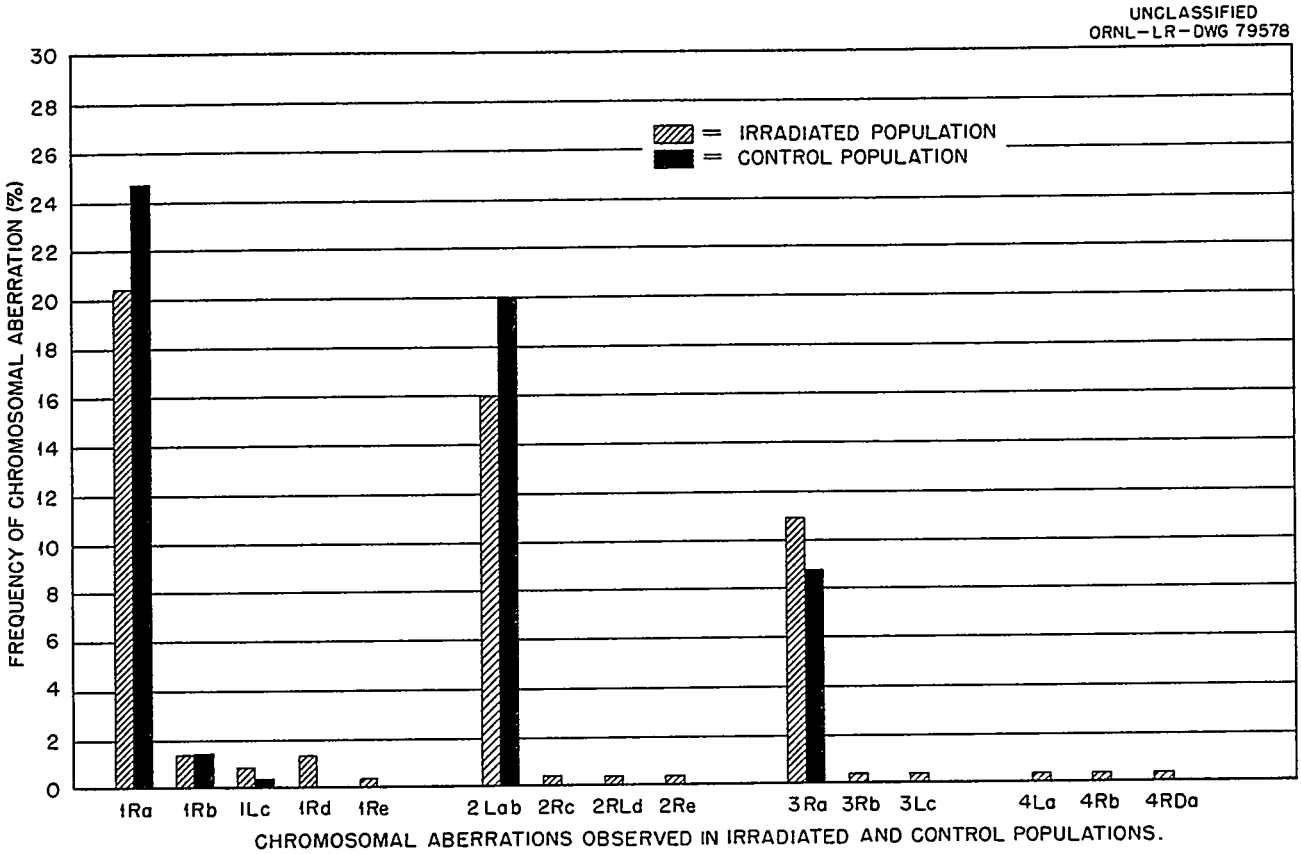

Fig. 11.4. Chromosomal Aberrations and the Frequencies at Which They Appeared in the Irradiated and Control Populations of *C. tentans*.

irradiated and the control population, but there was three times the variety of chromosomal aberrations found in the irradiated area. From this evidence it was concluded that chronic low-level irradiation from radioactive waste was increasing the variability of chromosomal aberrations without significantly increasing the frequency.

Five different inversions were found in both the irradiated and control populations; three inversions (1Ra, 2Lab, and 3Ra) were found at a relatively high frequency and were used in testing the seasonal and geographic distribution. In the White Oak Creek population the frequencies of the heterozygous inversions did not change significantly for a three-year period (1960–1962). Also, no seasonal changes were detected in the frequencies of these inversions from June through December of 1961 and September through December of 1962. There was no significant difference in the frequencies of these same heterozygous inversions between local geographic populations of *C. tentans*. It was concluded that the three inversions which occurred at the highest frequencies are endemic to the populations of East Tennessee and have been established in the population for a long time.

The frequencies of the standard arrangement, the heterozygous inversion, and the homozygous inversion of 1Ra (one of the endemic inversions) were determined in an uncontaminated area. The frequencies of these chromosomal arrangements were significantly different from the expected frequencies as predicted by the Hardy-Weinberg Law (Table 11.2). A deficiency of inversion heterozygotes was found, which is contrary to the theory of balanced chromosomal polymorphism but is consistent with a model proposed by Levene,[13] where

[13] H. Levene, "Genetic Equilibrium When More Than One Ecological Niche Is Available," *Amer. Naturalist* 87, 331–33 (1953).

Table 11.2. Distribution of Inversion 1Ra Compared to the Expected Frequencies as Determined by the Hardy-Weinberg Law in a Natural Population of *C. tentans*

	Standard Arrangement	Inversion Heterozygote	Inversion Homozygote	Number of Larvae Examined
Observed	94	55	43	192
Expected	76.8	89.3	25.9	

$X^2 = 28.30,\ P < 0.005$

under certain assumptions genetic equilibrium can be obtained without the heterozygote being superior. The assumptions of the model are that there be more than one ecological niche with one allele favored in one niche. Gene frequencies are dependent on the adaptive values of the homozygotes in the different niches. The requirements of the model stipulate that mating is at random in the entire population, so that the initial zygotic frequencies are q^2AA, $2q(1-q)$AA′, and $(1-q)^2$A′A′ where A and A′ are alleles with gene frequencies of q and $1-q$ respectively. The zygotes are deposited at random in large numbers in each of the niches, and the resulting individuals cannot move preferentially to niches for which they are better fitted. There is differential mortality ending with a fixed number of individuals in each niche with the frequencies of the allele in each niche dependent upon its adaptive value in the niche. At the time of reproduction, survivors leave the niche, and mating is at random in the entire population. The assumption must be made that the individuals cannot select the niche for which they are best fitted and that there is no tendency for mating to occur within a niche rather than at random over the whole population.

The natural population of *C. tentans* from this uncontaminated area appears to fulfill the conditions of Levene's model. The swarm-type matings and the restricted movement of the larvae of *Chironomus* make it an ideal organism for the model. These findings show that chromosomal polymorphism can be maintained in a natural population without superiority of the heterozygous individuals.

SAFETY EVALUATION OF CLINCH RIVER FISHERIES

S. I. Auerbach D. J. Nelson

As part of the Cooperative Clinch River Study (ORNL, U.S. Public Health Service, U.S. Geological Survey, Tennessee Valley Authority, Tennessee Game and Fish Commission, and Tennessee Department of Public Health), data were obtained on the radionuclide concentration in Clinch River fish, the commercial fish harvest in Watts Bar Reservoir, and the distribution of sports fishing pressure in this area. A total of 390 fish of 11 different species were caught in the Clinch River and analyzed radiochemically. Of these fish approximately one-half were analyzed at the USPHS laboratories in Cincinnati, and the remainder were analyzed at ORNL. Fish analyzed included both game and commercial food species, and these were processed in the field and laboratory to approximate, insofar as possible, normal human utilization. Data on the commercial fish harvest and its distribution to markets for human consumption were obtained from a local fish buyer. Additional information on the origin of fishermen active in the Clinch River–Watts Bar Reservoir area was developed from fish tag return data. These data were submitted to the Subcommittee on Safety

Evaluation of the Clinch River Steering Committee and will be used in their continuing analysis of Clinch River conditions.

RELATED ACTIVITIES

The section chief served as chairman of the Radioecology Committee of the Ecological Society of America. The Committee again sponsored a summer institute in radiation ecology. This institute, which was held in Oak Ridge, was attended by 20 college and university teachers and 2 staff members of other government agencies.

The section chief continued to serve as chairman of the Aquatic Biology Subcommittee of the Clinch River Project.

The section was visited by a graduate class in plant ecology from the University of Illinois. This group was given a tour of the field facilities and briefed on the ORNL program.

One member of the section participated in the ORNL–University of Tennessee educational program. He gave a graduate seminar course in "Ecological Models" to the Department of Botany.

Four senior members of the section served on the research committees of graduate students who are doctoral candidates at the University of Tennessee.

Part III. Radiation Physics and Dosimetry

G. S. Hurst

12. Theoretical Radiation Physics

J. Neufeld
R. H. Ritchie

R. F. Adkinson[1]
J. C. Ashley
F. J. Davis
R. N. Hamm[2]
W. S. Snyder
J. E. Turner
R. Woodyard[2]
H. A. Wright

DOSIMETRY OF HIGH-ENERGY PROTONS

J. E. Turner Jacob Neufeld

Calculations in collaboration with the Neutron Physics Division were completed for rad and rem doses in a tissue slab irradiated normally by protons in the energy range 50 to 400 Mev. These calculations are based on the Monte Carlo technique, with relative biological effectiveness (RBE) values as given by the National Committee on Radiation Protection and Measurements[3] (NCRP) to estimate the rem dose. The mathematical programming of the rem dose is such that the RBE can be varied within broad limits. Results of these calculations have been reported.[4]

Results of the calculations are shown in Figs. 12.1–12.7. These figures show (1) the total dose in rems and rads as a function of depth in tissue slabs for incident protons of energies 100, 150, 200, 250, 300, 350, and 400 Mev and (2) the rad dose due to heavy particles (i.e., particles with mass number $A \geqq 2$, which arise as recoil nuclei and as nuclear evaporation products). The total

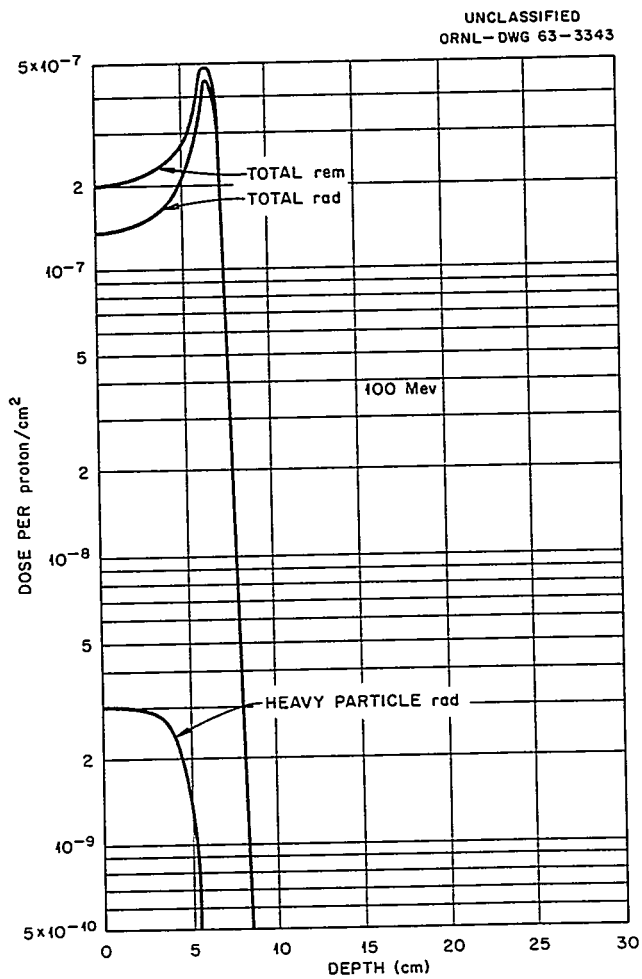

Fig. 12.1. Dose from 100-Mev Protons Normally Incident on a 30-cm Tissue Slab.

[1]Temporary employee.

[2]Consultant.

[3]G. Failla *et al.*, *Permissible Dose from External Sources of Ionizing Radiation, National Bureau of Standards Handbook 59*, p 48, National Bureau of Standards, Washington, D.C., 1954.

[4]J. E. Turner *et al.*, "The Calculation of Radiation Dose in Tissue from High-Energy Protons," paper D-7 in *Proceedings of the Symposium on the Protection Against Radiation Hazards in Space, Gatlinburg, Tenn., November 5–7, 1962*, TID-7652.

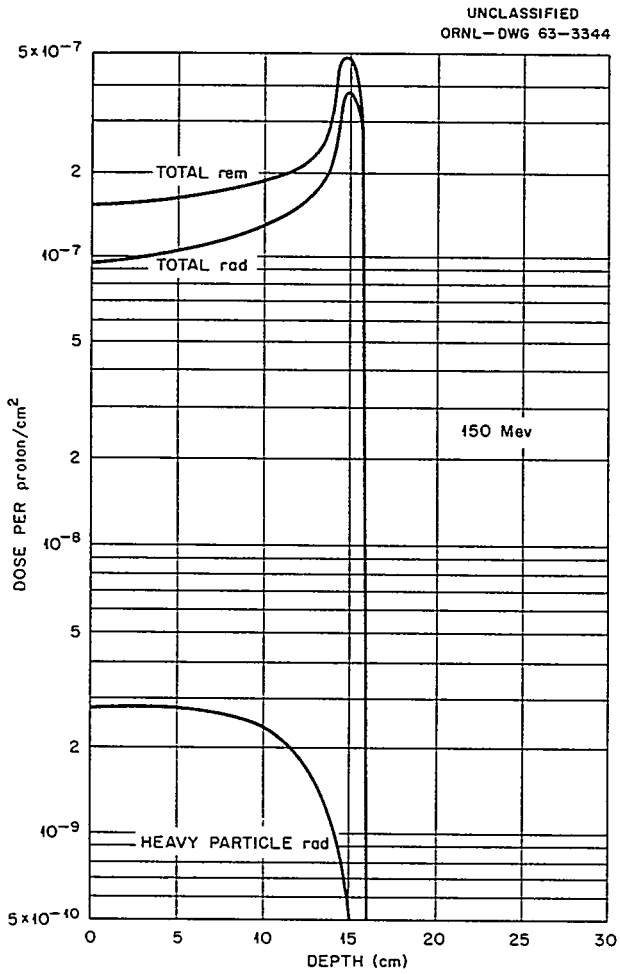

Fig. 12.2. Dose from 150-Mev Protons Normally Incident on a 30-cm Tissue Slab.

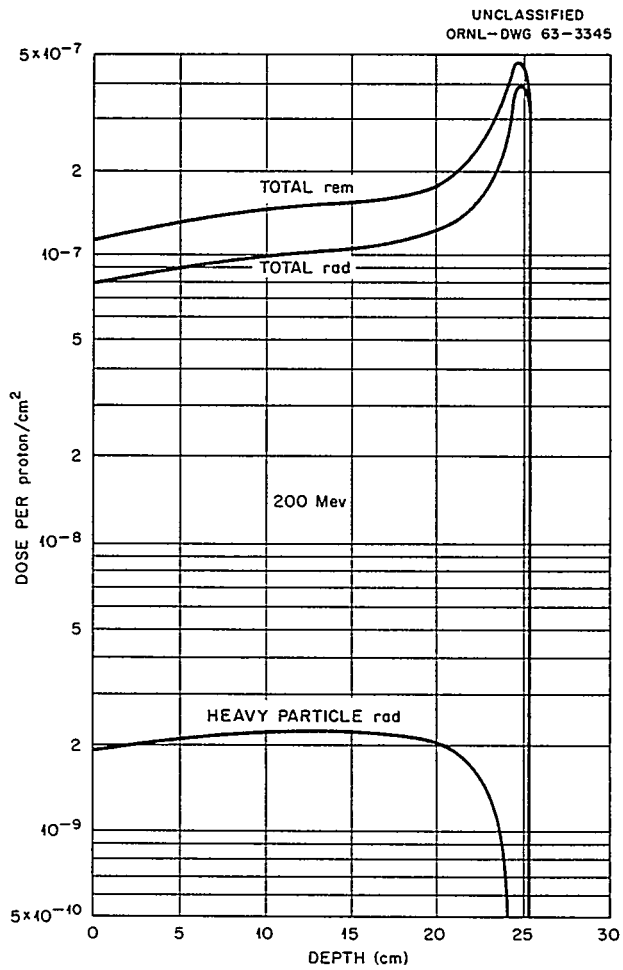

Fig. 12.3. Dose from 200-Mev Protons Normally Incident on a 30-cm Tissue Slab.

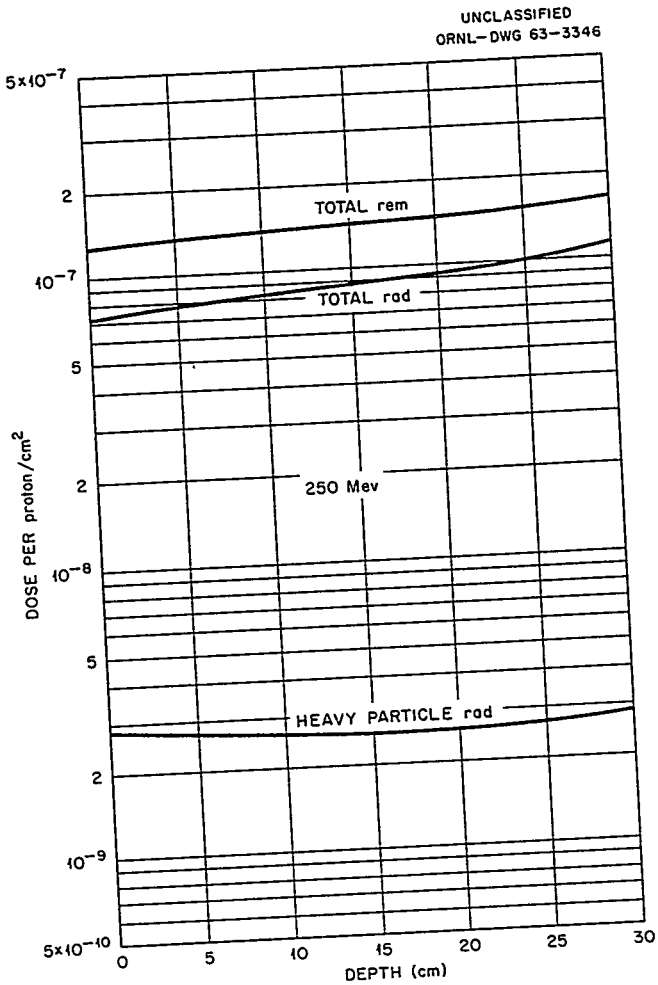

Fig. 12.4. Dose from 250-Mev Protons Normally Incident on a 30-cm Tissue Slab.

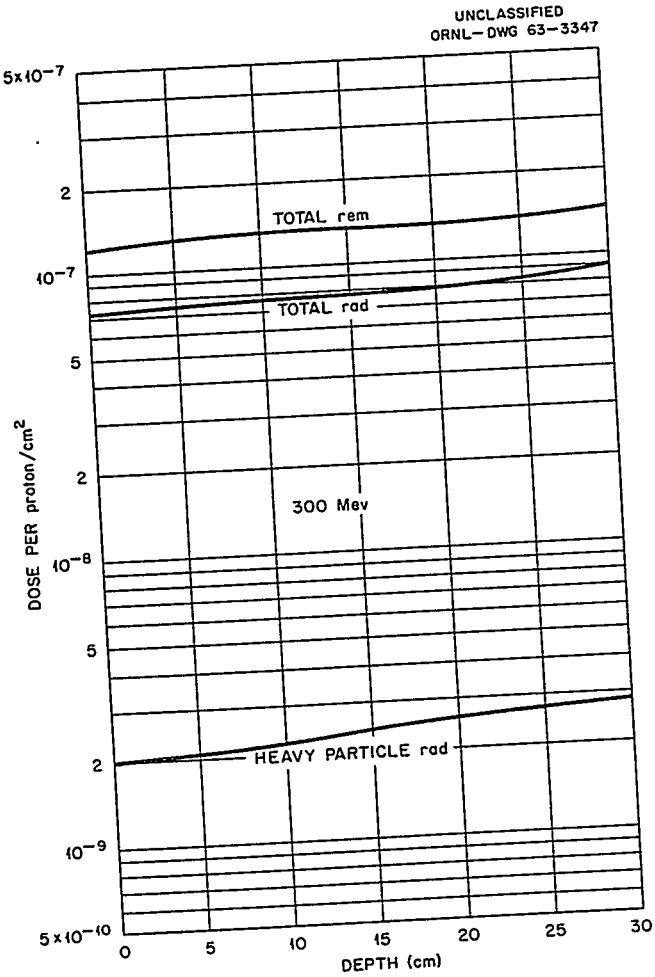

Fig. 12.5. Dose from 300-Mev Protons Normally Incident on a 30-cm Tissue Slab.

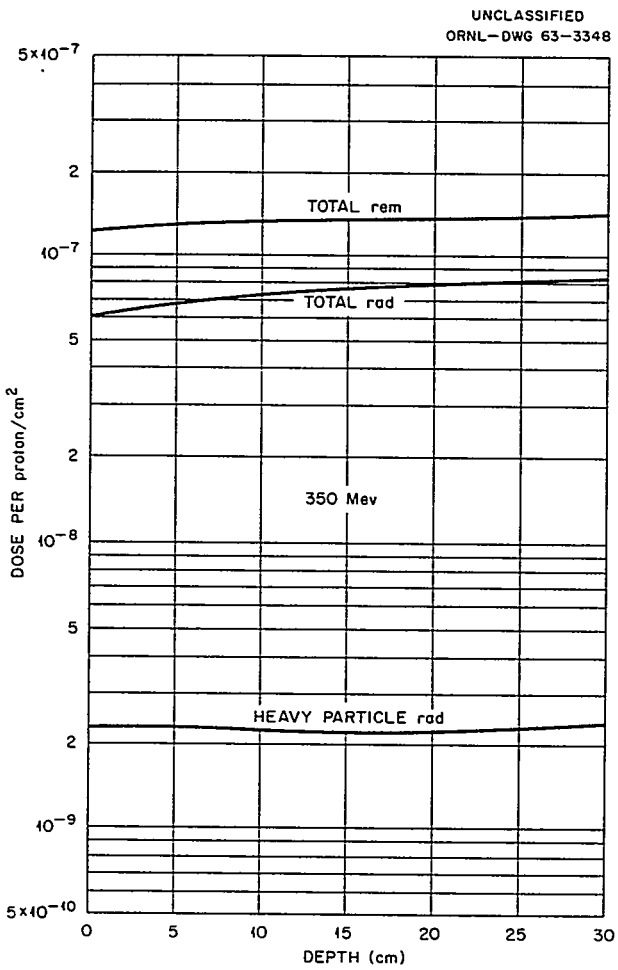

Fig. 12.6. Dose from 350-Mev Protons Normally Incident on a 30-cm Tissue Slab.

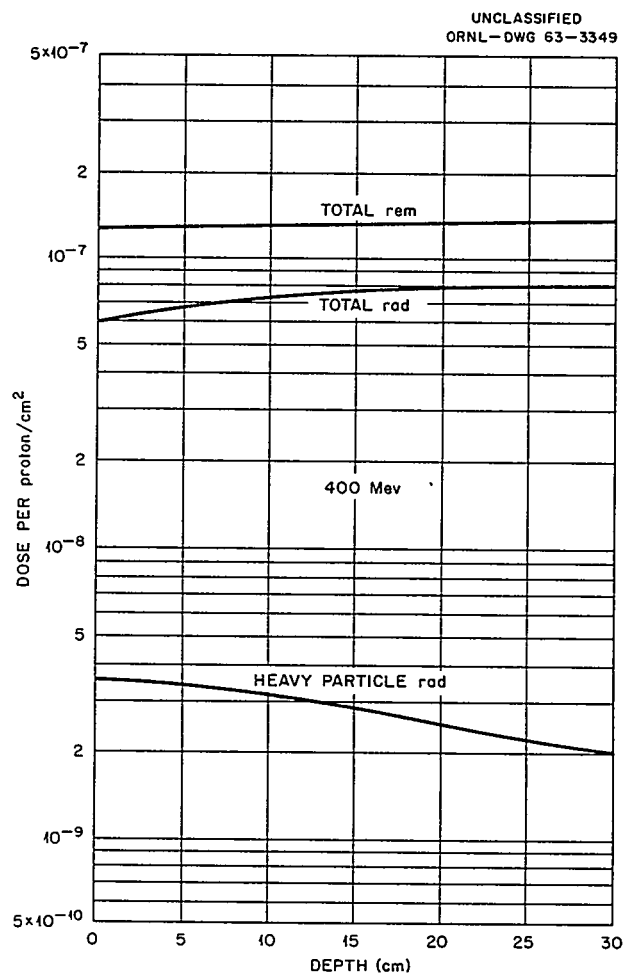

Fig. 12.7. Dose from 400-Mev Protons Normally Incident on a 30-cm Tissue Slab.

rad dose is generally quite uniform throughout the slabs in which the primary protons do not come to rest (Figs. 12.4–12.7). For 200 Mev and below, protons coming to rest show the familiar Bragg peak.

The RBE values used in the above calculations are based on current recommendations of the NCRP. The highest values of linear energy transfer (LET) for which recommendations are given is 1750 Mev per centimeter of path length. For the rem dose estimations the value RBE = 20 was used for particles having an LET greater than 1750 Mev/cm.

Additional calculations are being completed for a tissue phantom of finite geometry (parallelepiped) irradiated isotropically by protons in the energy range 50 to 400 Mev. A program for the calculation of rad and rem dose for this case has been completed, and detailed results are expected to be available soon.

Work is continuing on the extension of these calculations into the Bev region. Preliminary studies of the mean proton ranges were made, taking into account nuclear interactions in which pions originate.

STUDIES CONCERNING THE RELATION OF RBE TO LET

W. S. Snyder Jacob Neufeld

A code has been written to compute the distribution of dose with LET, primarily with a view to analyzing more precisely the biological response of animals exposed to neutron irradiation. Although many such experiments (particularly those using neutrons with energies at or below 14 Mev) have been reported, interpretation of the results in terms of RBE or LET is difficult because the flux of radiation within the tissue is not of uniform quality. Even in the case of a monoenergetic primary beam of neutrons, the recoil nuclei have a continuous distribution of energies; thus there is a continuous distribution of LET values. In general, when biological effects are interpreted in terms of LET, only an average LET value is employed. Except when the relation of RBE and LET is linear, such an interpretation may be misleading and might conceal the real form of the functional relation.

The code is designed to calculate the function $f(L)$, the fraction of dose within a prescribed volume element which is delivered at LET rates not exceeding L. In most instances the function $f(L)$ will vary with the position of the volume element considered. Figure 12.8 illustrates this concept in the case of a proton of energy E_0 absorbed in the volume element. If $E_1 < E_2$ are the two proton energies for which $dE/dx = L$, then $E_0 - E_2 + E_1$ is the amount of dose contributed to the volume element in question. The function $f(L)$ is defined as the ratio of the total of all doses delivered in the volume element with LET less than L to the total dose in the volume element. The code is designed to calculate $f(L)$ using as input data, the particle histories calculated by standard programs of the Monte Carlo type.

Although no machine results are available at this time, several first-collision calculations were carried out in order to test the usefulness of this type of analysis. Table 12.1 gives an estimated LET spectrum of first-collision dose calculated for modified fission-spectrum neutrons[5] and for 14-Mev neutrons. It is clear that in the first case the preponderance of dose is in the range 7 to 100 kev/μ, while much of this dose must be reassigned to lower or higher LET categories in the second case. Although not accurate for

[5] G. J. Neary *et al.*, *Chronic Radiation Hazards*, p 25, Pergamon, London, 1957.

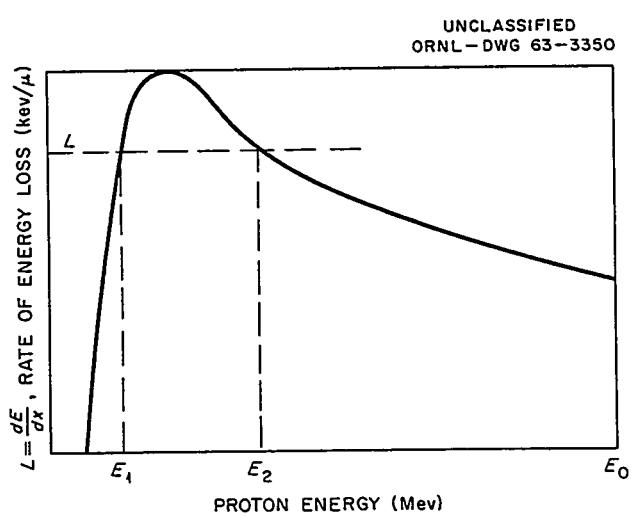

Fig. 12.8. Proton Dose for Various Ranges of LET.

Table 12.1. Percentage of Neutron Dose in Various Ranges of LET

LET (kev/μ)	Percentage of Dose for Specified Neutron Source	
	Modified Fission-Spectrum Neutrons	14-Mev Neutrons
<3.5	0.29	0.031
3.5–7	0.11	42.0
7–25	12.00	7.5
25–50	34.00	14.0
50–100	47.00	7.3
>100	6.6	29.0

irradiation of mice, these distributions should be qualitatively correct. It has been reported by Andrews and Berry[6] that there is no clear evidence of repair when mammalian tumor cells are irradiated by fission-spectrum neutrons; they also report,[7] similarly, that there is little or no oxygen effect present. However, oxygen effect and repair were reported for similar studies in which 14-Mev neutrons were used. This difference in response is not surprising in view of the pronounced difference of the LET distribution of dose in these two cases (see Table 12.1). It may be that a finer analysis of such mammalian data, with an accurate appraisal of the distribution of dose with LET, will reveal more clearly the regions of LET where RBE might be expected to decline.

SHELL CORRECTIONS TO ATOMIC STOPPING POWER

The stopping power, or average rate of energy loss dE/dx, of heavy charged particles in a material containing N atoms/cm^3 of atomic number Z can be written

$$-\frac{dE}{dx} = \frac{4\pi z^2 e^4}{mv^2} NZ \left[\ln \frac{2mv^2}{I(1-\beta^2)} - \beta^2 - \frac{C}{Z} \right], \quad (1)$$

where z and v are the charge and velocity of the incident particle, m and e are the electronic mass and charge, and I is the mean excitation energy of the stopping material. The quantity C denotes a shell correction term, which arises when the velocity of the incident particle cannot be considered as being large compared with the velocities of electrons in the ground state of the atoms of the stopping material.

An investigation of shell corrections in atomic stopping-power theory has been carried out in collaboration with U. Fano at the National Bureau of Standards, following an approach suggested by Fano. To extend stopping-power theory, one can retain more terms in the expansion of the inelastic form factor than are usually treated.[8] The additional contributions to stopping power which thus arise can be identified with parts of the traditional shell corrections C/Z to the theory and have the form of a power series in inverse powers of v^2, the square of the velocity of an incident particle. The coefficients of the series are well-defined properties of the ground state of the atoms of the stopping material[9] and can be evaluated numerically. The series was used to estimate tentative shell corrections for various elements at high incident particle energy, that is, in the limit $v \to c$, where c is the velocity of light. These estimates were used with smoothed stopping power and range data of Bichsel[10] and Whaling[11] to construct graphs for protons having the estimated value of C/Z at $v = c$, from which the total shell corrections for a stopping element can be found over a wide range of incident particle energy (see Fig. 12.9). Although only the general

[6] J. R. Andrews and R. J. Berry, *Radiation Res.* 16, 76 (1962).

[7] R. J. Berry and J. R. Andrews, "The Effect of Radiation Ionisation Density (LET) upon the Reproductive Capacity of Mammalian Tumour Cells Irradiated and Assayed *in Vivo*," unpublished data.

[8] U. Fano, "Penetration of Protons, Alpha Particles and Mesons," to be published in vol 13, *Ann. Rev. Nucl. Sci.*

[9] G. Placzek, *Phys. Rev.* 86, 377 (1952).

[10] H. Bichsel, *Passage of Charged Particles Through Matter*, University of Southern California Technical Report 2 (1961); *Higher Shell Corrections in Stopping Power*, University of Southern California Technical Report 3 (1961)[AEC contract AT(04-3)-136].

[11] W. Whaling, "The Energy Loss of Charged Particles in Matter," pp 193–217 in *Handbuch der Physik*, vol 34, Springer, Berlin, 1958.

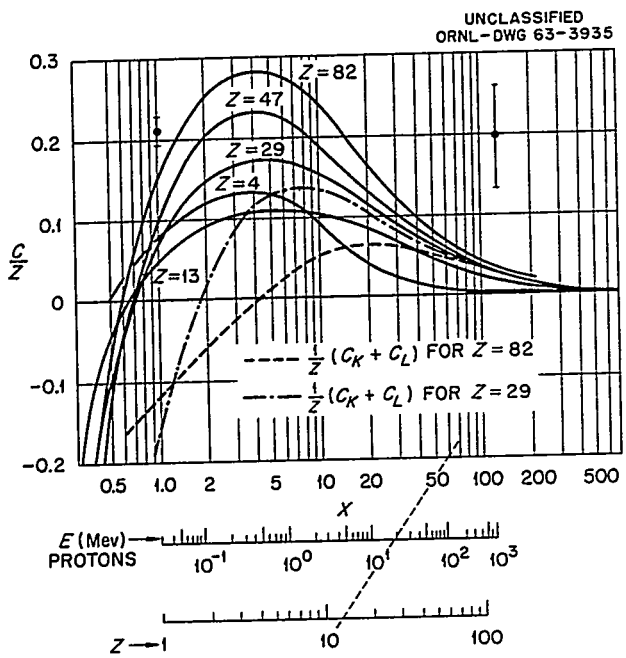

Fig. 12.9. Total Shell Corrections C/Z for Protons in Various Metals as a Function of $x = v^2/v_0^2 Z$, Where v_0 Is the Velocity of an Electron in the Ground State of a Hydrogen Atom. The example of nomogram use shows that $x = 59$ for 20-Mev protons in aluminum. The dashed curves show (for comparison) K- and L-shell corrections of Walske [*Phys. Rev.* 88, 1283 (1952) and 101, 940 (1956)].

features of the graphs can be regarded as experimentally significant at the present time, the graphs permit an evaluation of shell corrections which give values of stopping power to within a very few percent. The error bars in the figure show the approximate magnitude of the uncertainty in C/Z, which corresponds to an uncertainty of 1% in the value of the stopping power for all elements at the abscissas shown. A full report of this work will appear in the literature.[12]

LOW-ENERGY END OF THE SECONDARY ELECTRON CASCADE IN METALS

The importance of cascade and slowing-down processes of low-energy electrons in solids is self-evident. Any corpuscular radiation interacting with matter gives rise to a large number of electrons having energy of the order of a few electron volts. These electrons interact strongly with the medium in which they diffuse. Hence, in order to understand the ultimate effects of the primary radiation, one must investigate these processes in some detail.

Spencer and Fano[13] have given considerable attention to the high-energy end of the spectrum, where the detailed electronic structure of the stopping material is not important. Wolff[14] has considered slowing down and cascade in a free-electron gas by the use of cross sections taken from the Bohm-Pines theory. Ritchie[15] has computed interaction cross sections for low-energy electrons in a more systematic fashion using a consistent perturbation-theoretic treatment of the many-body problem in a free-electron gas. These cross sections have been employed to determine the cascade spectrum of electrons in an idealized metal.

The space- and angle-independent Boltzmann equation describing $u(x)$, the electron flux per unit energy interval at energy x due to a constant source emitting $S(x)\,dx$ electrons in the energy interval $(x, x + dx)$ may be written

$$u(x) \int_0^x \tau_L(x,t)\,dt = \int_x^\infty u(t)\tau_L(t,t-x)\,dt + \int_x^\infty u(t)\tau_S(t,x)\,dt + S(x)\,. \qquad (2)$$

In this equation

$\tau_L(x,t) = \tau_e(x,t) + \tau_P(x,t)$,

$\tau_P(x,t)\,dt$ = probability per centimeter that a primary electron with energy x will experience an energy loss t in the interval dt in exciting plasma oscillations in the free-electron gas,

$\tau_e(x,t)\,dt$ = corresponding probability for exciting a single electron with attendant loss by the primary in the interval $(t, t + dt)$,

$\tau_S(x,t)\,dt$ = probability per centimeter that a primary electron with energy x shall excite a single secondary electron to the energy interval $(t, t + dt)$.

[12] U. Fano (ed.), *NAS-NRC Report on Penetration of Charged Particles in Matter*, to be published.

[13] L. V. Spencer and U. Fano, *Phys. Rev.* 93, 1172 (1954).

[14] P. A. Wolff, *Phys. Rev.* 95, 56 (1954).

[15] R. H. Ritchie, *Phys. Rev.* 114, 644 (1959).

All energies are measured in units of the Fermi energy E_F from the top of the Fermi sea.

Figure 12.10 shows a plot of $a_0(x + 1)\tau_P(x,t)$ for a very high-energy primary electron ($x \gg 1$) at various electronic densities specified by different values of $\chi^2 \equiv (1/\pi)(\mathrm{Ry}/E_F)^{1/2}$, where $\mathrm{Ry} = e^2/2a_0$, and $a_0 = \hbar^2/me^2$. It is understood that electrons in the distribution must have positive energies. This cross section is subject to the restriction that momentum and energy must be conserved between the incident electron and the free-electron gas. This leads to a minimum value of energy loss t, which depends on x in a rather complicated way not shown here. Figure 12.11 gives plots of $a_0(x + 1)\tau_e(x,t)$, which depends only on t in the present approximation, for different values of χ^2. Figure 12.12 shows the function $a_0(x + 1)\tau_S(x,t)$ as a function of t for various values of x and for $\chi^2 = 0.344$.

When one has a monoenergetic source of energy x_0, and if $x_0 \lesssim 1$, $x \ll 1$, an analytic representation for $u(x)$ may be found. One obtains

$$u(x) \approx \text{const}\left(\frac{x_0^{0.56}}{x^{3.56}}\right),$$

showing an extremely large flux buildup at low energies, due primarily to the vanishing of the cross section τ_e as $x \to 0$.

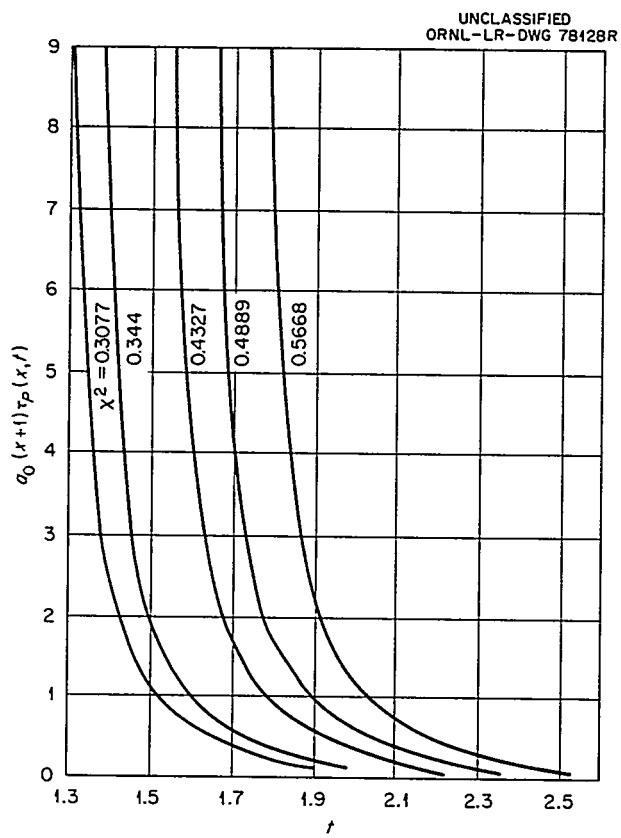

Fig. 12.10. $\tau_P(x, t)$ – Cross Section for Plasma Excitation.

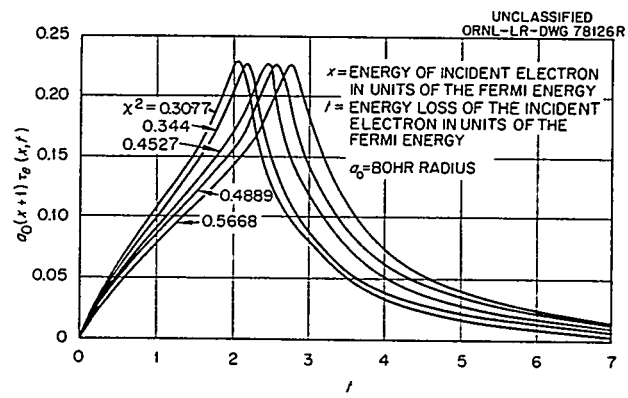

Fig. 12.11. $\tau_e(x, t)$ – Inverse Mean Free Path for One-Electron Excitation in a Free-Electron Gas.

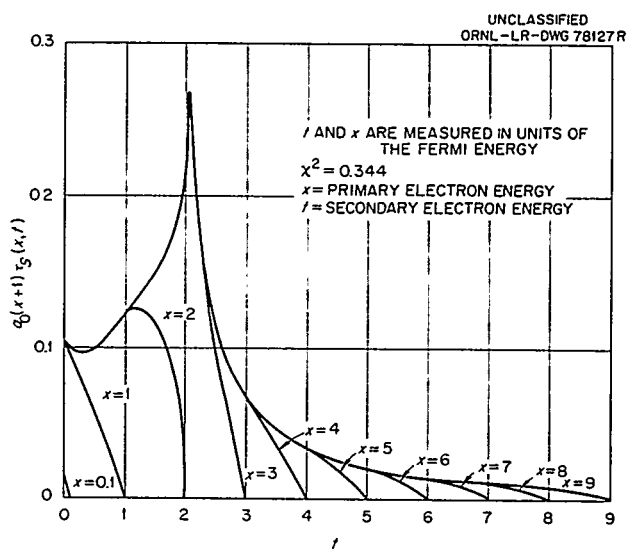

Fig. 12.12. $\tau_S(x, t)$ – Cross Section for Production of Secondary Electrons.

Preliminary results using a numerical method of solving Eq. (2) and employing larger values of x_0 indicate that the shape of the low-energy end of the spectrum $x \lesssim 1$ is nearly independent of x_0 and that the quantity $[u(x)/x_0 a_0]$ is nearly independent in magnitude as well for $x_0 \gg 1$. A comparison of $u(x)/x_0 a_0$ computed for $x_0 = 5$ with experimental data obtained by Finston *et al.*[16] is shown in Fig. 12.13. This comparison is rather encouraging since there are no adjustable parameters in the theory. More detailed comparisons will be reported elsewhere.

[16]R. A. Finston *et al.*, *Measurement of Electron Flux in Irradiated Media by AC Methods*, ORNL-2732 (Aug. 31, 1959).

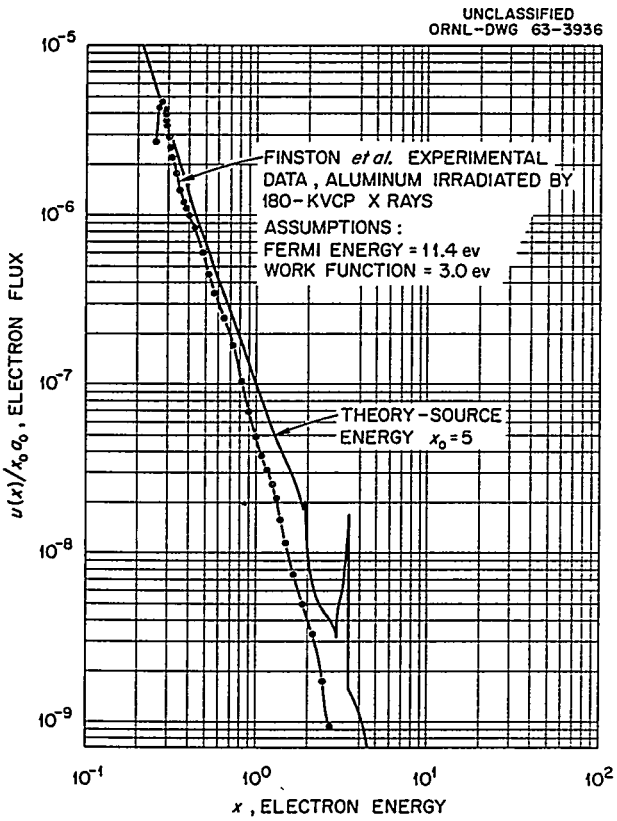

Fig. 12.13. Comparison of Experiment and Theory for the Low-Energy Electron Cascade Spectrum in Aluminum.

SURFACE PLASMON DISPERSION RELATION

Kanazawa[17] considered the dispersion relations and lifetimes for surface and volume plasmons in a metallic foil bounded on both sides by vacuum using the Bohm-Pines quantum-mechanical random-phase approximation.

His results for the dispersion relation of surface plasmons do not appear to agree with those obtained[18] using a semiclassical hydrodynamical description of these oscillations. Experimental work in the field of characteristic energy losses is becoming increasingly sophisticated, and soon it may be possible to determine by physical measurement which of these two theoretical results, both of which are necessarily approximate, is more nearly correct.

If one applies the hydrodynamical electron theory of Bloch[19–21] in its linearized form to an electron gas having an initially uniform density of electrons n_0 inside a planar foil bounded on both sides by vacuum, assumes that the density drops abruptly to zero at each surface, and requires that the component of the perturbed electron motion normal to the surface be zero at the surface, one obtains, as a condition for surface oscillation,

$$2\beta^2\gamma/\omega_p^2 - (1 - e^{-(K+\gamma)a})/(K+\gamma) = \pm e^{-\gamma a}\{2\beta^2\gamma/\omega_p^2 + [1 - e^{-(K-\gamma)a}]/(K-\gamma)\}\,, \quad (3)$$

where a = foil thickness; $\beta = \sqrt{3/5}\,x$ (Fermi velocity for the electron gas); the plasma frequency $\omega_p = (4\pi n_0 e^2/m)^{1/2}$; $\gamma^2 = (\omega_p^2 + \beta^2 K^2 - \omega^2 - i\alpha\omega)/\beta^2$; α = schematic damping constant for electronic motion; ω = frequency of oscillation; and $\vec{K}$ = component of the wave vector of the oscillation parallel to the foil surfaces.

One may obtain an approximate solution of this equation by iteration, if the conditions $\alpha \to 0$,

[17]H. Kanazawa, *Progr. Theoret. Phys. (Kyoto)* 26, 851 (1961).

[18]R. H. Ritchie, Ph.D. thesis, University of Tennessee, 1959 (unpublished).

[19]F. Bloch, *Z. Physik* 81, 363 (1933).

[20]F. Bloch, *Helv. Phys. Acta* 1, 358 (1934).

[21]H. Jensen, *Z. Physik* 106, 620 (1937).

$\beta^2K^2 \ll (\omega^2 - \omega_p^2)$, and $\gamma a \gg 1$ are fulfilled. The last of these conditions is satisfied if the foil is thick compared with the Debye length in the plasma and seems necessary if collective modes in the system are to exist. One finds

$$\omega = \frac{\omega_p}{\sqrt{2}}(1 \pm e^{-Ka})^{1/2} \times \left[1 + \frac{\beta K}{\sqrt{2}\omega_p}(1 \mp e^{-Ka})^{-1/2}\right]. \quad (4)$$

If the term involving β may be neglected, this agrees with a result obtained earlier by Ritchie.[22] In the limiting case of a thick foil, $Ka \gg 1$, one obtains

$$\omega = \frac{\omega_p}{\sqrt{2}}\left(1 + \frac{\beta K}{\sqrt{2}\omega_p}\right). \quad (5)$$

This does not agree with Kanazawa's Eq. (2.20), which in the present notation would read

$$\omega = \frac{\omega_p}{\sqrt{2}}\left(1 + \frac{2\beta^2K^2}{\omega_p^2}\right), \quad (6)$$

revealing quite a different dependence of "tangential" surface oscillations upon the wave vector K.

The case $Ka \ll 1$, which is designated case A in reference 12, yields the result

$$\omega_+ = \omega_p + \beta/\sqrt{2}a \quad (7)$$

for the choice of the plus sign in Eq. (7). This corresponds to "normal" oscillations at nearly the full plasma frequency. The minus sign yields

$$\omega_- = \sqrt{Ka}\left(\frac{\omega_p}{\sqrt{2}} + \frac{\beta K}{2}\right). \quad (8)$$

Equations (7) and (8) agree with the corresponding results obtained by Kanazawa if the term containing β may be neglected.

TRANSITION RADIATION FROM A TWO-LAYERED FOIL

The distribution of photons emitted when a charged particle passes through a single dielectric foil has been considered in detail in previous publications.[23,24] However, in experimental work a homogeneous plane foil is often difficult to achieve. Even in systems employing relatively high vacuums, impurity or oxide layers may form on exposed surfaces. Such layers may modify the emitted radiation appreciably.

A calculation has been made of the photon distribution from a foil consisting of two layers of arbitrary thicknesses and dielectric constants bombarded by normally incident charged particles of arbitrary velocity. These results may be applied not only to a foil and its oxide layer but also to a foil consisting of two different metals.

One supposes that a layer of material fills the region $0 < z < a$ and is characterized by a complex dielectric permittivity $\epsilon(\omega)$. A second layer having complex dielectric permittivity $\epsilon_0(\omega)$ fills the region $a < z < b$. The composite foil is taken to be bounded by vacuum on both sides. Normally incident particles of charge Ze and speed v move in the $+z$ direction, thereby stimulating currents in the foil which result in the emission of photons. Following the procedure of ref 23, one finds for $d^2N/d\Omega d\omega$, the number of photons emitted per unit in the solid angle around the angle θ measured relative to the $+z$ axis and per unit frequency at the frequency ω,

$$d^2N/d\Omega d\omega = \frac{z^2\alpha\beta^2}{\pi^2\omega}\mu^2(1-\mu^2)\left|\frac{\Lambda}{\Delta}\right|, \quad (9)$$

where

$$\mu = \cos\theta,$$
$$\beta = v/c,$$
$$t = a\omega/c,$$
$$t_0 = (b-a)\omega/c,$$
$$\Delta = e^{i\sigma t}\xi_-\left[a_+\alpha_-e^{i\sigma_0 t_0} - a_-\alpha_+e^{-i\sigma_0 t_0}\right] + e^{-i\sigma t}\xi_+\left[a_-\alpha_-e^{i\sigma_0 t_0} - a_+\alpha_+e^{-i\sigma_0 t_0}\right],$$

[22] R. H. Ritchie, *Phys. Rev.* 106, 876, Eq. 33 (1957).

[23] R. H. Ritchie and H. B. Eldridge, *Phys. Rev.* 126, 1935 (1962).

[24] A. L. Frank, E. T. Arakawa, and R. D. Birkhoff, *Phys. Rev.* 126, 1947 (1962).

$$\Lambda = \xi_+ e^{-i\sigma t}\left[2\epsilon_0\sigma_0 C_- - a_- B_+ e^{i(1+\beta\sigma_0)t_0/\beta} + a_+ B_- e^{i(1-\beta\sigma_0)t_0/\beta}\right] - \xi_0 e^{i\sigma t}\left[2\epsilon_0\sigma_0 C_+ + a_+ B_+ e^{i(1+\beta\sigma_0)t_0/\beta} - a_- B_- e^{i(1-\beta\sigma_0)t_0/\beta}\right] - 4\epsilon\epsilon_0\sigma\sigma_0 e^{-it/\beta}\left[\frac{1}{1-\beta^2\mu^2} - \frac{\mu\beta\epsilon+1}{\epsilon(1-\beta^2\sigma^2)}\right],$$

and, further,

$$B_\pm = \frac{\beta\sigma_0 \mp \epsilon_0}{1-\beta^2\mu^2} + \frac{1}{\beta\sigma_0 \pm 1},$$

$$C_\pm = \frac{\beta\sigma \mp \epsilon/\epsilon_0}{1-\beta^2\sigma_0^2} + \frac{1}{\beta\sigma \pm 1},$$

$$a_\pm = \sigma_0\epsilon \pm \sigma\epsilon_0,$$

$$\alpha_\pm = \sigma_0 \pm \mu\epsilon_0,$$

$$\xi_\pm = \sigma \pm \mu\epsilon,$$

$$\sigma^2 = \epsilon - 1 + \mu^2,$$

$$\sigma_0^2 = \epsilon_0 - 1 + \mu^2,$$

$$\alpha = e^2/\hbar c.$$

These results are derived for $0 \leqq \theta \leqq (\pi/2)$ but may be transformed so that they describe the photon distribution function in the other hemisphere of directions (i.e., $\pi/2 \leqq \theta \leqq \pi$). In this case one puts $\cos\theta \to |\cos\theta|$, $\beta \to -\beta$, $t \to t_0$, $t_0 \to t$, $\epsilon_0 \to \epsilon$, and $\epsilon \to \epsilon_0$. A computer program to evaluate this expression is being written.

PHOTON ABSORPTION IN METALS DUE TO IMPURITY SCATTERING CENTERS

A very simple semiclassical derivation of the absorption probability of photons in a free-electron gas owing to the presence of impurity scattering centers has been carried out.

One assumes that a spatially constant, time-varying transverse electromagnetic field exists in a large free-electron gas of volume V containing N randomly spaced scattering centers per unit volume. Let the electric vector of this field be $\mathbf{E}(t) = \mathbf{E}_0 e^{-i\omega_0 t}$. In the first approximation the electron gas will oscillate in response to this field, generating a current $\mathbf{j} = -en\xi(t)$. The displacement vector $\xi(t)$ of a representative electron is taken to be $\xi(t) = [e/(m\omega_0^2)]\mathbf{E}(t)$. This oscillating motion of the electron gas will give rise, through collisions via the scalar potential, to a time-varying force $\mathbf{F}_1$ on the scattering centers. This force is equal and opposite to the space-averaged force with which the ions react on the electron gas. To determine $\mathbf{F}_1$, one may transform to a moving system of coordinates in which the electrons are at rest and the centers move in a mode described by displacement vector $-\xi(t)$ from their original positions. In the usual way one computes the force acting at the position of a given atom by use of the dielectric theory of the free-electron gas, assuming that the displacement vector $\xi(t)$ times $\mathbf{k}$, the wave vector of the disturbance, is a small quantity. The total force $\mathbf{F}_1$ is obtained by summing over the NV centers, assuming no interference in the scattering processes. One now assumes that the space-averaged electric field acting on the electron gas in the direction of the applied field is given by $\mathbf{E}_0 \cdot \mathbf{F}_1[1/(enV|\mathbf{E}_0|)]$, where n is the electron density, so that the inverse conductivity of the system is given as the solution of

$$\frac{1}{\sigma_1} = \frac{\mathbf{E}(t)}{-en\xi(t) + \sigma_1[\mathbf{E}_0 \cdot \mathbf{F}_1(t)/enV|\mathbf{E}_0|]\hat{e}}. \qquad (10)$$

In this manner one obtains

$$\sigma_1 = \frac{i\omega_P^2}{4\pi}\left[\frac{1}{\omega_0 + \frac{4\pi Z_I^2 e^2}{m\omega_0}\frac{N}{n}\frac{1}{L^3}\sum_{\mathbf{k}}\left(\frac{\mathbf{k}\cdot\hat{e}}{k}\right)^2\left(\frac{1}{\epsilon_{\mathbf{k},0}} - \frac{1}{\epsilon_{\mathbf{k},\omega_0}}\right)}\right], \qquad (11)$$

which reduces in the limit $\omega_0 \to 0$ to the dc conductivity obtained by the procedure of Mott.[25] In this expression, ω_P is the plasma frequency and $Z_I e$ is taken to be the charge on a single scattering center. The unit vector $\hat{e}$ is taken in the direction of $\mathbf{E}_0$. This expression also

[25] N. F. Mott, *Proc. Phys. Soc. (London)* A62, 136 (1949).

reduces to that obtained by Ron and Tzoar[26] in the limit $\omega_0 \to \infty$ if one allows for the fact that they consider $Z_I = 1$ and $n = N$.

CONSTITUTIVE EQUATIONS FOR A MOVING MEDIUM

Maxwell's formulation of the phenomenological behavior of an electromagnetic field interacting with a material medium contains four equations relating the quantities **E**, **B**, **D**, and **H** (where **E** is the electric field intensity, **B** the magnetic induction, **D** the electric displacement, and **H** the magnetic intensity). Only two of these equations are independent; therefore the dynamical system described by these equations is not complete. In order to determine uniquely and unambiguously the behavior of this system, the two Maxwell equations should be combined with two "constitutive equations." The constitutive equations provide relations between the macroscopic field quantities **D** (or **P**), **H** (or **M**), and the corresponding microscopic quantities **E** and **B** (where **P** is the electric polarization, and **M** is the magnetic polarization).

Consider an extended and uniform medium comprised of a charged, equilibrated electron beam having density n and moving with the velocity $V = \beta c$ (where c is the velocity of light). The constitutive equations for such a medium are as follows:

$$\mathbf{P} = \alpha_{ee}\mathbf{E} + \alpha_{em}\mathbf{B}\,, \tag{12}$$

$$\mathbf{M} = \alpha_{me}\mathbf{E} + \alpha_{mm}\mathbf{B}\,, \tag{13}$$

where α_{ee} is the "*ee* susceptibility," α_{em} is the "*em* susceptibility," α_{me} is the "*me* susceptibility," and α_{mm} is the "*mm* susceptibility."

The constitutive macroscopic parameters α_{ee}, α_{em}, α_{me}, and α_{mm} are tensors. Only two of these are independent. Using x,y,z coordinates and assuming that **k** is aligned in the z direction, one obtains for an arbitrary direction of **v** the following expressions for the constitutive parameters α_{ee} and α_{em}:

$$\begin{aligned}
(\alpha_{ee})_{11} &= A\left(1 - \frac{v_x^2}{c^2}\right);\\
(\alpha_{ee})_{12} &= (\alpha_{ee})_{21} = -A\frac{v_x v_y}{c^2};\\
(\alpha_{ee})_{13} &= (\alpha_{ee})_{31} = -A\frac{v_x v_z}{c^2};\\
(\alpha_{ee})_{22} &= A\left(1 - \frac{v_y^2}{c^2}\right);\\
(\alpha_{ee})_{23} &= (\alpha_{ee})_{32} = -A\frac{v_y v_z}{c^2};\\
(\alpha_{ee})_{33} &= A\left(1 - \frac{v_z^2}{c^2}\right);
\end{aligned} \tag{14}$$

and

$$\begin{aligned}
(\alpha_{em})_{11} &= (\alpha_{em})_{22} = (\alpha_{em})_{33} = 0;\\
(\alpha_{em})_{12} &= -(\alpha_{em})_{21} = -A\frac{v_z}{c};\\
(\alpha_{em})_{13} &= -(\alpha_{em})_{31} = A\frac{v_y}{c};\\
(\alpha_{em})_{23} &= -(\alpha_{em})_{32} = -A\frac{v_x}{c};
\end{aligned} \tag{15}$$

where

$$A = \frac{ne^2(1-\beta^2)^{1/2}}{mc(\omega - ck\beta)}\,, \tag{16}$$

e is the electronic charge, and m is the mass of an electron.

The two remaining paramaters α_{me} and α_{mm} can be formulated by means of Eqs. (14) and (15). Thus α_{me} is directly obtained from Eq. (15) because of the following relation:

$$\alpha_{me} = -\alpha_{em}\,. \tag{17}$$

The expression for α_{mm} is directly obtained from α_{ee} because of the following relation:

$$\alpha_{mm} = \alpha_{ee} - AI\,, \tag{18}$$

where the symbol I designates a unit tensor.

[26] A. Ron and N. Tzoar, *Phys. Rev. Letters* 10, 45 (1963).

INSTABILITIES IN A PLASMA-BEAM SYSTEM IMMERSED IN A MAGNETIC FIELD

The interaction of an electron or an ion beam moving with velocity βc through a stationary plasma in the presence of a static magnetic field has been investigated theoretically under the assumption that the plasma is cold, that the intensity of the beam is very small, and that the beam, as well as the waves resulting from the interaction, are aligned along the direction of the magnetic field. It is well known that an electron beam moving with a velocity that exceeds the phase velocity of electromagnetic waves in a stationary plasma is capable of exciting such waves and that these waves (circularly polarized) rotate in the same direction and at the same angular frequency as the gyroelectrons of the beam. It has been shown in this investigation that there is an apparent reversal in the direction of rotation of these gyroelectrons as seen by the stationary observer. Consequently, the excited wave has a circular motion in the same direction as perturbed stationary ions. The frequency $\tilde{\omega}$ of the excited wave satisfies the inequality

$$|X| = \left|\frac{\tilde{\omega}}{\Omega_i}\right| < 1 , \tag{19}$$

where Ω_i is the gyrofrequency of perturbed stationary ions. Similarly, a wave excited by an ion beam has a circular motion in the same direction as perturbed stationary electrons. The frequency $\tilde{\omega}^i$ of the latter wave satisfies the

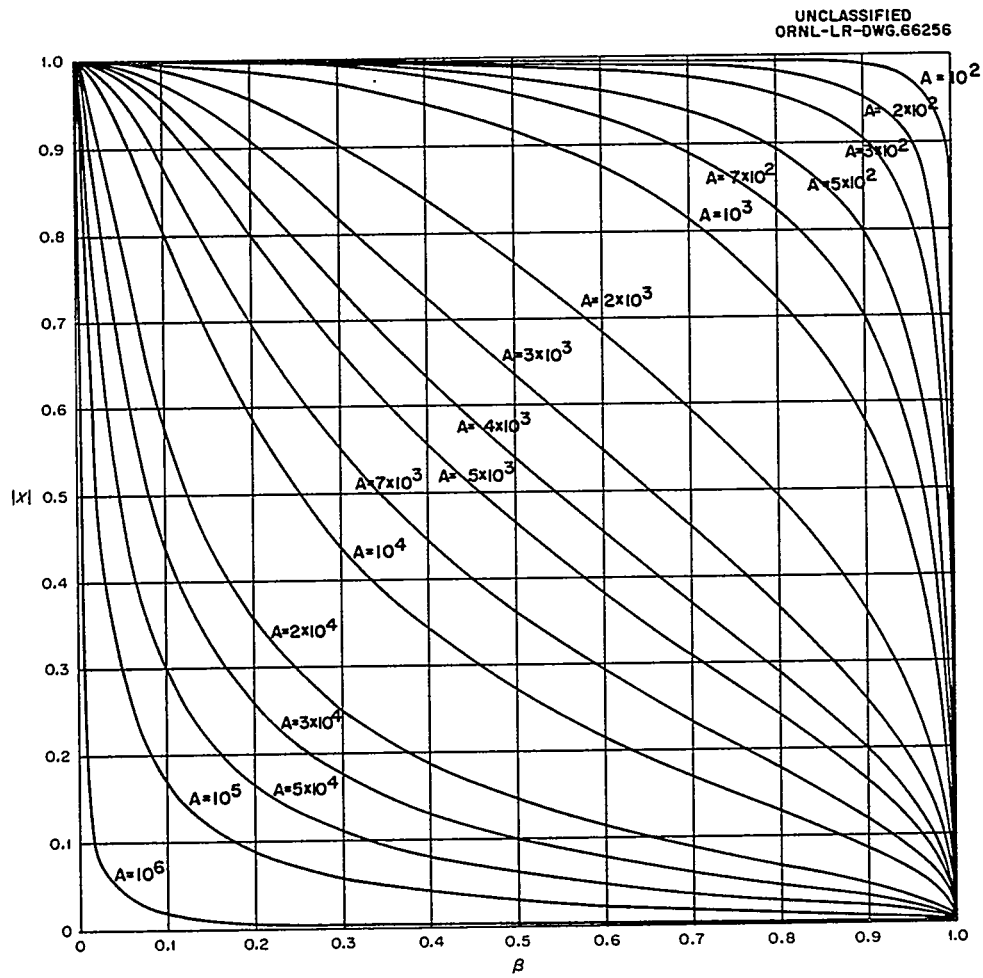

Fig. 12.14. Graphical Representation of the Relation Between $|X|$, A, and β (for an Electron Beam).

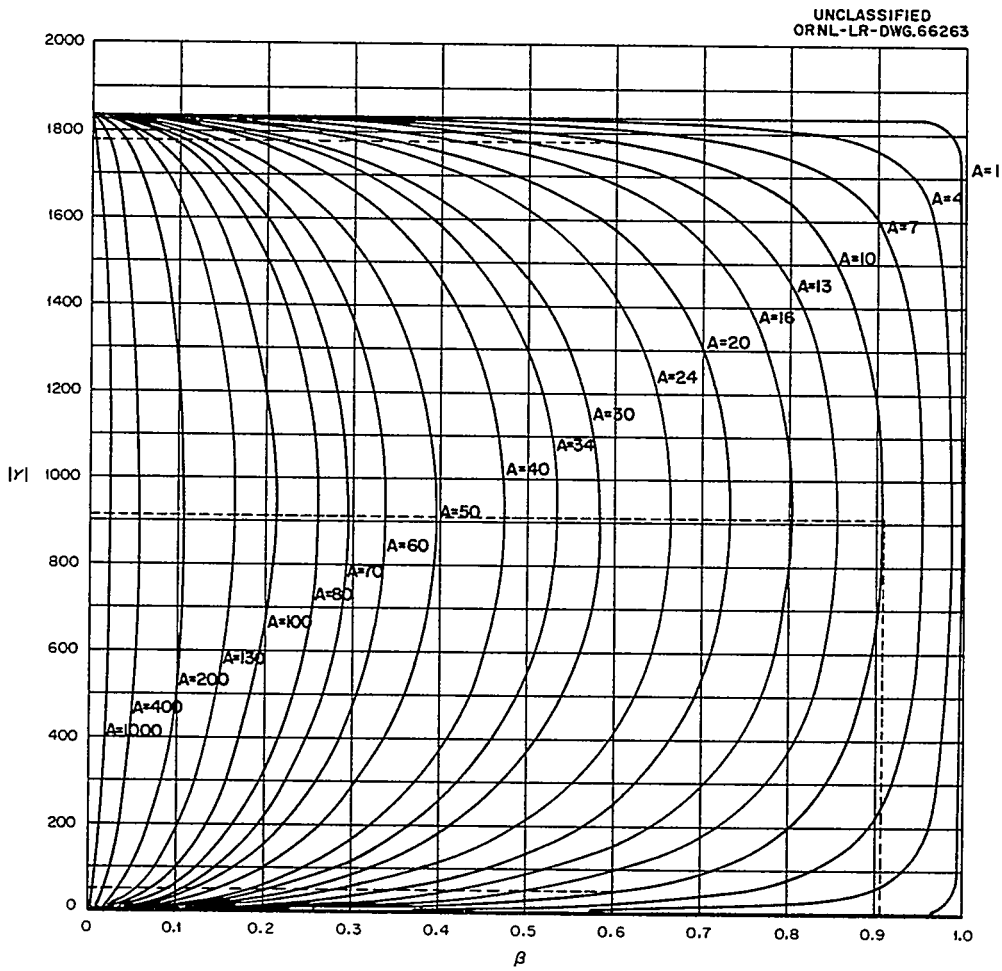

Fig. 12.15*a*. Graphical Representation of the Relation Between $|Y|$, A, and β (for an Ion Beam).

inequality

$$|Y| = \left|\frac{\tilde{\omega}^i}{\Omega_e}\right| < 1 , \qquad (20)$$

where Ω_e is the gyrofrequency of perturbed stationary electrons. It has been shown that an electron (ion) beam moving in the direction of the magnetic field can excite only a wave having negative (positive) helicity. The reverse situation occurs for a beam moving against the magnetic field.

Figure 12.14 graphically illustrates the relation between the quantity $|X|$ defined in Eq. (19) and the velocity β of an electron beam. Each of these graphs corresponds to a different value of the parameter A characterizing a plasma. One has

$$A = \frac{\omega_e}{\eta^{1/2}\Omega_i} , \qquad (21)$$

where ω_e is the plasma frequency and η is the ion-to-electron mass ratio.

A similar graph given in Figs. 12.15*a* and *b* gives the relation between the quantity $|Y|$ defined in Eq. (20) and the velocity β of an ion beam.

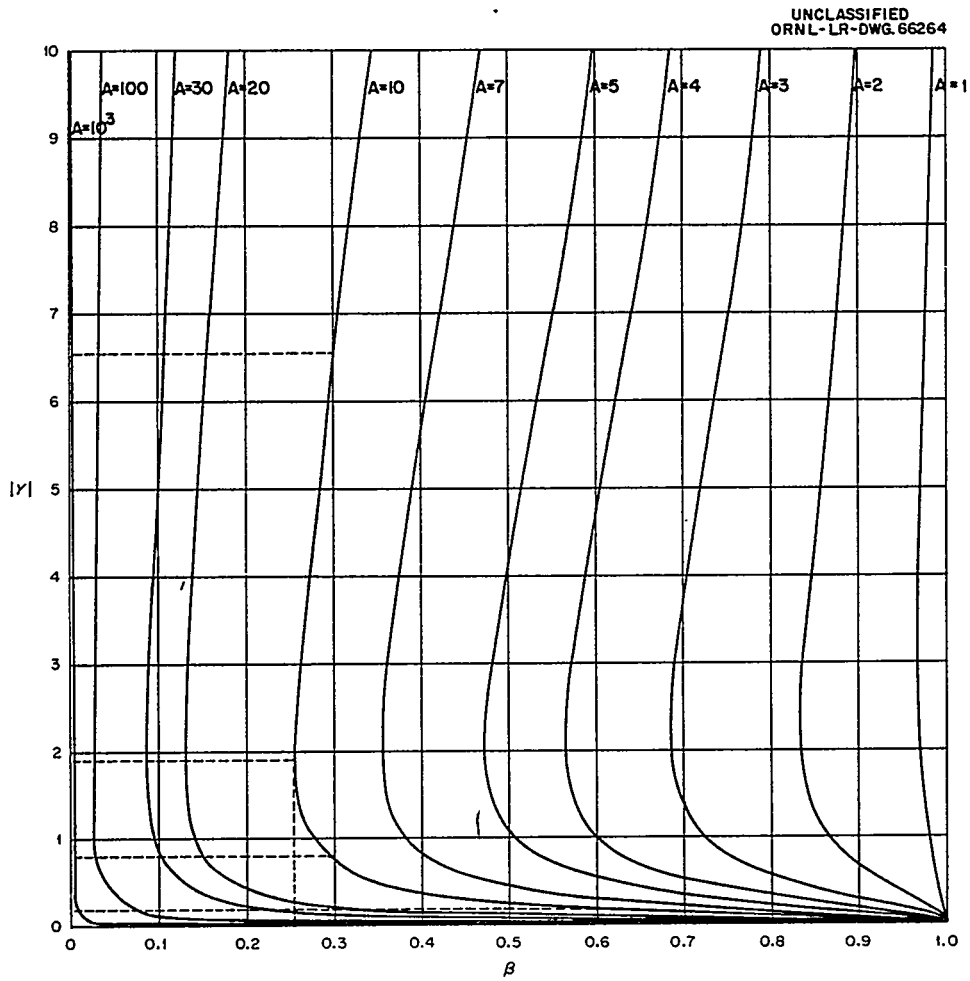

Fig. 12.15*b*. Enlarged Portion of the Graph of Fig. 12.15*a*.

13. Experimental Physics of Dosimetry

R. D. Birkhoff
E. T. Arakawa

T. E. Bortner[1]
A. E. Carter
N. O. Davis[2]
L. C. Emerson[3]
J. A. Harter
H. H. Hubbell, Jr.
G. S. Hurst
W. J. McConnell[2]
L. B. O'Kelly
J. E. Parks[4]
Devon Pittman[5]
R. M. Simmons
J. A. Sivinski[4]
J. L. Stanford[1]
J. A. Stockdale[6]
E. B. Wagner

ELECTRON INTERACTIONS WITH WATER MOLECULES

Low-Energy Interactions

The question of whether low-energy electrons (less than 1 ev) form negative ions in water vapor has been examined in a series of experiments.

Interaction of Low-Energy Electrons with Water Vapor and with Other Polar Molecules. – As previously described,[7] electron attachment coefficients and drift velocities have been measured in mixtures of H_2O vapor with N_2, CH_4, C_2H_4, and CO_2. Electron capture takes place only in the H_2O-CO_2 mixture, and even in this case the attachment coefficient is quite small. Thus low-energy (less than 1 ev) electrons do not, in general, form stable negative ions with H_2O.

Electron drift velocities are very sensitive to the addition of small quantities of H_2O in all the mixtures. When certain other polar molecules (acetone, heavy water, methyl alcohol, dimethyl ether, hydrogen sulfide, toluene, and nitrous oxide) were mixed with C_2H_4, it was found that the decreases in drift velocity correlated well with the magnitude of the electrical dipole moments. The drift velocity data were analyzed to obtain the cross sections for momentum transfer.[8] These cross sections are in fair agreement with the theory of Altshuler,[9] except for H_2O, D_2O, and H_2S, where the experimental values are a factor of 2 larger than theory. This discrepancy may be related to excitation of molecular rotation; or it may be due to the temporary formation of negative ions, an effect which would reduce the observed drift velocity. Analyses of diffusion coefficients for electron swarms released in H_2O-C_2H_4 mixtures[10] and independent drift velocity measurements[11] have confirmed the discrepancy with theory in the case of H_2O. In Fig. 13.1 the experimental results are compared with Altshuler's predictions.

Electron Capture in H_2O-O_2 Mixtures. – Recent data[11] do not confirm Bradbury and Tatel's[12] observation of electron capture in pure water vapor at low *E/P* (electric field in volts per cm, divided by total pressure in mm Hg). It was thought that small amounts of O_2 mixed with H_2O vapor might account for Bradbury and Tatel's observations. Measurements of electron attachment (by means of an apparatus described previously)[13] were made in mixtures of O_2 plus H_2O vapor with C_2H_4.

[1]Consultant.

[2]AEC Health Physics Fellow.

[3]AEC Advanced Health Physics Fellow.

[4]Summer employee.

[5]On loan from Instrumentation and Controls Division, ORNL.

[6]Guest from Australian Atomic Energy Research Establishment, Lucas Heights, Sydney, Australia.

[7]R. D. Birkhoff *et al.*, *Health Phys. Div. Ann. Progr. Rept. July 31, 1962*, ORNL-3347, p 80.

[8]G. S. Hurst, J. A. Stockdale, and L. B. O'Kelly, *J. Chem. Phys.* 38, 2572 (1963).

[9]Saul Altshuler, *Phys. Rev.* 107, 114 (1957).

[10]G. S. Hurst, L. B. O'Kelly, E. B. Wagner, and J. A. Stockdale, "Time of Flight Investigations of Electron Transport in Gases," to be published in the *Journal of Chemical Physics*.

[11]J. L. Pack, R. E. Voshall, and A. V. Phelps, *Phys. Rev.* 127, 2084 (1962); R. E. Fox, P. R. Malmberg, and R. B. Gosser, *Rev. Sci. Instr.* 32, 898 (1961).

[12]N. E. Bradbury and H. E. Tatel, *J. Chem. Phys.* 2, 835 (1934).

[13]T. E. Bortner and G. S. Hurst, *Health Phys.* 1, 39 (1958).

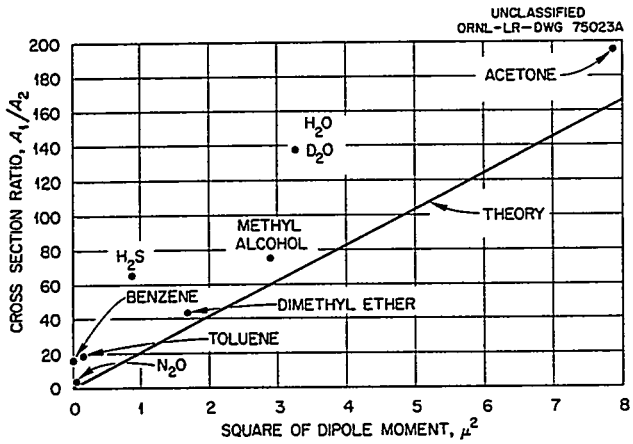

Fig. 13.1. Ratio of Cross-Section Parameters, A_1/A_2, for Various Polar Gases Added to Ethylene. (Points are experimental values; solid line is based on theory.)

Though the results show enhanced capture (above that which would be expected from non-dissociative capture of electrons by O_2),[14] the magnitude does not seem sufficient to explain the results of Bradbury and Tatel. The attachment coefficients are consistent with a process in which the H_2O molecule carries away the energy needed to stabilize the O_2 ion.[15]

Electron Transport Measurements in Mixtures of Water and Ethylene. – By use of the electron time-of-flight apparatus previously described,[16] the diffusion coefficient D and the drift velocity W for H_2O-C_2H_4 mixtures were measured. The results for D were analyzed to obtain the ratio of the cross section for momentum transfer for the two vapors and found to be in general agreement with those based on the measurement of W.[8]

In summary, all of the above work is consistent with the idea that the interaction of low-energy electrons with water vapor is a physical process in which the cross section for momentum transfer is larger (by a factor of 2) than that obtained from theory. There is no strong evidence for the formation of stable negative ions in H_2O; however, the possibility of short-lived negative ions remains a point for further investigation. More direct investigations with a time-of-flight negative-ion mass spectrometer will be undertaken.

Dissociative Capture of Electrons by D_2O Vapor

Recently data have been published on dissociative electron capture in H_2O,[17] indicating that the process peaks at an electron energy $\epsilon = 6.4$ ev with an energy-integrated cross section

$$\int_0^\infty \sigma(\epsilon)d\epsilon = 7.7 \times 10^{-18}\ \mathrm{cm}^2\ \mathrm{ev}\ .$$

A similar electron swarm measurement of these two parameters for D_2O has now been made yielding $\epsilon = 6.5$ ev and

$$\int_0^\infty \sigma(\epsilon)d\epsilon = 4.6 \times 10^{-17}\ \mathrm{cm}^2\ \mathrm{ev}\ .$$

TIME-OF-FLIGHT INVESTIGATIONS OF ELECTRON TRANSPORT IN GASES

With the electron time-of-flight apparatus previously described[16] (Geiger-Mueller counter used for single-electron detection), measurements have been made of drift velocities and diffusion coefficients in the following gases or gas mixtures: C_2H_4, CO_2, N_2, H_2, Ar + 4% H_2, and $C_2H_4 + H_2O$. In most cases the electron drift velocities obtained agree with independently determined values. Where slight differences arise, the data from the time-of-flight method may be more reliable, since the shape of the electron distribution arriving at the detector is taken into account.

More difficulty has been experienced in measurement of electron diffusion coefficients. Encouraging results have been obtained in a number of gases, but the method is limited by difficulties in operating the G-M tube as a consistent detector of single electrons.

A new electron time-of-flight apparatus has been designed and is now in the construction and test stages. As shown in Fig. 13.2, the new arrangement will consist of a new single-electron detection scheme and two stages of differential pumping to connect it to the reaction chamber.

[14] G. S. Hurst and T. E. Bortner, *Phys. Rev.* 114, 116 (1959).

[15] See, for instance, F. Bloch and N. Bradbury, *Phys. Rev.* 48, 689 (1935) and also ref 14, this chapter.

[16] R. D. Birkhoff *et al.*, *Health Phys. Div. Ann. Progr. Rept. July 31, 1962*, ORNL-3347, p 81.

[17] G. S. Hurst, L. B. O'Kelly, and T. E. Bortner, *Phys. Rev.* 123, 1715 (1961).

UNCLASSIFIED
ORNL-DWG 63-3937

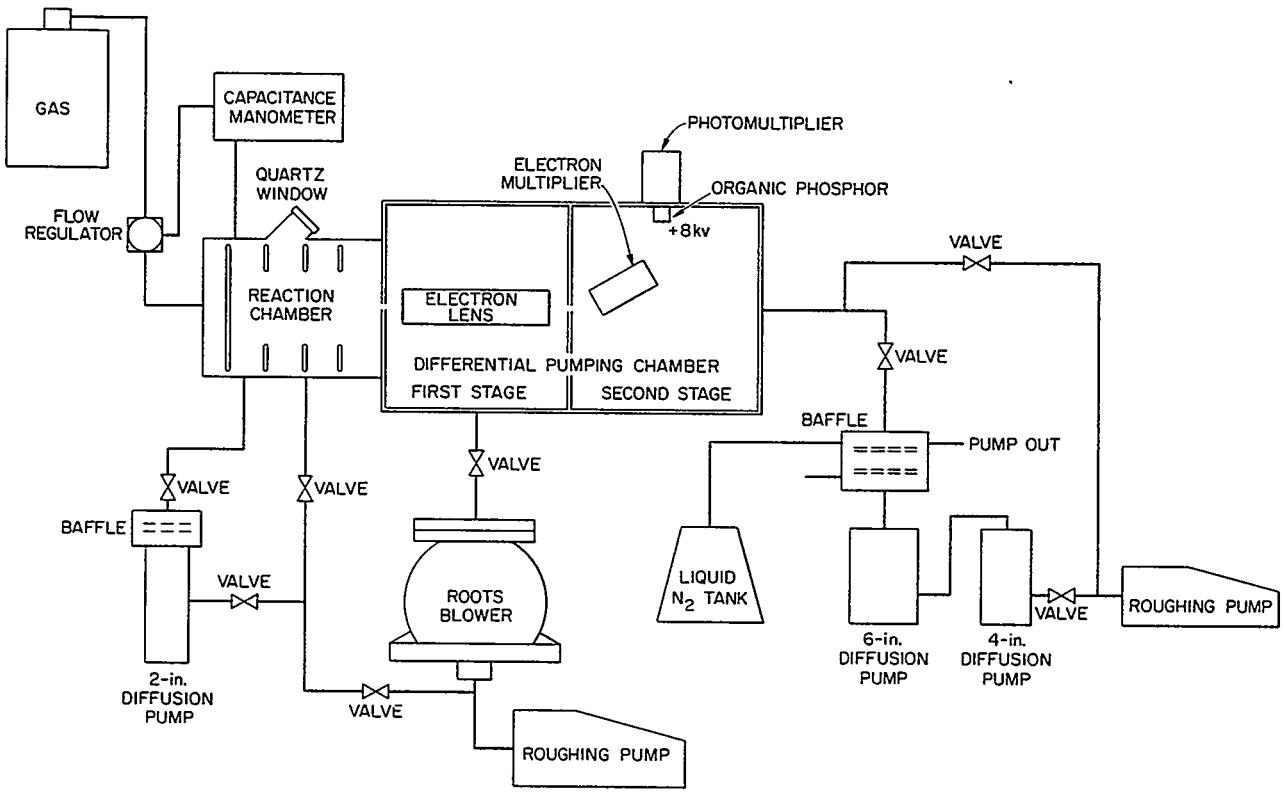

Fig. 13.2. Schematic Diagram of Electron Time-of-Flight Apparatus.

The first stage of differential pumping connects to both the reaction chamber and the second stage of differential pumping through 0.050-in. holes. The electron multiplier requires a vacuum of 1×10^{-4} mm Hg, or better, and present plans are to operate the reaction chamber with gas pressures ranging from 1 to 10 mm Hg. Although accurate calculations of the vacuum parameters are difficult, because the flow is in the transition region between molecular and viscous with the above apertures and pressures, it is believed that with the components chosen a pressure of 1×10^{-5} mm Hg will be obtained in the first stage, when the reaction chamber is at 1 mm Hg gas pressure.

The reaction chamber has been designed so that it may be cascaded with similar chambers to increase the length of the electron drift region from 25 cm to 100 cm. It contains field rings, a quartz window to allow entrance of ultraviolet light from the flash tube, a plate to produce photoelectrons, and both a roughing pump and a 2-in. diffusion pump to pump out and outgas the reaction chamber when necessary.

A capacitance manometer will be used to monitor the gas pressure in the reaction chamber and to supply a control signal to a pressure controller which is designed to automatically maintain the pressure in the reaction chamber at any desired preset level.

The first stage of differential pumping is pumped by a roots blower in order to obtain the desired pressure (1×10^{-2} to 1×10^{-3} mm Hg) with the high throughput of gas, which is ~1400 micron-liters per second. A four-section electrostatic quadrupole electron lens has been designed and is being evaluated for use in this stage as a means of focusing the electrons from the reaction chamber aperture and beaming them through the second aperture into the electron multiplier. The second stage of differential pumping is performed by a 6-in. diffusion pump cascaded with a 4-in. diffusion pump.

A new and relatively simple scheme for detecting single electrons is being evaluated. Electrons from the focused beam are picked up on the cathode of a modified electron multiplier. The secondary electrons, instead of being collected by an anode at the output end, are accelerated by an 8-kv potential to a plastic phosphor, giving rise to a light signal which is detected by an external photomultiplier. This scheme should have the following advantages: (1) exceptionally high gain should be obtained; (2) the Bendix multiplier as well as the photomultiplier can be operated at low gains and thus with low dark currents; and (3) complete electrical de-coupling between the electron multiplier and the photomultiplier is obtained, allowing versatility in biasing the input and output and good overall stability.

INTERACTION OF ENERGETIC CHARGED PARTICLES WITH ATOMIC ARGON

Spectroscopic investigations of light emission due to the passage of alpha particles in atomic argon show that two broad continua (at about 2300 A and at 1300 A) are emitted. The 2300-A continuum is quenched by a factor of 10 with the addition of CH_4, CO_2, O_2, and Kr at relative concentrations of about 2%. These observations provide strong support for the idea previously advanced[18] – that argon is left in at least two excited states. The 2300-A continuum probably originates from a collision process in which an excited dimer of argon is formed. A transition between two excited states in the dimer would account for the continuum at 2300 A. The 1300-A continuum apparently arises from radiation from the low-lying excited dimeric state to a ground state which is repulsive.

In the light emission experiments it was also found that N_2 quenched the 2300-A argon continuum, but associated with the effect was the emission of light which could be assigned to electronic transitions of N_2. Because of this it was predicted that Ar-N_2 mixtures would be less sensitive (compared with pure argon) to the addition of the molecular gases which produce ionization enhancement, in spite of the observation that N_2 is not ionized when added to argon. This effect was experimentally demonstrated and studied in detail for Ar-N_2 mixtures further mixed with CO_2, CH_4, H_2, Xe, and Kr.

When combined with optical measurements of the oscillator strengths for atomic argon (being done at the Institute of Molecular Biophysics, Florida State University), the work reported here will probably provide a detailed description of the processes involved when energetic charged particles interact with the argon atom.

[18] R. D. Birkhoff *et al.*, *Health Phys. Div. Ann. Progr. Rept. July 31, 1962*, ORNL-3347, p 79.

MEASUREMENT OF TRANSITION RADIATION AND OPTICAL BREMSSTRAHLUNG FROM ELECTRON-BOMBARDED METAL FOILS

The spectral distribution of photons emitted by silver foils, 660 and 1980 A thick, when bombarded by 40-kev electrons has been determined experimentally in the wavelength region 2500 to 5600 A. The spectra were determined for photons emitted at 0 to 150° from the foil normal by means of an angular distribution chamber which permitted the spectrometer to be rotated around the foil in a continuous fashion without breaking the vacuum. A Glan prism analyzer was used to separate the light into a component polarized parallel to the plane of the electron and photon and into another component perpendicular to it. Transition radiation has been predicted by Frank and Ginzburg[19] to be polarized in the parallel plane, whereas bremsstrahlung may be found in both planes.

The experimental results in the parallel plane were compared with the transition radiation theory of Ritchie and Eldridge[20] on an absolute scale for emission from both the front and back sides of the silver foils.

A comparison of the experiment with theory of the complete spectral distribution for transition radiation for the silver foils 660 A thick at 40 kev is shown for the angles on the front side of the foil in Figs. 13.3 and 13.4. For the small angles (θ = 5 to 40°), the sharp peak at λ = 3300 A is less intense than the theoretical peak. The continua on both sides of the peak agree closely with

[19] I. Frank and V. Ginzburg, *J. Phys. USSR* 9, 353 (1945).

[20] R. H. Ritchie and H. B. Eldridge, *Phys. Rev.* 126, 1935 (1962).

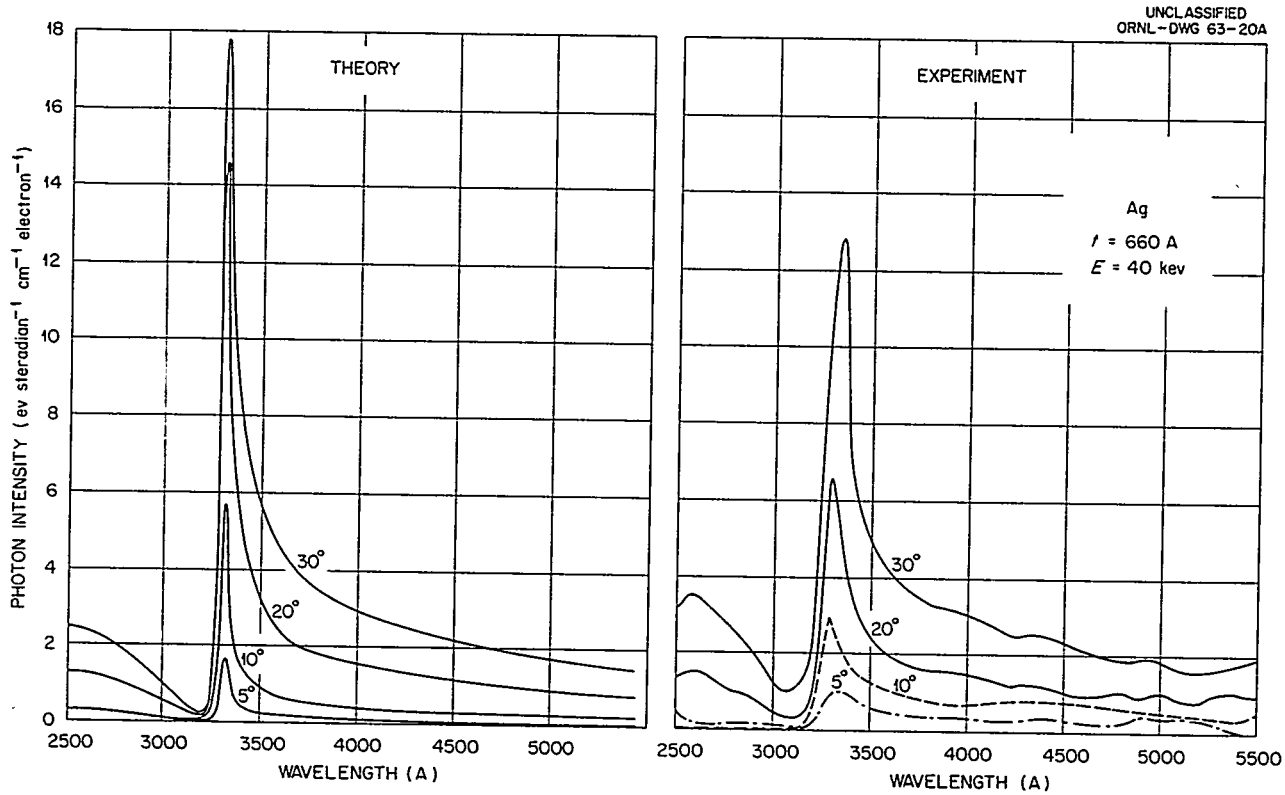

Fig. 13.3. Theoretical and Experimental Spectra from Silver Foil 660 A Thick ($\theta = 5$ to 30°; $E = 40$ kev).

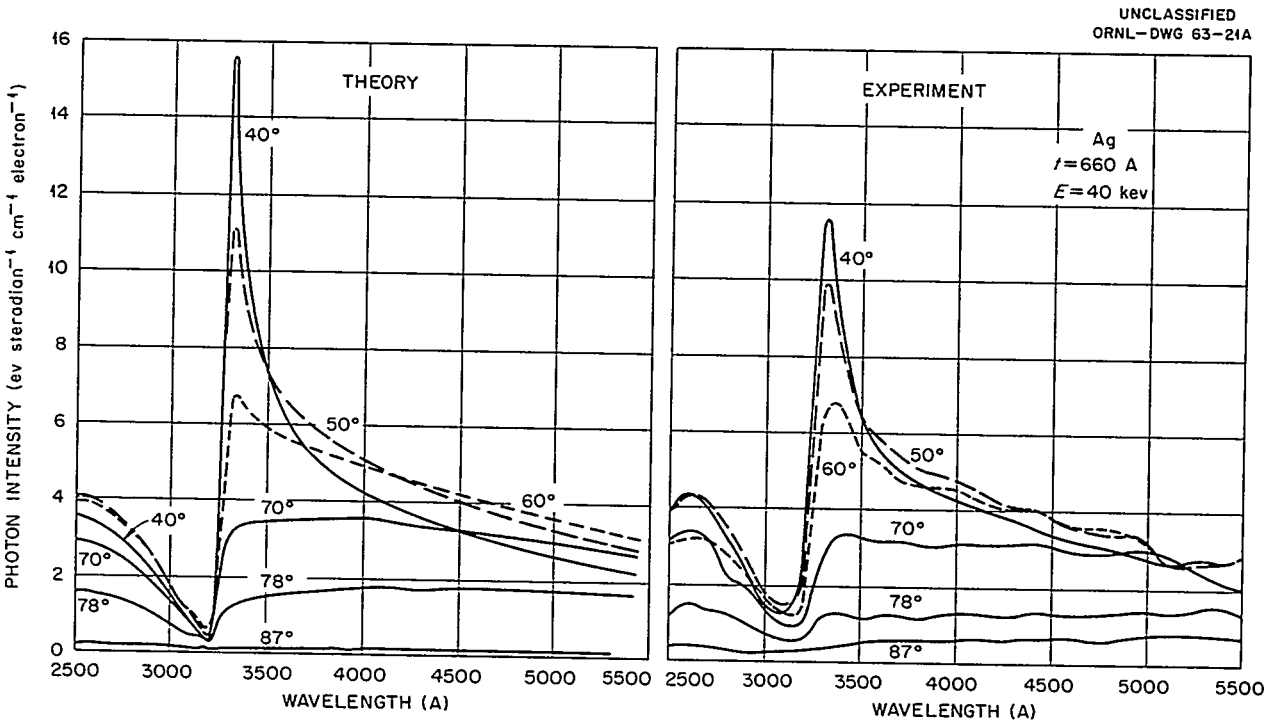

Fig. 13.4. Theoretical and Experimental Spectra from Silver Foil 660 A Thick ($\theta = 40$ to 87°; $E = 40$ kev).

theory. The spectral distributions found experimentally at the larger angles (θ = 50 to 87°) show good agreement with the theory for all wavelengths.

The experimental spectral distributions for the angles on the back side of the foil 660 A thick are compared with the theory in Figs. 13.5 and 13.6. Very close agreement was observed for the complete spectral distributions at these angles. Also, in the same figures the spectral distributions on the back side are compared with those on the front side at corresponding angles. The intensity is higher on the front side than it is on the back side because of the relativistic velocity of the electron.

The intensity at the silver peak as a function of angle for the foil 660 A thick is shown in Fig. 13.7. The solid line represents the theory, while the points represent experimental runs with two foils of equal thickness. The experimental angular distribution shows a maximum intensity at 30°, in agreement with theory; but the intensity is less than the theoretical intensity for the smaller angles ($\theta \leqq 40°$ and also θ = 140°). A comparison of the experiment with theory of the photon intensity at λ = 4500 and 2700 A (Fig. 13.7) shows good agreement for both the angular distribution and intensity. The maximum intensity for the continua occurs at θ = 50°, whereas the maximum intensity for the peak occurs at 30°.

The experimental results are shown in Fig. 13.8 for the light emitted in the perpendicular plane by the foil 1980 A thick for the front angles. Although detailed conclusions concerning this source of light cannot be presented, because the intensity observed in this plane was only two to three times the noise level, some general trends may be seen. The intensity is maximum in the direction of the electron beam and decreases with increasing angle, as is predicted theoretically for bremsstrahlung. The photon intensity for the foil 1980 A thick is greater than that for the foil 660 A thick, as expected for bremsstrahlung.

This experiment will be continued on other foils such as sodium and potassium in an effort to detect the plasma light which has been predicted from the decay of the collective oscillations of the conduction electrons in solids.

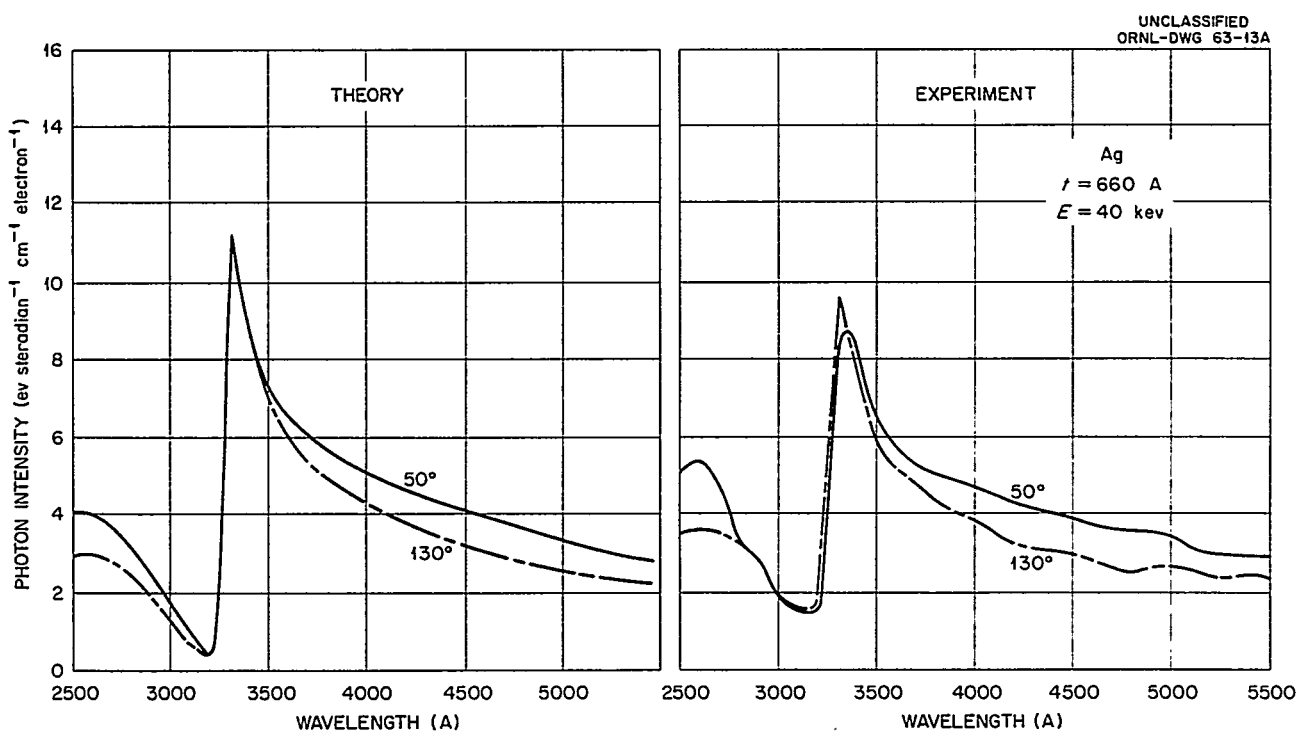

Fig. 13.5. Theoretical and Experimental Spectra for Corresponding Angles on Front and Back Sides of Silver Foil 660 A Thick (θ = 50° vs 130°).

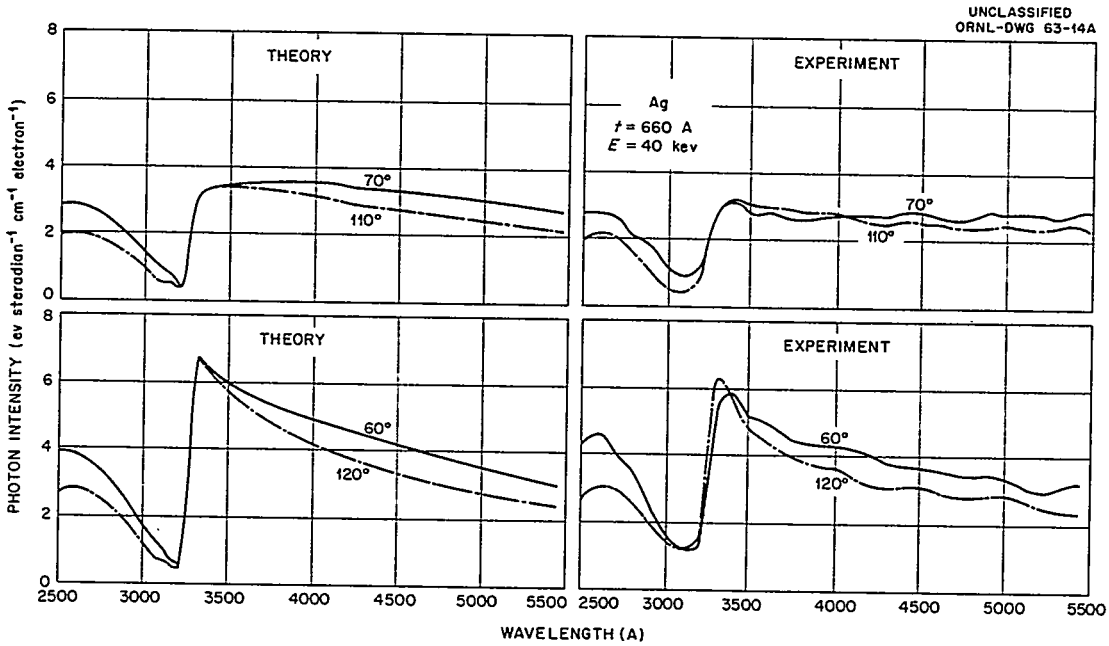

Fig. 13.6. Theoretical and Experimental Spectra for Corresponding Angles on Front and Back Sides of Silver Foil 660 A Thick ($\theta = 60$ and 70° vs 120 and 110° respectively; $E = 40$ kev).

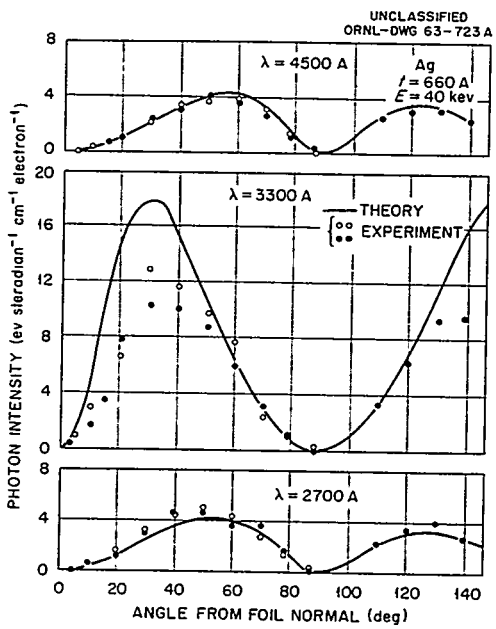

Fig. 13.7. Comparison Between Theory and Experiment of the Angular Distribution at $\lambda = 2700$, 3300, and 4500 A for Silver Foil 660 A Thick.

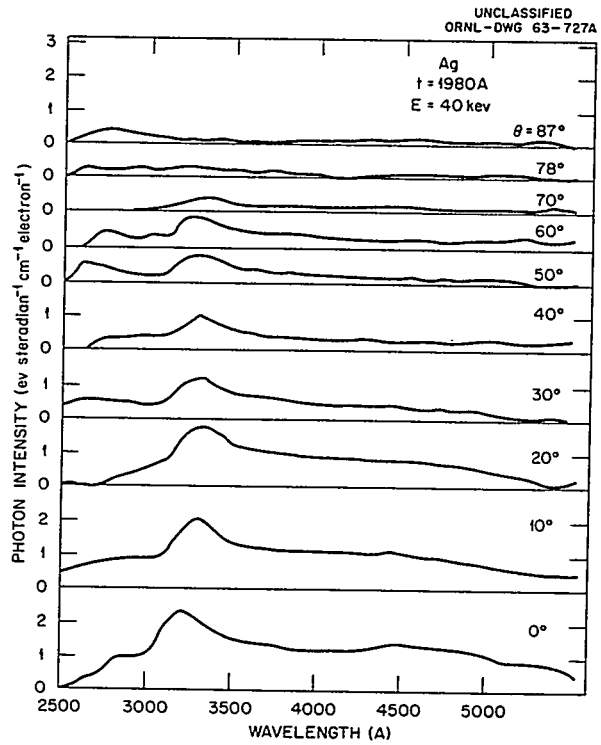

Fig. 13.8. Experimental Results for the Light Emitted in the Perpendicular Plane on the Front Side of a Silver Foil 1980 A Thick ($E = 40$ kev).

SPHERICAL ELECTROSTATIC ANALYZER AND ELECTRON SLOWING-DOWN SPECTRA IN COPPER

The spherical electrostatic beta-ray analyzer (the Keplertron) described previously[21] has undergone further tests and development, and flux spectra have been obtained from several types of sources. The transmission and resolution determined previously below 3 kev by means of an electron gun have been checked at higher energies with the Sm^{152} Auger line at 32.8 kev and the Ni^{64} Auger line at 6 kev resulting from electron capture in relatively thin sources of Eu^{152} and Cu^{64} respectively. For both sources the energy calibration was $E_0 = 1.37\ V_0$, where E_0 is the electron energy and V_0 is the outer sphere potential. This proportionality constant agrees with the value previously determined at lower energies. Line profiles of the Sm^{152} Auger line appeared to be in satisfactory agreement with theory, although not enough data were available for a detailed comparison. The Sm^{152} Auger line had a resolution of (7 ± 1)% and a transmission of (21 ± 5)% compared with the theoretical values of 6.3% and 25% respectively. These values were earlier verified[21] at lower energies.

The electron flux spectrum from a copper "cavity" source has been measured and is shown with the theoretical electron flux in Fig. 13.9. The contributions of the primary and secondary electrons to the theoretical flux are shown. The curves have not been fitted, and the intensities shown are absolute. The experimental flux is in absolute agreement with the theory from 37 kev to 1 kev. The large rise at lower energy and the peak at 3 ev are due to secondary electrons, but corrections are required for scattering from the Keplertron spheres. At present an effort is being made to determine the origin of these spurious secondary electrons and the magnitude of the correction.

A new inner sphere with anti-scattering ridges has been constructed from aluminum in an effort to reduce scattering. The smaller peak at 6 kev is composed of two unresolved peaks, the Cu K-$2L$ Auger line which results when an energetic electron collides with and ejects a K electron from a copper atom and the Ni K-$2L$ Auger line which results from electron capture in the nuclear decay of

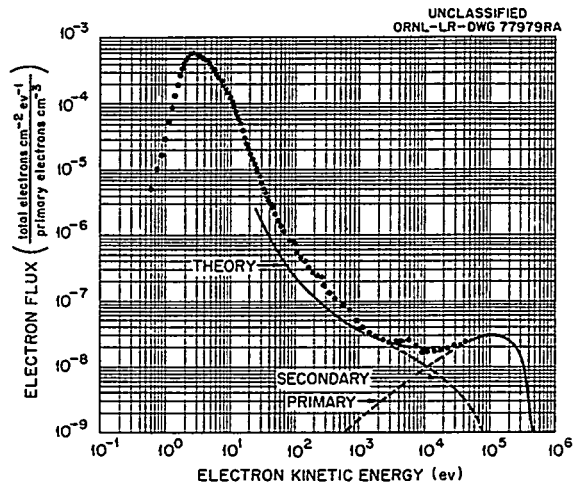

Fig. 13.9. Electron Flux Spectrum of Cu^{64} Beta Rays Absorbed in Copper.

Cu^{64}. Three other peaks, somewhat obscured by the logarithmic ordinate scale, were observed at 100, 250, and 300 ev. Similar peaks, from electron-beam-irradiated metal surfaces, have been reported by Lander[22] at 69, 160, 816, and 774 ev for nickel and at 185 and 63 ev for copper. The identification of the peaks found in the present research is now in progress.

An electron flux spectrum has also been obtained from a plane disk source of copper. The spectrum showed the same general features as the cavity source but was lower than theory at high energies, because the source was a semi-infinite medium rather than an infinite medium as assumed in the theory.

The experiments with the radioactive sources revealed several difficulties in experimental techniques. It was found that (1) the tools for mounting the multicurie sources were inadequate; (2) with no potential applied to the outer sphere, there were still significant numbers of electrons reaching the Faraday cup; and (3) a significant number of spurious low-energy electrons were reaching the Faraday cup. The first difficulty has been overcome by designing and constructing a new "pig" and a "rabbit" decapping tool and by improving existing facilities and tools. The second difficulty was assumed to be due to electrons ejected in the vicinity of the Faraday cup by gamma rays. This

[21] R. D. Birkhoff *et al.*, *Health Phys. Div. Ann. Progr. Rept. July 31, 1962*, ORNL-3347, p 82.

[22] J. J. Lander, *Phys. Rev.* 91, 1382 (1953).

assumption has been verified by measuring the Faraday cup current produced by an encapsulated Cs^{137} source. The current was measured with the Cs^{137} source unshielded and then with lead placed on all sides of the source except that side radiating into the angular acceptance range of the Keplertron. The latter geometry gave a much lower current at all outer sphere potentials. The spectrum shown in Fig. 13.9 has been corrected for this effect by subtracting from each observed current a corresponding properly normalized current obtained from the unshielded Cs^{137} source. More lead has been placed behind the source mount on the inner sphere, and it is hoped that the background caused by gamma rays will not be significant in future experiments. At present an effort is being made to locate the source of the spurious low-energy electrons by use of a newly designed electron gun.

The theory shown in Fig. 13.9 was calculated by means of a simplified version of the Spencer-Fano theory of electron slowing down[23] which included an approximation of the Möller cross section for electron-electron collisions. The calculation has since been programmed for the CDC 1604 computer and calculated by use of the complete Möller cross section. No difference was observed between the two calculations. A program has also been written to correct the experimental data for corona discharge at high outer sphere potential, grid transmissions, background due to gamma rays, source activity, and source decay.

Details of the theory and experiment have been discussed in a separate publication.[24]

AN OPERATIONAL ANALYZER FOR GENERALIZED DOSIMETRY

An operational analyzer has been built, based on the conceptual design described by Hurst and Ritchie.[25] This instrument is used to compute the sum

$$\sum_u 2^{r(u)} (-1)^{m(u)} \int_{E_1(u)}^{E_2(u)} n(\epsilon, E)\, d\epsilon \ ,$$

where

u = identification number of an instrument channel,

$E_1(u)$ = lower energy of the uth channel,

$E_2(u)$ = upper energy of the uth channel,

$r(u)$ = 0 or a positive integer,

$m(u)$ = either 1 or 2,

$n(\epsilon, E)$ = number of charged secondaries of energy ϵ generated per unit energy interval by primary radiation of energy E.

This instrument has been checked for electronic functioning of all stages but has not yet been used with a detector to supply the input data for an actual computation.

The analyzer is completely transistorized and is built in two chassis with standard rack-type 19-in. panels. The basic units of the analyzer are a linear amplifier, pulse sorter, binary scalers, addition-subtraction circuit, and the readout decade scaler. Commercial transistor plug-in-type modules were used where they were readily adaptable.

The linear amplifier consists of three feedback loops with an overall voltage gain of approximately 1200. This amplifier has an emitter follow output which is used to drive the pulse sorter.

The pulse sorter consists basically of seven single-channel analyzers with inputs connected in parallel to the output of the amplifier. Each single-channel analyzer has a window whose upper and lower level can each be varied from the lower threshold of 0.8 v to the upper limit of 10 v. These upper- and lower-level controls are 10-turn Helipots that can be calibrated to aid in rapidly setting up the instrument for a particular computation. The two lower single-channel analyzers have a linear window amplifier with a gain of 10.

There are two sets of binary scaling stages (one set for addition, the other set for subtraction), and each set contains seven binary stages in series. A patch cord arrangement is provided so that the output of any of the single-channel analyzers can be connected to the proper point in either the addition set or the subtraction set to allow computation

[23] L. V. Spencer and U. Fano, *Phys. Rev.* 93, 1172 (1954).

[24] W. J. McConnel, H. H. Hubbell, Jr., and R. D. Birkhoff, *Electron Slowing Down Spectrum in Cu of Beta Rays from Cu^{64}*, ORNL-3463 (to be published).

[25] G. S. Hurst and R. H. Ritchie, *Health Phys.* 8, 117 (1962).

of a particular dose calculation. The output of the add binary set is connected to the add input of the addition-subtraction (A-S) circuit, and the subtract binary set to the subtract input of the A-S circuit.

The A-S circuit is based on a glow-transfer tube which can be driven counterclockwise with pulses from the add set, and clockwise with pulses from the subtract set. The circuit utilizes a gating circuit so that the glow-transfer tube passes a count to the readout scaler only when the tube reads zero; thus it is a negative storage unit. The gating circuit also prevents the glow transfer from storing more than eight consecutive negative counts to prevent an ambiguity. However, since the subtract counts generally are only a fraction of the add counts, this provision would not be a necessity.

The readout circuit is a three-decade scaler and register combination. A single reset generator resets the readout scaler and all of the binaries.

Plans are under way to apply the instrument to the analysis of the output of appropriate detectors so that the dose received from exposure to high-energy radiations (e.g., exposures of interest to the NASA program) can be estimated.

14. Physics of Tissue Damage

R. D. Birkhoff

J. G. Carter D. R. Nelson

D. A. LaBar[1]

EFFECT OF ADSORBED GAS ON OPTICAL EMISSIONS OF IRRADIATED BIOCHEMICALS

As previously reported, the light emissions from x-irradiated powders of the aromatic amino acids and the enzyme trypsin were found to depend upon the gaseous atmosphere present during the irradiation. It was found that the intensity of thermoluminescence depended strongly upon the presence of a gas both during the irradiation of the sample and during the subsequent warmup. A dependence was observed not only for the organic materials studied but in a less important manner for the alkali halides, NaCl and KCl.[2] A portion of the effort this past year has been directed toward understanding mechanisms involved in this anomalous gas effect.

In one experiment an attempt was made to observe whether the ions or electrons formed in the gas during irradiation influenced the thermoluminescent intensity. A 200-mg sample of tyrosine powder was evenly spread on the bottom of a stainless steel holder. A Lavite ring containing a wire screen was then supported $\frac{1}{4}$ in. above the surface of the sample. A voltage of 300 v of either polarity was applied to the screen during both irradiation and subsequent warmup in order to prevent any ions or electrons originating in the gas from striking the surface of the sample. No effect on the resulting glow curve was noted. These results seem to indicate that the light intensity is not appreciably affected by action of an electric field on the sample or on the secondary electrons or ions ejected from the holder and gas environment.

An attempt was also made to detect by gas chromatography any gaseous emissions from the samples, particularly as these might correlate with the optical emissions. A series of preliminary experiments was performed in which all the gas in the sample chamber after an irradiation was pumped out through a liquid-nitrogen trap. No significant amounts of gases such as CO_2, NH_3, or H_2 were

[1]AEC Health Physics Fellow.

[2]J. G. Carter, D. R. Nelson, and L. G. Augenstein, *Appl. Phys. Letters* 2(11), 226 (1963).

found even when a Linde molecular sieve was included in the trap. It is believed that the most probable gas evolved from irradiated organics is hydrogen. Since the sensitivity of the gas chromatograph for hydrogen is about 50 ppm, a rough calculation of a reasonable hydrogen yield indicates that the present experiment is not sensitive enough. A more sensitive experiment using a smaller trapping system and more efficient gas transfer is under consideration.

Another experiment involving the technique of electron spin resonance was carried out with R. A. Weeks of the ORNL Solid State Division. Correlations between the numbers of radiation-induced spins and integrated thermoluminescent intensity for varying sample crystallinities and gaseous conditions were sought. Even though significant spin resonance signals were observed for irradiated tyrosine, no correlation of signal strength with the tyrosine glow curve as a function of warmup temperature was found. Also, no gaseous dependence of spin resonance signals was found. A vacuum treatment at 50 μ and 77°K after an irradiation did not decrease the spin signal, although there was a decrease in the observed thermoluminescence signal under similar conditions.

TIME-OF-FLIGHT ELECTRON BEAM MONOCHROMATOR

Studies of the electronic energy levels which are excited by the passage of fast electrons through solids and gases have been severely restricted because of the energy spread in the electron beam, characteristically of the order of 0.5 ev. Recently G. J. Schultz in the United States and H. Boersch in West Germany have succeeded in reducing this to about 0.1 ev using electron optical methods. In order to avoid space-charge effects which contribute to the spread of electron energy at focal points in lens systems, development of an electron beam monochromator utilizing a time-of-flight velocity selection technique was initiated during the past year. An avalanche transistor pulser supplies nanosecond gating pulses to a negatively biased grid of an electron gun located at the lower end of a drift tube. Electrons are accelerated by 1 to 15 v from a negatively biased filament into the drift tube, which is aligned with the earth's magnetic field in order to provide weak magnetic focusing. The electrons in their passage through the drift tube are dispersed spatially with the more energetic ones getting first to the exit aperture 83 cm from the electron gun. A method is under development to gate the electron beam at the aperture by either electrostatic or magnetic deflection to allow a nanosecond segment of the pulsed electron beam to pass through the aperture. These electrons should then be monoenergetic to within 0.01 ev. Operating characteristics of the system have been obtained using a flat collector at the aperture position. Pulses from the flat collector are amplified by a transistorized pulse amplifier,[3] delivered to a sampling oscilloscope, and displayed on a chart recorder. Three typical chart traces are superimposed in Fig. 14.1. By algebraically converting

[3]Plans for the transistorized pulse amplifier were furnished by C. W. Williams and J. H. Neiler of ORNL.

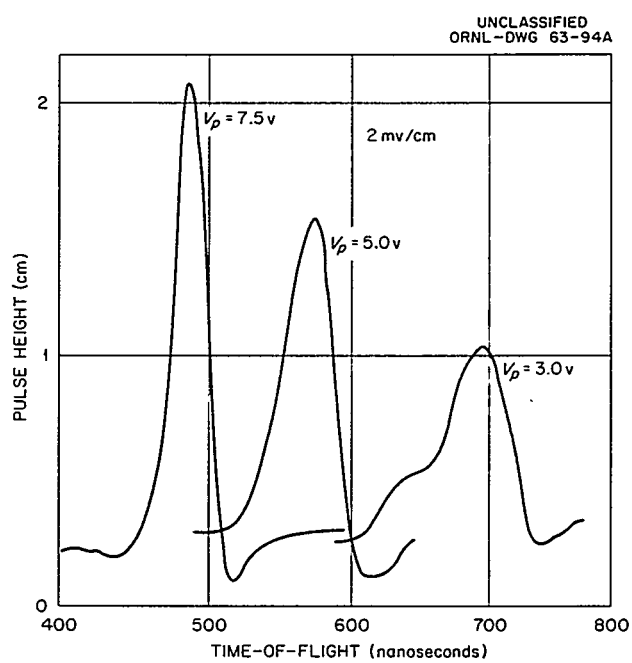

Fig. 14.1. Arrival Time Distribution of Pulsed Electron Beam.

the time distribution of the electron arrivals to an energy distribution, a spread in energy of about 0.5 ev is calculated for electron gun voltages between 2 and 15 ev. This value is consistent with that expected from thermal energy of emission from the filament source. The square of the reciprocal of the transit time is a linear function of the electron energy, as shown in Fig. 14.2.

The gate at the aperture will reject the majority of the arriving electrons so that the present system will not be able to detect this weak signal. An RCA model C7187J 14-stage copper-beryllium dynode, open-window electron multiplier will replace the present plane collector and transistorized amplifier for an increased gain and a faster response time. To preserve the cleanliness of the dynode surfaces of the multiplier, the present oil diffusion vacuum pump will be replaced with a turbo-molecular pump. Present data seem to indicate that there is an impedance mismatch between the 50-ohm pulser line and the grid of the electron gun. A new electron gun was designed and is being constructed which will preserve the impedance from the coaxial transmission line to the two parallel plates forming the grid and plate.

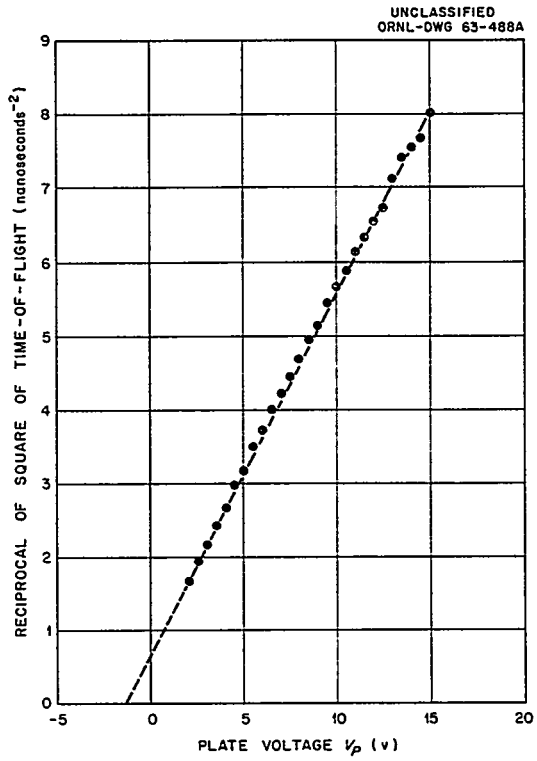

Fig. 14.2. Reciprocal of Square of Electron Time-of-Flight vs Electron Gun Voltage.

15. Radiation Dosimetry

J. A. Auxier

M. D. Brown[1]
J. S. Cheka
F. J. Davis
J. L. Ellis[1]
S. Fukushi[2]
L. W. Gilley[3]
F. F. Haywood[4]
D. R. Johnson
C. R. McAmis[5]
J. E. Parks[1]
P. W. Reinhardt
F. W. Sanders
W. H. Shinpaugh, Jr.
J. H. Thorngate

GAMMA-RAY SPECTROMETRY

During Operation BREN low instrument efficiency coupled with a high radiation background limited the usefulness of the Compton recoil gamma-ray spectrometer described previously;[6] low efficiency limited the number of energies and the distance at which measurements were made. The gamma spectrum measured at a range of 624 yd is given in Fig. 15.1; it shows a decrease in flux with increasing energy at low energies and then shows a peak near 8 Mev. Exact assignments of energies are difficult due to the uncertainty in the amount of energy lost in the Compton electron radiator foil. The measured spectrum appears reasonable, since a large part of the gamma rays from fission and fission products were absorbed by the dense uranium core of the reactor, which made the high-energy gamma rays from $_7N^{15*}$ an unusually large part of the measured field. These gamma rays have energies up to 8.89 Mev. Further measurements of the HPRR gamma spectrum are planned.

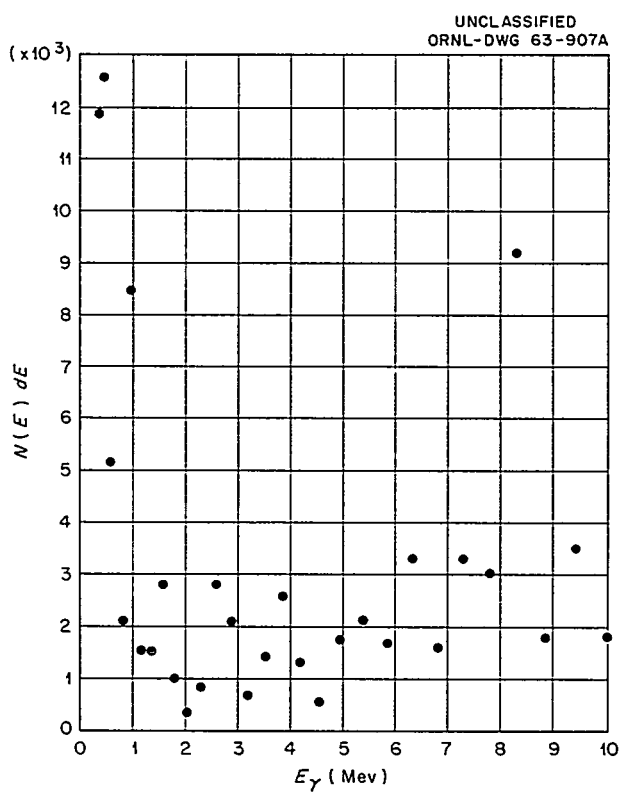

Fig. 15.1. Gamma-Ray Spectrum in Air Measured 624 yd from BREN Tower with Compton Spectrometer.

FAST-NEUTRON SPECTROMETRY

The thick-radiator proton-recoil telescope previously described[7] was used to measure neutron spectra as a function of the angle of incidence (see following section, "Gamma-Ray and Fast-Neutron Dose as a Function of Incidence Angle") during Operation BREN (reactor operations). Subsequent to BREN, it was operated with monoenergetic neutrons at the ORNL 5-Mev Van de Graaff facility. These results were used to normalize a calculated spectrometer efficiency curve and a calculated curve of light output vs proton energy for the anthracene crystals. The measured values fit the calculated curves well in both cases. Typical response of this spectrometer to 2.08-Mev neutrons

[1]Summer employee.

[2]Guest from the Japan Atomic Power Company, Tokyo, Japan.

[3]On loan from Neutron Physics Division, ORNL.

[4]On loan from Applied Health Physics Section, Health Physics Division, ORNL.

[5]On loan from Instrumentation and Controls Division, ORNL.

[6]J. A. Auxier *et al.*, *Health Phys. Ann. Progr. Rept. July 31, 1962*, ORNL-3347, p 88.

[7]J. A. Auxier *et al.*, *Health Phys. Ann. Progr. Rept. July 31, 1962*, ORNL-3347, p 87.

is shown in Fig. 15.2. The results of a measurement taken during BREN with the spectrometer aimed directly at the reactor are shown in Fig. 15.3. The dip in the spectrum at 1.5 Mev is probably due to selective absorption of neutrons in the air. However, data reduction is not complete but a detailed analysis of the BREN data is continuing.

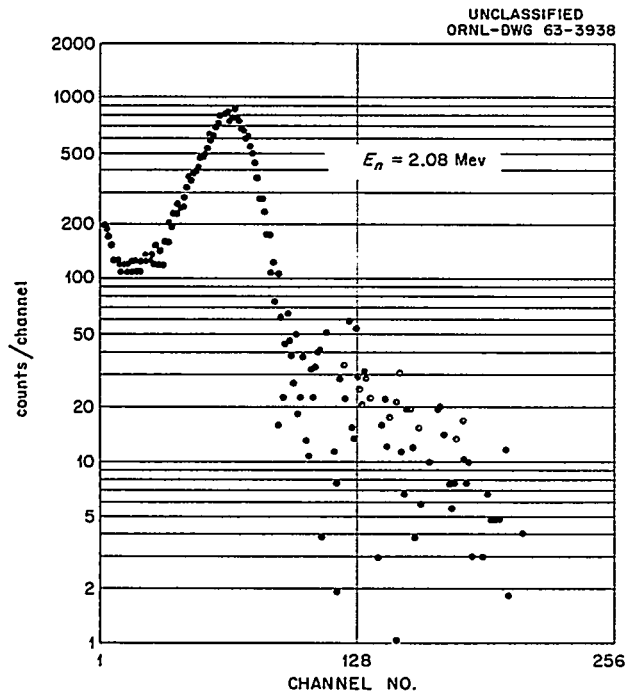

Fig. 15.2. Response of Neutron Spectrometer to 2.08-Mev Neutrons.

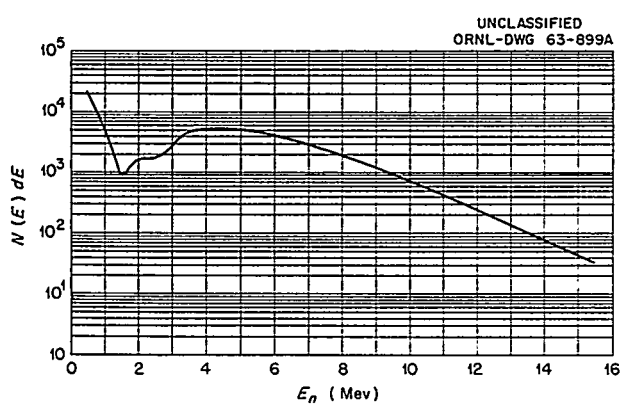

Fig. 15.3. Normalized BREN Neutron Spectrum at 0° Polar Angle (Slant Range 838 yd).

Continued studies of the HPRR neutron spectrum will be made at the ORNL Dosimetry Applications Research (DOSAR) facility.

GAMMA-RAY AND FAST-NEUTRON DOSE AS A FUNCTION OF INCIDENCE ANGLE

By using collimators with conical openings, the distribution of gamma and neutron dose in space was measured during Operation BREN. Previously, during weapons tests, it was found that the dose to a point from a unit solid angle of space above the air-ground interface depended solely upon the angle between the source-detector line and the axis of the collimator cone. Because this angle is similar to the polar angle in a system of polar coordinates, it is normally given this designation. Figure 15.4 is a graph showing the reactor-produced gamma dose as a function of polar angle measured

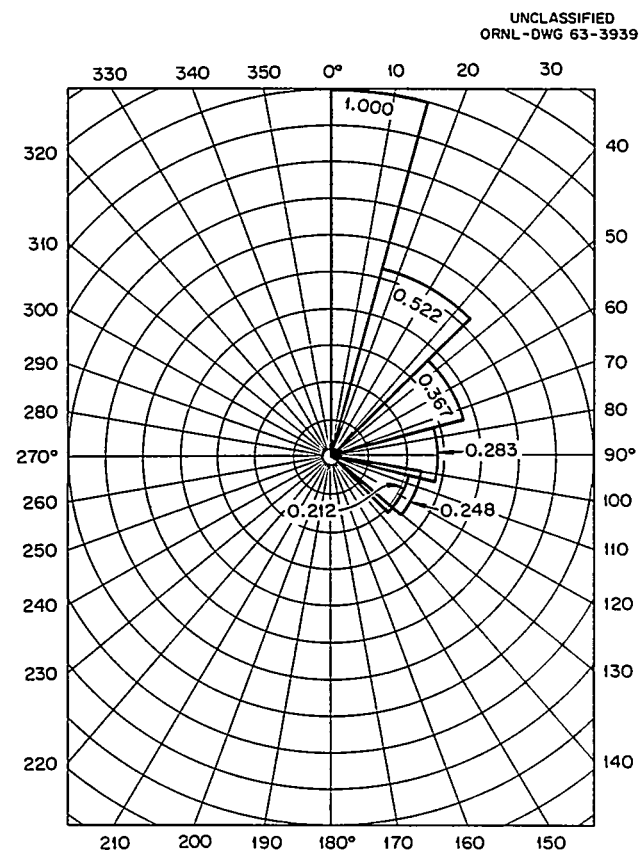

Fig. 15.4. BREN Gamma Dose per Unit Solid Angle vs Polar Angle (Normalized to 0°).

with a Phil dosimeter.[8] In this presentation the measured dose values have been normalized to the dose obtained where the polar angle equals 0°. The conical opening in the lead subtended an angle of 30°. To obtain more detail in the forward direction, the opening was reduced to 10°. These data are shown in Fig. 15.5. Similar plots for the dose from a Co^{60} source are given in Figs. 15.6 and 15.7. The data of Fig. 15.6 were obtained with a 30° cone and those of Fig. 15.7 with a 10° cone.

A Radsan[9] fast-neutron dosimeter was used to measure the reactor neutron dose as a function of angle. The results (by using a 30° water cone in the collimator) are given in Fig. 15.8. Figure 15.9 represents the neutron dose measured as a function of polar angle with a 10° water cone in the collimator.

All the measurements presented were taken at a slant range of 838 yd with the reactor at an elevation of 1125 ft. Measurements of the gamma dose as a function of angle at a slant range of 1117 yd with the reactor at 1500 ft were very similar to

[8]E. B. Wagner and G. S. Hurst, *Health Phys.* 5, 20 (1961).

[9]E. B. Wagner and G. S. Hurst, *Rev. Sci. Instr.* 29, 153 (1958).

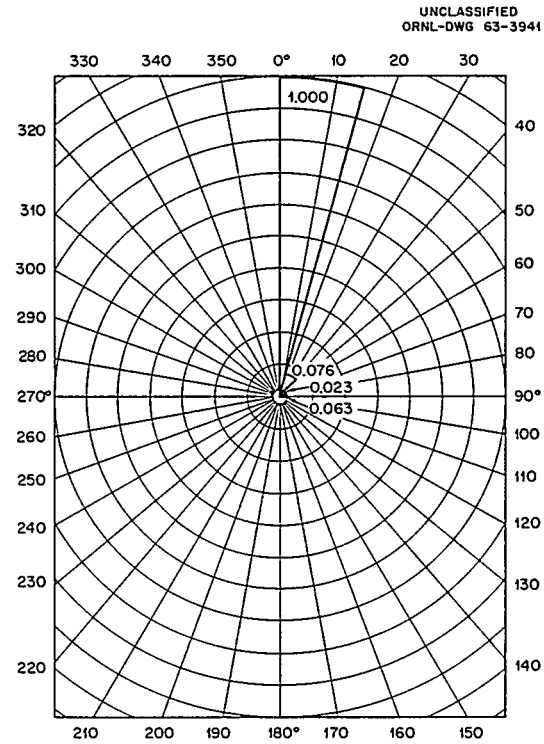

Fig. 15.6. BREN Gamma Dose per Unit Solid Angle vs Polar Angle for Co^{60} Source (Normalized to 0°).

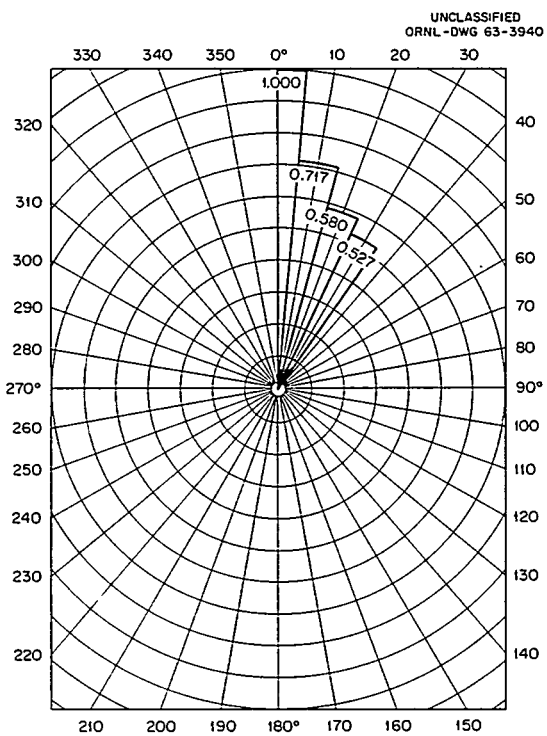

Fig. 15.5. BREN Gamma Dose per Unit Solid Angle vs Polar Angle (Normalized to 0°).

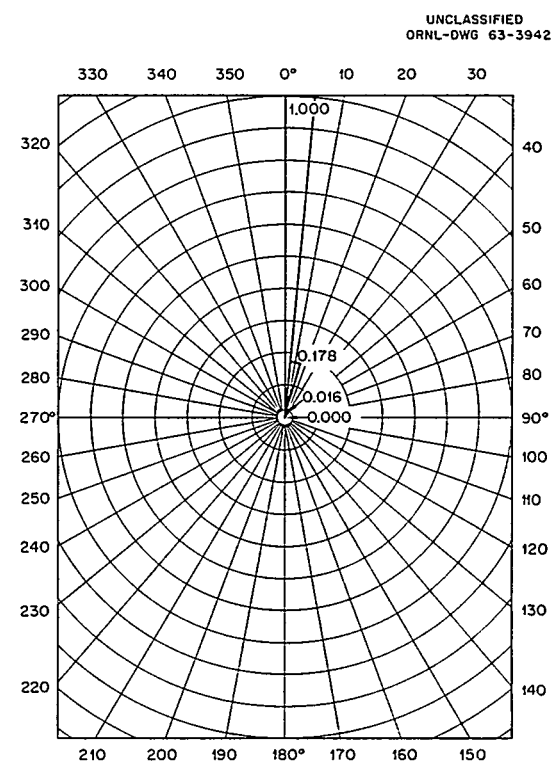

Fig. 15.7. BREN Gamma Dose per Unit Solid Angle vs Polar Angle for Co^{60} Source (Normalized to 0°).

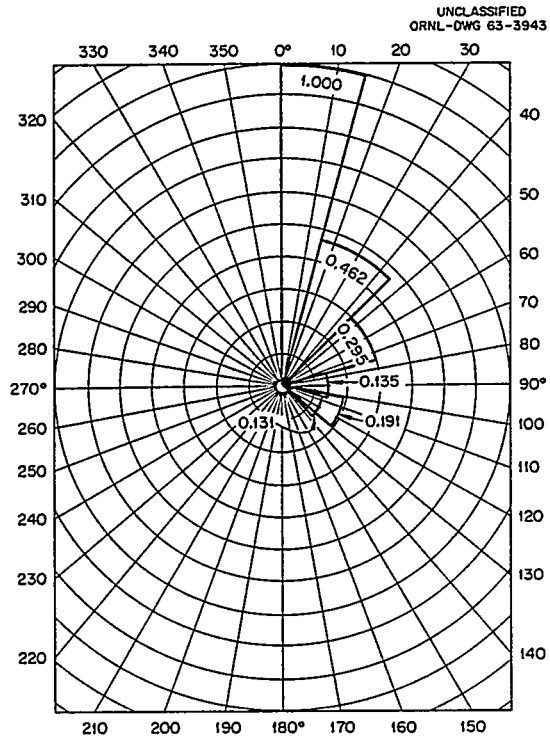

Fig. 15.8. BREN Neutron Dose per Unit Solid Angle vs Polar Angle (Normalized to 0°).

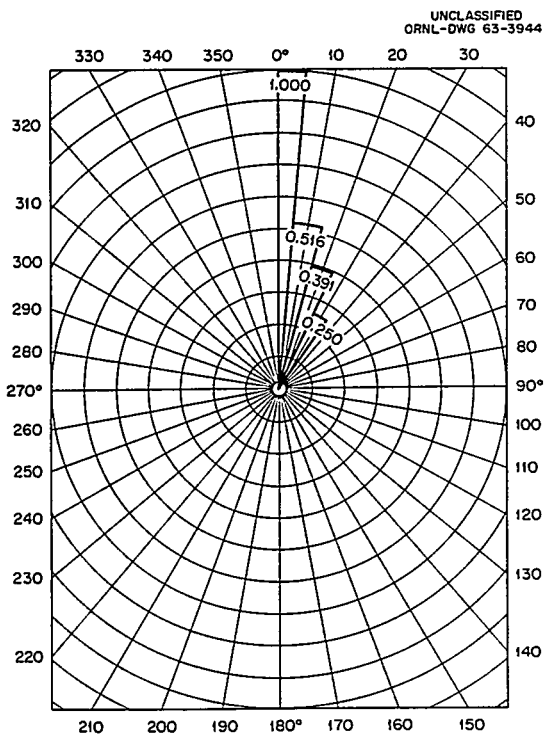

Fig. 15.9. BREN Neutron Dose per Unit Solid Angle vs Polar Angle (Normalized to 0°).

those shown. The neutron dose distribution measured at the greater range was less sharply peaked in the forward direction.

Although the neutron results are in good agreement with weapons test results, the gamma results with the reactor are less sharply peaked in the forward direction. This is attributed to the large percentage of gamma rays produced by inelastic interactions of neutrons with air. These neutron-produced gamma rays represent a considerably more diffuse source than the fission product gamma rays from a weapon. However, the same effect might be produced by the leakage of these high-energy photons through the collimator, and this possibility will be explored in the near future. That the difference between the BREN results and the weapons test results is due to the high-energy gamma rays is evident from the results obtained with the Co^{60} source, for which the gamma dose is sharply peaked in the forward direction.

The data shown in Figs. 15.10–15.12 are corrected so that they represent the total dose reaching the point between intervals of polar angle.

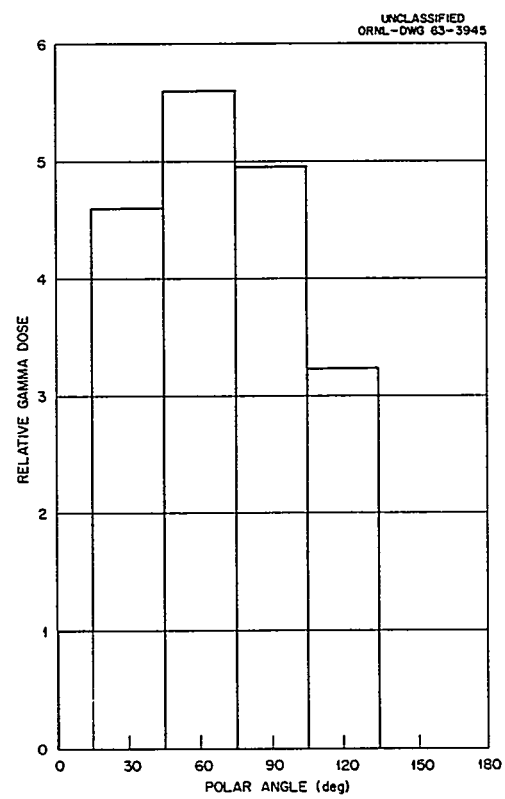

Fig. 15.10. BREN Reactor Gamma Dose vs Polar Angle Corrected to Total Solid Angle (Normalized to 0°, 30° Cone).

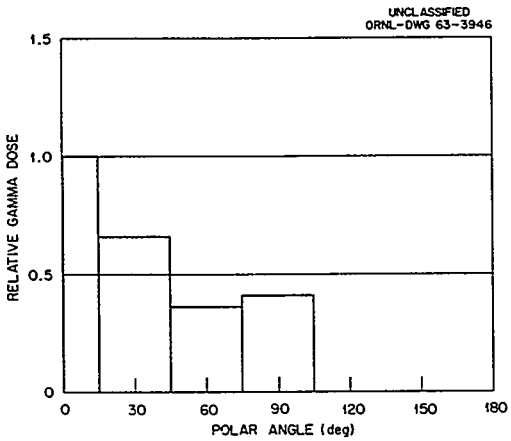

Fig. 15.11. BREN Co^{60} Gamma Dose vs Polar Angle Corrected to Total Solid Angle (Normalized to 0°, 30° Cone).

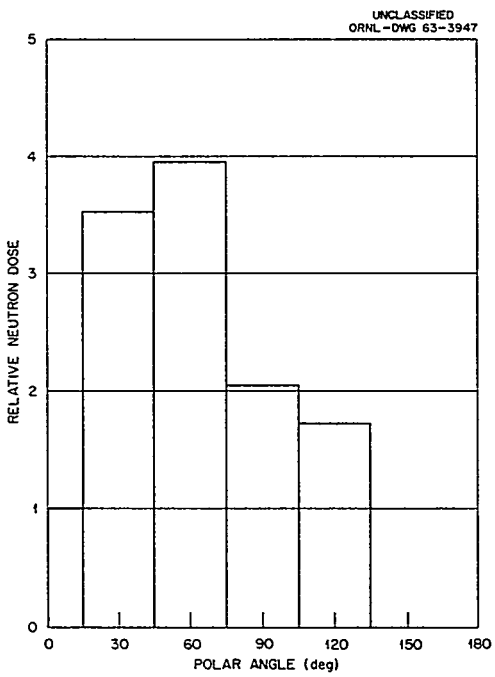

Fig. 15.12. BREN Neutron Dose vs Polar Angle Corrected to Total Solid Angle (Normalized to 0°, 30° Cone).

ENERGY RESPONSE OF BREN NORMALIZING COUNTER

In order to overcome geometry problems involved in operating the reactor at varying heights during Operation BREN, a simple cylindrical paraffin moderator was used with a BF_3 proportional counter to normalize reactor neutron flux. The cylinder was positioned with its axis perpendicular to the reactor-detector line. While it was not expected that such a simple device would exhibit the flat response vs neutron energy given by a Hanson and McKibben type "long counter," a flat response would be necessary only when large changes of neutron spectrum occurred; it was anticipated that the neutron spectrum would not change greatly as a function of source height during BREN. However, the opportunity arose to study the response of the BREN normalizing counter as a function of neutron energy. This was done with monoenergetic neutrons generated with the $H^3(p,n)He^3$ reaction on the ORNL 5-Mev Van de Graaff. The results are shown in Fig. 15.13. Shown for comparison is the response of a typical "long counter."[10] Because the actual number of counts per neutron for each detector depends upon source-detector geometry, the numbers given are true only for the experiment run. The response of the BREN normalizing counter proved to be quite satisfactorily flat. This device will be utilized further with the HPRR at the DOSAR.

[10] W. B. Allen, "Flat Response Counters," chap. IIIA in *Fast Neutron Physics* (ed by J. B. Marion and J. L. Fowler), Interscience, New York, 1960.

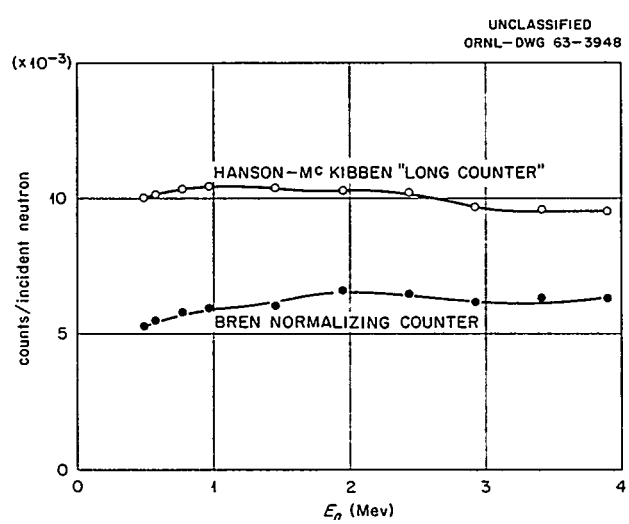

Fig. 15.13. Response vs Energy (E_n) for Hanson-McKibben "Long Counter" and BREN Normalizing Counter.

SPATIAL DOSE DISTRIBUTION IN AIR-OVER-GROUND GEOMETRY

Penetration of neutrons and gamma rays from a small reactor and a point gamma source (HPRR and 1200-curie Co^{60}, respectively) was studied for the case of air over ground. Data were taken at points ranging to 100 ft above the ground and to 4500 ft horizontally away from the sources.

The attenuation of neutron and gamma radiation in air for several source heights is shown in Figs. 15.14–15.16. The average relaxation lengths for neutron dose rate (D_n) and gamma-ray exposure rate (D_γ) for a density of 1.293 g/liter are 194 yd and 271 yd, respectively. Similarly, the average relaxation length for gamma-ray exposure rate from Co^{60} is 193 yd. These data are for detectors lying on the interface.

The dependence of neutron dose rate on source height and detector height is presented in Fig. 15.17 for a source-detector separation of 750 yd. The experimental data are compared to a theoretical model of French.[11] Good agreement is found in the case of neutron dose rate vs detector height for a fixed source height.

[11] R. L. French, personal communication.

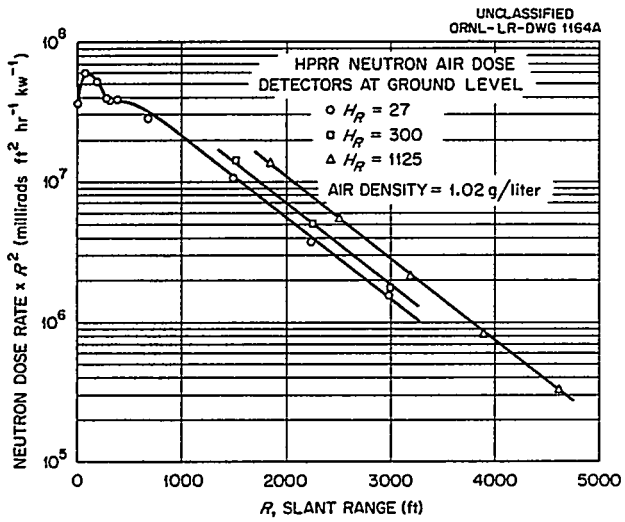

Fig. 15.14. Neutron Air Dose Curves for Reactor Heights (H_R) of 27, 300, and 1125 ft.

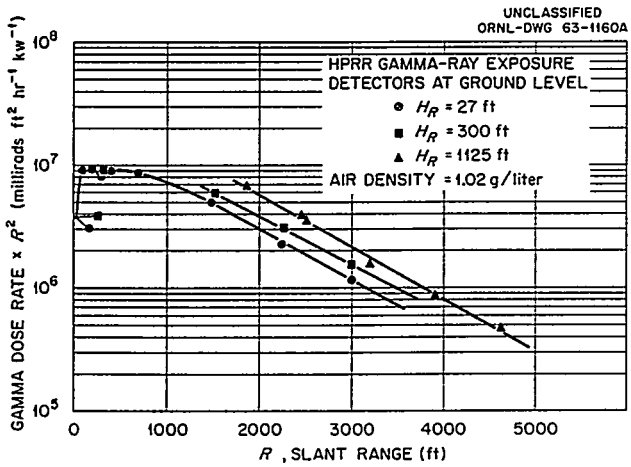

Fig. 15.15. Gamma-Ray Air Exposure Curves for Reactor Heights of 27, 300, and 1125 ft.

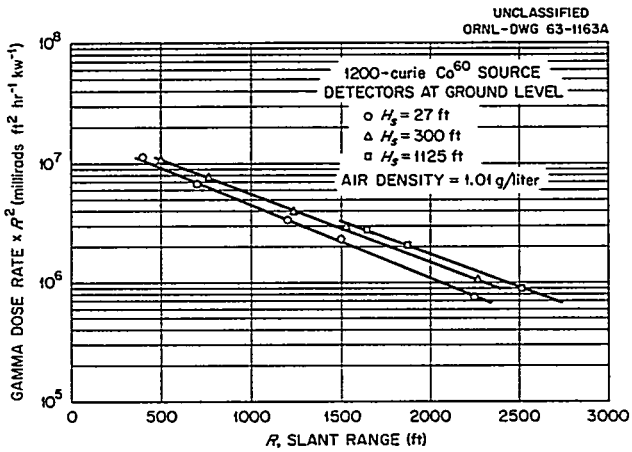

Fig. 15.16. Gamma-Ray Exposure Curves for Co^{60} Source Heights of 27, 300, and 1125 ft.

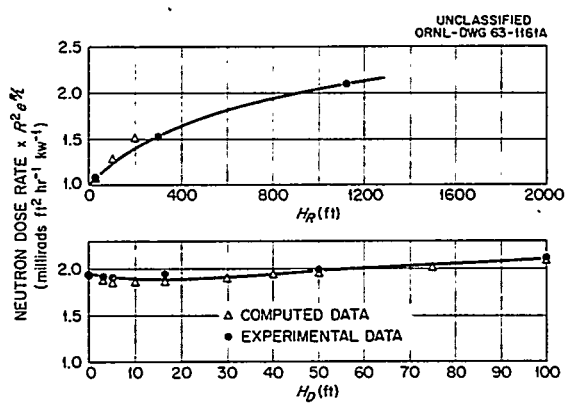

Fig. 15.17. Dependence of Neutron Dose Rate on Variations in Detector Height (H_D) and Reactor Height (H_R).

The ratios of neutron dose rate to gamma-ray exposure rate vs slant range (slant distance between source and detector) for two source heights and two detector heights are presented in Fig. 15.18. The ratio D_n/D_γ, where D_n is neutron dose rate and D_γ is gamma-ray exposure rate, is independent of source height above the interface but is dependent on detector height. This statement is substantiated further by data points (which do not appear here) for other reactor heights.

The air-ground interface increases the dose rate at small source-detector separations and at larger separations decreases the dose rate. Figure 15.19 presents curves which represent Co^{60} gamma-ray exposure buildup factor vs mean free path. Curves are presented for three source heights and for two infinite-media cases (computed). One infinite-medium case is for buildup of Co^{60} gamma-ray exposure in an infinite water medium,[12] and the other is for 1-Mev gamma rays in an infinite air medium.[13] The range of crossover points indicates that the presence of the interface causes a decrease in dose rate at large distances, but these distances are dependent on the height of the source above the air-ground interface.

[12]M. J. Berger, *J. Appl. Phys.*, 28, 1502 (1957).

[13]M. B. Wells, "A Monte Carlo Calculation of Gamma-Ray and Fast Neutron Scattering in Air," pp 308–95 in *NRDL-OCDM Shielding Symposium Proceedings, 1960*, Reviews and Lectures No. 110, 1961.

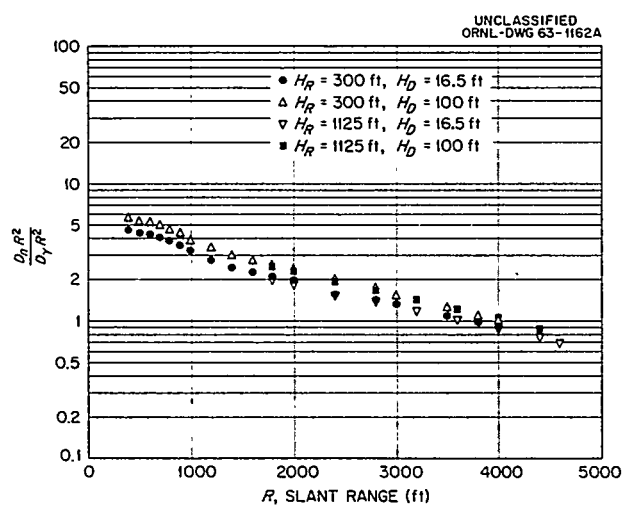

Fig. 15.18. Ratio of Health Physics Research Reactor Neutron Dose Rate to Gamma-Ray Exposure Rate vs Range.

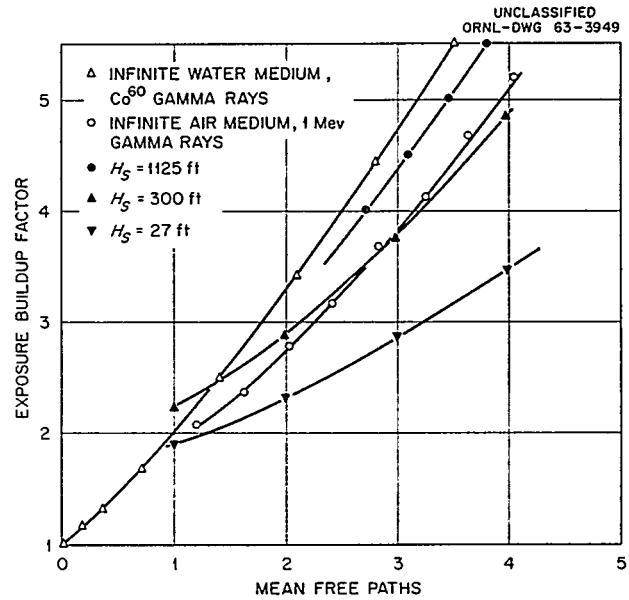

Fig. 15.19. Gamma-Ray Exposure Buildup Factor vs Mean Free Paths.

RADIATION MEASUREMENTS OVER SIMULATED PLANE SOURCES

Gamma-ray spectral measurements were made at the Nevada Test Site utilizing the 1527-ft BREN tower. A 9- by 8½-in. NaI crystal was supported 100 ft to one side of the tower by cables controlled by winches so that measurements could be made from ground level to 1200 ft. The signal pulses from the crystal were fed through a 2000-ft signal cable to a 512-channel analyzer which was housed in an underground bunker.

A simulated plane source array was laid out with positions at 100-ft intervals in the form of a square with sides 2000 ft in length. The square was arranged with one corner beneath the position of the detector so that by symmetry it would be equivalent to a quadrant of a square 4000 ft on each side. The field was bulldozed free of brush but was still quite rough. Two sets of sources (3.5 mc of Co^{60} and 14.3 mc of Cs^{137}) were available to be used in the array positions. The sources were mounted on sticks so they could stand 6 in. above the ground and be in line of sight from the detector, or they could be laid on the ground to give the effect of ground roughness. Three point sources of approximately 0.8 curie of Co^{60}, 1.6 curies of Cs^{137}, and 0.065 curie of Hg^{203} were also used.

Using the source array, gamma-ray spectral measurements were made at heights from 3 to 1000 ft for both sets of sources 6 in. above the ground. Measurements with sources lying on the ground showed differences only in the first 100 ft above ground. At 3 ft above ground the integrated count rates for the two source positions differed by only 10%.

Spectral measurements were made (by using the point sources) at various heights above the three sources and also with the sources at different distances horizontally from a point directly below the detector. In two experiments the height of the detector and horizontal distance of the source were varied so as to maintain a constant distance between source and detector with only the angle between the line joining the two and the horizontal plane being changed. All three sources were employed at a separation of 50 ft but only Co^{60} and Cs^{137} could be used at a separation of 500 ft. To study the ground backscattering and air scattering the sources were tied 50 ft below the detector and comparisons were made between spectra obtained with the sources just touching the ground and at 250 ft above ground. The gamma-ray spectral data were taken on punched tape and are now in process of analysis.

METAPHOSPHATE GLASS MICRODOSIMETERS

Investigation of the additivity of moderately small doses in three types of metaphosphate glass rod microdosimeters, previously mentioned,[14] was reported as a note[15] when the accumulated exposure at 500 mr of radium gamma per working day had reached 95.5 r over a period of 39 weeks. After the experiment had been continued for another 37 weeks, the total exposure was 182.5 r. Table 15.1 presents a condensed summary of the results.

The investigation of change of fluorescence with time after single exposures has been completed. This experiment comprised exposures from 100 to 100,000 r of Co^{60} gamma of the three types of fluorods. These were read after intervals of one day to one year of storage. While these exposures were outside the range encountered in personnel monitoring, they were exaggerated to provide both a high enough response to make predose readings insignificant and an indication of the possible dose dependence of the change of fluorescence with time.

[14] J. A. Auxier *et al.*, *Health Phys. Ann. Progr. Rept. July 31, 1962*, ORNL-3347, p 93.

[15] J. S. Cheka, *Health Phys.* 8, 551 (1962).

Table 15.1 Summary of Response of Various Fluorods to 500 mr per Working Day

Date	Elapsed Time (days)	Accumulated Exposure (r)	Divisions per r		
			B and L Hi-Z[a]	B and L Lo-Z[a]	Toshiba[b]
4/28/61	14	6	0.192 ± 0.010	0.198 ± 0.012	0.328 ± 0.013
6/9/61	56	20.5	0.165 ± 0.026	0.206 ± 0.022	0.366 ± 0.014
7/21/61	98	35.0	0.167 ± 0.014	0.204 ± 0.014	0.369 ± 0.004
9/7/61	146	52.0	0.160 ± 0.014	0.209 ± 0.009	0.371 ± 0.007
1/12/62[c]	273	95.5	0.161 ± 0.001[d]	0.203 ± 0.019	0.374 ± 0.008
8/10/62	483	168.0	0.158 ± 0.001[d]	0.206 ± 0.023	0.381 ± 0.007
9/28/62	532	182.5	0.148 ± 0.001[d]	0.200 ± 0.021	0.373 ± 0.003

[a] Bausch and Lomb Optical Company.

[b] Shibaura Electric Company, Tokyo.

[c] Last values previously reported.

[d] Only two fluorods intact from a group of six.

HEALTH PHYSICS RESEARCH REACTOR (HPRR)

The HPRR became operational in its permanent location at the DOSAR facility on May 31, 1963. Installation of cable-handling equipment for supporting the control cables during movement of the reactor positioning device was completed on June 15, 1963. Figure 15.20 shows the assembled reactor on its positioning device. Experiments during June 1963 included calibration and dosimetry studies, and exposures were made for three radiobiological studies (mice, for W. L. Russell, ORNL; rats, for N. Wald, University of Pittsburgh; and silkworms, for S. Kondo, Japanese Institute of Genetics).

UNCLASSIFIED
PHOTO 61950

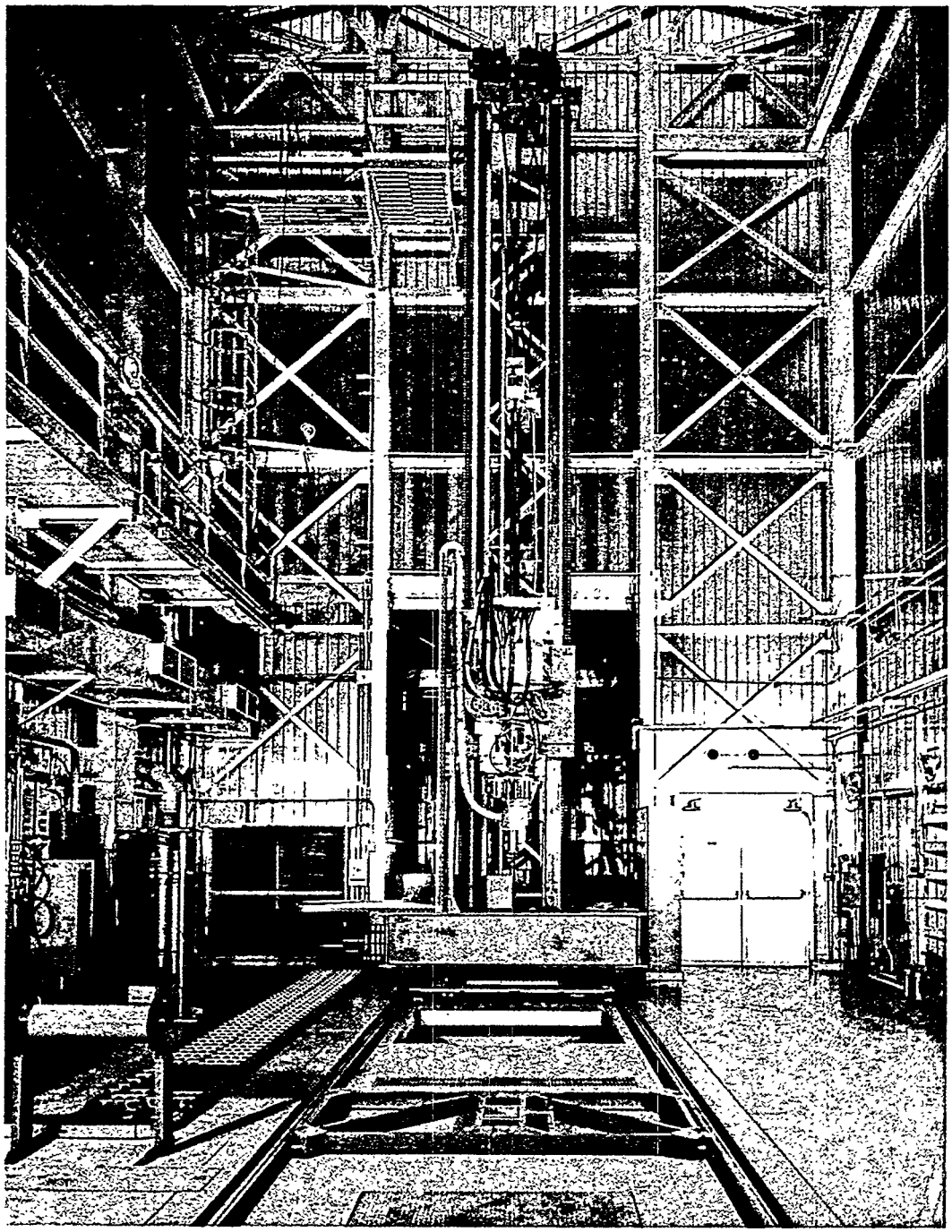

Fig. 15.20. Health Physics Research Reactor on Its Positioning Device.

Part IV. Internal Dosimetry

W. S. Snyder

16. Estimation of Internal Dose

$(MPC)_w$ VALUES FOR OCCUPATIONAL EXPOSURE TO Sr^{90}, Sr^{89}, AND Sr^{85}

W. S. Snyder Mary Jane Cook
Mary R. Ford

Since the beginning of large-scale work with atomic energy, the metabolism of strontium has been the subject of intensive research efforts. The ICRP and NCRP Internal Dose Committees have recommended 2 μc as the maximum permissible body burden for Sr^{90}. In this study an attempt has been made to calculate occupational MPC values for Sr^{90}, Sr^{89}, and Sr^{85} which would limit the body burden of Sr^{90} to 2 μc over 50 yr of occupational exposure. No attempt has been made to assess the evidence concerning the carcinogenic potency of the strontium isotopes, but rather only the metabolic problem. Due to the lack of human data covering such an extended period, it is necessary to establish metabolic models. Several models have been considered, and the MPC values based upon each have been estimated. The first is a representation of the retention of a single intake to blood as a sum of three exponential functions; the second consists in using a power function to represent the retention; and the third involves the comparison of metabolism of calcium and strontium and centers about the observed ratio (OR), that is, $(Sr/Ca)_{bone}/(Sr/Ca)_{diet}$. Finally, data on stable strontium are considered and may be regarded in their own right as established directly, although only roughly, from the relation of intake and body burden.

The Exponential Model

In Table 16.1 the human studies which are the principal basis of the exponential model are summarized. According to the cited references, the subjects might be considered as "grossly normal" in all cases. No attempt was made here to study the many cases in which strontium metabolism has been studied in subjects who were aged or hospitalized for various ailments.

Figure 16.1 shows retention following a single intravenous injection of two individuals, "A" and "B," and an accidental puncture wound of the thumb in the case of the third individual, "C." In the case of "A" and "B" the radionuclide was Sr^{85}, which emits a 0.51-Mev gamma ray, so that retention was determined by whole-body counting. Fractional retention may also be estimated as 1 − excretion; however, this method is not considered as accurate as whole-body counting due to incomplete collection of excreta (i.e., sweat is known to include some of the material) and inaccuracies in analysis. It is found that the

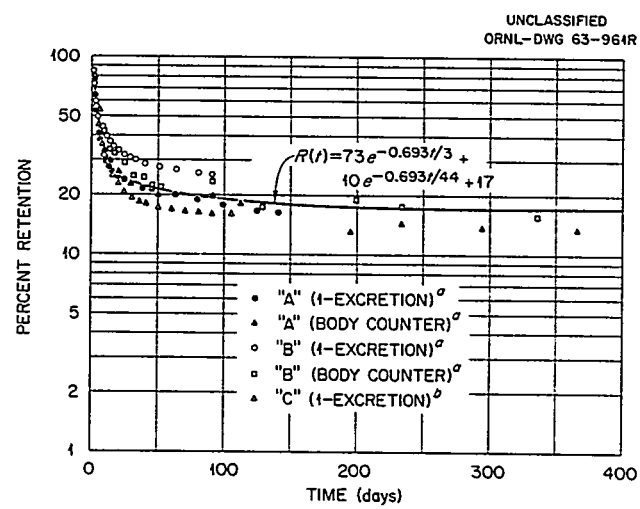

Fig. 16.1. Retention of Strontium Following Intravenous Administration. (Symbols *a* and *b* refer to footnotes of Table 16.1.)

Table 16.1. Description of Strontium Studies on Normal Human Subjects

Subject	Length of Study	Type of Analysis	Dose and Route of Entry	Comments
"A," "B"[a] (males; age, 47, 53; weight, ~80 kg)	140 days 1 yr	Excretion (fecal, urinary) Whole-body counting	Sr^{85} chloride; 0.5 μc; intravenously	"A" determined to be approximately in calcium balance
"C"[b] (male; age, 32; weight, ~84 kg)	115 days	Excretion (fecal, urinary)	($Sr^{90} + Y^{90} + Ca^{45}$) chloride; puncture wound; 0.0074 μc (estimated)	Dietary calcium increased 2 to 3 times average after wound
"D," Japanese male[c,d] (age, 53; weight, ~68 kg)	163 days 212 days	Excretion (fecal, urinary) Whole-body counting	Sr^{85} chloride; ~5 μc; oral	Subject determined to be approximately in calcium balance
Sr-1, -2, -3[e] (males; age, adult; weight, ~74 kg)	160 days	Whole-body counting	Sr^{85}; 1.07 μc; oral	
"E" (REF)[e]	60 days	Whole-body counting	Sr^{85}; oral	
"F," "A"[f] (males; age, 40, 45; weight, 80, 85 kg)	20 to 25 days	Excretion (fecal, urinary)	Sr chloride, stable; intravenously; "F," 100 mg; "A," 20 mg	"A" determined to be approximately in calcium and strontium balance before study
"F," "B"[f] (males; age, 40, 50; weight, 85, 77 kg); "G" (female; age, 29; weight, 73 kg)	20 to 25 days	Excretion (fecal, urinary)	Sr chloride, stable; oral; males, 250 mg; "G," 100 mg	

[a]Margaret Bishop *et al.*, *Intern. J. Radiation Biol.* 2(2), 125 (1960).

[b]L. B. Farabee, *Health Phys. Div. Ann. Progr. Rept. July 31, 1961*, ORNL-3189, pp 224–26; L. B. Farabee and B. R. Fish, *Health Phys. Div. Ann. Progr. Rept. July 31, 1962*, ORNL-3347, pp 153–54; ORNL unpublished data.

[c]M. Fujita *et al.*, *Health Phys.* 9(4), 407 (1963).

[d]Susumu Suguri *et al.*, *Health Phys.* 9(5), 529 (1963).

[e]J. E. Furchner *et al.*, *Retention of Strontium-85 by Man*, LAMS-2780 (1962).

[f]G. E. Harrison, W. H. A. Raymond, and H. C. Tretheway, *Clin. Sci.* 14, 681 (1955).

formula

$$R(t) = 0.73e^{-0.693t/3} + 0.10e^{-0.693t/44} + 0.17 \quad (1)$$

fits the data rather well.

In the case of "C," Sr^{90} was accidentally injected, which meant that the intake was somewhat uncertain, and the retention was estimated only on the basis of excretion data. The shape of the retention curve for "C" is the most significant independent bit of information to be inferred from this exposure for the present purpose. It is seen that these three subjects have a reasonably consistent common pattern. The final constant term of Eq. (1) must be presumed to represent material which is being excreted from the body at a very

slow rate. On the basis of these data, it is not possible to determine whether this 17% consists of one, two, or three exponentials, but by analogy with radium, it must be supposed that some fraction of it will remain in bone after many years.

Before discussing the long-term retention, it is illuminating to consider the relation of Eq. (1) to the excretion data. These excretion data are shown in Fig. 16.2. The solid curve is the derivative of (1) except that the last term is taken as $0.17e^{-0.693t/4000}$, as discussed below. The agreement is remarkably good as excretion data go. It is likely that the low values measured are somewhat uncertain because of the very low level. Thus Eq. (1) seems adequate, so far as these individuals are concerned, for interpretation of the early metabolism of strontium ($t < 200$ days).

If the 17% retained at about 1 yr is the sum of several components with different elimination rates, the replacement of these exponentials by a single exponential will lead to the same body burden as the use of several, provided the elimination rate is chosen to achieve this. Assuming that all this material is eliminated slowly (half-life long compared to a year), then the error will not be a gross one if all such components are grouped together. For example, if one had $0.07e^{-0.693t/10} + 0.10e^{-0.693t/20}$ instead of $0.17e^{-0.693t/20}$ (time in years), then in 50 yr the error in the body burden would be 20%. Thus the short-term studies only fix the size of the long-term-retention component, but with this size fixed, one may use an average rate of elimination for it and hope to estimate the body burden with reasonable accuracy provided one long-term retention value can be estimated to represent an average rate of elimination over this period.

Data on stable strontium provide such a check value provided the model can be modified suitably for oral intakes. Figure 16.3 shows excretion data on "B" and "F," who took stable strontium both intravenously and orally. The excretion values do differ by a fairly consistent factor over the entire period of observation. To avoid exogenous material and the uncertainty of the lowest values, the two sets of values have been averaged over the period from 4 to 20 days. The ratio of the average values was found to be 0.36.

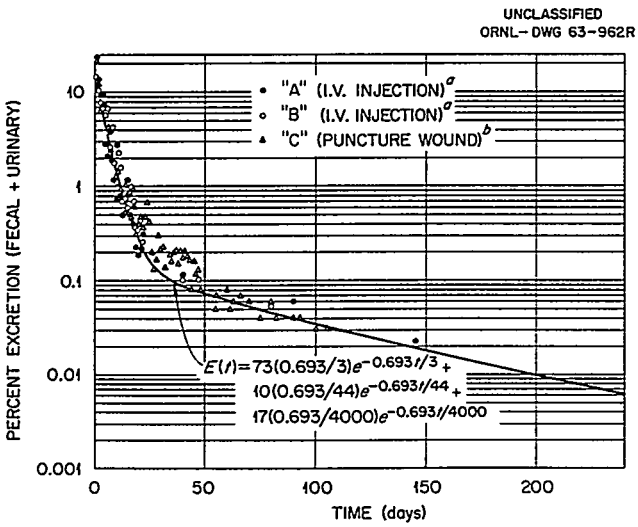

Fig. 16.2. Excretion of Strontium Following Intravenous Administration. (Symbols *a* and *b* refer to footnotes of Table 16.1.)

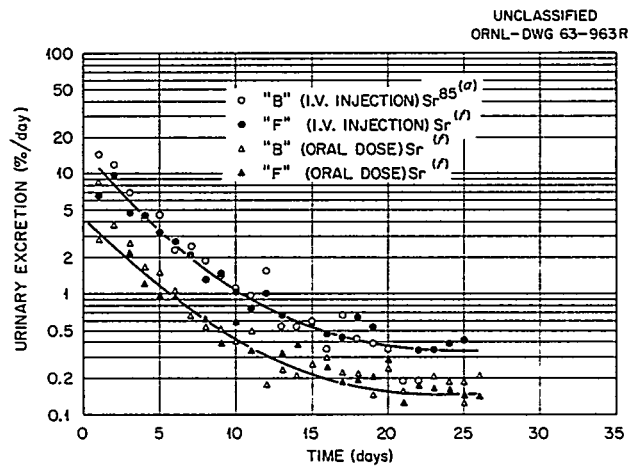

Fig. 16.3. Urinary Excretion of Strontium Following Oral or Intravenous Administration. (Symbols *a* and *f* refer to footnotes of Table 16.1.)

Figure 16.4 shows data on five male adults who took Sr^{85} orally. Equation (1) has been modified by a suitably chosen factor f_1 in each case, and it has been found that the data do tend to follow the formula when so adjusted. Thus the use of a constant factor, that is, a constant percentage shift of all portions of the curve, seems a reasonable assumption. It will be noted that the values of f_1 that must be used range from 0.17 to 0.5.

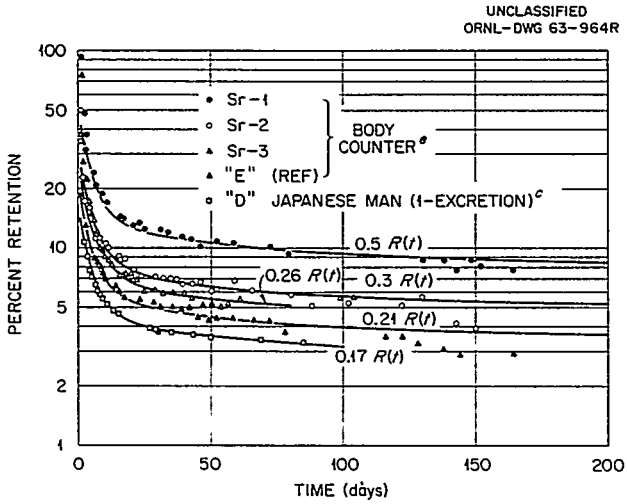

Fig. 16.4. Retention of Strontium after Oral Administration. (See Table 16.1, footnotes c and e.)

Table 16.2 shows data on the Sr/Ca ratio in diet and bone. These data undoubtedly leave much to be desired. In many cases the number of individual samples is small, and in no case is it known whether or not an individual that contributed a bone sample really consumed something like the diet which was sampled. Despite these grave shortcomings, it may be that these data are the best human data now available on the long-term accumulation of a body burden of strontium. It must be remembered that the standard man can only represent some kind of average or typical individual, and thus it is somewhat more excusable to use "average" values of diet and bone samples to obtain his elimination rate.

The English data predict that the adult body burden should average 209 daily intakes, and the total of United States data would predict 182 daily

Table 16.2. $(MPC)_w$ for Sr^{90} Estimated from Diet-Bone Data on Stable Strontium

Bone				Food			
Source of Sample	Sample Size	Responsible for Analysis	μg of Sr per g of Ca	Source of Sample	Responsible for Analysis	Intake (mg/day)	$(MPC)_w$ (μc/ml)
							$\times 10^{-6}$
San Francisco	24	ORNL	378	San Francisco	HASL	1.90	4.6
San Francisco	5	HASL	300	San Francisco	HASL	1.90	5.8
Chicago	4	ORNL	286	Chicago	HASL	1.82	5.8
Chicago	6	HASL	290	Chicago	HASL	1.82	5.8
New York	6	HASL	250	New York	HASL	1.53	5.6
New York	127	Lamont	410	New York	HASL	1.53	3.4
United States	171	ORNL	320	Av { New York, San Francisco, Chicago }	HASL	1.75	4.5
England	31	Harwell	355	England	British Agricultural Research Council	1.6	4.3
Montreal		Chalk River	280	Canada	Chalk River	1.3	4.2
San Juan	5	HASL	503	San Juan	HASL	1.23	2.2

intakes. Since the data on American diets are less extensive (as represented here), it may be better at present to use the British data. If this is done directly, the daily intake to produce a body burden of 2 μc of Sr^{90} is at least 2/209 μc/day = 9.5×10^{-3} μc/day. The corresponding $(MPC)_w = 9.5 \times 10^{-3}/2200 = 4.3 \times 10^{-6}$ $\mu c/cm^3$, 168 hr/week. These values are conservative on several counts: (1) no allowance is made for radioactive decay, and (2) the young adult has already accumulated a considerable body burden of stable strontium. Nevertheless, the value must be regarded as highly uncertain. The data on U.S. diets and bone would give $(MPC)_w = 5.1 \times 10^{-6}$ $\mu c/cm^3$, 168 hr/week.

Returning to the exponential model and assuming a state of equilibrium, the body burden for unit daily intake with $f_1 = 0.3$ would be

$$0.3 \left[\frac{0.73 \times 3}{0.693} + \frac{0.10 \times 44}{0.693} + \frac{0.17 \times T_b}{0.693} \right] ;$$

setting the above result equal to 210, one obtains $T_b = 2800$ days. Most British experimenters report $f_1 \approx 0.20$ (ref 1), and if this is used, one obtains $T_b = 4300$ days. Thus a value of T_b of the order of 3000 to 4000 days seems indicated by the dietary-bone data. The U.S. data would give a smaller value.

One other bit of data, again somewhat tenuous, may be used to check on the long-term elimination rate. Rowland has estimated an average turnover rate of 3 to 5% a year for bone.[2] Although the bone samples may not be representative of total bone and of "standard" man, it seems worthwhile to see if it is grossly out of line with the above model. The average turnover rate of the long-term compartment is $0.693/T_b \times 365 \times 100\%$ per year. With $T_b = 3000$ this amounts to 8%, and for $T_b = 4000$, to about 6%. The value of $T_b = 4000$ is preferred here, partly because of this slightly closer agreement with Rowland's estimate and partly because the MPC it determines is more conservative. Even if the U.S. "standard" man has $f_1 = 0.3$, one obtains $(MPC)_w = 4.3 \times 10^{-6}$ $\mu c/cm^3$, 168 hr/week.

[1] J. F. Loutit, *Irradiation of Mice and Men*, The University of Chicago Press, 1962.

[2] R. E. Rowland, p 339 in *Radioisotopes in the Biosphere* (ed. by R. S. Caldecott and L. A. Snyder), University of Minnesota, Minneapolis, 1960.

Power-Function Model

Power-function models for retention have been given by ICRP Committee II,[3] by Marinelli,[4] and by Bishop *et al.*[5] The retention function given by Bishop *et al.*[5] more closely resembles the animal models as summarized by Rowland.[6] The $(MPC)_w$ values for Sr^{90} corresponding to these retention functions are given below.

If the retention function following intravenous administration is $R(t) = at^{-b}$, then the body burden following 50 yr of intake of I μc/day is given by

$$q(t) = If_1 \int_0^t d\tau\, a(t-\tau)^{-b}\, e^{-\lambda_r(t-\tau)}$$

$$= If_1 \int_0^t dx\, ax^{-b} e^{-\lambda_r x} ,$$

where $t = 50 \times 365$. Using the function as recommended by Marinelli, $R(t) = 0.95t^{-0.25}$, and taking $q = 2$ μc and $f_1 = 0.3$, one obtains for Sr^{90} $I = 5.7 \times 10^{-3}$ and $(MPC)_w = 2.6 \times 10^{-6}$ $\mu c/cm^3$, 168 hr/week. The formula $R(t) = 0.65t^{-0.35}$ given in *ICRP, Report of Committee II* yields $I = 1.8 \times 10^{-2}$ μc/day and $(MPC)_w = 8.3 \times 10^{-6}$ $\mu c/cm^3$, 168 hr/week. The formula $R(t) = 0.51t^{-0.23}$ given by Bishop *et al.*[5] yields $I = 8.5 \times 10^{-3}$ μc/day and $(MPC)_w = 3.9 \times 10^{-6}$ $\mu c/cm^3$, 168 hr/week.

Comparison with Calcium

Many investigators have reported that

$$OR = (Sr/Ca)_{bone}/(Sr/Ca)_{diet} \cong 0.25 .$$

It is known that the value of the observed ratio can be perturbed by grossly altering the diet. However, for a normal diet the value of 0.25 has been considered as rather well established. Nevertheless, the bone-diet data reported from HASL (Table 16.2) yield lower values, but again the sampling is not very extensive. If OR = 0.25 is used to estimate

[3] *Report of Committee II on Permissible Dose for Internal Radiation*, ICRP Publication 2, Pergamon, London, 1959.

[4] L. D. Marinelli, *Estimates of Bone Pathology to Be Expected from Sr^{90}*, ANL-5716 (1957).

[5] Margaret Bishop *et al.*, *Intern. J. Radiation Biol.* 2(2), 125 (1960).

[6] R. E. Rowland, *Retention and Plasma Clearance of the Alkaline Earth Elements*, ANL-6104, pp 34–37 (1959).

Table 16.3. Reported Observed Ratio Values

Observed Ratio (OR)	Method	Reference
0.2–0.25	Hospital patients; double tracer Ca^{45} and Sr^{85}	J. L. Kulp and A. R. Schulert, *Sr^{90} in Man and His Environment, Part I*, NYO-9934, pp 152–53 (May 1962).
0.25	Comparison of diet and bone levels	J. L. Kulp and A. R. Schulert, *Science* **136**, 619 (1962).
0.25	Stable strontium and calcium, Wales and north and west England	F. J. Bryant, A. C. Chamberlain, and G. S. Spicer, *Brit. Med. J.* **1958**, 1371.
0.23	Stable strontium and calcium, England	J. D. Burton and E. R. Mercer, *Nature* **193**, 846 (1962).
0.16	Stable strontium and calcium in adults, New York	J. Rivera, *Fallout Program Quarterly Summary Report April 1, 1963–July 1, 1963*, HASL-138, pp 235–38.
0.16	Stable strontium and calcium in adults, Chicago	
0.16	Stable strontium and calcium in adults, San Francisco	
0.2	Stable strontium and calcium in adults, San Francisco	ORNL unpublished data to W. S. Snyder from S. R. Koirtyohann and C. Feldman, 1962; J. Rivera, *Fallout Program Quarterly Summary Report April 1, 1963–July 1, 1963*, HASL-138, pp 235–38.
0.16	Stable strontium and calcium in adults, Chicago	
0.18	Stable strontium and calcium in adults, average for U.S.	
0.16	Japanese	Y. Hiyama, quoted by J. D. Burton and E. R. Mercer, *Nature* **193**, 846 (1962).
0.18	Stable strontium and calcium; human rib samples from U.S.	G. V. Alexander and R. E. Nussbaum, *J. Biol. Chem.* **234**, 418 (1959).
0.35	Double tracer Sr^{85} and Ca^{45}; hospital patients	Herta Spencer, D. Laszlo, and M. Brothers, *J. Clin. Invest.* **36**, 680 (1957).
0.53	Double tracer Sr^{85} and Ca^{45}	C. L. Comar *et al.*, *Proc. Soc. Exptl. Biol. Med.* **95**, 386 (1957).
0.35	Double tracer Sr^{85} and Ca^{45}; two patients on nonmilk diets	C. L. Comar, R. S. Russell, and R. H. Wasserman, *Science* **126**, 485 (1957).
0.31	Stable strontium and calcium in infants (0–1 yr); New York	J. Rivera, *Fallout Program Quarterly Summary Report April 1, 1963–July 1, 1963*, HASL-138, pp 235–38.
0.48	Stable strontium and calcium in infants (0–1 yr); Chicago	
0.31	Stable strontium and calcium in infants (0–1 yr) San Francisco	
Body/diet, average = 0.92; std deviation = ±0.27; range, 0.54–1.48	Fourteen infants; at beginning of observation period, ages ranged from 25 to 46 days	S. A. Lough, J. Rivera, and C. L. Comar, *Proc. Soc. Exptl. Biol. Med.* **112**, 631 (1963).

uptake and retention of strontium, the intake to give a uniform labeling of the skeleton at the level of 2 μc burden is (μc of Sr^{90} per g of Ca)$_{diet}$ × OR × (g of Ca in standard man) = q (μc of Sr^{90}), that is,

$$(I/1) \times 0.25 \times 10^3 = 2$$

or

$$I = 8 \times 10^{-3}\ \mu c/\text{day}\ .$$

This gives an $(MPC)_w = 3.6 \times 10^{-6}\ \mu c/cm^3$, 168 hr/week. The value is conservative insofar as it neglects radioactive decay of Sr^{90}.

The observed ratio (OR) model is very attractive on several counts. First, it purports to control the local concentration of strontium in the bone, since the model assumes that the new bone formed will be at the level of the plasma at the time of formation. For constant exposure level this would ensure a nearly uniform concentration. Moreover this model is the one of the four discussed here that seems most immediately applicable to the child or the infant. With the other models it must be assumed that the parameters might change with age. There is the possibility that the OR may be greater, particularly during the first year following birth. Some human data as well as some animal studies have suggested such a change.[7,8] If this discrimination exists, it is supposed to be partially offset by placental discrimination and, in any case, is easily taken into account for application to infants. Table 16.3 lists various OR values that have been reported, from which it is seen that the value of 0.25 is rather conservative. However, some of the lower values rest on relatively few samples.

Sr^{89} and Sr^{85}

Merely by changing the radioactive half-life, the $(MPC)_w$ values for Sr^{89} and Sr^{85} are readily obtained either by the power-function model or from the exponential model. It is not so easy to adapt the OR model or the direct data on diet and bone since no elimination rate is implied by the model. The $(MPC)_w$ values obtained from the exponential and power-function models are listed in Table 16.4.

Table 16.4. $(MPC)_w$ Values for Sr^{90}, Sr^{89}, and Sr^{85} as Computed by Various Models[a]

Model	Radionuclide		
	Sr^{90}	Sr^{89}	Sr^{85}
	$\times 10^{-6}$	$\times 10^{-4}$	$\times 10^{-3}$
$R(t) = 0.65t^{-0.35}$	8.3	4.1	6.2
$R(t) = 0.95t^{-0.25}$	2.6	2.1	3.0
$R(t) = 0.51t^{-0.23}$	3.9	3.6	5.3
$R(t) = 0.73e^{-0.693t/3} + 0.10e^{-0.693t/44} + 0.17e^{-0.693t/4000}$	4.3	3.3	4.7
OR	3.6		
Diet-bone data (British)	4.3		
Diet-bone data (U.S.)	4.5		
NCRP values (Handbook 69)	1	1	1

[a] $\mu c/cm^3$, 168 hr/week; critical organ, bone.

MAXIMUM PERMISSIBLE BODY BURDENS AND MAXIMUM PERMISSIBLE CONCENTRATIONS ESTIMATED BY AN EQUIVALENCE RELATION BETWEEN EXTERNAL DOSE AND INTERNAL DOSE

S. R. Bernard

The purpose in this work is to suggest a possible method for estimating the maximum permissible body burden, q, and maximum permissible concentration, MPC, for Sr^{90} from a different model than the critical-organ concept employed by ICRP and NCRP. Use is made of the toxicity data on mice published by Finkel[9] and of Henshaw's[10] life-shortening data from chronic whole-body external exposure of mice to x rays. With these data an equivalence between external exposure and internal exposure can be derived; then from the

[7] A. C. Andersen, *The Effects of Continual Sr^{90} Ingestion During the Growth Period of the Beagles and Its Relation to Ra^{226} Toxicity*, UCD-106 (June 1962).

[8] R. J. Della Rosa and R. Pool, *Radiation Res.* 19(1), 179 (1963).

[9] M. P. Finkel, *Proc. Second Intern. Conf. Peaceful Uses At. Energy* 22, 65 (1958).

[10] P. S. Henshaw, *J. Natl. Cancer Inst.* 4, 521 (1944).

life-shortening data on American radiologists,[11] this equivalence relation can be extrapolated to man, and some estimates can be made of an equivalent q and MPC for man.

The equivalence relation between external external exposure and internal exposure is based on Henshaw's data in Fig. 16.5, which presents a plot of R, the roentgens per day external exposure of mice, vs the median life span S in days. The equation fitted to the data is

$$R = 40\left[\frac{1-(S/320)}{1-e^{-0.7S/37}}\right], \qquad (1)$$

in r/day, and it is a fairly adequate representation over the entire region. In this equation the life span S_0 of control animals is ~320 days. With $x = S/S_0$ and values of $x \to 1$, the equation simplifies to

$$R \sim 40(1-x), \qquad (2)$$

in r/day.

An expression similar to (1) can be obtained from a fit of Finkel's Sr^{90} data. Figure 16.6 shows a plot of the single-injection dose q_0/m, in μc/g, into mice vs the median life span S, in days. The equation fitted to Finkel's data is

$$q_0/m = \left[\frac{1-(S/600)}{1-e^{-0.7S/180}}\right], \qquad (3)$$

in μc/g. Here S_0 is 600 days. For values of

[11] Discussed in *Report of the United Nations Scientific Committee on the Effects of Atomic Radiation*, suppl No. 16 (A/5216), p 144, 1962.

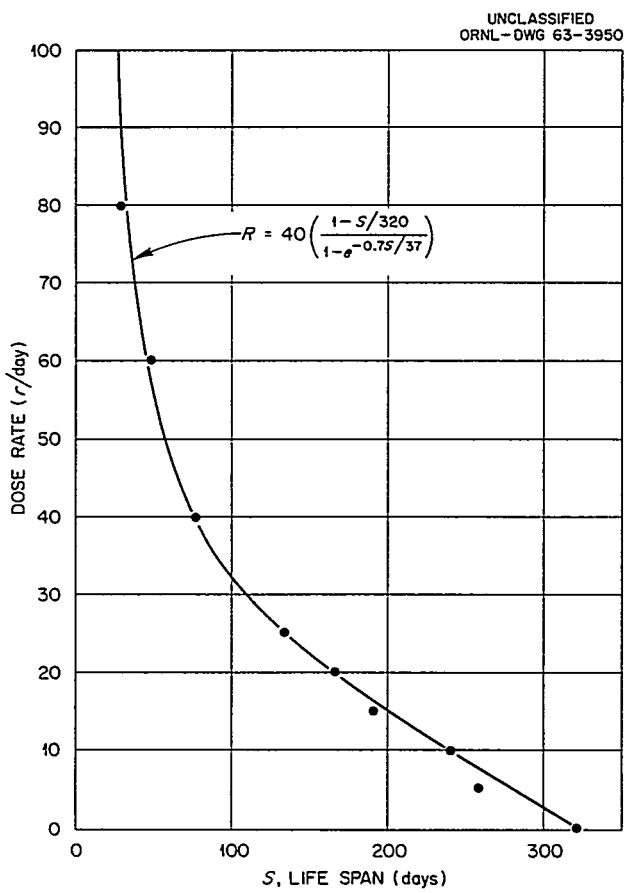

Fig. 16.5. Henshaw's Data; Mice, Chronic Irradiation (X Rays).

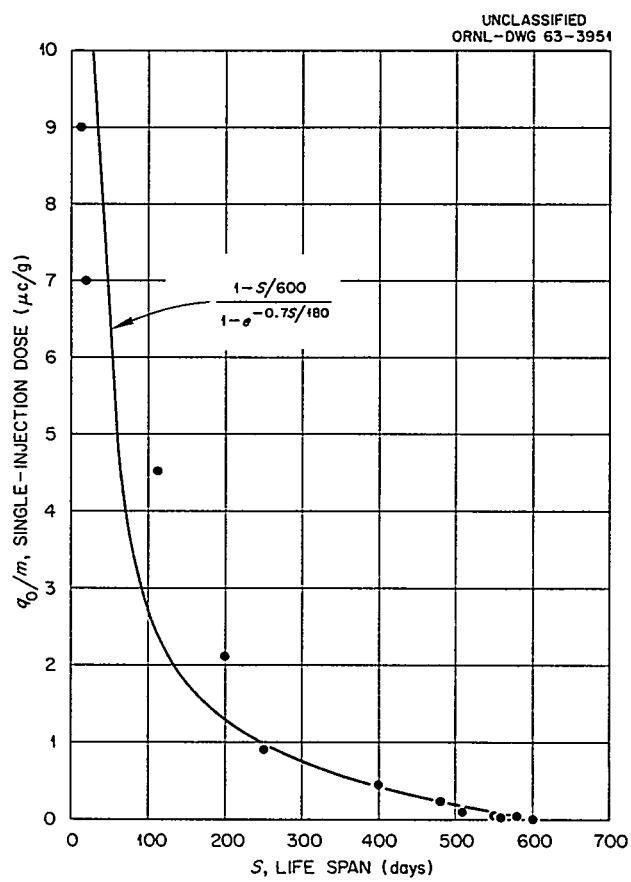

Fig. 16.6. Finkel's Strontium Data; Mice, Injection Dose (μc/g) vs Survival Time (days).

$S/S_0 = x \to 1$, the expression

$$q_0/m \sim (1 - x) , \qquad (4)$$

in μc/day, is a fair representation.

From (2) and (4), x can be eliminated, and we obtain the equivalence

$$q_0/m = R/40 . \qquad (5)$$

From this equation, we may say that a single-injection dose of 1 μc of Sr^{90} per g of body weight produces the same percentage of life shortening in mice as does chronic, external, whole-body exposure of mice to 40 r/day. We can use this expression to estimate q_0 and MPC for man *if we can assume that the same equivalence relation between external dose and internal dose in man would hold.* However, some extrapolation from mouse to man must be made. Use is made of the data on American radiologists to extrapolate formula (1) for man.

Braestrup[12] has estimated the external dose to American radiologists of ~100 rads/yr (0.4 rad/day). Their average life span was 60.5 yr. Other physicians had a life span of ~65.7 yr. Thus, the fractional life span

$$x = \frac{60.5}{65.7} = 0.921 .$$

From (2) we would find that R = 3.16 r/day when x = 0.921. We can equate the absorbed dose rate, rads/day, to the exposure dose rate since the mice were exposed to 200-kvp x rays. Thus, mice require eight times the dose rate that man does to give a fractional life span of 0.921. A similar check on the extrapolation of (4) is desirable, but corresponding data on man are not available. The permissible external dose rate for man is 0.1 rad/week (0.02 rad/day, occupational exposure), which is equivalent to 0.16 rad/day exposure of mice. From (5) we estimate q_0/m equivalent to 0.16 rad/day and obtain

$$q_0/m = \frac{0.16}{40} = 0.004 ,$$

in μc/g. This would suggest that man could take 0.004 μc/g × 70,000 g = 280 μc as a single injection, and the injury in terms of life shortening would be equivalent to that resulting from exposure to 0.1 rad/week, *providing this equivalence relation holds for man* and the above extrapolation from mouse to man is valid. The bone burden would be 0.3 × 280 $\mu c \cong$ 84 μc. (Here the value of 0.3, the fraction going from blood to bone, was taken from *ICRP, Report of Committee II.*) The body burden would be 84/0.99 $\cong$ 84 μc since f_2, the fraction in the bone to that in the body, which is also taken from the handbook, is given as 0.99. This value of 84 μc is not comparable with the 2-μc value recommended by ICRP and NCRP for body burden that results from chronic intake.

To estimate an $(MPC)_w$, actually, we should have continuous ingestion data on mice to construct a plot of the $\mu c/cm^3$ vs the median life span and employ a similar equivalence relation. For a crude estimate we can calculate the daily incremental amount put into man over a period of 50 yr such that the total intake would be 280 μc. In 50 yr there are 200 quarters, and the quarterly intake would be 280/200 μc per quarter = 1.4 μc per quarter. This is the input into the blood. Since only 0.3 is assumed to be absorbed from the gut into blood, then man could ingest 1.4/0.3 = 4.6 μc per quarter. This is to be compared with the permissible quarterly intake of 0.2 μc recommended by ICRP and NCRP. It is a factor of 23 times higher.

Note in this equivalence-relation method no adjustment for radiological decay is made. The value of q_0 indicates an amount which can be put into the body but only as a single quantity or parceled out over a period of 50 yr of exposure. Thus, insofar as the q_0 value is concerned, no direct comparison with the usual body burden should be made. As for the $(MPI)_w$ value (quarterly permissible intake in water), it is permissible to compare this value with the ICRP or NCRP recommendations. It would appear that the ICRP or NCRP recommendations are conservative. However, this estimation method should not be used without checking with data on more species of animals which were administered lower injection levels or which experienced continuous feeding and inhalations of the radionuclides. In addition to the need for data to permit interspecies extrapolation, other biological effects should be considered also. When such data become available, a more firm basis for conclusions about q and MPC may evolve.

[12]Cited by P. R. J. Burch, *Nature* 185, 135–42 (1960).

$(MPC)_w$ FOR Rn^{222}

S. R. Bernard

In a previous progress report[13] an $(MPC)_w$ for Rn^{222} was estimated to be $\sim 2 \times 10^{-4}$ $\mu c/cm^3$ based on yellow bone marrow which was considered as a blood-forming organ. This is now believed to be a factor of 2.5 too low because the decay chain of Rn^{222} contains chiefly alpha emitters whose ranges are short enough so that the energy will be dissipated in the yellow marrow and not in the nearby red marrow. Thus, a revision upward by a factor of 2.5 is suggested in order to prevent compounding of safety factors.

$(MPC)_w$ values for various organs and tissues based on Nussbaum's[14] experimentally determined f_2 values have been calculated and appear in Table 16.5. For these calculations the method of estimation previously described[13] was employed. As can be noted, fat and yellow marrow are the critical organs, and the $(MPC)_w$ is 5×10^{-4} $\mu c/cm^3$ (168 hr/week) for occupational exposure.

The dose to the stomach has also been considered, for which Nussbaum does not have measurements. The ICRP model was employed for

[13]S. R. Bernard, *Health Phys. Div. Ann. Progr. Rept. July 31, 1961*, ORNL-3189, p 192.

[14]E. Nussbaum, *Radon Solubility in Body Tissues and in Fatty Acids*, UR-503 (1957).

Table 16.5. $(MPC)_w$ for Occupational Workers Exposed 168 hr/week

Organ	m (g)[a]	f_2	m/f_2	R (rem/week)	$(MPC)_w$ ($\mu c/cm^3$)
			$\times 10^5$		$\times 10^{-3}$
Muscle	30,000	0.07	4.3	0.1	5.2
Skin	6,100	0.01	6.1	0.3	22
Fat	10,000	0.71	0.14	0.3	0.5
Skeleton	7,000	0.016	4.4	0.3	16
Red marrow	1,500	0.0095	1.6	0.1	1.9
Yellow marrow	1,500	0.11	0.14	0.3	0.5
Blood	5,400	0.035	1.5	0.3	5.4
GI tract	2,000	0.092	2.2	0.3	7.9
Liver	1,700	0.008	2.1	0.3	7.6
Brain	1,500	0.007	2.1	0.3	7.6
Lungs	1,000	0.004	2.5	0.3	9
Lymphoid tissue	700	0.003	2.3	0.3	8.3
Kidneys	300	0.0012	2.5	0.3	9
Heart	300	0.0011	2.7	0.3	9.7
Spleen	150	0.0006	2.5	0.1	3
Urinary bladder	150	0.0003	5	0.3	18
Testes	70	0.0001	4	0.1	4.8
Balance	884	0.004	2.2	0.3	7.9
Total body	70,000	1	0.7	0.1	0.84

[a]From *ICRP Handbook*, p 151.

estimating the dose to the stomach, which was determined not to be a critical organ. However, the ICRP model does not take into account the possibility of diffusion of inert gases into the stomach walls. Some rough calculations were made of the amounts diffusing into the stomach walls and indicated that diffusion was slow enough such that the stomach will not be overirradiated upon ingestion of 5×10^{-4} $\mu c/cm^3$. Experimental data are needed to confirm this conclusion.

In all these estimations, it is implicitly assumed that the short-lived daughters of the Rn^{222} in the organ or tissue undergo decay *in situ*. Some experimental data collected by Hollcroft *et al.*,[15,16] Scott,[17] and Morken[18] implicate the kidney as a possible critical organ. We must, therefore, estimate the dose to this organ which results from the intake and decay of Rn^{222} and translocation of its daughters in the body.

There are at least two ways to estimate the dose to the kidneys from the short-lived daughters. One way is to estimate the level of daughters released to the bloodstream each day from each organ and then take the fraction f_2' of these daughters going from the blood to the kidney and calculate its burden of short-lived daughters. The available biological data are not adequate to make this calculation. Needed here are the biological half-lives of all daughters in each organ. Also, since these daughters have very short half-lives, some data on the transport times from organs to kidneys are needed. Thus we are forced to estimate the dose to kidneys in another – a second, simpler – way.

In this second way we estimate the level of daughters present in the whole body produced by the decay of Rn^{222}. We can then estimate the level in the kidneys by multiplying the body burden by f_2, the fraction of that in the total body present in the kidneys, in which case an estimate of f_2 is available in the handbook. Or another way, from the equation $qf_2 = 2.8 \times 10^{-3}\ RM/\epsilon$, we can calculate the value of q, the permissible body burden, and compare it with the estimated level of daughters present in the whole body.

Let N_i denote the number of atoms of ith daughter present in the body and produced from decay of Rn^{222} and also from intake of I_i' atoms per day into the body from the gut. The body burden N_i of these ith atoms is governed by the equation

$$\frac{dN_i}{dt} = I_i' + \lambda_{i-1}^r N_{i-1} - (\lambda_i^r + \lambda_b^i) N_i ,$$

$$i = 1, 2, \ldots , \qquad (1)$$

where λ_i^r is the radiological decay constant, λ_b^i is the biological decay constant, and the 0th kind of atoms are Rn^{222}. Assume the steady state exists, that is, neglect the buildup and only examine the case of equilibrium. Solving (1), we find that

$$N_i = \frac{I_i' + \lambda_{i-1}^r N_{i-1}}{(\lambda_i^r + \lambda_b^i)} . \qquad (2)$$

The biological half-life λ_b^i is small for these daughters compared to λ_i^r, so we can neglect λ_b^i and calculate q_i, the number of μc of the ith atoms, where

$$q_i = \frac{\lambda_i^r N_i \,(\text{atoms/day})}{3.7 \times 10^4 \,(\text{dis sec}^{-1}\ \mu c^{-1}) \times 8.6 \times 10^4 \,(\text{sec/day})} , \qquad (3)$$

and obtain from (2) and (3)

$$q_i = \frac{I_i'}{3.7 \times 10^4 \times 8.6 \times 10^4} + q_{i-1} . \qquad (4)$$

Now

$$I_i' = I_i \,(\mu c/\text{day}) \times 3.7 \times 10^4 \,(\text{atoms sec}^{-1}\ \mu c^{-1})$$

$$\times\ 8.6 \times 10^4 \,(\text{sec/day})/\lambda_r^i \,(\text{day}^{-1}) , \qquad (5)$$

where I_i is the μc/day intake into the gut. From (4) and (5)

$$q_i = (I_i/\lambda_i^r) + q_{i-1} , \qquad (6)$$

[15] J. W. Hollcroft and E. Lorenz, *Nucleonics* 5, 63–71 (1951).

[16] J. W. Hollcroft *et al.*, *J. Natl. Cancer Inst.* 15(4), 1059–1067 (1955).

[17] J. K. Scott, *Histopathology of Mice Exposed to Radon*, Atomic Energy Project Report UR-411 (1955).

[18] D. A. Morken, A. M. A. *Arch. Ind. Health* 20, 69–73 (1959).

and since I_i will be the same for all daughters (assuming equilibrium with Rn^{222} at the time of ingestion) and because λ_i^r is relatively large, the first term of (6) is negligible and (6) simplifies to

$$q_i \sim q_{i-1} \,. \tag{7}$$

Now from Eq. (5), p 194, ORNL-3189, we obtain q_0, and inserting q_0 into Eq. (7) gives

$$q_1 = \frac{(\mathrm{MPC})_w}{8.3 \times 10^{-3}}\ \mu c = q_2 = q_3 = q_4 \,. \tag{8}$$

Since $(\mathrm{MPC})_w = 5 \times 10^{-4}\ \mu c/cm^3$,

$$q_i = 0.06\ \mu c\,, \qquad i = 0, 1, 2, 3, 4 \,. \tag{9}$$

Thus we have at equilibrium 0.06 μc of Rn^{222} and each of its short-lived daughters present in the body. Now we must calculate the permissible q_i for each of the short-lived daughters, for which we need values of f_2, m, and ϵ. Since the kidney is the critical organ for each of these daughters, m = 300 g, and the value of f_2 can be obtained from Table 12 of the *ICRP Handbook*. The value of ϵ is computed from a table of isotopes by Strominger, Hollander, and Seaborg.[19]

Table 16.6 presents the calculated values of q. The first column shows the isotope; the second column shows the value of ϵ estimated by the procedures set forth in Sec VI of the *ICRP Handbook*; the third, the f_2 value; and the fourth, the value of q calculated from Eq. (1). As can be seen in the fourth column, the permissible body burden for Po^{218} is 0.06 μc present in the body from decay of Rn^{222}. Also, the 0.05-μc burden permissible for Po^{214} is slightly lower than the 0.06 μc present. Thus, these calculations indicate that the $(\mathrm{MPC})_w$ of $5 \times 10^{-4}\ \mu c/cm^3$ is too high since the body burdens of the short-lived polonium daughters are too high, and, subsequently, the kidneys would receive an exposure of ~0.6 rem/week from the short-lived polonium daughters produced by decay of Rn^{222}.

In the kidney dose estimation, from Table 16.6 it is noted that the $(\mathrm{MPC})_w$ for Rn^{222} would have

Table 16.6. Values of q for the Short-Lived Daughters of Rn^{222} Based on Kidneys as the Critical Organ

Isotope	ϵ (Mev)	f_2[a]	q (μc)
Po^{218}	62	0.067	0.06
Pb^{214}	<0.4[b]	0.13	5[c]
Bi^{214}	<1.6[b]	0.3	0.5[c]
Po^{214}	80	0.067	0.05

[a]Estimated from Eq. (41) in the *ICRP Handbook* and data in Table 12 and assuming $T^x = T^t$.

[b]These energies are slight upper-bound estimates of ϵ because they were based on the body as the organ of reference; since they have large gamma components in their decay scheme, the energy absorption will be less in kidneys because of their smaller dimensions.

[c]These are lower-bound estimates because the value of ϵ employed in their calculation is somewhat too high.

to be lowered by about a factor of 2 to prevent the overirradiation of kidney tissue from uptake of short-lived polonium daughters. However, we find that the $(\mathrm{MPC})_w$ might have a hidden safety factor of about 2.2 contained in it, and, due to this and the extreme conservatism in the assumption, it is not necessary to reduce the $(\mathrm{MPC})_w$. The factor of 2.2 comes from considering a daily intake of 2200 cm^3/day for water – a customary procedure – but in fact the standard man only consumes 1000 cm^3 of fluids per day (Table 9 of the *ICRP Handbook*). The other 1200 cm^3 comes from intake of foods. Arguing that in the processing of foods Rn^{222} would have greater chances to escape by diffusion during heating, decay by sitting on shelves, and loss by other kinds of processing, then it would seem that we should employ 1000 cm^3 rather than 2200 cm^3 as the daily intake. Thus we apparently have a safety factor of at least 2 in the $(\mathrm{MPC})_w$ for Rn^{222} (minus its daughters). Hence, it is not necessary to reduce by a factor of 2 the $(\mathrm{MPC})_w$ based on radiation exposure of kidneys by the polonium daughters. Also, in making the above calculations we were extremely conservative in assuming that a short-lived polonium atom formed anywhere in the body will reach the kidney to undergo disintegration. It seems more probable that the 3-min half-life of Po^{218} would perhaps be long enough to favor its transferring from, say,

[19]D. J. Strominger, J. M. Hollander, and G. T. Seaborg, *Table of Isotopes*, UCRL 1928 (2nd Rev); *Radiological Health Handbook*, pp 195–454, U. S. Dept. Health, Education and Welfare, Public Health Service, September 1960.

fat in a limb to kidney rather than the 1.6×10^{-4} sec Po^{214}, which would probably disintegrate at or near the site of its production.

The question of dose to the lungs from exhalation of ingested Rn^{222} must be considered too. In order to estimate this dose we need to know the fraction f of the daughters in the lung air which exists as free ions. This is evidently not known as no experimental data for this case were found. However, we can make a crude estimate of dose by considering the following argument. Since the daily intake of Rn^{222} by ingestion is 5×10^{-4} ($\mu c/cm^3$) $\times$ 2200 (cm^3/day) = 1.1 μc/day, assuming 2200-cm^3/day intake, and since ~99% of this is eliminated by the body (we assume via exhalation), the μc/day exhaled by a worker ingesting the $(MPC)_w$ is $0.99 \times 1.1 = 1.0$ μc/day.

The standard man exhales 2×10^7 cm^3/day, and thus the concentration of Rn^{222} exhaled is

$$\frac{1.0}{2 \times 10^7} = 5 \times 10^{-8}\ \mu c/cm^3 .$$

A worker who inhales the $(MPC)_a$ for Rn^{222} (equal to 10^{-8} $\mu c/cm^3$) would be expected in the steady state to exhale about the same concentration, that is, 10^{-8} $\mu c/cm^3$. This level is a factor of 5 lower than the level exhaled by the worker who chronically ingests the $(MPC)_w$.

The calculation of lung dose implies that the lungs are overexposed to radiation. However, the $(MPC)_a$ is for the case of inhalation of Rn^{222} *and its daughters* and depends upon the level at which the radium A daughter exists in the form of free ions, since these unattached atoms deliver all but a small fraction of the dose to the bronchi of lungs. For inhalation of Rn^{222} and daughters, the *ICRP Handbook* (p 23) uses the formula

$$(MPC)_a = \frac{3 \times 10^{-6}}{1 + 1000f}\ \mu c/cm^3 \text{ (40-hr week)} ,$$

where f is the fraction of the equilibrium amount of radium A ions which are unattached to nuclei. In the case of Rn^{222} that originates in the deep parts of the lung, we do not have an experimental value for f. Provided that f is not larger than 0.02, the dose rate delivered to lungs from ingested Rn^{222} at the level of 5×10^{-4} $\mu c/cm^3$ will not be in excess of the permissible dose rate. It seems unlikely that f could be as high as 0.02, since there is probably little time for the decay of Rn^{222} atoms to form radium A atoms (i.e., a turnover time for lung air is probably much less than the half-life of the radium A daughter, so that radium A could not equilibrate with Rn^{222}), and because of the presence of a high concentration of water vapor relative to ordinary air in exhaled air, serving as nuclei for attachment of radium A atoms. However, this is mere speculation, and an experimental measurement of f for this case would be required to estimate adequately the dose to lungs from exhalation of ingested Rn^{222}.

In view of the following considerations, that is, there is a possibility that the dose to kidneys might be as high as ~0.6 rem/week from deposition of short-lived daughters and that the lungs could possibly be overexposed due to exhalation of Rn^{222}, it does not seem to be advisable to remove the safety factor of 2 and increase the $(MPC)_w$. When more adequate data are made available, then if it is indicated that neither the kidneys nor the lungs will be overexposed, an increase in the $(MPC)_w$ can be justified.

MAXIMUM PERMISSIBLE CONCENTRATION AND BODY BURDEN VALUES FOR VARIOUS TRANSURANIC RADIONUCLIDES

Mary R. Ford W. S. Snyder

Maximum permissible concentrations in air, $(MPC)_a$, and in water, $(MPC)_w$, and body burden limits, q, have been computed for occupational exposure to 20 radionuclides of importance in the Transuranium Program. The specific radionuclides were U^{240}, Pu^{243}, Pu^{244}, Am^{242m}, Am^{242}, Am^{244}, Cm^{247}, Cm^{248}, Cm^{249}, Bk^{250}, Cf^{251}, Cf^{253}, Cf^{254}, Es^{253}, Es^{254m}, Es^{254}, Es^{255}, Fm^{254}, Fm^{255}, and Fm^{256}. The basic biological and physical assumptions which are the basis of the calculations were adopted after discussion with Committee II of ICRP and Subcommittee 2 of NCRP and conform to their recommendations. Values were tabulated in each case for (1) insoluble material, using both the lungs and the GI tract as organs of reference, and for (2) soluble material, using total body, bone, GI tract, and other organs wherever indicated as organs of reference. The computations were made according

to the formulas and assumptions of the NCRP[20] and ICRP[21] internal-dose reports. In cases where the radionuclide decays to a stable state through a chain of radioactive daughters, the computations become quite involved, and originally these determinations were programmed for the Oracle. However, since the Oracle was being disassembled when the transuranic computations were needed, the problem was reprogrammed for the IBM 7090 computer.

Biological data used in the computations were taken from Table 12 of the *ICRP, Report of Committee II,*[21] where these data were given, that is, for U, Pu, Am, Bk, and Cf. The literature was searched for biological data for the other transuranics, Es and Fm, and none were found, no doubt because of the small quantity of material available for study. However, since the chemical properties of any one of the transcurium elements are known to be very similar to those of the rest,[22] the assumption was made that the biological properties were similar; and, thus, the biological parameters for these elements were taken to be identical to the values given in the *ICRP, Report of Committee II* for Bk and Cf. The biological parameters for each radionuclide and each organ of reference considered were listed in a table entitled "Biological and Related Physical Constants."

Physical data for determining radioactive half-lives, type and mode of decay, and energy quantities and intensities were taken principally from refs 23 and 24. Energies absorbed by the various organs of reference were computed from these data and listed in a table entitled "Effective Energies." In conformity with recommendations of ICRP[21] these energies were weighted by RBE; by n, the relative damage factor for radionuclides deposited in bone; and by F, the ratio of disintegrations of daughter atoms to the disintegrations of the parent. A more detailed table entitled "Effective Energies for Chains" was also included which gave the breakdown of F values (as computed by the IBM 7090) and average energies multiplied by RBE and n for parent-daughter chains.

One problem arose with the new group of radionuclides that was not encountered in the previous group. This was the matter of radionuclides in which the prominent mode of decay is spontaneous fission. A survey of the pertinent literature revealed that the quantity and distribution of spontaneous fission energy for most of the radionuclides involved are not precisely known as yet. However, it has been shown both theoretically and experimentally[25] that the energy release in spontaneous fission is similar to the energy release in the neutron-induced fission of U^{235}. The approximate distribution[26] of neutron-induced fission energy is:

Energy Group	Mev
1. Kinetic energy of fission fragments	168 ± 5
2. Instantaneous gamma-ray energy	5 ± 1
3. Kinetic energy of fission neutrons	5 ± 0.5
4. Beta particles from fission products	7 ± 1
5. Gamma rays from fission products	6 ± 1
6. Neutrinos	~10
Total fission energy	201 ± 6

The energy in groups (1), (2), and (3) is released at the time of fission (considering for this purpose the time of the delayed neutrons as negligible), while that in groups (4) and (5) is set free gradually as the fission products decay. Since neutrinos do not interact appreciably with matter, the energy from that source can be neglected.

The calculations that involved spontaneous fission in the present list made use of data contained in Table 16.7. Since not all the spontaneous fission energy distributions for the different

[20] *Maximum Permissible Body Burdens and Maximum Permissible Concentrations of Radionuclides in Air and in Water for Occupational Exposure,* NBS Handbook 69, Superintendent of Documents, Washington, 1959.

[21] *Report of Committee II on Permissible Dose for Internal Radiation,* ICRP Publication 2, Pergamon, London, 1959.

[22] G. H. Higgins, *The Radiochemistry of the Transuranic Elements,* AEC Nuclear Science Series NAS-NS 3031 (1960).

[23] E. K. Hyde, *The Radioactive Decay of the Isotopes of the Transuranium Elements,* UCRL-9148 (January 1961); UCRL-9036 (January 1960).

[24] Landolt-Bornstein, *New Series, Energy Levels of Nuclei: A = 5 to A = 257,* Springer-Verlag, Berlin, 1961.

[25] A. B. Smith, P. R. Fields, and A. M. Friedman, *Phys. Rev.* 104(3), 699 (1956).

[26] Samuel Glasstone, *Principles of Nuclear Reactor Engineering,* p 22, Van Nostrand, New York, 1955.

Table 16.7. Distribution of Spontaneous Fission Energy

	Radionuclide					
	U^{235} (neutron induced)	Pu	Cm	Cf	Es	Fm
Kinetic energy of fragments, Mev[a]	167		(180)[b]	185	(180)	176
ν, neutrons per fission[a]	2.42		(2.8)	3.86	(3.95)	4.05
Energy per neutron,[a] average-Mev	2.0		(2)	2.15	(2.18)	2.2
Total gamma-ray energy per fission[a]						
Prompt, average-Mev	7.5 (first few μsec)		(9)	9	(9)	(8.5)
Delayed, average-Mev	(+10 to 20% for gammas up to a millisecond)		(+10 to 20%)	(+10 to 20%)	(+10 to 20%)	(+10 to 20%)
Energy, prompt gammas per fission,[a] average-Mev	0.8		(0.8)	0.8–0.9	(~0.9)	(~0.9)
Total average beta energy from fission products per fission,[c] Mev	7.6	(7.5)	(7.4)	(7.0)	(7.0)	(7.0)
Energy per beta,[c] average-Mev	1.2	(1.17)	(1.12)	(1.05)	(1.05)	(1.05)
Total gamma energy from fission products per fission,[c] Mev	6.0	(5.8)	(5.6)	(5.2)	(5.2)	(5.2)
Energy per fission product gamma,[c] average-Mev	1.6 at 10^2 sec 0.5 at 10^5 sec Average ~1.3	(1.26)	(1.19)	(1.15)	(1.15)	(1.15)

[a]From literature survey by H. W. Schmitt, private communication.
[b]Values in parentheses were estimated from measured values of neighboring elements.
[c]From literature survey by G. D. O'Kelley, private communication.

isotopes of an element are known at present but are considered to be quite similar,[27] the values given in the table for an element have been used for all isotopes of that element. Also, in cases where values are not available from the literature for an element, for example, plutonium, values were extrapolated from those used for neighboring elements in Table 16.7. Such values in the table are enclosed in parentheses.

In keeping with the assumptions of the NCRP[20] and ICRP[21] internal-dose reports, n was taken as 1 and 5 for the gamma and beta radiations, respectively, arising from spontaneous fission. Since the kinetic energy of the fragments and the neutron components was considered to be as damaging as alpha rays, n was taken equal to 5 for these energies. An RBE of 20 was used

[27]H. W. Schmitt and G. D. O'Kelley, private communication.

for the kinetic energy of fission fragments. This value was recommended by ICRP Committee II at its meeting in New York, September 1961. Using Fig. 14 of the *United States National Bureau of Standards Handbook 63* as a guide, RBE for spontaneous fission neutrons was taken equal to 8; and, as in the internal-dose reports, 1 was used for the beta and gamma components. In computing effective energies for the GI tract, only 1% of the kinetic energy release of the fission fragments was included since it was assumed that this energy, like the energy from alpha particles, would fail to penetrate the mucosa to an appreciable extent.

Both the NCRP and ICRP committees have reviewed the material on the transuranics in regard to basic philosophy, format, and parameters used; and after certain revisions resulting from an interchange of ideas, the ICRP committee has adopted the values listed here. They also will appear in the forthcoming ICRP Publication 6, *Recommendations of the International Commission on Radiological Protection, as Amended 1959 and Revised 1962.* Subcommittee 2 of NCRP has these values under consideration. Only the values of MPC and q are given in Table 16.8.

Table 16.8. Maximum Permissible Body Burdens and Maximum Permissible Concentrations of Radionuclides in Air and Water for Occupational Exposure

Radionuclide and Type of Decay	Solubility	Organ of Reference[a]	Maximum Permissible Burden in Total Body, q (μc)	Maximum Permissible Concentrations (MPC)			
				40-hr Week		168-hr Week	
				Water (μc/cm^3)	Air (μc/cm^3)	Water (μc/cm^3)	Air (μc/cm^3)
$_{92}U^{240} + Np^{240}$	sol	GI(LLI)		10^{-3}	2×10^{-7}	3×10^{-4}	8×10^{-8}
$\alpha, \beta^-, \gamma, e^-$		Kidney	4	0.4	2×10^{-6}	0.1	5×10^{-7}
		Total body	20	2	10^{-5}	0.8	4×10^{-6}
		Bone	2	3	10^{-5}	1	4×10^{-6}
	insol	GI(LLI)		10^{-3}	2×10^{-7}	3×10^{-4}	6×10^{-8}
		Lung			10^{-6}		5×10^{-7}
$_{94}Pu^{243}$	sol	GI(ULI)		0.01	2×10^{-6}	3×10^{-3}	6×10^{-7}
$\alpha, \beta^-, \gamma, e^-$		Bone	7	10^3	10^{-5}	400	5×10^{-6}
		Kidney	30	5×10^3	7×10^{-5}	2×10^3	2×10^{-5}
		Liver	40	6×10^3	7×10^{-5}	2×10^3	3×10^{-5}
		Total body	50	8×10^3	10^{-4}	3×10^3	4×10^{-5}
	insol	GI(ULI)		2×10^{-6}	2×10^{-6}	3×10^{-3}	8×10^{-7}
		Lung		0.01	2×10^{-5}		6×10^{-6}
$_{94}Pu^{244}$	sol	Bone	0.04	10^{-4}	2×10^{-12}	4×10^{-5}	6×10^{-13}
$\alpha, \beta^-, \gamma, e^-$ (99.7%);		GI(LLI)		3×10^{-4}	7×10^{-8}	10^{-4}	2×10^{-8}
spontaneous		Kidney	0.4	6×10^{-4}	8×10^{-12}	2×10^{-4}	3×10^{-12}
fission (0.3%)		Total body	0.3	9×10^{-4}	10^{-11}	3×10^{-4}	4×10^{-12}
	insol	Lung			3×10^{-11}		10^{-11}
		GI(LLI)		3×10^{-4}	6×10^{-8}	10^{-4}	2×10^{-8}
$_{95}Am^{242m}$	sol	Bone	0.07	10^{-4}	6×10^{-12}	4×10^{-5}	2×10^{-12}
$\alpha, \beta^-, \gamma, \epsilon, e^-$		Kidney	0.1	10^{-4}	6×10^{-12}	5×10^{-5}	2×10^{-12}
		Liver	0.3	2×10^{-4}	9×10^{-11}	7×10^{-5}	3×10^{-12}
		Total body	0.3	3×10^{-4}	2×10^{-11}	10^{-4}	5×10^{-12}
		GI(LLI)		3×10^{-3}	6×10^{-7}	9×10^{-4}	2×10^{-7}
	insol	Lung			3×10^{-10}		9×10^{-11}
		GI(LLI)		3×10^{-3}	5×10^{-7}	9×10^{-4}	2×10^{-7}

Table 16.8 (continued)

Radionuclide and Type of Decay	Solubility	Organ of Reference[a]	Maximum Permissible Burden in Total Body, q (μc)	Maximum Permissible Concentrations (MPC) 40-hr Week Water ($\mu c/cm^3$)	40-hr Week Air ($\mu c/cm^3$)	168-hr Week Water ($\mu c/cm^3$)	168-hr Week Air ($\mu c/cm^3$)
$_{95}Am^{242}$ $\alpha, \beta^-, \gamma, \epsilon, e^-$	sol	GI(LLI)		4×10^{-3}	8×10^{-7}	10^{-3}	3×10^{-7}
		Liver	0.06	0.9	4×10^{-8}	0.3	10^{-8}
		Kidney	0.1	2	8×10^{-8}	0.6	3×10^{-8}
		Bone	0.1	2	8×10^{-8}	0.6	3×10^{-8}
		Total body	0.3	4	2×10^{-7}	1	6×10^{-8}
	insol	Lung			5×10^{-8}		2×10^{-8}
		GI(LLI)		4×10^{-3}	7×10^{-7}	10^{-3}	2×10^{-7}
$_{95}Am^{244}$ $\alpha, \beta^-, \gamma, e^-$	sol	GI(SI)		0.1	3×10^{-5}	0.05	10^{-5}
		Bone	0.2	90	4×10^{-6}	30	10^{-6}
		Kidney	0.2	100	4×10^{-6}	30	10^{-6}
		Liver	0.2	100	5×10^{-6}	40	2×10^{-6}
		Total body	0.4	200	10^{-5}	80	3×10^{-6}
	insol	Lung			2×10^{-5}		8×10^{-6}
		GI(SI)		0.1	2×10^{-5}	0.05	8×10^{-6}
$_{96}Cm^{247}$ $\alpha, \beta^-, \gamma, e^-$	sol	Bone	0.04	10^{-4}	5×10^{-12}	4×10^{-5}	2×10^{-12}
		Liver	0.5	2×10^{-4}	9×10^{-12}	7×10^{-5}	3×10^{-12}
		Kidney	0.2	2×10^{-4}	9×10^{-12}	7×10^{-5}	3×10^{-12}
		Total body	0.4	3×10^{-4}	10^{-11}	10^{-4}	5×10^{-12}
		GI(LLI)		6×10^{-4}	10^{-7}	2×10^{-4}	5×10^{-8}
	insol	Lung			10^{-10}		4×10^{-11}
		GI(LLI)		6×10^{-4}	10^{-7}	2×10^{-4}	4×10^{-8}
$_{96}Cm^{248}$ α(89%); spontaneous fission (11%)	sol	Bone	5×10^{-3}	10^{-5}	6×10^{-13}	4×10^{-6}	2×10^{-13}
		Liver	0.06	2×10^{-5}	10^{-12}	8×10^{-6}	4×10^{-13}
		Kidney	0.03	3×10^{-5}	10^{-12}	9×10^{-6}	4×10^{-13}
		Total body	0.04	4×10^{-5}	2×10^{-12}	10^{-5}	6×10^{-13}
		GI(LLI)		4×10^{-5}	8×10^{-9}	10^{-5}	3×10^{-9}
	insol	Lung			10^{-11}		4×10^{-12}
		GI(LLI)		4×10^{-5}	7×10^{-9}	10^{-5}	2×10^{-9}
$_{96}Cm^{249}$ $\alpha, \beta^-, \gamma, e^-$	sol	GI(S)		0.06	10^{-5}	0.02	5×10^{-6}
		Bone	1	300	10^{-5}	100	4×10^{-6}
		Total body	4	800	3×10^{-5}	300	10^{-5}
	insol	GI(S)		0.06	10^{-5}	0.02	4×10^{-6}
		Lung			5×10^{-5}		2×10^{-5}
$_{97}Bk^{250}$ $\alpha, \beta^-, \gamma, e^-$	sol	GI(ULI)		6×10^{-3}	10^{-6}	2×10^{-3}	5×10^{-7}
		Bone	0.05	10	10^{-7}	4	5×10^{-8}
		Total body	0.3	80	10^{-6}	30	4×10^{-7}
	insol	GI(ULI)		6×10^{-3}	10^{-6}	2×10^{-3}	4×10^{-7}
		Lung			2×10^{-6}		8×10^{-7}

Table 16.8 (continued)

Radionuclide and Type of Decay	Solubility	Organ of Reference[a]	Maximum Permissible Burden in Total Body, q (μc)	Maximum Permissible Concentrations (MPC) 40-hr Week Water ($\mu c/cm^3$)	40-hr Week Air ($\mu c/cm^3$)	168-hr Week Water ($\mu c/cm^3$)	168-hr Week Air ($\mu c/cm^3$)
$_{98}Cf^{251}$ α, γ	sol	Bone	0.04	10^{-4}	2×10^{-12}	4×10^{-5}	6×10^{-13}
		GI(LLI)		8×10^{-4}	2×10^{-7}	3×10^{-4}	6×10^{-8}
		Total body	0.3	9×10^{-4}	10^{-11}	3×10^{-4}	4×10^{-12}
	insol	Lung			10^{-10}		3×10^{-11}
		GI(LLI)		8×10^{-4}	10^{-7}	3×10^{-4}	5×10^{-8}
$_{98}Cf^{253}$ $\alpha, \beta^-, \gamma, e^-$	sol	GI(LLI)		4×10^{-3}	9×10^{-7}	10^{-3}	3×10^{-7}
		Bone	0.04	0.06	8×10^{-10}	0.02	3×10^{-10}
		Total body	0.3	0.5	6×10^{-9}	0.2	2×10^{-9}
	insol	Lung			8×10^{-10}		3×10^{-10}
		GI(LLI)		4×10^{-3}	7×10^{-7}	10^{-3}	3×10^{-7}
$_{98}Cf^{254}$ Spontaneous fission	sol	GI(LLI)		4×10^{-6}	8×10^{-10}	10^{-6}	3×10^{-10}
		Bone	7×10^{-4}	4×10^{-4}	5×10^{-12}	10^{-4}	2×10^{-12}
		Total body	5×10^{-3}	3×10^{-3}	4×10^{-11}	10^{-3}	10^{-11}
	insol	Lung			5×10^{-12}		2×10^{-12}
		GI(LLI)		4×10^{-6}	6×10^{-10}	10^{-6}	2×10^{-10}
$_{99}Es^{253}$ $\alpha, \beta^-, \gamma, e^-$	sol	GI(LLI)		7×10^{-4}	10^{-7}	2×10^{-4}	5×10^{-8}
		Bone	0.04	0.06	8×10^{-10}	0.02	3×10^{-10}
		Total body	0.3	0.4	5×10^{-9}	0.1	2×10^{-9}
	insol	Lung			6×10^{-10}		2×10^{-10}
		GI(LLI)		7×10^{-4}	10^{-7}	2×10^{-4}	4×10^{-8}
$_{99}Es^{254m}$ $\alpha, \beta^-, \gamma, e^-$	sol	GI(LLI)		5×10^{-4}	10^{-7}	2×10^{-4}	4×10^{-8}
		Bone	0.02	0.4	5×10^{-9}	0.1	2×10^{-9}
		Total body	0.1	3	4×10^{-8}	1	10^{-8}
	insol	Lung			6×10^{-9}		2×10^{-9}
		GI(LLI)		5×10^{-4}	10^{-7}	2×10^{-4}	3×10^{-8}
$_{99}Es^{254}$ $\alpha, \beta^-, \gamma, e^-$	sol	GI(LLI)		4×10^{-4}	9×10^{-8}	10^{-4}	3×10^{-8}
		Bone	0.02	10^{-3}	2×10^{-11}	5×10^{-4}	6×10^{-12}
		Total body	0.2	10^{-2}	10^{-10}	3×10^{-3}	5×10^{-11}
	insol	Lung			10^{-10}		4×10^{-11}
		GI(LLI)		4×10^{-4}	7×10^{-8}	10^{-4}	3×10^{-8}
$_{99}Es^{255}$ α, β^-, γ	sol	GI(LLI)		8×10^{-4}	2×10^{-7}	3×10^{-4}	6×10^{-8}
		Bone	0.04	0.04	5×10^{-10}	0.01	2×10^{-10}
		Total body	0.3	0.3	4×10^{-9}	0.09	10^{-9}
	insol	Lung			4×10^{-10}		10^{-10}
		GI(LLI)		8×10^{-4}	10^{-7}	3×10^{-4}	5×10^{-8}

Table 16.8 (continued)

Radionuclide and Type of Decay	Solubility	Organ of Reference[a]	Maximum Permissible Burden in Total Body, q (μc)	Maximum Permissible Concentrations (MPC) 40-hr Week Water ($\mu c/cm^3$)	40-hr Week Air ($\mu c/cm^3$)	168-hr Week Water ($\mu c/cm^3$)	168-hr Week Air ($\mu c/cm^3$)
$_{100}Fm^{254}$	sol	**GI(ULI)**		4×10^{-3}	8×10^{-7}	10^{-3}	3×10^{-7}
α, γ, e^- (99.9448%);		Bone	0.02	5	6×10^{-8}	2	2×10^{-8}
spontaneous		Total body	0.1	30	4×10^{-7}	10	2×10^{-7}
fission	insol	Lung			7×10^{-8}		2×10^{-8}
(5.52×10^{-2}%)		**GI(ULI)**		4×10^{-3}	6×10^{-7}	10^{-3}	2×10^{-7}
$_{100}Fm^{255}$	sol	**GI(LLI)**		10^{-3}	2×10^{-7}	3×10^{-4}	7×10^{-8}
α, γ		Bone	0.04	1	2×10^{-8}	0.4	6×10^{-9}
		Total body	0.3	9	10^{-7}	3	4×10^{-8}
	insol	Lung			10^{-8}		4×10^{-9}
		GI(LLI)		10^{-3}	2×10^{-7}	3×10^{-4}	6×10^{-8}
$_{100}Fm^{256}$	sol	**GI(ULI)**		3×10^{-5}	6×10^{-9}	9×10^{-6}	2×10^{-9}
Spontaneous		Bone	8×10^{-4}	0.2	3×10^{-9}	0.07	10^{-9}
fission		Total body	5×10^{-3}	1	2×10^{-8}	0.5	7×10^{-9}
	insol	Lung			2×10^{-9}		6×10^{-10}
		GI(ULI)		3×10^{-5}	5×10^{-9}	9×10^{-6}	2×10^{-9}

[a]The abbreviations GI, S, SI, ULI, and LLI refer to gastrointestinal tract, stomach, small intestine, upper large intestine, and lower large intestine respectively; critical organ is in bold-face type.

RELATED ACTIVITIES

Members of the Internal Dose Estimation Section have participated in the iodine studies reported by the Health Physics Technology Section, in the Clinch River Survey Program Evaluation Study reported by the Radioactive Waste Disposal Section, and in the program of High-Energy-Proton Dosimetry carried out under NASA and reported in the Radiation Physics and Dosimetry Section.

During the year several members of the Section have participated in two meetings of the National Committee on Radiation Protection Subcommittee 2. The Section also has assisted in the preparation of material for the forthcoming Publication 6 of the International Commission on Radiological Protection.

Members of the Section have participated in conferences held at Argonne Cancer Research Hospital and at Hanford Atomic Operations on the Biology of Radioiodine and at similar conferences on program reviews at Wayne State University and at The Lovelace Foundation.

One member of the Section serves as Editor-in-Chief of the journal *Health Physics* and another serves as Editor.

In cooperation with the Education and Training Section, one member presented six lectures and another presented four lectures in the AEC Fellowship Course of Applied Radiation Physics, Vanderbilt University, Nashville, Tennessee.

Two members each presented one lecture at the University of Tennessee for Physics 599E, Seminars in Health Physics.

17. Stable-Element Metabolism by Man

INFLUENCE OF AGE, RACE, AND GEOGRAPHICAL LOCATION ON THE TRACE ELEMENT CONCENTRATION IN HUMAN TISSUE

Isabel H. Tipton Mary Jane Cook
Jane Shafer

Data from spectrographic analysis of trace elements in the tissues of children from the United States, India, and Africa, of caucasoid and negroid adults from the United States and Africa, and of caucasoid adults from India have been treated statistically by nonparametric methods which have been described elsewhere.[1] In tests of variation, adult males of the same age group (20–59 yr) but from different geographical locations or of different races were compared. All children (0–19 yr), male and female, from one location were compared with all adults, male and female, from the same location. Females from one location were compared with males of the same age (20–59 yr) from the same location. Table 17.1 shows the number of individuals in each group and the number of samples of aorta, kidney, liver, and lung for which data were available.

On the whole the concentrations of trace elements in children were not different from those in adults, but certain elements in certain tissues showed significant variations.

Calcium in aorta was significantly lower (probability $p \leqq 0.01$) in the American children than in the American adults, but the two samples of aorta available from Indian children were not different from those from Indian adults with respect to this element. (No samples of aorta from African children were analyzed.) The median value for the calcium in aorta for American children was lower than that for the African and Indian adults. This value for the American adults, however, was significantly higher ($p \leqq 0.01$) than for the African and Indian adults.

Concentrations of cadmium in kidney were significantly lower ($p \leqq 0.01$) in the children of each group. The median concentration of this

[1] I. H. Tipton *et al.*, *Health Phys.* 9(2), 89 (1963).

Table 17.1. Number of Individuals and Organs from Each Group

		Adults (20–59 yr)					Children (0–19 yr)				
		Total	Aorta	Kidney	Liver	Lung	Total	Aorta	Kidney	Liver	Lung
United States	All subjects[a]	118	80	115	118	113	23	8	21	22	22
	All females	30	21	27	29	27					
	Male, caucasoid	52	40	52	52	51					
	Male, negroid	21	12	21	21	21					
Africa	All subjects	49	15	44	41	40	5	0	5	4	5
	All females	15	2	12	11	12					
	Male, caucasoid	4	4	4	4	4					
	Male, negroid	30	9	28	26	24					
India	All subjects	29	10	23	26	26	9	2	9	9	9
	Female, caucasoid	5	1	4	4	4					
	Male, caucasoid	24	9	19	22	22					

[a] Fifteen subjects, race unknown.

element in the kidneys of American children, however, was slightly higher than that for the African adults. Cadmium in liver was lower in children also, but this difference was not so highly significant as that for kidney.

Lead showed interesting variations (see Figs. 17.1–17.3). In the group of children from the United States, lead was consistently significantly lower than it was in adults, while in the groups of children from India and from Africa, this element showed no significant difference in any tissues. In the American group, tissues of males showed higher lead than the same tissues of females, and negroid males showed higher lead in lung and liver than caucasoid males. American males in general showed higher lead than African or Indian males. These differences in the levels of lead reflect the difference in exposure to lead in the atmosphere. Butt and his colleagues have observed that the concentration of lead in serum is higher the longer the period of daily travel in an automobile.[2]

There appeared to be no significant differences due to race *per se*. Except for the higher lead in lung and kidney (which is probably a reflection of occupational exposure), the American negroid group was not significantly different ($p \leqq 0.01$) from the American caucasoid group in any respect. The African negroids differed from African caucasoids at this level of significance only in higher calcium in kidney and molybdenum in liver. On the other hand, the American negroids were significantly different ($p \leqq 0.01$) from African negroids for many elements, and the American caucasoids were significantly different ($p \leqq 0.01$) from the African caucasoids for approximately the same elements. The Africans were higher in aluminum in aorta, kidney, and liver and much lower in cadmium and lead in kidney, liver, and lung. The Indian caucasoids did not differ from the African negroids in as many respects nor as significantly as they did from the American caucasoids. The

[2]Private communication.

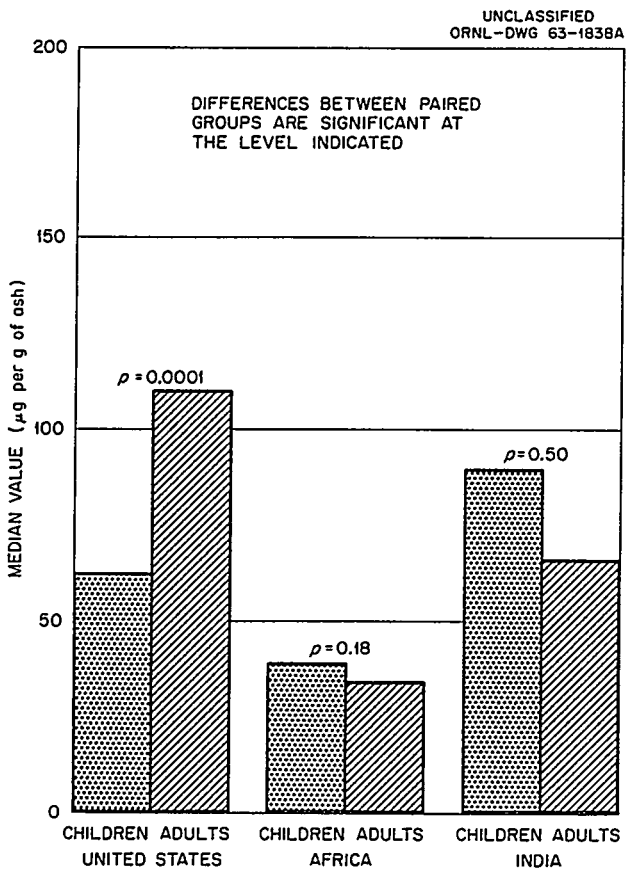

Fig. 17.1. Lead in Kidney, Age Differences.

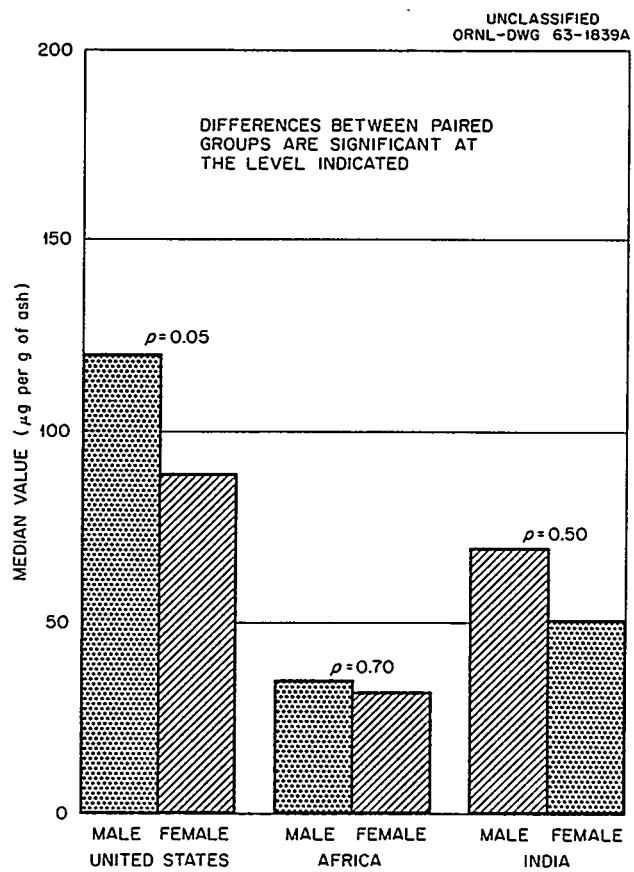

Fig. 17.2. Lead in Kidney, Sex Differences.

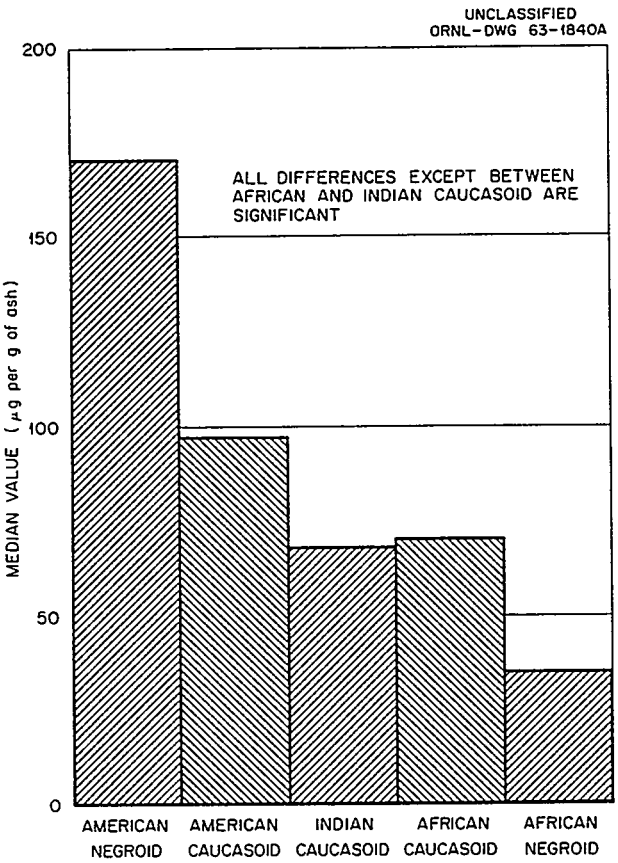

Fig. 17.3. Lead in Kidney, Geographic and Race Differences.

differences between the American subjects and the African and Indian subjects are not surprising in view of the differences in diet and nutritional status and the differences in exposure to contaminants.

Except for higher lead ($p \leqq 0.05$) in kidney, liver, and lung of males, there were no sex differences in the American group. The African females had significantly higher ($p \leqq 0.01$) cadmium in kidney than African males. The Indian males and females showed no significant differences.

TISSUE ANALYSIS LABORATORY PROGRESS REPORT

S. R. Koirtyohann C. Feldman

During the past year about 415 bone samples were analyzed for 20 elements by three different procedures. The trace elements were determined by the method previously described.[3] Sodium and calcium were determined in solutions of these samples using a flame as the light source on the Quantometer. Potassium was determined in these same solutions by use of a conventional flame spectrophotometer. Phosphorus values were obtained from the San Francisco bone samples by a colorimetric method.

The data obtained from the San Francisco bone samples are given in Table 17.2. These data show much less variability than the soft tissues in the values for Mg, Sr, Zn, Ca, P, and Na in the ash. This is especially true in the case of Ca and P, where the extreme values are less than 10% different from the average.

A few bone samples were analyzed repeatedly over a period of several months to test the long-term reproducibility of the method used for the trace element determinations. Standard deviations were calculated in the cases where the data were sufficiently complete. They are summarized below:

Standard Deviation (%)	No. of Values
<5	2
5–10	7
10–20	8
>20	1

The precision of the flame methods used for the Na, Ca, and K determinations is much better than this (≈ 2%).

The accuracy of the Quantometer values was checked for several elements by using independent methods. The results for iron and strontium are given in Table 17.3, and other comparisons are discussed below.

In addition to the analysis of bone samples, about 400 samples of soft tissues from Atlanta and New York and 36 samples of whole blood from the New Jersey Department of Health[4] were analyzed for 23 trace elements. These blood samples were from people who had been employed in the radium-dial-painting factories. A cursory comparison indicated that these values were within the range usually regarded as normal.

[3]W. S. Snyder *et al.*, *Health Phys. Ann. Progr. Rept. July 31, 1962*, ORNL-3347, p 109.

[4]These samples were supplied through the courtesy of L. A. Barrer, Director, Radium Research Project.

Table 17.2. Analyses of San Francisco Bone Samples

Concentrations are expressed as μg per gram of ash except for Na, Ca, K, and P, which are as percent in the ash. Numbers in parentheses are estimates from photographic exposures.

ORNL Sample No.	% Dry	% Ash	Co	Fe	Cu	Ni	Cr	Pb	Al	Mn	Mo	Sn	Mg	Sr	Ba	Zn	Cd	Au	%Na	%Ca	%K	%P
300 B	76	31		320	(10)			33	28	(2)			5000	99		190			1.10	36.8	0.50	18.4
302 B	58	14		1200	10	(2)		96	46	(3)		(5)	5800	120		240			1.62	34.0	0.96	16.2
303 B	67	24		350	(5)	(2)		140	(15)	(2)			5100	160		220			1.66	36.0	0.79	16.2
304 B	72	26		500	(5)			34	(20)	(2)			4200	91		180			1.14	35.4	0.54	16.4
305 B	66	29		150	(20)			46	(20)	(2)		(5)	4800	120		160			1.23	35.3	0.56	16.4
306 B	63	25		540	(5)			70	22	(2)			5600	120		180			1.46	37.4	0.66	16.4
307 B	65	34		100				(10)	(20)	(2)			5300	120		140			1.06	35.5	0.39	17.5
308 B	58	23		660	(2)			77	32	(2)			5600	120		200			1.18	36.8	0.75	17.2
309 B	74	32		540	13			30	(20)	(2)			4900	120		200			1.18	36.2	0.39	17.2
310 B	80	35		400	(2)			64	27	(2)		(20)	5000	220		200			1.18	36.2	0.36	17.2
312 B	76	46		180				(10)	(15)	(2)			4000	160		130			1.09	37.9	0.23	17.5
313 B	54	15		860	(5)	(2)		71	23	(5)			5200	180		230			1.70	34.5	0.86	17.0
314 B	81	33		160	(2)			30	24	(3)		(10)	4400	140		190			1.06	36.4	0.34	17.2
315 B	61.7	25.1		660	(2)			76	(5)	(2)			4800			270			1.53	32.9	0.56	15.5
316 B	66	32		320	(2)			46	(15)	(2)		(5)	5000	160		160			1.04	36.2	0.44	17.0
317 B	63	26		520	(5)			46	(10)	(2)		(5)	4400	130		160			1.50	34.4	0.56	16.2
319 B	64	23		480	(2)			32	(10)	(2)		(5)	5000	120		200			1.14	35.9	0.54	17.8
320 B	66	28		950	(2)	(5)		30	(30)	(2)			5200	110		160			1.12	35.8	0.58	17.0
321 B	69	28		910	(2)			67	(15)	(2)			4900	130		180			1.25	37.3	0.40	17.2
322 B	69	27		540	(2)			28	(15)	(2)			4600	89		150			1.22	36.6	0.30	17.5
323 B	73	24		600				70	(10)	(2)			4500	220		140			1.22	36.2	0.66	17.2
324 B	64	25		280	(2)			62	(10)	(2)		(20)	4400	160		170			1.29	37.2	0.44	17.2
325 B	64	27		410	(2)			40	(10)	(2)		(10)	3900	120		180			1.29	34.7	0.40	16.2
326 B	67	24		480	(2)			63	(10)	(3)			4400	110		180			1.28	37.0	0.48	17.0
327 B	76	28		410				39	(5)	(2)		(10)	4900	170		200			1.25	34.9	0.39	17.0
Av	58	27		494	4.3			51	19	2.3			4800	130		180			1.27	35.9	0.52	17.0
Detection limits			(2)	(20)	(2)	(2)	(2)	(5)	(5)	(2)	(2)	(5)		(1)	(20)	(50)	(5)	(2)				

Table 17.3. Colorimetric and Flame-Spectrophotometric Values for Iron and Strontium in Bone

Sample No.	Fe		Sr	
	Quantometer	Colorimetric	Quantometer	Flame
302 B	1200	970	120	120
303 B	350	315	160	140
304 B	500	470	91	92
305 B	150	175	120	125
306 B	540	540	120	115

Radium was not determined. An average of 2.2 ppm of Sr in whole blood ash was reported. This is believed to be one of the first values published for Sr in blood and should be checked against blood from persons who have not been employed in the radium dial factories. Gofman[5] reported a 0.00-ppm value in serum.

Atomic absorption spectroscopy is a very valuable tool for checking the accuracy of the Quantometer values for several elements. In this method light of proper wavelength is passed through a flame into which the sample solution is aspirated. Atoms of the test element, which are liberated in the flame, absorb the light and reduce the intensity by an amount proportional to their concentration. This method is capable of very good sensitivity. Concentrations as low as single parts per billion (10^{-9} g/ml) of some elements can be detected in the sample solution. Detection limits based on concentrations in the ash are generally not as good as in the arc because a rather dilute solution of the ash (0.1–1.0%) must be used. Interferences and interelement effects are generally much less serious than with other spectrochemical methods. Precision of 1–2% of the amount present can be obtained under favorable conditions. The method yields results on only one element at a time and is not applicable to elements that form refractory oxides in the flame (Al, Ti, Si).

[5]J. W. Gofman, p 1 in *Advances in Biological and Medical Physics*, vol VIII (ed. by C. A. Tobias and J. H. Lawrence), Academic Press, New York, 1962.

The atomic absorption method has been used to check the Quantometer values for Zn, Pb, Cd, and Mn in soft tissues and for Zn and Mg in bone. The results from the soft tissues are given in Table 17.4. This table can be summarized as follows:

Difference Between Results (%)	No. of Values
<10	13
10–20	10
20–40	7

The data on bone in Tables 17.3 and 17.5 can be summarized as follows:

Difference Between Results (%)	No. of Values
<10	7
10–20	15
20–40	1

These figures represent the combined errors of the two methods and include any sampling error that might be present. They indicate satisfactory accuracy of the Quantometer values.

Plans have been developed to provide the Quantometer with an automatic readout based on punched paper tape. This tape, containing calibration and sample data, will be processed by computer to yield elemental concentrations in the sample. The necessary components for building the tape punch attachment have been ordered, and the computer program for processing the tape is being written.

Table 17.4. Emission Spectrographic (Quantometer) and Atomic Absorption Values from Soft-Tissue Ash (μg per Gram of Ash)

Sample No.	Zn		Cd		Pb		Ni		Mn	
	Quantometer	At. Absorp.	Quantometer	At. Absorp.	Quantometer	At. Absorp.	Quantometer	At. Absorp.	Quantometer	At. Absorp.
YN-1 (kidney)	1700	1610	500	465			500	400	60	63
YN-2 (kidney)							350	320		
YN-3 (kidney)							220	240		
YN-4 (kidney)							160	150		
YN-7 (kidney)	7400	6240	1800	1380					68	73
276 K	3300	3770	1300	1290					82	112
307 K	3000	3440	1200	1280					110	142
312 K	2000	2990	600	790					90	124
323 K	4400	4920	4800	4850	80	100			88	110
307 L	5900	5550	140	132	150	120			240	207
324 L	5100	4520	220	212	180	150				

Methods have been considered for pulverizing large samples of wet tissue so that small representative samples can be obtained. Impact pulverization of the tissue at dry ice temperature appears to offer the best possibility. Other methods for grinding wet tissue involve metal-to-metal wear in the mill, which results in severe sample contamination. Test samples of beef muscle, fat, and bone were sent to the Pulverizing Machinery Company for trial processing in an impact mill. The samples were pulverized satisfactorily but showed contamination from the stainless steel mill that was used. A mill of this same type but made from hardened carbon steel has been ordered. This should reduce the sample contamination problem, but if it is still serious a special liner made from tungsten or some similar material will be made for the mill.

The analysis of bone for both trace and major constituents and of soft tissues for trace elements is being carried out on a routine basis. Flame spectrophotometry, colorimetry, and atomic absorption spectroscopy were used to test the accuracy of the Quantometer values. In each case the agreement was generally good.

Table 17.5. Emission Spectrographic and Atomic Absorption Values from Bone Ash (μg per Gram of Ash)

Sample No.	Zn		Sample No.	Mg	
	Quantometer	At. Absorp.		Quantometer	At. Absorp.
300 B	190	190	253 B	4700	4620
303 B	220	270	254 B	4600	4450
304 B	180	260	263 B-1	4100	4430
305 B	160	165	263 B-2	4300	4360
306 B	180	200	346 B	5300	5740
			352 B	3600	4260
			372 B	4200	4430
			376 B	4900	4620

Part V. Health Physics Technology

B. R. Fish

18. Aerosol Physics

B. R. Fish G. W. Royster, Jr.
J. L. Thompson

F. G. Karioris[1] P. Kotrappa[4]
Liliana Masironi[2] A. J. Moll[5]
R. S. Sager[3] J. E. Swander[6]
R. L. Walker[7]

Dispersion of particles and vapors in semi-isolated environments is being studied, particularly regarding deposition and retention on environmental surfaces. At present, the major emphasis of the program is as follows: (1) developing standardized methods for measuring contamination on surfaces, (2) delimiting the normal range of environmental conditions affecting deposition and redispersion, and (3) applying new measuring techniques and the results of redispersion tests to the establishment of contamination control criteria.

STUDIES OF SURFACE CONTAMINATION

G. W. Royster, Jr.

Studies directed toward establishing realistic control practices for radioactive surface contamination are being continued. Major emphasis is on the development of reproducible sampling techniques for measuring particulate contamination on surfaces and application of redispersion test results to the establishment of contamination control criteria.

Comparisons of methods have been reported[8–10] for measuring surface contamination as they relate to measurement techniques and surface characteristics. Test results from the earlier studies show that the smear and adhesive paper sampling methods are affected rather strongly by surface characteristics as well as by the total concentration of the contaminant on the surface. The "smair" measuring technique, which employs air impingement to redisperse loose contamination from a surface, is essentially independent of surface roughness as well as degree of surface dustiness. The efficiency of the smair technique is, however, dependent upon the particle size of the contaminant. Stainless steel surfaces were contaminated with ThO_2 dust of 0.5-μ particle size, and the redispersion efficiency was observed as a function of air velocity (Fig. 18.1). As expected, the removal efficiency increased with

[1]Temporary summer employee, Marquette University, Milwaukee, Wis.

[2]NATO Postdoctoral Fellow, citizen of Italy.

[3]ORINS undergraduate trainee, Texas Lutheran College, Seguin.

[4]Atomic Energy Establishment, Trombay, Bombay, India.

[5]Temporary summer employee, University of Washington, Seattle.

[6]Temporary summer employee, University of California, Berkeley.

[7]USAEC Graduate Fellow in Health Physics.

[8]G. W. Royster, Jr., and B. R. Fish, *Studies of Surface Contamination. I. Intercomparison of Methods for Measuring "Removable" Contamination*, paper presented at the Annual Health Physics Society Meeting, June 12–16, 1961, Las Vegas, Nev.; ORNL CF-61-3-39 (1960).

[9]G. W. Royster, Jr., and B. R. Fish, *Studies of Surface Contamination. II. Surface Characteristics Affecting the Measurement and Redispersion of Particulates*, paper presented at the Annual Health Physics Society Meeting, June 11–16, 1962, Chicago, Ill.

[10]G. W. Royster, Jr., and B. R. Fish, *Studies of Surface Contamination. III. Effect of Particle Size on the Measurement and Redispersion of Particulates*, paper presented at the Annual Health Physics Society Meeting, June 10–14, 1963, New York.

velocity of the impinging air. These stainless steel surfaces were seen to follow the same pattern of increased redispersion with higher air velocity when contaminated with 5.0-μ particles of ThO_2 dusts with the exception that a greater percentage of the 5.0-μ dust was removed at each measured air velocity. When the contaminant is a mixture of two particle sizes the removal curve more nearly approximates the curve for the larger particles.

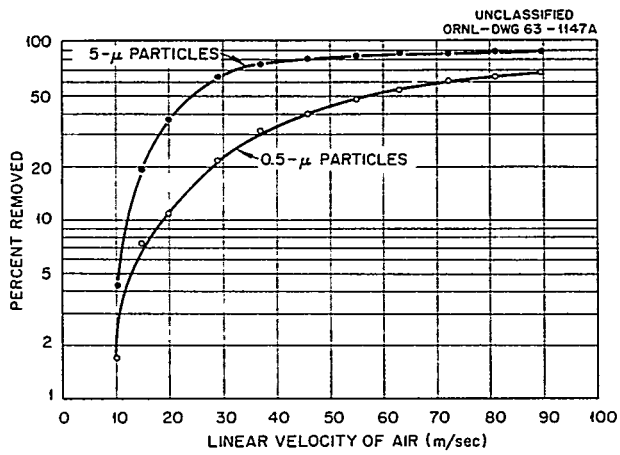

Fig. 18.1. Smair Removal of ThO_2 from Stainless Steel.

The individual variation of smearing techniques among monitoring personnel may contribute greatly to differences in cleanup requirements in contaminated areas. An effort was made to assess the magnitude of this variation by identically contaminating 21 stainless steel surfaces and allowing 21 different surveyors to take 8 smears (estimated 100 cm^2 of surface per smear), 8 adhesive paper samples, and 8 smair samples. All surfaces were contaminated with 3.65-μ ThO_2 dust particles dispersed uniformly over the surface (standard deviation <5% of the mean). Figure 18.2 shows that there was very little variation between the individuals using the smair method (72.5 m/sec). The overall average was 54.5% (σ = 5.7) removed by the smair technique; the individual standard deviations (σ) ranged from 3 to 9.2%. The adhesive paper technique resulted in

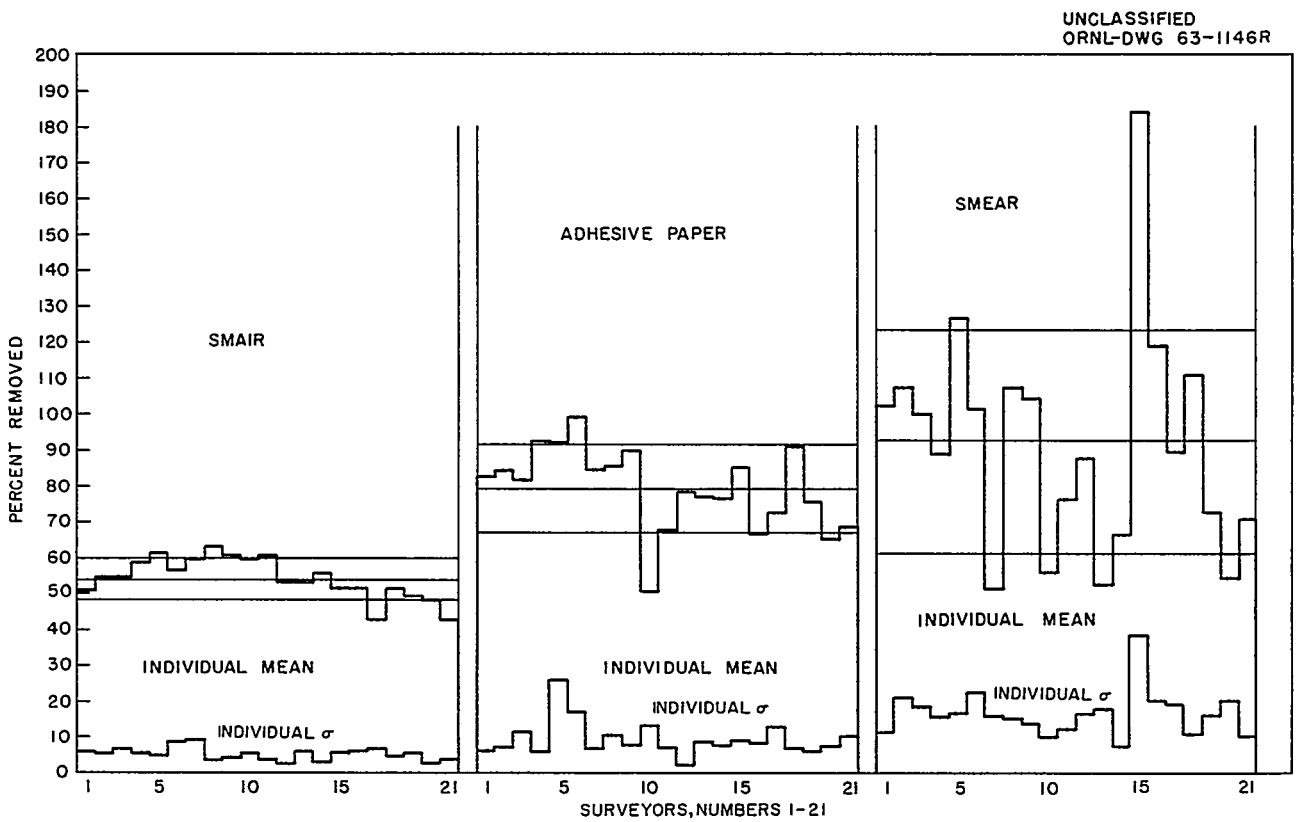

Fig. 18.2. Personal Variance in Area Survey Techniques.

greater removal with an overall average of 79.9% (σ = 11.5), and the individual σ's ranged from 2.7 to 24. Smear results showed the largest overall average removal of 92.9% (σ = 31.2). These data deviate from the data reported by Barry and Solon,[11] which show the adhesive method to be more variable than the smear method. The individual σ's ranged from 8.4 to 39.5%. Since the 100-cm^2 area was approximated for the smear method and not fixed as in the other two techniques, errors in estimating 100 cm^2, no doubt, contributed greatly to the large variation in results. However, it is believed that under these conditions of a smooth surface and a visible dust film, the errors in estimating a given area should be at a minimum. For variations in surfaces that would normally be encountered in actual smearing practice, the errors would be expected to be much greater than under the conditions of this study.

[11]E. V. Barry and L. R. Solon, *Radioactive Contamination Sampling by Smears and Adhesive Discs*, NYO-4525 (May 1953).

STUDY OF THE ADSORPTION OF IODINE VAPOR ONTO AEROSOLS

R. L. Walker

A study is being made of the adsorption of iodine vapor onto various aerosols, which include particles of silver and of platinum in the size range 0.01 to 0.1 μ. Figure 18.3 shows schematically the general arrangement of apparatus used in this work. At present aerosols are produced in the exploding wire aerosol generator which has been described in previous reports.[12,13] A wire of the selected material is exploded, and the resulting aerosol is pulled into a flexible walled chamber which is used to dilute and store the aerosol. Particle concentration in the storage chamber immediately after filling is approximately 10^6/cm^3 as determined with a condensation nuclei

[12]F. G. Karioris and B. R. Fish, *J. Colloid Sci.* 17, 155–61 (1962).

[13]F. G. Karioris, B. R. Fish, and M. B. Edwards, *Health Physics Div. Ann. Progr. Rept. July 31, 1960*, ORNL-2994, pp 266–69.

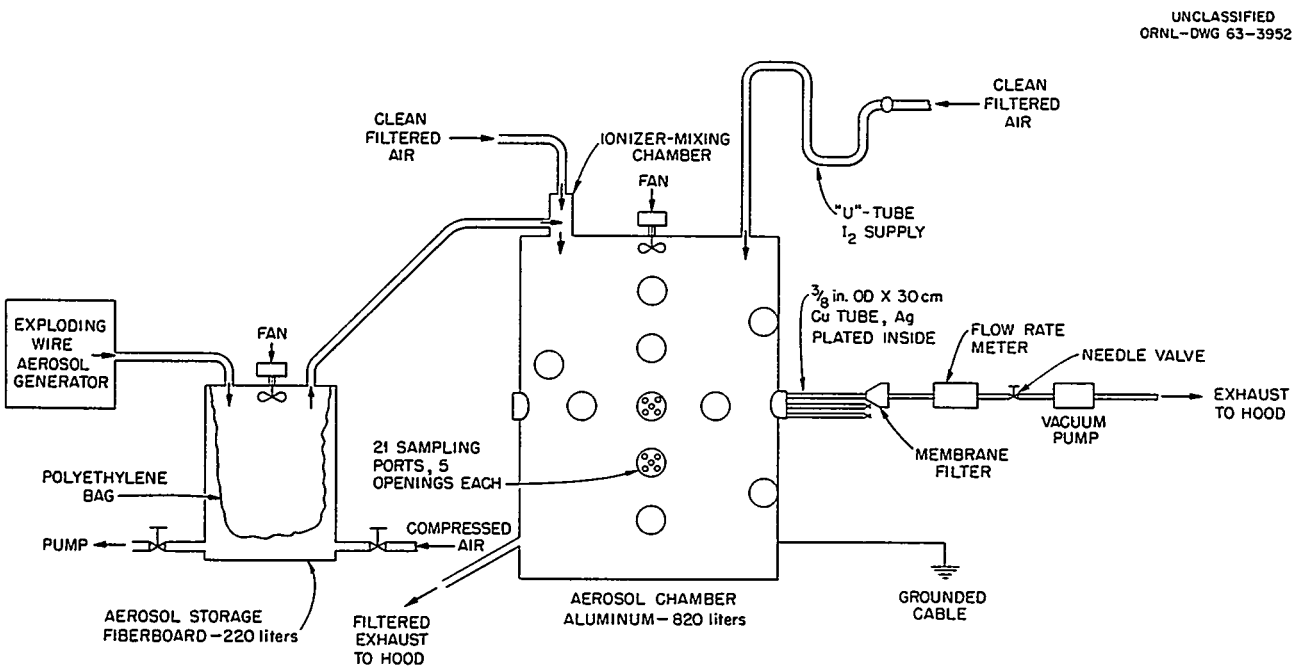

Fig. 18.3. Diagram of I_2 Adsorption Apparatus.

counter.[14] Aerosol can be transferred directly to the aluminum test cylinder or run through an ionizer of a type described by Whitby.[15] Concentration in this chamber is usually about 10^5 particles per cm^3 at the beginning of the run. At present iodine vapor is generated by passing clean filtered air through a U-tube containing 1 mc I^{130} plus 10 mg I^{127}; earlier runs were made using 0.1 mc I^{131} plus 10 mg I^{127}. Samples are withdrawn through a ⅜-in. copper tube and can be obtained from virtually any point in the chamber. It is possible to take as many as five sequential samples from approximately the same point. The flow rate and tube length are selected so that the iodine vapor will diffuse to the walls of the tube while most of the particles will pass the length of the tube. Thus, the activity on the filter at the end of the tube will be due mainly to iodine adsorbed onto particles. At first the copper tubes were used as they were received, but this resulted in erratic count rates along the length of the tube. The tubes now being used have been silver plated on the inside and yield a monotonic decreasing count rate along the tube.

When the silver aerosol is mixed with I_2^{131} vapor there is only a very small amount of activity detectable on the diffusion tubes, whereas 96% of I_2 vapor is retained on the tubes in the absence of the aerosol. With the addition of silver aerosol most of the I^{131} penetrates to and is collected on the membrane filter. This suggests that there is very little free iodine vapor left in the tank and that the iodine on the particles going through the tube stayed on the particles. With the platinum there is always a high activity on the tube as well as on the filter, which indicates that iodine vapor is present in the tank and/or that the vapor is not completely retained on the particles as they pass through the tube.

By using an equation for deposition in a cylindrical diffusion channel derived from the equation of Gormley and Kennedy,[16]

$$n = n_0 \frac{D}{Q} (9.4033e^{-11.48DZ/Q} + 6.8270e^{-70.02DZ/Q} + 5.8169e^{-178.98DZ/Q}),$$

where

n = number of particles deposited per unit length,

n_0 = number of particles entering the channel,

D = diffusion coefficient of the particles (or molecules),

Q = volumetric flow rate of carrier gas,

Z = distance from channel entrance,

it has been found that the activity in the diffusion tube when platinum aerosol is used has an effective diffusion coefficient of 0.085 cm^2/sec (Fig. 18.4). Thus it appears that some free vapor is present and the remainder is carried out of the diffusion tube along with platinum particles.

The total amount of I^{130} in the diffusion tube plus the filter tends to decrease with time (Table 18.1); however, it is observed that considerable amounts of iodine are deposited in dead-end tubes, although the iodine does not penetrate more than 1 cm into the tube. Thus, the radioactivity deposited along the first centimeter of the tube is ignored in the tabulation of Table 18.1. In this study, airborne iodine vapor is lost by

[14]Gardner Associates, Inc., Schenectady, N.Y., Small-Particle Detector type CN.

[15]K. T. Whitby *et al.*, "Generator for Producing High Concentrations of Small Ions," *Technical Report No. 12*, Mechanical Engineering Department, University of Minnesota, to USPHS, July 1960.

[16]P. G. Gormley and M. Kennedy, *Proc. Roy. Irish Acad., Sect. A* 52, 163–69 (1949).

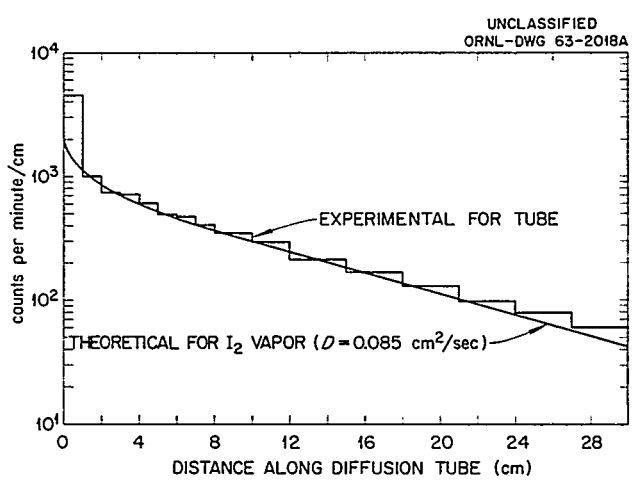

Fig. 18.4. Diffusion Deposition in a Silver-Plated Copper Tube Using Platinum Aerosol and I^{130} + I^{127} Vapor.

Table 18.1. Partitioning of I^{130} plus I^{127} Between the Vapor State and a Filterable Particulate Phase[a]

Time (hr)	Iodine Only		Iodine plus Platinum Aerosol	
	Diffusion Tube[b] (counts/min)	Filter (counts/min)	Diffusion Tube[b] (counts/min)	Filter (counts/min)
0.25			8590	3140
0.50			8040	3220
0.75	7350	270		
1.00	3780	193		
1.25			3470	2860
1.50	2920	61		
1.75			1650	2790
2.00	1550	89		
2.25			1170	2480
2.50	1270	110		
3.00	876	98		
4.25			326	2100

[a]Corrected for radiological decay.
[b](Total tube) − (activity on 1st centimeter) = 76% of total free I_2.

deposition on the walls of the chamber with a concentration half-life of 49 min when no large numbers of condensation nuclei are present. When aerosol particles are not present, a relatively small and variable amount of iodine is collected on the membrane filter; still, this small amount is approximately 90% of the vapor that has traversed the length of the tube. When platinum aerosol particles were mixed with iodine vapor, approximately 17% of the total airborne iodine was associated with a particulate phase which is collected on the membrane filter. The airborne concentration of the particulate phase decreased with a half-life of 6.9 hr, while the concentration of free molecular iodine decreased with a 41-min half-life.

DEPOSITION OF DUST IN AN ANNULAR IMPACTOR

P. Kotrappa[17] B. R. Fish

The high-volume annular impactor is an air-sampling device employing inertial forces to deposit airborne particulates onto a collecting surface. Although its design and application have been described by a number of authors,[18–22] very little information has been published concerning the basic principles of its operation. Figure 18.5*a* shows that dust-laden air enters the device through an annular opening, impinges on the collecting surface, and is withdrawn through the central tube. If one assumes the device to behave as a rectangular slit sampler extended as a figure of revolution into a circular shape, the deposit might be expected to be most dense at the radius of impingement and become gradually thinner toward the center. This is observed not to

[17]Atomic Energy Establishment, Trombay, Bombay, India.

[18]G. W. C. Tait, *Nucleonics* 14, 53 (January 1956).

[19]J. E. Hoy, *Annular Kinntic Impactor*, AECU-3439 (August 1956).

[20]D. C. Stevens, *Air Sampling with the Annular Impactor*, AERE HP/M 110 (August 1956).

[21]*Air Sampling Instruments*, 2d ed., pp B-3-17–18, American Conference of Governmental Industrial Hygienists, Cincinnati, Ohio, 1962.

[22]P. Kotrappa, *Deputation Report — (1963)*, Atomic Energy Establishment, Trombay, Bombay, India.

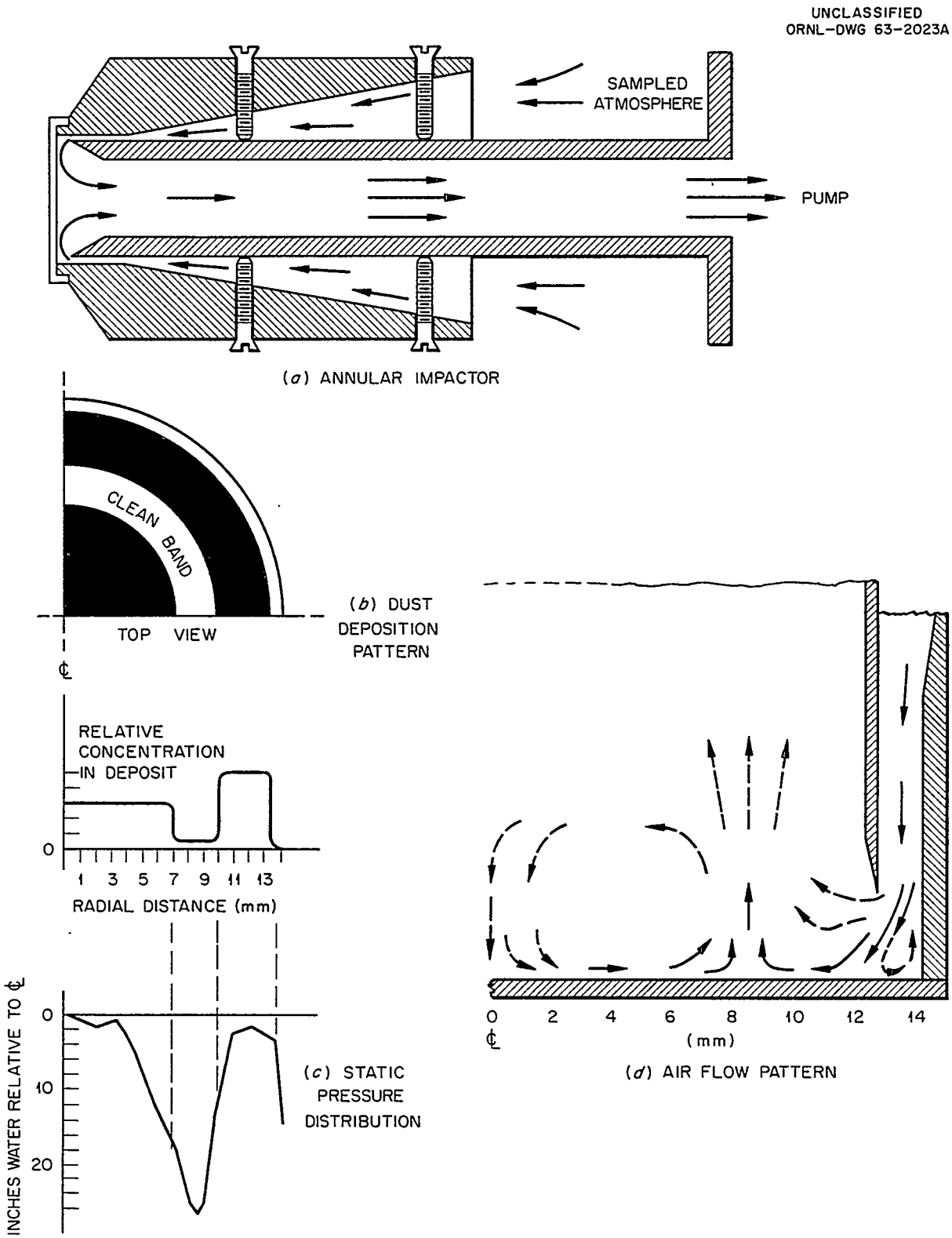

Fig. 18.5. Annular Impactor and Dust Deposition.

be the case; in fact, the dust deposition patterns usually include a central circular deposit and one or more annuli of deposited dust with definite minima or clear areas separating deposition areas (Fig. 18.5*b*). It has been suggested that the central deposit appears only after long sampling times,[20] and that it is dust which had been deposited on the primary impaction annulus, then blown off. Contrary to this hypothesis, we observe that deposition at the center begins as soon as the sampling is started and that all parts of the deposition pattern develop concurrently. This pattern of deposition has been observed with aerosols of uranyl nitrate,[22] MgO, and carbonyl iron.

In preparation for a more detailed investigation of the design and operating parameters, it was decided to explore the airflow patterns in the region near the collecting surface. Measurement of the static pressure pattern at the surface was accomplished by means of a number of pressure taps which were designed to be as small as possible and still reach an equilibrium response in about 2 sec. A 19-gage hypodermic needle was found to be adequate for this purpose. The pressure distribution pattern shown in Fig. 18.5c is the result of five replicate determinations separated by about 90° in angular position at radial distance intervals of 1 mm. The patterns of static pressure distribution and of dust deposition appear to be correlated to a considerable degree. Airflow lines (Fig. 18.5*d*), deduced from the gradient of the static pressure pattern, indicate the presence of at least two stable, toroidal vortices contiguous to the surface. Changes in the system parameters may result in the formation of additional flow structure, which can account for the observation of more than one clean band under some conditions.

An abrupt change in the surface concentration of deposited dust occurs, in this study, at points where the pressure gradient along the surface is in the range 9 to 11 mm Hg per mm and at which there is no significant component of velocity normal to the surface. This observation is consistent with the interpretation that, at some definite air velocity near the surface, the adhesive forces between particle and surface are exceeded by aerodynamic forces, thus precluding the retention of particles that may impinge on the surface. If this is true, it may be anticipated that the width of the clean band will vary directly with the "aerodynamic equivalent" size of the larger dust particles. In addition, the absolute value of the width of the clean band may be expected to depend upon composition of the particles and of the surface as well as depending upon relative humidity and other factors affecting the adhesion of solid particles to solid surfaces.[23,24] Preliminary studies suggest that this is a tenable explanation of the observed phenomena. Additional detailed studies are planned to examine this and other questions concerning the annular impactor.

PRODUCTION OF SUBMICRON AEROSOLS

F. G. Karioris B. R. Fish
A. J. Moll

Tests to explore the capabilities of the exploding conductor aerosol generator[25,26] to produce and disperse a wide variety of submicron aerosols[27] were continued. These aerosols differ greatly in chemical composition, density, electrical and thermal conductivity, permittivity, and other physical properties which may be of interest in testing instruments or in simulating health physics field problems in the laboratory. The generator has been used also to produce aerosols of platinum and silver for a study of the adsorption of radioactive I^{130} vapor on particulates.[28]

A series of 18 different metal wires or foils was exploded, with 10 kv on the 20-μf capacitor bank, in an atmosphere of nitrogen at barometric pressure; the pertinent data regarding yield and composition of the resulting aerosols are given in Table 18.2. Although nitrides were not detected

[23] M. C. Kordecki and C. Orr, *Environ. Health* 1, 1 (1960).

[24] M. Corn, *The Adhesion of Solid Particles to Solid Surfaces. I and II*, papers presented at the 54th Annual Meeting of APCA, June 11–15, 1961, New York.

[25] F. G. Karioris and B. R. Fish, *J. Colloid Sci.* 17, 155–61 (1962).

[26] F. G. Karioris and J. W. Youngblood, *Health Phys. Div. Ann. Progr. Rept. July 31, 1961*, ORNL-3189, pp 227–29.

[27] F. G. Karioris and A. J. Moll, *Health Phys. Div. Ann. Progr. Rept. July 31, 1962*, ORNL-3347, pp 145–47.

[28] R. L. Walker, "Study of the Adsorption of Iodine Vapor onto Aerosols" (a preceding section in this chapter, this report).

Table 18.2. Aerosols from Wires Exploded in Nitrogen[a]

Metal	Aerosol Collected (mg)	Relative Yield[b] (%)	Color of Deposit on Filter	Constituents of Aerosol[c]			Crystallite Size[d] (A)
				Major	Minor	Trace	
Ag	22	74	Brown	Ag			1500
Al	9	43	Gray	Al	AlN		2000
Au	15	63	Black	Au			340
Cd	11	85	Dark brown	CdO		Cd	250
Cu	8	71	Matte black	Cu		Cu_2O	570
Fe	7	96	Matte black	Fe, FeN			570
In	14	92	Brown	In	In_2O_3	InN	2000, 210
Mg	23	110	Gray	Mg		MgO	1700
Mo	13	49	Dark gray	Mo			1200
Ni	26	100	Black	Ni	NiO		860, 590
Pb	41	64	Charcoal gray	Pb	PbO (red)	$PbCO_3 \cdot Pb(OH)_2$	1700, 270, 1200
Pt	19	75	Dull black	Pt			>1000
Sn	16	84	Gray	β-Sn			>1000
Ta	8	75	Black	Ta_2N	?		590, 140
Th	9	92	Blue-black	ThO_2		ThN	50
U	7	72	Matte black	UN_2	UN		120, 550
W	10	58	Black	α-W, β-W	β-WN		
Zr	9	99	Matte black	ZrN	Zr		550

[a]Two centimeters of wire exploded by 20 μf at 10 kv in nitrogen at barometric pressure.

[b]This is 100 times (mass of aerosol collected)/(mass of wire exploded).

[c]Estimated from x-ray diffraction line intensity. Trace: 0 to 1%; minor: 1 to 20%; major: 20 to 100%.

[d]Estimated from x-ray line broadening. Sizes greater than ~1000 A cannot be considered reliable by this method.

in the aerosols from wires exploded in air,[29] they occur frequently when wires are exploded electrically in nitrogen.[30] It is interesting to note that uranium dinitride, which cannot be prepared by reaction of metal and nitrogen unless a high pressure of nitrogen is used,[31] is the major constituent of the aerosol resulting from the explosion of uranium in nitrogen. Oxides in these aerosols are probably due to contamination of the nitrogen or exposure of the samples to humid air after collection. In all cases the aerosol yield is relatively high. There are indications that the particle size distribution is multimodal when two or more chemical species are present in the aerosol.

To establish further the characteristics of the generator for the production of aerosols comprised

[29]A. G. Barkow, F. G. Karioris, and J. J. Stoffels, "X-Ray Diffraction Analysis of Aerosols from Exploding Wires," to be published in *Proceedings of Eleventh Annual Conference on Applications of X-Ray Analysis, Denver, Colo., Aug. 8–10, 1962*, Plenum Press.

[30]F. G. Karioris and J. J. Woyci, *X-Ray Investigation of Aerosols from Wires Exploded in Nitrogen*, a paper to be presented at Twelfth Annual Conference on Applications of X-Ray Analysis, Denver, Colo., Aug. 7–9, 1963.

[31]J. J. Katz and G. T. Seaborg, *The Chemistry of the Actinide Elements*, p 151, Wiley, New York, 1957.

of uranium compounds, two series of uranium ribbons of different mass were exploded in nitrogen at barometric pressure. The ribbons were made by cutting strips of different width from a strip of 0.001-in. foil and exploding 2-cm lengths at 4 kv and 8 kv. The uranium nitride aerosol yield curves (Fig. 18.6) are similar to those for uranium metal

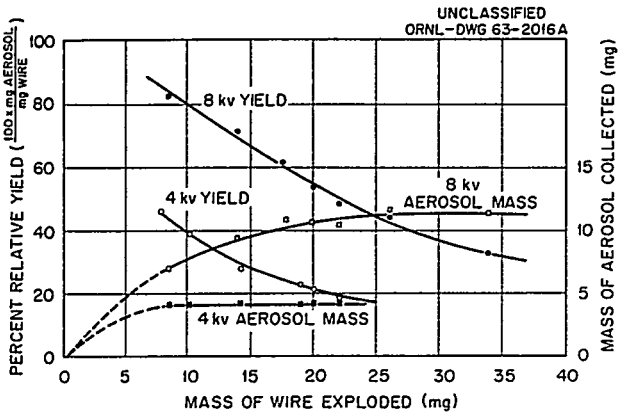

Fig. 18.6. Yield of Uranium Nitride Aerosols from Uranium Wires Exploded in Nitrogen.

exploded in air[32] and illustrate the relationship of yield to the mass of metal and voltage. Uniform aluminum wires were exploded in dry air with various voltages on the capacitor bank, and the resulting Al_2O_3 aerosols were collected on membrane filters. For most of these explosions, the mass of aerosol collected exceeded the mass of wire exploded because of the reaction of the aluminum with oxygen. The yield curves (Fig. 18.7) have the same general form as those for uranium and copper exploded in air.[32]

[32]F. G. Karioris, B. R. Fish, and G. W. Royster, Jr., "Aerosols from Exploding Wires," pp 299–311 in *Exploding Wires*, vol 2, Plenum Press, New York, 1962.

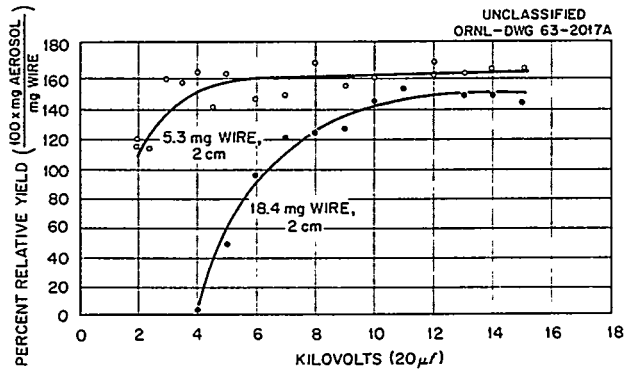

Fig. 18.7. Yield of Al_2O_3 Aerosol from Aluminum Wires Exploded in Dry Air.

Since it had been reported that the gas pressure influences the particle size of condensate from metal vapors,[33] nickel and thorium wires were exploded in nitrogen at pressures ranging from 50 to 750 mm Hg and at various voltages. The aerosol yield was found to increase with pressure at all voltages used, but the primary particle size was not affected dramatically either by the pressure or the voltage. This independence of particle size with respect to ambient pressure, together with the evidence that certain reactions with nitrogen do not proceed except at high pressure, may indicate that particle formation in the exploding wire phenomenon occurs in the shock wave.

A Zeiss particle size analyzer, TGZ 3, has been installed in the laboratory, and personnel are becoming familiar with its operation and use. A computer program has been written to process the data from the analyzer and determine size distribution parameters.[34]

[33]W. E. Gibbs, *Clouds and Smokes*, p 33, J. S. Churchill, London, 1924.

[34]A. J. Moll to B. R. Fish, unpublished data.

19. Applied Internal Dosimetry

ORNL IN VIVO GAMMA-RAY SPECTROMETRY FACILITY

P. E. Brown
L. B. Farabee
G. R. Patterson, Jr.
J. L. Thompson
W. H. Wilkie, Jr.
L. S. Barden[1]
J. H. Dobkins[3]
B. A. Flores[2]
D. L. Mason[4]
S. L. Wood[5]

The ORNL in Vivo Gamma-Ray Spectrometer Facility, in operation since June 1960, has been applied primarily as a monitoring device to aid in the detection and measurement of internal exposures. As a result of instrumentation and program improvements made during the past year, it has been possible to increase the rate of routine counting for monitoring purposes and, at the same time, initiate a limited program of research. A computer program, which was being developed and tested during the early part of this report period, was designed to reduce the amount of facility time required for routine data processing and reporting. The program has been completed; however, several major revisions were required during the last few months in order to use the program on the new digital computer which was installed at ORNL in February and March 1963. The routine monitoring program, previously confined to examination of known or suspected exposure cases, has been expanded in scope. Increased emphasis is being placed on routine counting of potentially exposed persons and also on obtaining base-line counts for individuals prior to their entering new work involving potential internal exposure. During the past year, 492 human counts were made. The current rate of counting is about 110 persons per month, excluding instrumentation downtime. Table 19.1 summarizes the data for those cases in which measurable amounts of internal radioactive contamination were observed.

[1]ORINS undergraduate trainee, Hendrix College, Conway, Ark.

[2]Mathematics Division.

[3]Temporary summer employee, North Carolina State College, Raleigh, N.C.

[4]Temporary summer employee, Austin Peay State College, Clarksville, Tenn.

[5]ORINS research participant, Austin Peay State College, Clarksville, Tenn.

Table 19.1. Measurable Radioactivity Found in Routine Whole-Body Monitoring Program During the Period June 1, 1962, to May 31, 1963

Isotope	Number of People	Highest Quantity[a] Measured (μc)	Maximum Permissible[a] Burden (μc)
Cs^{137}	64	0.57	30
Na^{24}	1	0.14	7
I^{131}	19	0.28[b]	0.7[b]
Zr^{95}	21	0.014	20
Sb^{125}	4	0.006	40
Sr^{90}	2	0.04[c]	0.8[c]
Co^{60}	5	0.002	10
Zn^{65}	4	0.003	60

[a]Whole body, except as noted.
[b]Thyroid.
[c]Lung.

HUMAN UPTAKE AND EXCRETION OF I^{131}: ACCIDENTAL INHALATION AND CHRONIC AND SINGLE INGESTION OF IODINE IN MILK

G. R. Patterson, Jr.
G. W. Royster, Jr.
S. R. Bernard
L. B. Farabee
B. R. Fish
P. E. Brown

In the previous progress report,[6] Dowex 1-X8 resin was shown to be about 90% effective in removing I^{131} from cow's milk. The 10% I^{131} content lost to the column effluent milk was shown to be bound to protein. During the present report period, a study was undertaken to investigate whether or not the uptake and excretion of protein-bound I^{131} are significantly different from the uptake parameters utilized by the ICRP and NCRP[7] in estimating thyroid radiation dose and maximum permissible concentrations of I^{131}.

[6]L. B. Farabee, *Health Phys. Div. Ann. Progr. Rept. July 31, 1962*, ORNL-3347, pp 149–52.

[7]Report of Committee II on Permissible Dose for Internal Radiation (1959), *Health Phys.* 3 (1960); and *Natl. Bur. Std. (U.S.), Handbook 69* (1959).

The study was conducted in two separate phases. In the first phase, three male volunteers each day for 11 consecutive days ingested 150 $\mu\mu c$ of the protein-bound I^{131} contained in resin-treated milk. With the use of a 4- by 4-in. lead-collimated NaI(Tl) crystal, in vivo determinations indicated that the protein-bound I^{131} was taken up by the human thyroid.

The second phase of the study was undertaken in cooperation with the Internal Dose Estimation Section to obtain human data with which to evaluate the ICRP-NCRP parameters, assumptions, and predictions. In this phase, two of the volunteers who had participated in the first phase each ingested single intakes of 92 nanocuries of protein-bound I^{131} in milk. Three additional volunteers each ingested 1.84 nanocuries/day for 63, 8, and 4 consecutive days. As nearly as possible, the time interval between consecutive doses was maintained at 24 hr. Table 19.2 shows the age and weight of subjects, amount of ingested activity, estimated peak dose rate, and total dose received by the thyroid gland. All subjects were found to be euthyroid, as indicated by standard tests of protein-bound iodine in blood.

Thyroid counts were made using a 3- by 3-in. lead-collimated NaI(Tl) crystal connected to an RIDL 200-channel analyzer. Figure 19.1 shows a subject in the thyroid counting position.

Figure 19.2 presents the thyroid-gland data for the two subjects who ingested 92 nanocuries. Plotted on the ordinate is the percent of ingested dose present in the thyroid; on the abscissa is the time after ingestion. At first the buildup of I^{131} in the thyroid gland is very rapid, but it levels off at about four days, at which time the amount of I^{131} begins to decrease along a single exponential path. The data from the decay curve for I^{131} in the thyroid were treated by the method of least squares according to the equation

$$\phi = \sum_{i=0}^{n} W_i (Y_i - Y_{oi})^2 ,$$

where

ϕ = residual sum of squares,

Y_i = calculated ith value of the ordinate,

Y_{oi} = observed value,

W_i = weight factor.

The least-squares method was programmed for the IBM 7090 computer by George Atta of the Mathematics Division. Calculations were made using two sets of weight factors in which $W_i = 1$ (i.e., unit weight) and $W_i^{-1} = \text{var } Y_i$. Because it was assumed that all the variance in the ordinate value was due to counting, the variance was

Table 19.2. Data on Human Subjects Participating in the Protein-Bound I^{131} Experiment

Subject[a]	Age (yr)	Weight (lb)	Daily Intake ($\mu\mu c$/day)	Duration of I^{131} Ingestion (days)	Single Intake ($\mu\mu c$)	Maximum Dose Rate to Thyroid Gland (rem/week)	Total Dose to Thyroid (rem)
A	36	220	150	11	92,000	0.110	0.176
B	36	187	150	11	92,000	0.055	0.076
C	37	225	1840	63	0	0.005	0.056
D	53	170	1840	8	0	0.005	0.010
E	42	152	150 1840	11 4	0 0	0.005	0.015
Av	41	191					

[a]All subjects were euthyroid, as indicated by tests of protein-bound iodine in blood performed by the ORNL Health Division.

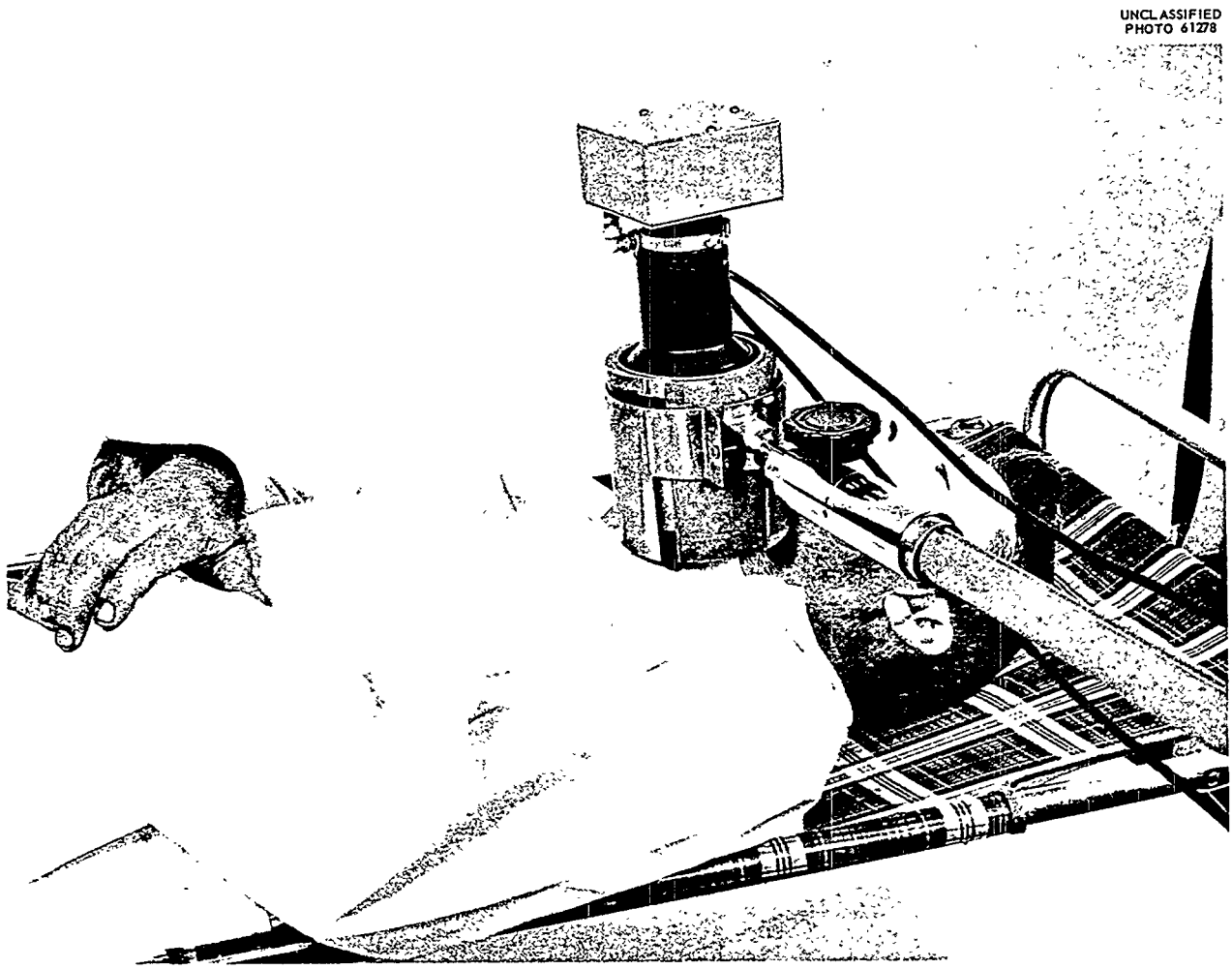

Fig. 19.1. Subject in Thyroid Counting Position.

estimated from the counts. The effect of weighting the residuals is to remove the bias of the smallest ordinate values (those containing the largest error) on the best-fitting curve. Figure 19.3 is a plot of the least-squares treatment of raw data for the two single-intake subjects. Figure 19.3*a* shows the data, together with the plot of the best-fitting curve for the case of $W_i = 1$ (i.e., unweighed data) and the equations for the curves. The errors on the parameters are two standard errors. On the ordinate are plotted the counts per minute in the thyroid gland, while on the abscissa is plotted the time in days.

Figure 19.3*b* is a plot of the data together with the best-fitting curves obtained when $W_i^{-1} = \text{var } Y_i$. Plotted along the ordinate are the counts per minute of the thyroid gland, while on the abscissa is the time in days following the single ingestion. Table 19.3 presents the rounded-off values of f_w and T_b for these two subjects. Using intercepts of the best-fitting curves and dividing by the amount ingested, estimates are obtained of f_w, the fraction going from the gut to the thyroid gland.

Although the f_w values (Table 19.3) for subjects A and B differ, the weighted and unweighted data have little influence on the f_w value for each individual subject. The biological half-lives T_b are quite different for subject A when the estimates are based on weighted and unweighted data. This is due to the fact that the effective decay constant λ approaches the radiological decay constant λ_r in the denominator of the equation

Table 19.3. Biological Values Estimated from Best-Fitting Parameters Obtained by Least-Squares Treatment of I^{131} Decay in Thyroid

Subject	Ingested Dose[a] (counts/min)	Fraction from GI Tract to Thyroid, f_w			Biological Half-Life, T_b (days)		
		Weighted	Unweighted	Weighted[b]	Weighted	Unweighted	Weighted[b]
A	10,090	0.28	0.27	0.29	291	1823	153
B	10,090	0.14	0.14		37	36	

[a]Based on 92 nanocuries at 4.94% thyroid counting efficiency.

[b]Last three measurements of curve for subject A omitted from least-squares calculation (see text).

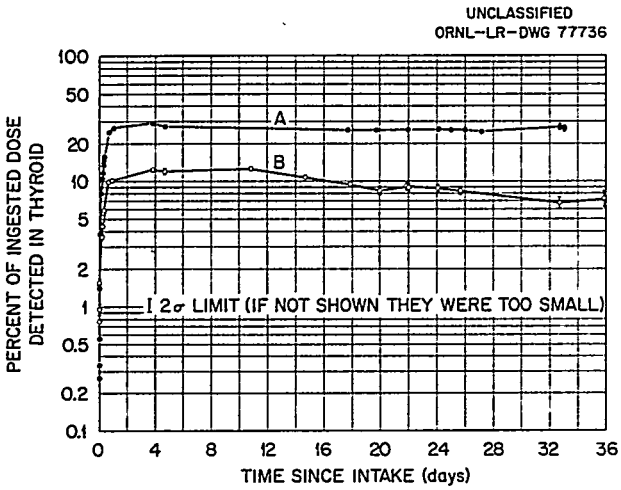

Fig. 19.2. Thyroid Gland Data for Two Subjects Who Ingested 92 Nanocuries of Protein-Bound I^{131} in Milk.

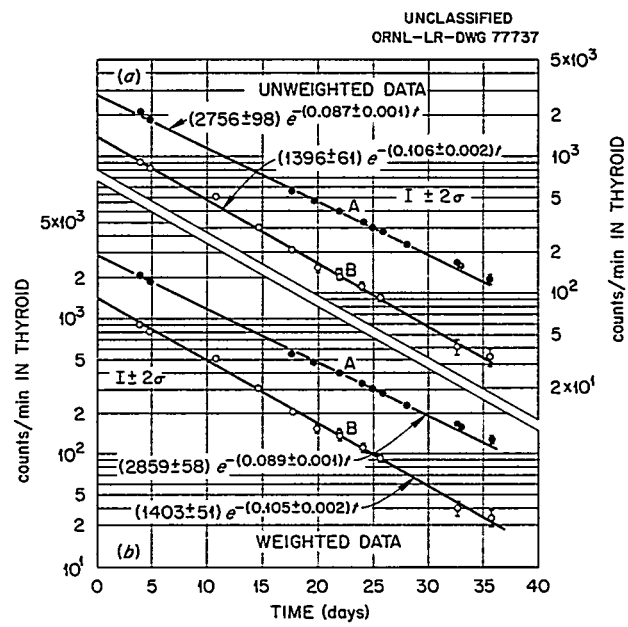

Fig. 19.3. Least-Squares Treatment of Thyroid Decay Curves.

for T_b [$= 0.693/(\lambda - \lambda_r)$], and T_b is quite sensitive to small changes in the denominator. The last three measurements for subject A markedly affect the value of λ and, hence, the calculated value of T_b. These last three points have larger variance than any of the other points. It was felt that these points might be biased because his intake of milk contained I^{131} from fallout. At the time of these measurements, the dietary milk in his community was increasing in its content of I^{131}. Therefore, the last three points were omitted from the least-squares calculation, and subject A's indicated biological half-life of I^{131} in the thyroid became 153 days.

Subjects A, B, and E also ingested, daily for 11 days, 150 $\mu\mu$c of I^{131} in resin-treated milk, and their thyroid glands were counted. Figures 19.4–19.6 show the measured thyroid burdens of these subjects and the burden predicted by extrapolation of the single-intake data. Also shown for comparison is the predicted burden using ICRP-NCRP parameter values. On the ordinates of these figures are plotted the I^{131} ($\mu\mu$c) in the thyroid, while on the abscissa is plotted the time following ingestion of the first dose. The ICRP-NCRP-predicted burden overestimates the measured burdens for all three subjects. In the cases of subjects A and B the extrapolated burden agrees more closely with actual measurements

than the ICRP-NCRP-predicted burden; nevertheless, it is an overestimate also.

The thyroid gland measurements on subjects C, D, and E, who were counted both during the period of ingestion and after intake stopped, will be shown later in this report. First, the measurements of the thyroid gland burden after stopping the intake will be examined. Figure 19.7 presents the data for I^{131} in the thyroid of subject C, who ingested 63 daily intakes, and of subject D, who ingested 8 daily intakes. Figure 19.7*a* shows the graph of the data and the best-fitting curves together with the parameters of the best-fitting equations estimated from least-squares treatment of the unweighted data. Figure 19.7*b* shows the same data, but the best-fitting curves and parameters were estimated from the least-squares treatment of weighted data. As can be seen in Fig. 19.7 the influence of the smallest ordinate value (the last point) is reduced when the weighted sum of squares is used. From these best-fitting equations, the values for the parameters f_w and T_b can be obtained for these two subjects, and the iodine burdens in the thyroid glands during the period of chronic intake can be predicted and compared with the measured burdens.

Table 19.4 presents the values for f_w and T_b obtained from the numerical data appearing in Fig. 19.7. For subject C the f_w value is quite different, depending on whether the weights were set equal to unity or to 1/(var Y_i). The same is true for the T_b for subject C. The parameters

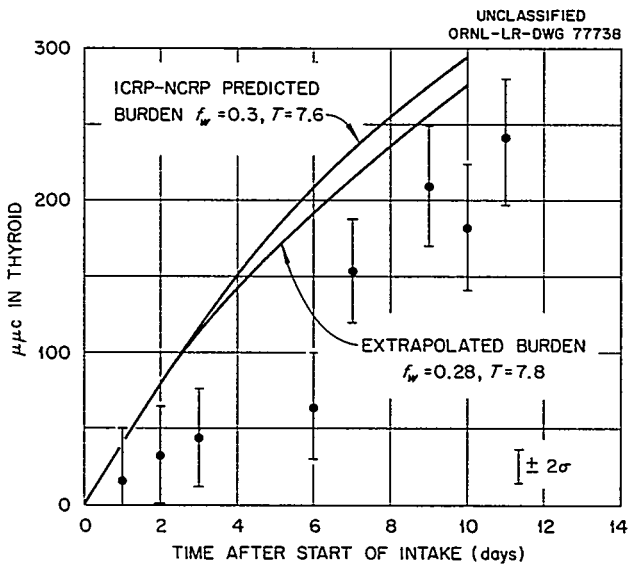

Fig. 19.4. Thyroid Gland Burden of I^{131}. Subject A ingested 150 μμc daily for 11 days in resin-treated milk.

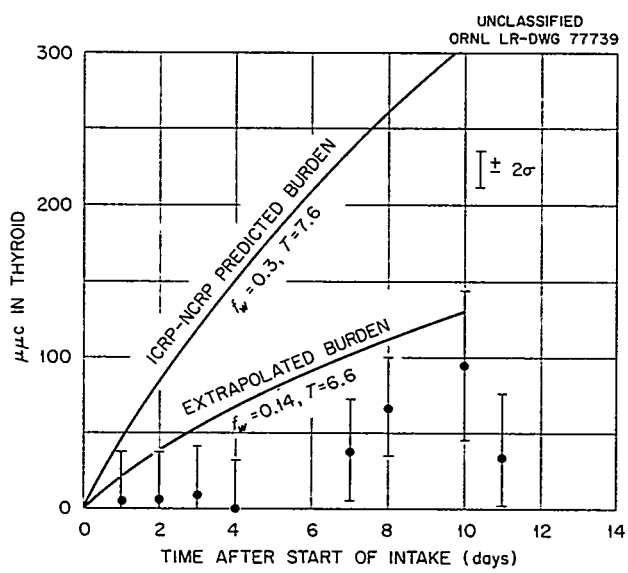

Fig. 19.5. Thyroid Gland Burden of I^{131}. Subject B ingested 150 μμc daily for 11 days in resin-treated milk.

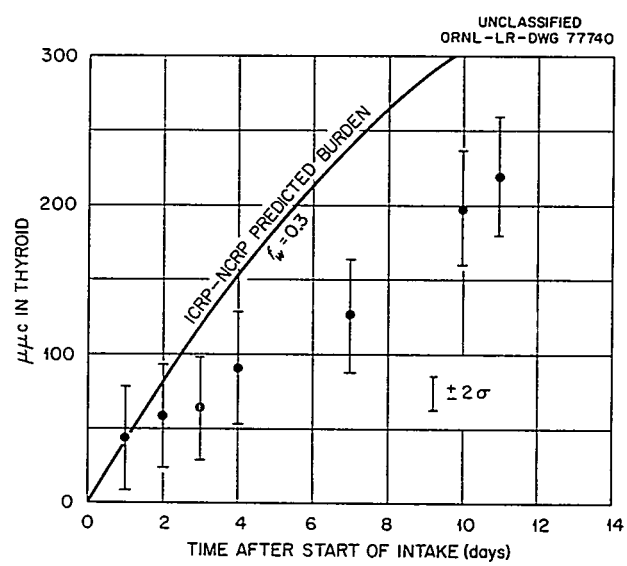

Fig. 19.6. Thyroid Gland Burden of I^{131}. Subject E ingested 150 μμc daily for 11 days in resin-treated milk.

obtained from the weighted least-squares treatment are employed to predict the thyroid uptake of I^{131} during daily ingestion.

Figures 19.8 and 19.9 show the thyroid burden measurements on these two subjects both during their period of daily intake and in the following period after the intake was stopped. Plotted on the ordinate is the I^{131} ($\mu\mu c$) in the thyroid, while plotted on the abscissa is the time in days from the first intake. Also shown in these figures are the predicted thyroid burdens employing ICRP-NCRP data and the extrapolated thyroid burdens based on the f_w and T_b values appearing in Table 19.4 (weighted data). For both subjects the ICRP-NCRP-predicted burdens overestimate the observed burdens. Also, in the case of subject C, the extrapolated burden from single-intake data slightly overestimates the observed level in thyroid.

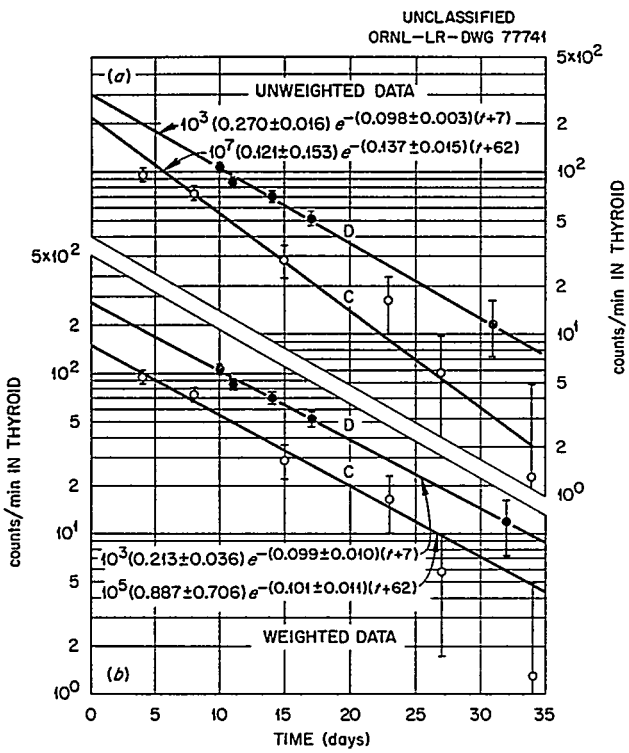

Fig. 19.7. Least-Squares Treatment of Thyroid Decay Curves.

Subjects A and B submitted urine samples for the first five days following their single ingestions; subject C submitted urine samples during the entire 63 days of continuous intake and 4 days following the end of intake. The samples constituted essentially total voiding during the above periods. An average of (64 ± 5)% of the ingested dose was excreted in urine during the first day after a single intake. In the continuous-intake case, the daily urinary excretion increased to about 95%/day when equilibrium was apparently reached.

The urinary excretion of I^{131} for subject C is shown in Fig. 19.10. Plotted on the ordinate is the percent of daily intake of I^{131}. The time in days after the first intake is plotted on the abscissa. During the first ten days, the measured excretion rate rises from 75%/day to a level of about 90 to 95%/day and from then fluctuates around 95%/day. Note that the point at 60 days is ~15%/day. On this day the subject had influenza, accompanied by diarrhea and vomiting. His urinary volume on this and the succeeding two days was quite low since he was on a negative water balance. It can be noted also that the rate of I^{131} excretion on these days was lower than usual. After the intake was stopped, the rate of excretion decreased precipitously. On the 66th day, three days after the ingestion of I^{131} had been stopped,

Table 19.4. Biological Values Estimated from Best-Fitting Parameters Obtained by Least-Squares Treatment of Thyroid-Decay-Curve Data

Subject	Daily Dose[a] (counts/min)	Fraction from GI Tract to Thyroid, f_w		Biological Half-Life, T_b (days)	
		Weighted	Unweighted	Weighted	Unweighted
C	202	0.08	0.17	47	14
D	202	0.14	0.14	57	61

[a]Based on 1.84 nanocuries per day at 4.94% thyroid counting efficiency.

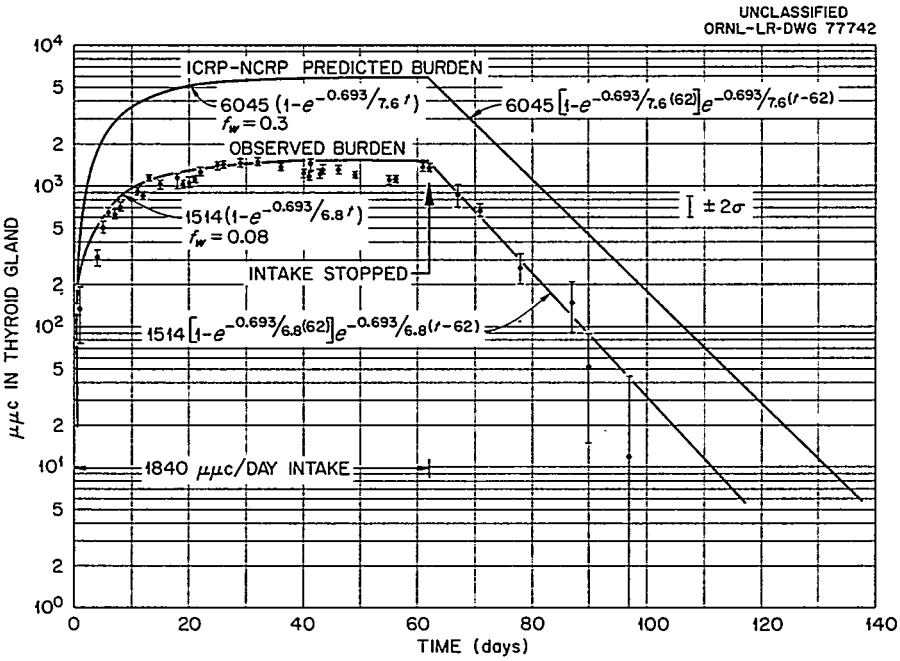

Fig. 19.8. Thyroid Gland Burden of I^{131}. Subject C ingested 1840 μμc daily for 63 days.

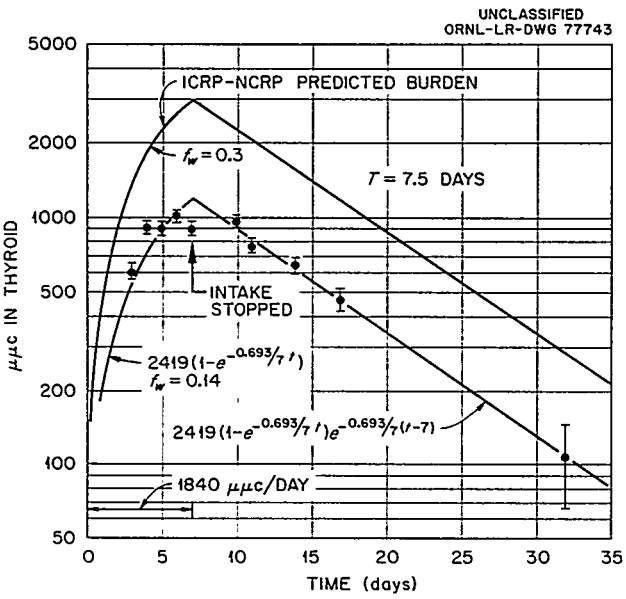

Fig. 19.9. Thyroid Gland Burden of I^{131}. Subject D ingested 1840 μμc daily for 8 days.

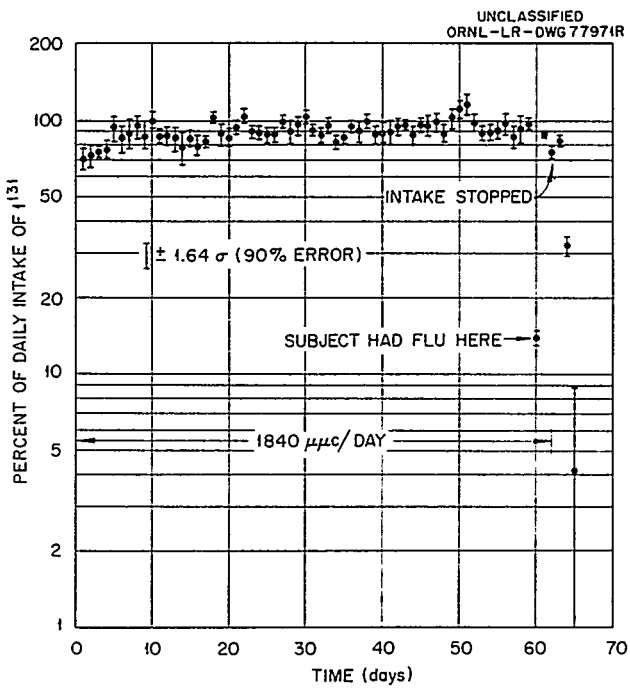

Fig. 19.10. Daily Urinary Excretion of I^{131}. Subject C ingested 1840 μμc daily in resin-treated milk for 63 days.

the level in urine was less than the limit of sensitivity for detecting I^{131} in urine.

Coincidentally, just before the second phase of the study began, an ORNL employee inhaled a small quantity of I^{131} vapor when a sample which was being poured out reacted with the slightly acid waste in the hot-sink drain trap. The employee was first counted for I^{131} thyroid activity 4 hr after the exposure incident; during the next 42 days, he was counted seven times for I^{131} thyroid activity and seven times to determine the whole-body burden. Figure 19.11 shows the spectrum from a typical thyroid count with the 3- by 3-in. crystal positioned over the employee's thyroid gland and in contact with his throat.

Figure 19.12 compares the decrease in thyroid burden for the inhalation case with the burdens for the two ingestion volunteers for the first 18 days following intake. The data points were not corrected for radiological decay; consequently, they are compared with the rate of elimination from the thyroid predicted by the ICRP-NCRP, $T_{eff} = 7.6$ days.[7]

The urinary excretion pattern of the inhalation case shows rather good agreement with excretion patterns for the two ingestion cases. The employee exposed by inhalation submitted essentially his total voiding for the first four days following exposure, beginning approximately 30 min after exposure. The two ingestion volunteers submitted essentially their total voiding during the same period. Figure 19.13 shows the comparison of urinary excretion for the three cases. Urine sample counts were corrected for radiological decay back to the time of intake in order to provide cumulative excretion data.

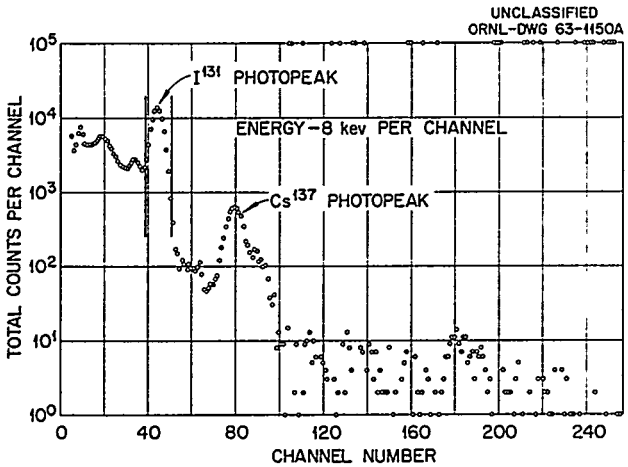

Fig. 19.11. Typical I^{131} Gamma-Ray Spectrum of 3- by 3-in. Lead-Collimated NaI(Tl) Crystal Positioned over Thyroid Gland.

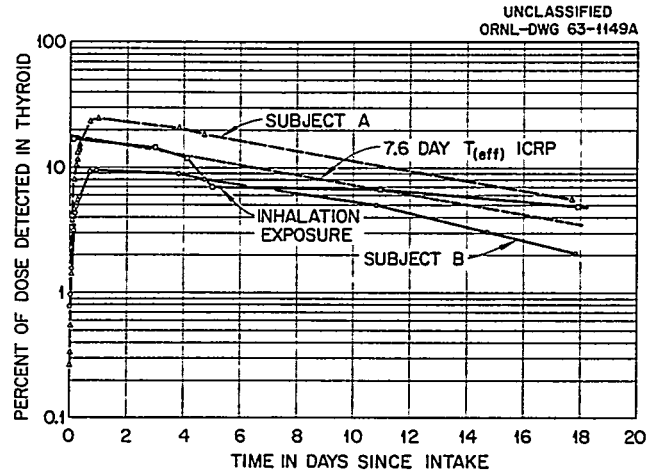

Fig. 19.12. Percent of Initial I^{131} Intake Found in Human Thyroid. Comparison of two cases of single oral ingestion (A and B: 0.092, in milk) with one case of single inhalation of I^{131} vapor (estimated 0.740 μc, WBB).

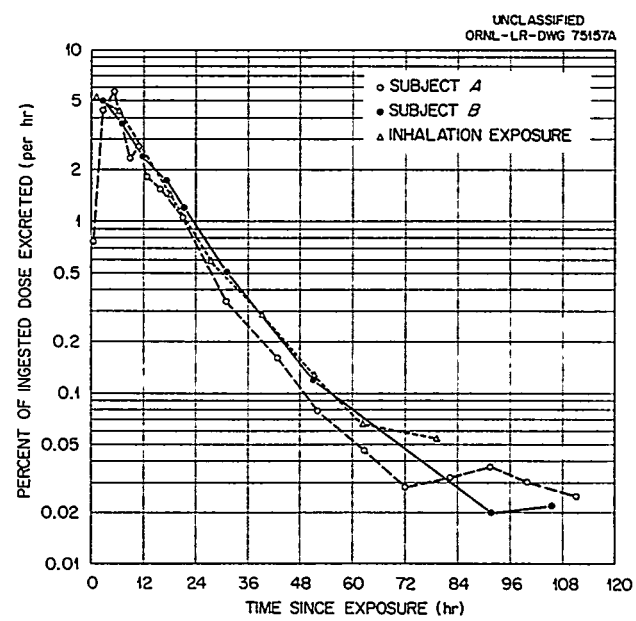

Fig. 19.13. Comparison of Urinary Excretion for Three Cases.

From Figs. 19.12 and 19.13, it is seen that subject A had a higher thyroid uptake and lower excretion; subject B had a high excretion and lower thyroid uptake. Although two subjects do not constitute a good statistical sample, these two apparently provide a reasonably good average excretion factor. Keating *et al.*[8] found the average cumulative excretion for apparently normal thyriod cases to be approximately 64.5% of the dose at the end of 48 hr; the average for the two volunteer subjects was approximately 65% of the ingested dose excreted by 48 hr.

The patterns for thyroid uptake and urinary excretion of radioiodine appear to be strikingly similar, whether the dose is acquired by inhalation or ingestion. Since this seems to be true, the data obtained from the I^{131} ingestion study were useful in estimating the extent of the inhalation exposure. Based on the ingestion data, the initial inhalation exposure was estimated to have been approximately 740 nanocuries in the whole body. Extrapolating thyroid counts for the inhalation case back to time of intake gives approximately 135 nanocuries in the thyroid. This is approximately 18% of the whole-body burden.

For the sake of comparison, had the exposure been sustained at the original level, it would be approximately 96% of the MPC for continuous exposure (ICRP-NCRP).[7] It is more nearly correct, however, to compare this single acute inhalation with the maximum permissible quarterly intake by inhalation (ICRP-NCRP, 4.4 μc), in which case this exposure amounted to approximately 16.8% of the permissible quarterly intake.

In conclusion, the present study suggests that the single-intake data can be extrapolated to the case of continuous intake when the parameters are estimated for each individual. It is also suggested that the single-exponential-compartment model of ICRP-NCRP is a fairly adequate representation of the data on I^{131} uptake by human thyroid glands. It is to be remembered that the foregoing statements are only suggestions, and they rest on relatively few cases observed over periods of time that are short compared with a 50-yr-exposure period. It is indicated from these few human studies that the ICRP-NCRP recommendations of $(MPC)_w$ are conservative and differ by a factor of only ~ 2.

[8] F. R. Keating *et al.*, *J. Clin. Endocrinol.* 10, 1425 (1950).

COMPUTER PROGRAM FOR IN VIVO COUNTING DATA

G. R. Patterson, Jr. B. A. Flores

Program WBC is designed to process data from the RIDL 200-channel analyzer and the Nuclear Data 512-channel analyzer. Data in the form of punched paper tape are transferred to magnetic tape on the CDC 160-A computer and are merged on the CDC 1604 computer with other information concerning the in vivo count. The 1604 program processes the individual spectra according to the indicated counting geometry and stores the original spectrum, coded information, net spectrum, and output information on magnetic tape for future use.

The code strips K^{40} and Cs^{137} from the net spectrum and calculates two estimates of the grams of total potassium according to the summation of counts both in the photopeak and in the Compton scatter band, the nanocuries of Cs^{137}, and the standard deviations of these estimates. A plotting subroutine prepares instructions on magnetic tape, which is used with a Calcomp plotter to graph the net spectrum and the net spectrum minus K^{40} and Cs^{137}. This subroutine can be instructed to sum two or more adjacent channels and plot as a single data point, permitting a rudimentary form of curve smoothing.

Figure 19.14*a* shows a portion of the computer printout for a routine in vivo count of an ORNL employee. The personal information identifying the count was supplied to the computer from in vivo count data sheets. Figure 19.14*b* shows the Calcomp plot of the spectrum for the same employee. Each point shown is the sum of two adjacent channels plotted at the "midpoint" position. Note the net spectrum, showing peaks for K^{40} around channel 180, Cs^{137} around channel 81, and I^{131} around channel 45. In the second curve (net spectrum minus K^{40} and Cs^{137}), the potassium and cesium peaks have been stripped out, but the I^{131} peak is still very much in evidence, reduced only slightly by the stripping of the potassium and cesium contribution.

The program originally was written for the IBM 7090 to be processed at Central Data Processing, ORGDP. In this format, the program was almost ready for use in December 1962, but changes in computer equipment, both at Central Data Processing and at ORNL, necessitated a major program

UNCLASSIFIED
ORNL-DWG 63-2423

PART A

NAME BADGE DEPT. BLDG. DATE 3-22-63 TENN SPEC. SURVEYOR TIME 1023

RUN NO. 1484 BKG. NO. 14872 COUNT CODE 601 TIME (MIN.) 20 GROSS INT. CT. 91943 GROSS CT. (M.E.A.) 10718

MONITOR INT. CT. 23300 WT.(KG)=03.0 HT.(CM)=88.6 CHEST TK.=11IN CHEST CIRC.=41IN WAIST=42IN AGE= 57.0

BODY 0 SEX M EPPL 0 CLASS 1 EXPOSURE 2 DATA 0 ANALYZER 0 PREVIOUS NO. 0

BANDS	LOW 14- 74	CS137 71- 89	K40-SCATTER 100- 163	K40-PHOTO 170- 192	TOTAL 14- 199	HI
SUMS(C/M)	1524.70	178.34	184.25	82.00	2449.45	530.55
SUM/KG	14.81	1.73	1.01	.80	23.79	5.15
STD. DEV. NET			4.891E+000	3.208E+000	1.557E+001	
NET-K40		4.745E+000	8.599E+000			
NET-K40-CS	1.776E+001					
ESTIMATES		22.9920 NANOC.	223.2984 GRAMS	144.0776 GRAMS		
STD. DEV. OF ESTIMATES		6.162E-001		5.814E+000		

NET SPECTRUM

386.50	15.95	19.95	27.50	35.40	43.65	53.05	56.45	62.60	62.35
63.30	58.75	65.45	65.15	68.35	65.05				
62.45	56.35	50.05							

PART B

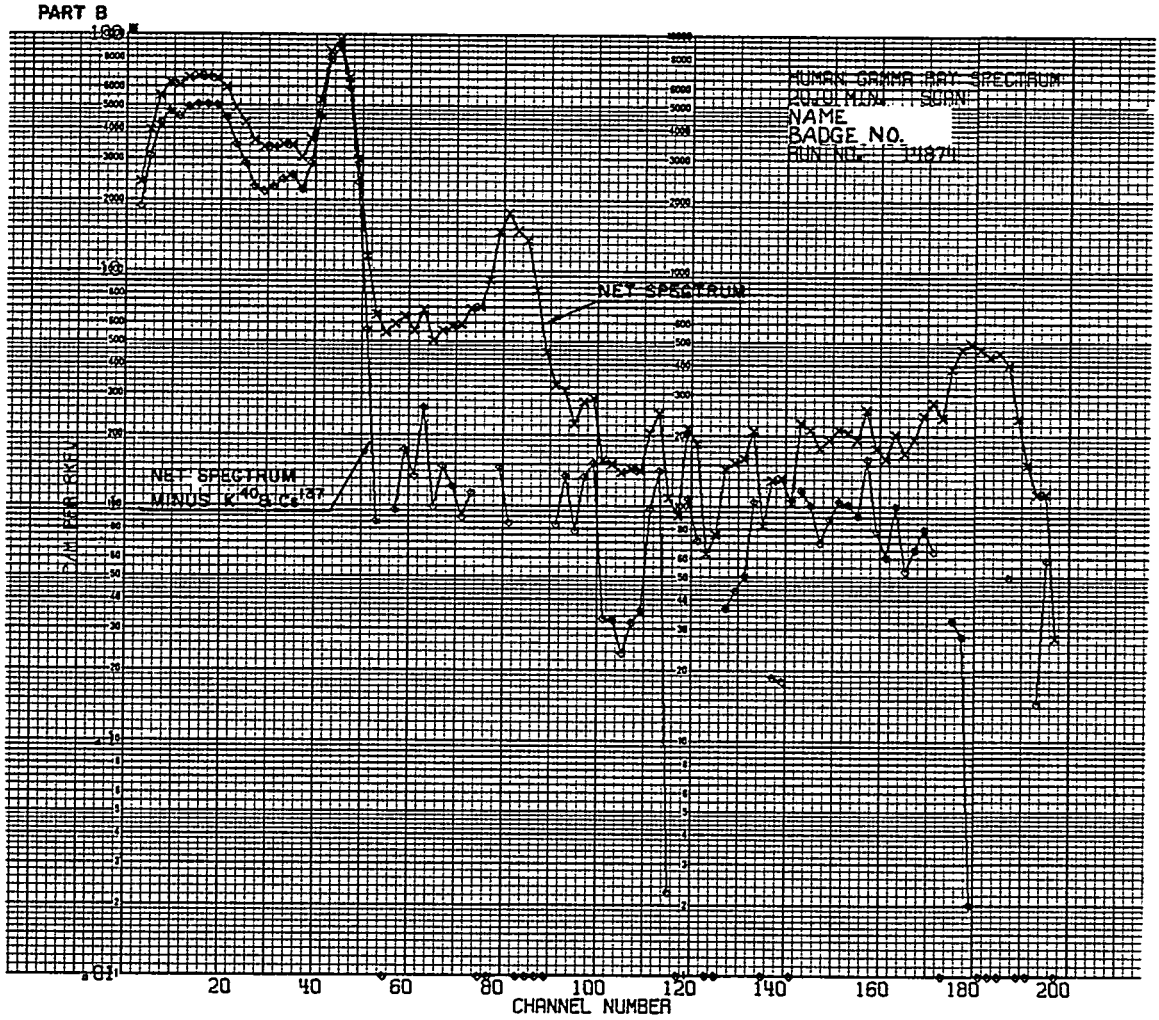

Fig. 19.14. In Vivo Data Printout.

rewrite. The CDC 160-A, on which punched paper tapes were transferred to magnetic tape, was moved from Central Data Processing to the High Voltage Laboratory at ORNL and was replaced with an IBM 1401. The 1401 could not handle the WBC program input without a major program rewrite, and the 160-A in its new location at ORNL had been modified so that it no longer could handle the WBC program input. The decision was made to rewrite the program to utilize the new CDC 160-A and 1604 complex which was being installed at ORNL to replace the Oracle. This rewrite has been accomplished and is being debugged. At the present time the program seems to be capable of handling the data for routine in vivo counts and of providing satisfactory estimates of total K and Cs^{137}.

DEVELOPMENTS IN THE ORNL IN VIVO GAMMA-RAY SPECTROMETRY FACILITY

W. H. Wilkie, Jr.

During the past year several improvements have been made in the IVGS Facility. All routine human in vivo counts are now made in a scanning bed geometry in which an individual lying horizontally on a bed is moved beneath a NaI(Tl) crystal. At the same time that the gamma spectrum is being analyzed, a strip-chart recorder traces the gross counting rate as a function of detector position along the body. The scanning bed replaces the chair geometry formerly used in our routine program. Although a thorough study has not yet been completed, it is estimated that the efficiency for gamma detection using the scanning bed geometry is approximately equal to that of the chair geometry for radionuclides uniformly distributed in the body and is less sensitive to changes in geometry resulting from nonuniformly distributed radionuclides or from variations in size between individuals.

A thin-crystal assembly is now available for use in the spectral analysis of electromagnetic radiation in the energy region below 150 kev. The assembly consists of three 5-in.-diam by $\frac{1}{16}$-in.-thick NaI(Tl) crystals with a 5-mil beryllium entrance window and mounted on 5-in. photomultiplier tubes. Signals from these three tubes are linearly mixed, amplified, and sorted in a multichannel pulse-height analyzer. A normal human spectrum obtained with the thin-crystal assembly is composed of counts due to the K^{40} and Ba^{137} gamma rays, a Ba^{137} x ray, and a residual gamma flux. Figure 19.15 shows a typical thin-crystal-assembly spectrum of the residual portion of a human chest count (average of seven unexposed males); that is, the spectrum with the contributions from K^{40} and Ba^{137} removed. The origin of the residual spectrum has not been adequately explained and is being studied further.

The thin-crystal spectrum of an individual containing a small amount of Sb^{125} is shown in Fig. 19.16. The amount was determined to be less than 10^{-4} times the maximum permissible body

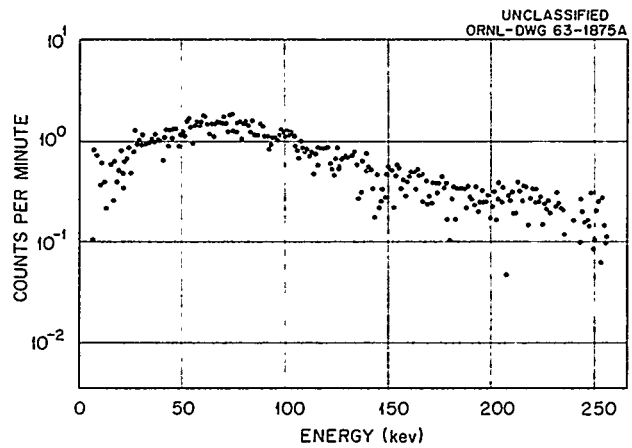

Fig. 19.15. Typical Thin-Crystal-Assembly Spectrum of a Residual Portion of a Human Chest Count.

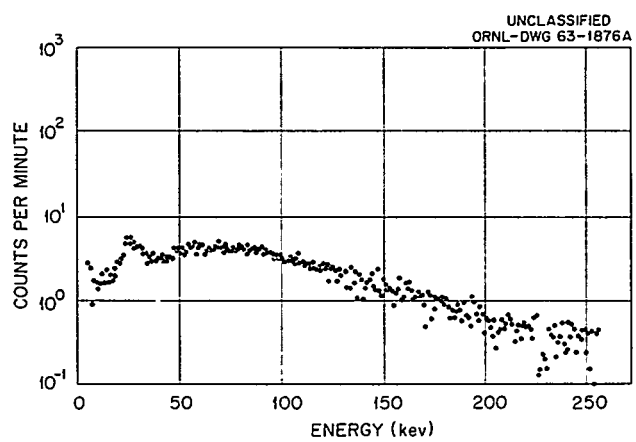

Fig. 19.16. Thin-Crystal-Assembly Spectrum of an Individual Containing a Small Amount of Sb^{125}.

burden (MPBB).[9] The thin-crystal assembly is of particular importance in the study of lung burdens of plutonium. In its present state of development the assembly is capable of detecting less than 40 nanocuries of Pu^{238} in the human lung in a 40-min chest count, provided that a background is available on the individual prior to the Pu^{238} inhalation. If no prior background is available, the Pu^{238} burden detectable is 80 nanocuries or less. Figure 19.17 shows a typical calibration spectrum for Pu^{238} in the lung. The lowest-energy peak is due to the 17-kev x-ray group of uranium.

An attempt was made to reduce the background in the iron room by installing a graded shield over the existing ⅛-in. lead lining of the room. A layer of tin and cadmium approximately 0.04 in. thick was laid on top of the lead on the floor, a layer of copper 0.01 in. thick was placed over the tin and cadmium, and the original vinyl tile was then replaced. On the basis of similar background counts, using the 8- by 4-in. NaI(Tl) crystal before and after the operation described, it was concluded that the background below 2 Mev had been reduced by 24%. Further developments include the installation of the thin-crystal assembly adjacent to the large NaI(Tl) crystal, permitting their use concurrently.

[9]Report of Committee II on Permissible Dose for Internal Radiation (1959), *Health Phys.* 3 (1960).

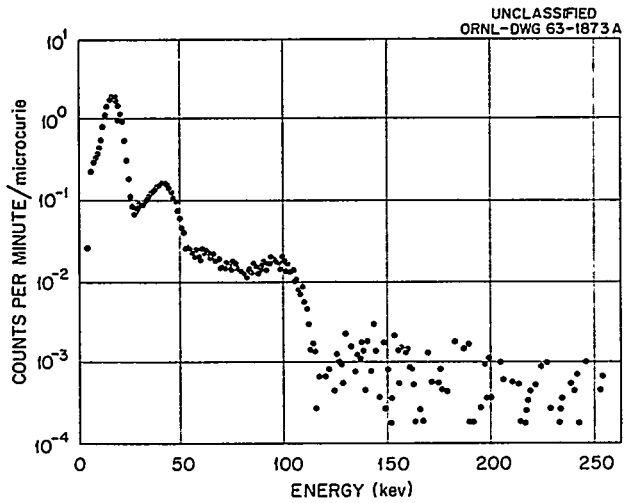

Fig. 19.17. Typical Calibration Spectrum for Pu^{238} in the Lung.

METHOD FOR REMOVAL OF ALPHA CONTAMINANTS IN PHOSPHORIC ACID

L. B. Farabee

Gross alpha transuranic radionuclides in a urine sample are determined most expediently by a cursory method which concentrates the total alpha activity by a bismuth phosphate–lanthanum fluoride precipitation ($BiPO_4$-LaF_3). This procedure isolates as a group the isotopes of Th, Np, Pu, Am, Cm, Bk, and Cf. Since the urinary alpha radioactivity excretion rates of these radionuclides associated with a maximum permissible exposure are very low, the chemical reagents used in the isolation procedure must be free of extraneous alpha activity in order that the background be held to a minimum. The elimination of alpha-active impurities from lanthanum has been described.[10] This study is concerned with identification of alpha-radioactive impurities in phosphoric acid (H_3PO_4) and a method for their removal.

Although phosphates are normal constituents of urine, excess phosphate (as H_3PO_4) is added to ensure complete precipitation of the bismuth "carrier" in the $BiPO_4$ procedure. In one procedure for isolating plutonium from a 1500-ml urine sample by $BiPO_4$ precipitation,[11] the 10 ml of added H_3PO_4 increased the alpha background by 0.4 dis/min. Radium D (Pb^{210}) and its daughters were found in this H_3PO_4, and the alpha of Po^{210} is no doubt the cause of the increased background counts in the reagent blank.

The radioactive contaminants in H_3PO_4 are so low that concentration of these radionuclides on a cation exchange resin column is necessary before identification can be made. The presence of Pb^{210} and Bi^{210} in H_3PO_4 was proved by a procedure of Baratta and Herrington,[12] while Po^{210} was determined by a plating technique.[13] Decay and/or growth studies confirmed the presence of Pb^{210} and Bi^{210}. Radium D and its daughters were found in samples from five different sources

[10]L. B. Farabee, *The Removal of Alpha Contamination from Lanthanum by Ion Exchange*, TID-7591, pp 78–80 (Oct. 1–2, 1959).

[11]L. B. Farabee, *Procedure for the Determination of Plutonium in Human Urine*, MonH-218 (April 1947).

[12]E. J. Baratta and A. C. Herrington, *The Determination of Isotopic Radium*, WIN-118 (September 1960).

[13]E. S. Spoerl, *Urine Assay Procedure at the Mound Laboratory*, AECD-3811 (April 1950).

of H_3PO_4. The Po^{210} alpha activity ranged from 70 to 1330 dis min^{-1} $liter^{-1}$. The H_3PO_4 was also analyzed for Ra^{226}; however, the Ra^{226} contribution was seen to be less than 1 part in 500 of the Po^{210} alpha activity of the reagent. Apparently Ra^{226} is removed in the process of preparing H_3PO_4.

Quantitative removal of the contaminants is achieved by passing a 2 *M* H_3PO_4 solution through a cation exchange resin column (35 ml of Dowex 50-X12 (–50 + 100 mesh) in a 1.8-cm-ID cylindrical glass column) at a flow rate of 3.8 ml cm^{-2} min^{-1}. This purification will reduce the alpha background of H_3PO_4 from about 0.4 to <0.08 dis/min per sample.

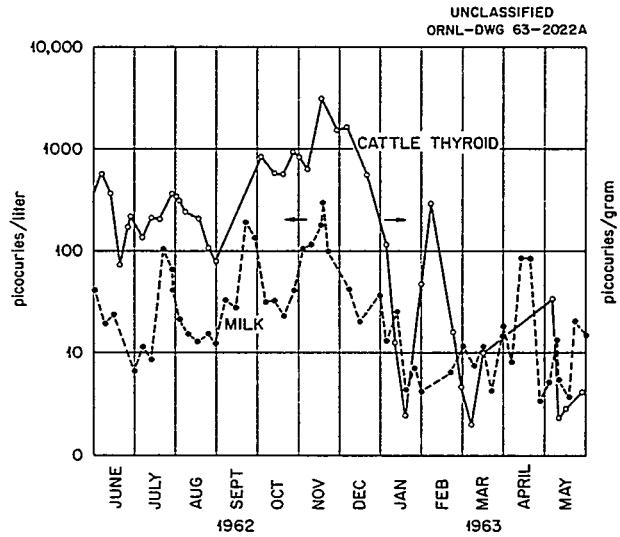

Fig. 19.18. Iodine-131 in Cattle Thyroids and in Milk in the East Tennessee Area.

IODINE-131 IN MILK AND IN CATTLE THYROIDS

J. L. Thompson B. R. Fish

During the period June 1, 1962, to May 31, 1963, a total of 285 cattle thyroids and 70 milk samples have been analyzed for I^{131}. It has been observed that the I^{131} concentration can differ by a factor of 3 or more in thyroids from cattle on the same farm and in milk from cows on the same farm. Thus, it is important to collect a fairly large number of samples from a given region in order to get a reasonable average for the concentration of I^{131} in milk. During the period of highest I^{131} levels, through December (Fig. 19.18), a larger number of samples were collected on each date; therefore, these data are considered to be more representative of the average I^{131} levels than the results of spot sampling in the later five months. These data suggest that the average concentration of I^{131} per liter in milk is about 8% of the average concentration per gram in cattle thyroids.

The I^{131} content in 280 liters of milk is approximately equal to the total I^{131} in one thyroid of cattle (average weight of thyroid, 22.4 g). For equal detection sensitivities the milk must be reduced about 8000 to 1 in volume. These facts emphasize the utility of including cattle thyroid sampling in a program for the monitoring of I^{131} in the environment. In addition to the milk sampling program the cattle thyroid monitoring program is suggested as another biological monitor which provides an extremely sensitive detection limit but requires a minimum amount of laboratory preparation.

Part VI. Education, Training, and Consultation

M. F. Fair

20. Education, Training, and Consultation

Nineteen students completed the course in Applied Radiation Physics at Vanderbilt University in May 1963. Thirteen of the students were AEC Fellows, four were from the Nuclear Engineering Department of the University, one was an Air Force officer, and one was a citizen of Pakistan.

Thirteen AEC Fellows, one Air Force officer, and one citizen of Pakistan reported to the Health Physics Division in June for Applied Health Physics training. Nine of the Fellows were granted extensions to their fellowships to complete the requirements for the M.S. degree.

Twenty-two students for the 1963–64 AEC Fellowship program were selected in March 1963. Nineteen will enroll at Vanderbilt University and three at the University of Tennessee in September 1963.

A 60-hr course in Health Physics was presented by the Division for the ORSORT program. The course consisted of lectures and tours covering various aspects of health physics.

Two 5-hr lecture series were given to NSF-AEC Institutes in Radiation Biology for High School Teachers – one at Florida State University and the other at the University of Wyoming.

Lectures and tours of the Laboratory were given for:

- U.S. Public Health Service, Cincinnati, Ohio
- ORNL Orientation Program
- ORINS Radioisotope Techniques Course
- ORINS Medical Division (courses in clinical techniques)
- American Industrial Hygiene Association
- University of North Carolina, School of Public Health
- ORINS-ORNL Ecology Course
- Applied Health Physics Section, Health Physics Division, ORNL

Training programs were coordinated by the Education and Training Section for C. Koh from Korea (one year), A. Gopez from the Philippines (three months), and A. Ziv from Israel (one year).

Papers, Publications, and Lectures

Papers

E. T. Arakawa, L. C. Emerson, D. C. Hammer, and R. D. Birkhoff

Transition Radiation and Optical Bremsstrahlung from Electron Bombarded Thin Gold Foils, American Physical Society, April 22–25, 1963, Washington, D.C.

E. T. Arakawa, A. L. Frank, L. C. Emerson, D. C. Hammer, and R. D. Birkhoff

Optical Emission from Metal Foils Irradiated by High Energy Electrons, International Congress of Radiation Research, August 5–11, 1962, Harrogate, England.

L. G. Augenstein, James Carter, Jaynati Nag-Chaudhuri, D. R. Nelson, and Edward Yeargers

Comparison of Emission from Excited States Produced in Proteins and Amino Acids by Ultraviolet Light and Ionizing Radiation, International Symposium on Physical Processes in Radiation Biology, May 5–8, 1963, East Lansing, Michigan.

J. A. Auxier

The Characteristics, Phenomenology and Attenuation of Fallout, U.S. Army Nuclear Science Seminar, August 1, 1962, Oak Ridge, Tennessee.

J. A. Auxier and F. W. Sanders

Dosimetry Studies for Hiroshima and Nagasaki, Health Physics Society, June 10–13, 1963, New York, New York.

A. G. Barkow, F. G. Karioris, and J. J. Stoffels

X-Ray Diffraction Analysis of Aerosols from Exploding Wires, Conference on Applications of X-Ray Analysis, August 8–10, 1962, Denver, Colorado.

S. R. Bernard

Mathematical Biological Approach to the Problem of Radiation-Induced Carcinogenesis, International Congress of Radiation Research, August 5–11, 1962, Harrogate, England.

An Expanding Compartment Model for Interpreting Radionuclide Metabolism by Various Species, International Congress of Radiation Research, August 5–11, 1962, Harrogate, England.

An $(MPC)_w$ *for* Rn^{222}, Health Physics Society, June 10–13, 1963, New York, New York.

Human Thyroid Uptake and Bodily Elimination of I^{131} *for the Case of Single and Continual Ingestion of Bound Iodine in Resin-Treated Milk,* Symposium on Radioiodine: Biological Considerations, June 17–19, 1963, Hanford, Washington.

R. D. Birkhoff

Energy Loss Spectra for Charged Particles Traversing Metal and Plastic Films, International Symposium on Physical Processes in Radiation Biology, May 5–8, 1963, East Lansing, Michigan.

J. O. Blomeke, R. L. Bradshaw, J. J. Perona, and J. T. Roberts

Estimated Costs for Management of High-Activity Power Reactor Wastes, American Nuclear Society, June 17–19, 1963, Salt Lake City, Utah.

W. J. Boegly, Jr.

Engineering Design of Demonstration Experiment 1. Mine Renovation, National Academy of Sciences–National Research Council Earth Sciences Committee on Waste Disposal, June 7, 1963, Washington, D.C.

W. J. Boegly, Jr., R. L. Bradshaw, F. M. Empson, Hisashi Kubota, and F. L. Parker

Laboratory and Field Studies in Salt at Oak Ridge Since December 1961, National Academy of Sciences–National Research Council Earth Sciences Committee on Waste Disposal, June 7, 1963, Washington, D.C.

R. L. Bradshaw

Ultimate Storage of High-Level Radioactive Waste Solids and Liquids in Salt Formation, Symposium on the Treatment and Storage of High-Level Radioactive Wastes, October 8–13, 1962, Vienna, Austria; International Colloquium on the Retention and Migration of Radioactive Ions in the Soil, October 15–19, 1962, Saclay, France.

R. L. Bradshaw, J. J. Perona, and J. O. Blomeke

Demonstration Disposal of High-Level Radioactive Solids in Lyons, Kansas, Salt Mine: Background and Preliminary Design of Experimental Aspects, National Academy of Sciences–National Research Council Earth Sciences Committee on Waste Disposal, June 7, 1963, Washington, D. C.

K. E. Cowser

Economic and Safety Evaluations, Conference on Transport of Radionuclides in Fresh Water, January 30–February 1, 1963, Austin, Texas.

K. E. Cowser, W. S. Snyder, and Mary Jane Cook

Estimates of Radiation Exposure Doses to Man from Radionuclides Released to the Clinch River, Health Physics Society, June 10–13, 1963, New York, New York.

D. A. Crossley, Jr.

Radioecology Studies of Millipedes (Dixidesmus erasus), American Association for the Advancement of Science, December 26–30, 1962, Philadelphia, Pennsylvania.

Use of Radioactive Tracers in the Study of Insect-Plant Relationships, IAEA Symposium on the Use and Application of Radioisotopes and Radiation in the Control of Plant and Animal Insect Pests, April 22, 1963, Athens, Greece.

Wallace de Laguna

Final Report of Second Fracturing Experiment and Preliminary Report on ORNL's Plans for Experimental Injections of Real Waste by Hydraulic Fracturing, National Academy of Sciences–National Research Council Earth Sciences Committee on Waste Disposal, June 7, 1963, Washington, D.C.

P. B. Dunaway and S. V. Kaye

Hematology of Cotton Rats on a Radioactive Area, American Association for the Advancement of Science, December 26–30, 1962, Philadelphia, Pennsylvania.

L. C. Emerson, E. T. Arakawa, R. H. Ritchie, R. D. Birkhoff, and D. C. Hammer

Investigation of Collective Effects in the Absorption of Radiation in Matter, Health Physics Society, June 10–13, 1963, New York, New York.

F. M. Empson

Radioactive Waste Disposal in Salt, International Conference on Saline Deposits, November 12–17, 1962, Houston, Texas.

Problems in Disposal of Radioactive Liquid Wastes in Salt, American Institute of Chemical Engineers, May 5–8, 1963, Buffalo, New York.

B. R. Fish

Exponentials versus Power Functions for Representing the Retention and Excretion of Elements by the Human Body, International Congress of Radiation Research, August 5–11, 1962, Harrogate, England.

B. R. Fish, S. R. Bernard, G. W. Royster, Jr., L. B. Farabee, P. E. Brown, and G. R. Patterson, Jr.

Human Uptake and Excretion of I^{131}: Single Inhalation Compared with Single and Continual Ingestion of Iodine in Milk, Health Physics Society, June 10–13, 1963, New York, New York.

F. F. Haywood

Operation BREN, Program I – Spatial Dose Distribution in Air Over Ground Geometry, Health Physics Society, June 10–13, 1963, New York, New York.

H. H. Hubbell, Jr., R. D. Birkhoff, and W. J. McConnell

Electron Slowing Down Spectra in Copper, American Physical Society, March 25–28, 1963, St. Louis, Missouri.

G. S. Hurst, L. B. O'Kelly, and J. A. Stockdale

Interaction of Subexcitation Electrons with Water Vapor, International Congress of Radiation Research, August 5–11, 1962, Harrogate, England.

D. G. Jacobs

Ion Exchange in the Deep-Well Injection of Radioactive Wastes, International Colloquium on the Retention and Migration of Radioactive Ions in the Soil, October 15–19, 1962, Saclay, France.

Mineral Exchange Work at Oak Ridge National Laboratory, AEC Working Meeting on the Use of Inorganic Exchange Materials for Radioactive Waste Treatment, August 13–14, 1962, Washington, D.C.

S. V. Kaye

Miniature Glass Rod Dosimeters in Radiation Ecology, American Association for the Advancement of Science, December 26–30, 1962, Philadelphia, Pennsylvania.

Use of Glass Rod Dosimetry in the ORNL Ecology Program, Health Physics Society, June 10–13, 1963, New York, New York.

David LaBar, J. A. Harter, and R. D. Birkhoff

Time-of-Flight Electron Beam Monochromator, American Physical Society, Southeastern Section, April 4–6, 1963, Knoxville, Tennessee.

T. F. Lomenick

Movement of Ruthenium in the Bed of White Oak Lake, International Colloquium on the Retention and Migration of Radioactive Ions in the Soil, October 15–19, 1962, Saclay, France.

K. Z. Morgan

Medical X-Ray Exposure, Tennessee Valley Industrial Health Conference, October 12–13, 1962, Gatlinburg, Tennessee.

The Body Burden of Long-Lived Isotopes, Pollution Medical Research Conference, January 28–29, 1963, San Francisco, California.

Permissible Dose for Internal Radiation, American Industrial Hygiene Conference, May 7–9, 1963, Cincinnati, Ohio.

D. J. Nelson

Chemical Morphology of Fresh-Water Clam Shells, International Congress of Limnology, August 20–25, 1962, Madison, Wisconsin.

Role of Bottom Organisms in Ecological Transport, Conference on Transport of Radionuclides in Fresh Water, January 30–February 1, 1963, Austin, Texas.

Use of Specific Activities for Interpretation of Ecological Tracer Studies, American Association for the Advancement of Science, December 26–30, 1962, Philadelphia, Pennsylvania.

D. R. Nelson and J. G. Carter

Comparison of Excited State Emissions Produced in Proteins and Amino Acids by Ultraviolet Light and Ionizing Radiation, Health Physics Society, June 10–13, 1963, New York, New York.

D. R. Nelson, J. G. Carter, and L. G. Augenstein

Thermoluminescence from X- and γ-Irradiated Biochemicals, International Congress of Radiation Research, August 5–11, 1962, Harrogate, England.

Jacob Neufeld

Distant Ionization Produced by Heavy Ions in Tissue, International Congress of Radiation Research, August 5–11, 1962, Harrogate, England.

Constitutive Equations for a Plasma-Like Medium, American Physical Society, January 22–25, 1963, New York, New York.

J. S. Olson

Gross and Net Production of Terrestrial Vegetation, British Ecological Society, March 30, 1963, London, England.

J. S. Olson and R. E. Shanks

Altitudinal Cover and Species Influences on Breakdown of Deciduous Litter in Southern Appalachian Forests, Ecological Society of America, August 26–30, 1962, Corvallis, Oregon.

Litter Breakdown in Relation to Chemical Cycling in Southern Appalachian Ecosystems, Ecological Society of America, August 26–30, 1962, Corvallis, Oregon.

F. L. Parker

Clinch River Studies, Conference on Transport of Radionuclides in Fresh Water, January 30–February 1, 1963, Austin, Texas.

Clinch River Studies, Health Physics Society, June 10–13, 1963, New York, New York.

Laboratory-Field Studies in Salt at Oak Ridge, Hutchinson, and Lyons, Kansas, National Academy of Sciences–National Research Council Earth Sciences Committee on Waste Disposal, June 7, 1963, Washington, D.C.

J. J. Perona, J. O. Blomeke, R. L. Bradshaw, and J. T. Roberts

Effects of Fission Product Removal on Waste Management Costs, American Nuclear Society, June 17–19, 1963, Salt Lake City, Utah.

J. J. Perona, R. L. Bradshaw, J. T. Roberts, and J. O. Blomeke

Economic Evaluation of Tank Storage, Pot Calcination, and Shipping of Power Reactor Fuel Reprocessing Wastes, Symposium on the Treatment and Storage of High-Level Radioactive Wastes, October 8–13, 1962, Vienna, Austria.

R. M. Richardson and E. G. Struxness

Environmental Factors That Affect Disposal Operations at ORNL, Health Physics Society, June 10–13, 1963, New York, New York.

R. H. Ritchie

Optical Absorption in Alkali Metals, American Physical Society, April 22–25, 1963, Washington, D.C.

R. H. Ritchie and J. C. Ashley

Transition Radiation and Bremsstrahlung from Irradiated Dielectric Media, Health Physics Society, June 10–13, 1963, New York, New York.

R. H. Ritchie, L. C. Emerson, and J. C. Ashley

Optical Bremsstrahlung from Dielectric Media, American Physical Society, Southeastern Section, April 4–6, 1963, Knoxville, Tennessee.

R. H. Ritchie and M. T. Harkrider

Low Energy End of the Secondary Electron Cascade in Metals, Health Physics Society, June 10–13, 1963, New York, New York.

R. H. Ritchie and G. S. Hurst

A Generalized Concept for Radiation Dosimetry, Symposium on Neutron Detection, Dosimetry, and Standardization, December 10–14, 1962, Harwell, England.

G. W. Royster, Jr., and B. R. Fish

NS "Savannah" Bioassay Program, Bio-Assay and Analytical Chemistry Conference, October 18–19, 1962, Augusta, Georgia.

Studies of Surface Contamination. III. Effect of Particle Size on the Measurement and Redispersion of Particulates, Health Physics Society, June 10–13, 1963, New York, New York.

W. S. Snyder

Estimation of Intake and Body Burden of Plutonium from Urinalysis Data, International Congress of Radiation Research, August 5–11, 1962, Harrogate, England.

Some Data on the Relationship of RBE and LET, Symposium on Protection Against Radiation Hazards in Space, November 5–7, 1962, Gatlinburg, Tennessee.

W. S. Snyder, Mary Jane Cook, and Mary R. Ford

An Estimate of $(MPC)_w$ *for Occupational Exposure to* Sr^{90}, Health Physics Society, June 10–13, 1963, New York, New York.

J. A. Stockdale, G. S. Hurst, L. B. O'Kelly, and E. B. Wagner

Electron Time-of-Flight Measurements of Diffusion and Drift Velocity, Gaseous Electronics Conference, October 10–12, 1962, Boulder, Colorado.

Tsuneo Tamura

Hydrofracture Mix Development, National Academy of Sciences–National Research Council Earth Sciences Committee on Waste Disposal, June 7, 1963, Washington, D.C.

Mineral Exchange Work at Oak Ridge National Laboratory, Working Meeting on Use of Inorganic Exchange Materials for Radioactive Waste Treatment, August 13–14, 1962, Washington, D.C.

Selective Sorption Reactions for Cesium and Strontium by Soil Minerals, International Colloquium on Retention and Migration of Radioactive Ions in Soils, October 15–19, 1962, Saclay, France.

J. H. Thorngate

Operation BREN, Program 1, Health Physics Society, East Tennessee Chapter, September 20, 1962, Oak Ridge, Tennessee.

Operation BREN, Program 1 – Spectrometry, Health Physics Society, June 10–13, 1963, New York, New York.

J. E. Turner, J. F. Feuerbacher, C. D. Zerby, W. E. Kinney, Jacob Neufeld, and W. S. Snyder

The Calculation of Radiation Dose in Tissue from High-Energy Protons, Symposium on Protection Against Radiation Hazards in Space, November 5–7, 1962, Gatlinburg, Tennessee.

H. O. Weeren

Shale Fracturing Experiment – Description and Hazards, National Academy of Sciences–National Research Council Earth Sciences Committee on Waste Disposal, June 7, 1963, Washington, D.C.

W. H. Wilkie, Jr., and R. D. Birkhoff

Measurement of Spectral Distribution of Positron Flux in an Infinite Copper Medium Containing Cu^{64}, American Physical Society, April 22–25, 1963, Washington, D.C.

J. P. Witherspoon, Jr.

Cycling of Cesium-134 in White Oak Trees, American Association for the Advancement of Science, December 26–30, 1962, Philadelphia, Pennsylvania.

Radiation Ecology and Mineral Cycling, Association of Southeastern Biologists, April 18–20, 1963, Gainesville, Florida.

Martin Witkamp

Factors Influencing Microbial Immobilization of Certain Radionuclides in Leaf Litter, American Society for Microbiology, Oak Ridge–Kentucky–Tennessee Branch, October 26–27, 1962, Oak Ridge, Tennessee.

Influence of Environmental Factors on Microbial Immobilization of Certain Radionuclides in Forest Litter, American Association for the Advancement of Science, December 26–30, 1962, Philadelphia, Pennsylvania.

Uptake, Concentration, and Release of Radioisotopes by Fungi in Leaf Litter, International Congress for Microbiology, August 19–24, 1962, Montreal, Canada.

Edward Yeargers, D. R. Nelson, Jayanti Nag-Chaudhuri, J. C. Carter, and L. G. Augenstein

Comparison of Emission from Excited States Produced by Ultraviolet Light and Ionizing Radiation, Radiation Research Society, May 27–29, 1963, Milwaukee, Wisconsin.

Publications

E. T. Arakawa, L. C. Emerson, D. C. Hammer, and R. D. Birkhoff
"Transition Radiation and Optical Bremsstrahlung from Electron-Bombarded Thin Gold Foils," to be published in the *Physical Review.*

S. I. Auerbach and Vincent Schultz
Onsite Ecological Research of the Division of Biology and Medicine at the Oak Ridge National Laboratory, TID-16890 (December 1962).

J. A. Auxier
"Dosimetry and Exposures in Nuclear Accidents," to be published in the *Journal of Nuclear Safety.*

J. A. Auxier, F. F. Haywood, and L. W. Gilley
"General Correlative Studies, Operation BREN," CEX-62.03 (to be published).

R. D. Birkhoff
"Electron Spectroscopy in Health Physics Research," submitted for publication in *Health Physics.*

R. E. Blanco and F. L. Parker
Waste Treatment and Disposal Quart. Progr. Rept. August–October 1962, ORNL TM-482 (Mar. 25, 1962).

R. E. Blanco and E. G. Struxness
Waste Treatment and Disposal Progr. Rept. February and March 1962, ORNL TM-252 (Sept. 10, 1962).

Waste Treatment and Disposal Progr. Rept. April and May 1962, ORNL TM-376 (Nov. 5, 1962).

Waste Treatment and Disposal Progr. Rept. June and July 1962, ORNL TM-396 (Dec. 19, 1962).

J. O. Blomeke, R. L. Bradshaw, J. J. Perona, and J. T. Roberts
Estimated Costs for Management of High-Activity Power Reactor Processing Wastes, ORNL TM-559 (May 13, 1963).

T. E. Bortner, G. S. Hurst, Mildred Edmundson, and J. E. Parks
Alpha Particle Ionization of Argon Mixtures – Further Study of the Role of Excited States, ORNL-3422 (May 23, 1963).

R. L. Bradshaw, W. J. Boegly, Jr., F. M. Empson, H. Kubota, F. L. Parker, J. J. Perona, and E. G. Struxness
"Ultimate Storage of High-Level Waste Solids and Liquids in Salt Formations," pp 153–75 in *Treatment and Storage of High-Level Radioactive Wastes,* International Atomic Energy Agency, Vienna, 1963.

P. R. J. Burch
"A Biological Principle and Its Converse: Some Implications for Carcinogenesis," *Nature* **195**, 241–43 (1962).

J. G. Carter, R. A. MacRae, D. R. Nelson, R. D. Birkhoff, and E. T. Arakawa
"Interference Filter Spectrometer for Low Intensity Extended Sources," to be published in *Applied Optics.*

J. G. Carter, D. R. Nelson, and L. G. Augenstein
"Dependence of Thermoluminescence upon Sample Surface Area and Environmental Gas Pressure," *Appl. Phys. Letters* **2**, 226–27 (1963).

J. S. Cheka
"Metaphosphate Glass as an Integrating Dosimeter," *Health Phys.* **8**, 551–52 (1962).

"Stability of Radiophotoluminescence in Metaphosphate Glass," submitted for publication in *Health Physics.*

K. E. Cowser, W. S. Snyder, and Mary Jane Cook
"Preliminary Safety Analysis of Radionuclide Release to the Clinch River," *Working Conference on Transport of Radionuclides in Fresh Water, Jan. 30, 31, and Feb. 1, 1963, Austin, Texas.*

D. A. Crossley, Jr., and Mary P. Hoglund
"A Litter-Bag Method for the Study of Microarthropods Inhabiting Leaf Litter," *Ecology* **43**(3), 571–73 (1962).

N. O. Davis, L. C. Emerson, E. T. Arakawa, and R. D. Birkhoff
Angular and Spectral Distribution of Light Emitted from Electron-Bombarded Silver Foils, ORNL-3485 (to be published).

F. J. Davis and P. W. Reinhardt
"Radiation Measurements Over Simulated Plane Sources," *Health Phys.* **8**, 233–43 (1962).

F. J. Davis and P. W. Reinhardt (eds.)
Extended- and Point-Source Radiometric Program, CEX-60.3 (Aug. 8, 1962).

P. B. Dunaway
"Litter Size Record for Eastern Harvest Mouse," *J. Mammalogy* **43**, 428–29 (1962).

H. B. Eldridge
Pulse Height Calculations for a Parallel Plate Ionization Chamber Containing Electron Attaching Gases, ORNL-3090 (Oct. 24, 1962).

L. C. Emerson, E. T. Arakawa, R. H. Ritchie, and R. D. Birkhoff
Emission Spectra of Electron Irradiated Metal Foils, ORNL-3450 (to be published).

B. R. Fish
Trip Report, July 27–Aug. 20, 1962: Second International Congress of Radiation Research, Harrogate, England; Visits to Whole Body Counting Facilities; and Discussions Concerning Proposed Symposium on Surface Contamination and Nuclear Safety Micrometeorology, ORNL CF-62-9-32 (Sept. 18, 1962).

B. R. Fish and G. R. Patterson, Jr.
Preliminary Review of Potential Biological Hazards from Deposition of Nuclear Rocket Debris in the Earth Biosphere, ORNL TM-501 (Feb. 25, 1963) (confidential).

B. R. Fish and G. W. Royster, Jr.
"Bioassay Development Program," pp 19–21 in *Maritime Reactor Program Ann. Progr. Rept. Nov. 30, 1962,* ORNL-3416.

A. L. Frank, E. T. Arakawa, R. D. Birkhoff, R. H. Ritchie, and H. B. Eldridge
Optical Emission from Irradiated Thin Metallic Foils, ORNL-3114 (July 2, 1962).

D. C. Hammer, E. T. Arakawa, and R. D. Birkhoff
"A Simple Grating Calibrator for the Visible and Vacuum Ultraviolet," to be published in *Applied Optics.*

D. C. Hammer, E. T. Arakawa, L. C. Emerson, and R. D. Birkhoff
Optical Emission from Electron Irradiated Thin Gold Foils, ORNL-3468 (to be published).

G. S. Hurst, L. B. O'Kelly, and J. A. Stockdale
"Quasi-Trapping of Low Energy Electrons in Water Vapor," *Nature* **195**, 66–67 (1962).

G. S. Hurst, L. B. O'Kelly, E. B. Wagner, and J. A. Stockdale
"Time-of-Flight Investigations of Electron Transport in Gases," to be published in the *Journal of Chemical Physics.*

G. S. Hurst and R. H. Ritchie
"Applications to Radiation Dosimetry," pp 367–90 in *Nuclear Instruments and Their Uses,* vol 1, Wiley, New York, 1962.

G. S. Hurst, J. A. Stockdale, and L. B. O'Kelly
"Interaction of Low Energy Electrons with Water Vapor and with Other Polar Molecules," *J. Chem. Phys.* **38**, 2572–78 (1963).

D. G. Jacobs
"Mineral Exchange Work at ORNL," pp 187–99 in *The Use of Inorganic Exchange Materials for Radioactive Waste Treatment,* TID-7644 (January 1963).

F. G. Karioris, B. R. Fish, and G. W. Royster, Jr.
"Aerosols from Exploding Wires," *Exploding Wires* **2**, 299–311 (1962).

N. R. Kevern
"Primary Productivity and Energy Relationships in Artificial Streams," PhD Thesis, Michigan State University, 132 pp (1962).

D. A. LaBar, R. D. Birkhoff, and J. A. Harter
Time-of-Flight Electron Beam Monochromator, ORNL-3484 (to be published).

W. de Laguna
"Engineering Geology of Radioactive Waste Disposal," *Eng. Geol.* **1**, 129–60 (1962).

W. T. Lammers
"Density Gradient Separation of Plankton and Clay from River Water," *Limnol. Oceanog.* **7**(2), 224–29 (1962).

T. F. Lomenick
The Geology of a Portion of the Hutchinson Salt Member of the Wellington Formation in the Mine of The Carey Salt Company, Lyons, Kansas, ORNL TM-597 (submitted for publication).

W. J. McConnell, H. H. Hubbell, Jr., and R. D. Birkhoff
Electron Slowing Down Spectrum in Cu of Beta Rays from Cu-64, ORNL-3463 (to be published).

A. L. Mohan, D. G. Jacobs, and E. G. Struxness
Ruthenium Sorption by Minerals, ORNL TM-329 (Aug. 31, 1962).

K. Z. Morgan
"Techniques of Personnel Monitoring and Radiation Surveying," p 391 in *Nuclear Instruments and Their Uses,* vol 1, Wiley, New York, 1962.

"Permissible Exposure to Ionizing Radiation," *Science* **139**(3555), 565–71 (Feb. 15, 1963).

R. J. Morton (ed.) *et al.*
Status Report No. 3 on Clinch River Study, ORNL-3370 (Nov. 21, 1962).

R. J. Morton (ed.) *et al.*
Status Report No. 4 on Clinch River Study, ORNL-3409 (submitted for publication).

D. J. Nelson and D. C. Scott
"Role of Detritus in the Productivity of a Rock-Outcrop Community in a Piedmont Stream," *Limnol. Oceanog.* **7**, 396–413 (1962).

J. Neufeld
"Constitutive Equations for a Plasma-Like Medium," to be published in *Journal of Applied Physics.*

"Electromagnetic Properties of a Plasma-Beam System," *Phys. Rev.* **127**, 346–59 (1962).

"Formulation of the Energy Density and the Energy Flow in Terms of Constitutive and 'Electromagnetic' Parameters," submitted for publication in the *Physical Review.*

"Interaction of a Stationary Plasma with an Electron Beam," submitted for publication in the *Physics of Fluids.*

"Plasma-Beam Instability in the Hartree-Appleton Approximation," submitted for publication in the *Physics of Fluids.*

J. Neufeld and H. A. Wright
"Instabilities in a Plasma-Beam System Immersed in a Magnetic Field," *Phys. Rev.* **129**, 1489–1507 (1963).

"Magnetodynamic Instabilities in a Plasma-Beam System," to be published in the *Physical Review.*

J. Neufeld and W. S. Snyder
"A Basis for Calculation of Depth Dose of High Energy Particles," pp 105–107 in *Premier Colloque International sur la Protection Aupres des Grands Accelerateurs (Shielding Around High Energy Accelerators) Orsay et Saclay, Jan.. 18–20, 1962,* Presses Universitaires de France, Paris, 1962.

J. S. Olson
"Surveys of Environmental Radioactivity," *Nucl. Safety* 4(1), 88–95 (1962).

F. L. Parker and R. E. Blanco
Waste Treatment and Disposal Progr. Rept. November–December 1962 and January 1963, ORNL TM-516 (June 12, 1963).

J. J. Perona, J. O. Blomeke, R. L. Bradshaw, and J. T. Roberts
Evaluation of Ultimate Disposal Methods for Liquid and Solid Radioactive Wastes. V. Effects of Fission Product Removal on Costs of Waste Management, ORNL-3357 (June 12, 1963).

H. M. Perry, Jr., Isabel H. Tipton, H. A. Schroeder, and Mary Jane Cook
"Variability in the Metal Content of Human Organs," *J. Lab. Clin. Med.* **60**, 245–53 (1962).

G. L. Plummer
"Growth Responses of Helianthus Annuus to Internal Calcium-45," *Botan. Gaz.* **123**(4), 272–78 (1962).

R. H. Ritchie
"On Surface Plasma Oscillations in Metal Foils," to be published in *Progress of Theoretical Physics (Kyoto)*.

R. H. Ritchie, V. E. Anderson, and H. B. Eldridge
ORNL-3116 (July 12, 1962) (classified).

F. W. Sanders and J. A. Auxier
"Neutron Activation of Sodium in Anthropomorphous Phantoms," *Health Phys.* **8**, 371–79 (1962).

H. A. Schroeder, J. J. Balassa, and Isabel H. Tipton
"Abnormal Trace Metals in Man: Titanium," *J. Chronic Diseases* **16**, 55–69 (1963).

J. M. Schurr and W. N. Stamper
"A Model for the Accumulation of Strontium and Calcium by Recently Molted Crayfish (*Cambarus longulus longerostris* Ort.)," *Limnol. Oceanog.* **7**(4), 474–77 (1962).

T. M. Sims
Low Temperature Thermoluminescence of Gamma Irradiated Potassium Dihydrogen Phosphate, ORNL-3346 (Oct. 5, 1962).

W. S. Snyder
"The Estimation of a Body Burden of Pu from Urinalysis Data," p 13 in ANL-6637.

"Major Sources of Error in Interpreting Urinalysis Data to Estimate the Body Burden of Pu^{239}: A Preliminary Study," *Health Phys.* **8**(6), 767 (1962).

"Some Data on the Relationship of RBE and LET," p 402 in TID-7652.

W. S. Snyder and Mary Jane Cook
"Variability of Relative Organ Concentration of Trace Elements in Human Tissue," *Health Phys.* **9**(1), 57 (1963).

"The Distribution of Dose Resulting from a Constant Level of Contamination of the Environment by Sr^{90} and Various Other Radionuclides," *Health Phys.* **9**(4), 417 (1963).

T. D. Strickler
"Ionization by Alpha Particles in Binary Gas Mixtures," *J. Phys. Chem.* **67**, 825 (1963).

T. Tamura
"Cesium Sorption Reactions as Indicator of Clay Mineral Structures," *Clays and Clay Minerals, Proc. Natl. Conf. Clays Clay Minerals* **X**, 389–98 (1963).

"Mineral Exchange Work at ORNL," pp 29–45 in *The Use of Inorganic Exchange Materials for Radioactive Waste Treatment*, TID-7644 (January 1963).

J. H. Thorngate
"A Medium Speed Coincidence Circuit Using Tunnel Diodes," submitted for publication in the *Review of Scientific Instruments*.

Isabel H. Tipton and Mary Jane Cook
"Trace Elements in Human Tissue. Part II. Adult Subjects from the United States," *Health Phys.* **9**(2), 103 (1963).

Isabel H. Tipton, Mary Jane Cook, R. L. Steiner, C. A. Boye, H. M. Perry, Jr., and H. A. Schroeder
"Trace Elements in Human Tissue. Part I. Methods," *Health Phys.* **9**(2), 89 (1963).

J. E. Turner and Hal Hollister
"The Possible Role of Momentum in Radiation Dosimetry," *Health Phys.* **8**, 523–31 (1962).

C. J. Weinberg, J. G. Carter, D. R. Nelson, and R. D. Birkhoff
Thermoluminescence Spectra and Activation Energies for Aromatic Amino Acids, Trypsin, and Spores of Bacillus Megaterium, ORNL-3115 (June 7, 1963).

W. H. Wilkie, Jr., and R. D. Birkhoff
Measurement of Spectral Distribution of Positron Flux in an Infinite Copper Medium Containing Cu^{64}, ORNL-3469 (to be published).

J. P. Witherspoon, Jr., S. I. Auerbach, and J. S. Olson
Cycling of Cs^{134} in White Oak Trees on Sites of Contrasting Soil Type and Moisture, ORNL-3328 (1962).

M. Witkamp
"Influence of Environmental Factors on Microbial Immobilization of Certain Radionuclides in Forest Litter" (Abstract), *Bull. Ecol. Soc. Am.* 43(4), 121 (1963).

"Factors Influencing Microbial Immobilization of Certain Radionuclides in Leaf Litter" (Abstract), *J. Tenn. Acad. Sci.* 38(2), 78 (1962).

Lectures

S. I. Auerbach
Soil-Plant Transfer of Fission Products as Derived from Ecological Studies at Oak Ridge National Laboratory, UT-AEC Agricultural Research Laboratory, May 8, 1963, Oak Ridge, Tennessee.

Radiation Ecology, Department of Zoology, University of Tennessee, May 22, 1963, Knoxville; Lecture for the Radiological Health Specialists Group of the Consolidated University of North Carolina, ORNL, September 12, 1962, Oak Ridge, Tennessee.

Radioecological Studies, Naval Research Reserve, U.S. Army Nuclear Science Seminar, August 8, 1962, Oak Ridge, Tennessee.

Introduction to Ecology, Health Physics Course, ORINS, October 26, 1962, Oak Ridge, Tennessee.

Special Topics in Ecology, Health Physics Course, ORINS, November 5, 1963, Oak Ridge, Tennessee.

J. A. Auxier
Human Radiobiological Investigations, Department of Physics, University of Tennessee, November 26, 1962, Knoxville.

R. D. Birkhoff
Experiments on Electron Interactions in Solids, Department of Physics, University of Tennessee, November 5, 1962, Knoxville.

R. L. Bradshaw
Radioactive Waste Disposal in Natural Salt Formations, Reactor Safety and Hazards Evaluation Course for U.S. Public Health Service Personnel, May 15, 1963, Oak Ridge, Tennessee.

Disposal of Radioactive Wastes, U.S. Army Nuclear Science Seminar, ORINS, August 8, 1962, Oak Ridge, Tennessee.

Mary Jane Cook
Internal Dose, East Tennessee Rabbit Association, January 8, 1963, Knoxville, Tennessee; Catholic High School, January 21, 1963, Knoxville, Tennessee.

K. E. Cowser
Origin, Treatment and Disposal of Radioactive Waste (three lectures), ORSORT, January 3–5, 1963, Oak Ridge, Tennessee.

D. A. Crossley, Jr.

Insect-Plant Relationships in a Radioactive Waste Area, Institute of Radiation Biology, Texas Woman's University, May 18, 1963, Denton; Alpha Mu Epsilon, University of Georgia, October 23, 1962, Athens; Department of Entomology, University of Maryland, November 5, 1962, College Park.

Biological Half-Life of Radioisotopes as an Ecological Research Tool, Science Department, Bethany College, November 7, 1962, Bethany, West Virginia; Biology Department, University of Florida, November 29, 1962, Gainesville; Institute of Marine Sciences, University of Miami, November 30, 1962, Miami, Florida; Midwestern University, January 9, 1963, Wichita Falls, Texas; Oklahoma State University, January 10, 1963, Stillwater; Zoology Department, Louisiana State University, January 11, 1963, Baton Rouge; Institute of Radiation Biology, Texas Woman's University, May 18, 1963, Denton.

Wallace de Laguna

Geological Consideration in Ground Disposal, U.S. Public Health Service Reactor Safety and Hazards Evaluation Course, March 6, 1963, Oak Ridge, Tennessee; U.S. Public Health Service Program on Radioactive Waste and Disposal, September 6, 1962, Oak Ridge, Tennessee; U.S. Public Health Service Reactor Safety and Hazards Evaluation Course, May 16, 1963, Oak Ridge, Tennessee.

P. B. Dunaway

Effects of Ionizing Radiation on Mammalian Populations, Alabama College, May 7, 1963, Montevallo.

B. R. Fish

Radioactivity in Man, ORINS Special Training Division, October 5, 1962, Oak Ridge, Tennessee.

Whole Body Counters in Health Physics, ORINS Special Training Division, October 10, 1962, Oak Ridge, Tennessee.

Measurement of Radioactivity in the Human Body, Department of Physics, University of Tennessee, November 12, 1962, Knoxville.

D. G. Jacobs

Mineral Exchange Reactions of Cesium, Seminar at Illinois State Geological Survey, November 30, 1962, Urbana.

Reactions of Fission Products in Mineral Systems, Seminar at Harvard University, April 11, 1963, Cambridge, Massachusetts.

S. V. Kaye

Use of Radioactive Tags for Marking Animals, Radiation Biology-Ecology Institute, ORINS, June 25, 1963, Oak Ridge, Tennessee.

N. R. Kevern

Primary Productivity and Energy Relationships in Artificial Streams, ORNL, April 25, 1963, Oak Ridge, Tennessee.

T. F. Lomenick

Waste Disposal Activities at ORNL, Lecture for the Radiological Health Specialists Group of the Consolidated University of North Carolina, ORNL, September 12, 1962, Oak Ridge, Tennessee.

Disposal of Radioactive Wastes, AEC Short Course in Health Physics, October 26, 1962, and November 5, 1962, Oak Ridge, Tennessee.

Tour – Waste Management Facilities, U.S. Public Health Service Radioactive Wastes and Their Disposal Course, September 6, 1962, Oak Ridge, Tennessee; U.S. Public Health Service Reactor Safety and Hazards Evaluation Course, March 6, 1963, Oak Ridge, Tennessee.

Handling, Treatment, and Disposal of Chemical Processing Wastes, U.S. Public Health Service Reactor Safety and Hazards Evaluation Course, March 6, 1963, Oak Ridge, Tennessee.

Waste Management at ORNL, U.S. Public Health Service Reactor Safety and Hazards Evaluation Course, May 16, 1963, Oak Ridge, Tennessee.

K. Z. Morgan

Health Physics, AEC Fellowship Course in Health Physics, ORNL, July 11–12, 1962, Oak Ridge, Tennessee.

Introduction to Health Physics, Department of Physics, University of Tennessee, September 24, 1962, Knoxville.

Radioactive Fallout, U.S. Civil Defense Council Conference, Civic Auditorium, October 16, 1962, Knoxville, Tennessee.

Requirements of the Rem Unit to Meet the Needs of Internal Dose, ORNL, October 17, 1962, Oak Ridge, Tennessee

Internal Exposure Calculations, ORINS Training Division, October 22 and 24, 1962, Oak Ridge, Tennessee.

History and Functions of the Health Physics Society, AEC Short Course in Health Physics, ORNL, November 8, 1962, Oak Ridge, Tennessee.

Maximum Permissible Exposure to Ionizing Radiation, Texas A and M College, November 29, 1962, College Station; Bishop College, December 1, 1962, Dallas, Texas.

Health Physics, North Carolina State College, December 14, 1962, Raleigh.

Maximum Permissible Exposure, ORSORT, ORNL, January 14, 16, and 18, 1963, Oak Ridge, Tennessee.

Internal Dose Calculations, ORSORT, ORNL, January 25 and 31 and February 1, 1963, Oak Ridge, Tennessee.

Permissible Exposure to Ionizing Radiation, University of Georgia, March 7, 1963, Athens.

A Perspective on Radiation Health Hazards; Health Physics Research at Oak Ridge National Laboratory, ORINS Deans' Conference, March 14–15, 1963, Oak Ridge, Tennessee.

Dental Education in the Proper Use of Ionizing Radiation, American Association of Dental Schools, March 25–26, 1963, Pittsburgh, Pennsylvania.

Health Physics Lectures, AEC Fellowship Course in Health Physics, Vanderbilt University, April 1–2, 8–9, and 15–16, 1963, Nashville, Tennessee.

Permissible Exposure to Ionizing Radiation, Lebanon Valley College, April 19–20, 1963, Annville, Pennsylvania; University of Cincinnati, April 23–24, 1963, Cincinnati, Ohio; Lees-McRae College, May 3, 1963, Banner Elk, North Carolina; Bennett College, May 6, 1963, Greensboro, North Carolina.

Problems of Internal Dosimetry, University of Pittsburgh Graduate School of Public Health, May 6, 1963, Pittsburgh, Pennsylvania.

Permissible Allowable Exposure, Radiation Safety Training Program, ORNL, May 21, 1963, Oak Ridge, Tennessee.

Internally Deposited Radionuclides, Department of Health, Education, and Welfare, May 29, 1963, Rockville, Maryland.

D. J. Nelson

The Distribution of Strontium with Respect to Growth and Morphology of Unionidae Shells, Department of Zoology, University of Tennessee, October 9, 1962, Knoxville.

Radioecological Research at Oak Ridge National Laboratory, Department of Zoology and Entomology, Iowa State University, November 30, 1962, Ames.

Specific Activity Ratios in Ecological Research, Institute in Radioecology, ORINS, June 14, 1963, Oak Ridge, Tennessee.

J. Neufeld

Magnetic Properties of Plasma-Like Medium and Instabilities Resulting from the Interaction of an Electron Beam with a Stationary Medium, Symposium on Theory of Plasma, Summer School sponsored by Faculty of Sciences of University of Paris, September 10–21, 1962, Orsay, France.

Interaction of Ions with Matter, Department of Physics, University of Tennessee, December 10, 1962, Knoxville.

F. L. Parker

Radioactive Waste Disposal, AEC Fellowship Course in Health Physics, Vanderbilt University, April 22–23, 1963, Nashville, Tennessee.

Disposal of Radioactive Waste into Fresh Water Streams, Sigma Xi Lecture, Clemson College, November 19, 1962, Clemson, South Carolina.

Radioactive Waste Disposal, Physics Seminar, University of Tennessee, December 3, 1962, Knoxville.

Disposal of Radioactive Wastes into the Clinch River, Fluid Mechanics Seminar, Pennsylvania State University, May 10, 1963, University Park.

R. H. Ritchie

Transition Radiation, Conference on Electromagnetic Theory and Its Application to Dispersive Media, September 10–21, 1962, Orsay, France.

Theory of Electron Interactions in Solids, Department of Physics, University of Tennessee, October 29, 1962, Knoxville.

W. S. Snyder

Maximum Permissible Exposure to Fast and Thermal Neutrons, USAEC Short Course in Health Physics, ORINS, October 2, 1962, Oak Ridge, Tennessee.

The Problem of Ingested Radioisotopes, Physics 599e Seminars in Health Physics, Department of Physics, University of Tennessee, October 8, 1962, Knoxville.

Relative Biological Effectiveness, Neutrons, International Commission on Radiological Protection, and National Committee on Radiation Protection, AEC Fellowship Course in Health Physics, Vanderbilt University, April 29–30, 1963, Nashville, Tennessee.

Strontium, Radon, GI Tract, Addition of Internal and External Dose, AEC Fellowship Course, Vanderbilt University, May 6–7, 1963, Nashville, Tennessee.

E. G. Struxness

Radioactive Waste Disposal, Summer Symposium on Radioecology, ORINS, June 17, 1963, Oak Ridge, Tennessee.

Isabel H. Tipton

Instrumentation for Optical Spectroscopy, Health Physics Society, June 1962, Chicago, Illinois.

Correlations Between Trace Elements in Human Tissue, International Physiological Congress, September 1962, Leiden, Netherlands.

Statistical Analysis of Data on Trace Elements in Human Tissue, Conference on Air Pollution, January 1963, San Francisco, California.

Statistical Interpretation of Trace Element Data, American Physical Society, Southeastern Section, April 1963, Knoxville, Tennessee.

J. E. Turner

Generalized Approach to Dosimetry, Department of Physics, University of Tennessee, October 15, 1962, Knoxville.

Martin Witkamp

Microbial Ecology, Department of Botany, University of Tennessee, May 8, 1963, Knoxville.

ORNL-3492
UC-41 – Health and Safety
TID-4500 (22nd ed.)

INTERNAL DISTRIBUTION

1. C. E. Larson
2. Biology Library
3–5. Central Research Library
6. Laboratory Shift Supervisor
7. Reactor Division Library
8–9. ORNL – Y-12 Technical Library, Document Reference Section
10–60. Laboratory Records Department
61. Laboratory Records, ORNL R.C.
62. A. M. Weinberg
63. J. A. Swartout
64. K. Z. Morgan
65. S. E. Beall
66. M. L. Nelson
67. S. C. Lind
68. A. S. Householder
69. C. S. Harrill
70. F. L. Parker
71. E. H. Taylor
72. W. H. Jordan
73. T. A. Lincoln
74. A. Hollaender
75. F. L. Culler
76. H. E. Seagren
77. M. T. Kelley
78. R. S. Livingston
79. C. D. Susano
80. W. J. Boegly
81. E. G. Struxness
82. W. E. Cohn
83. M. L. Randolph
84. M. J. Skinner
85. G. C. Williams
86. T. H. J. Burnett
87. G. S. Hurst
88. S. R. Bernard
89. J. A. Lane
90. W. S. Snyder
91. L. B. Holland
92. J. L. Gabbard
93. A. C. Upton
94. D. M. Davis
95. R. L. Clark
96. L. C. Johnson
97. O. D. Teague
98. A. J. Miller
99. A. D. Warden
100. J. A. Auxier
101. S. I. Auerbach
102. F. C. Maienschein
103. B. Fish
104. R. B. Parker
105. R. D. Birkhoff
106. J. A. Harter
107. R. W. Peelle
108. R. M. Richardson
109. J. S. Olson
110. R. J. Morton (consultant)
111. T. E. Bortner (consultant)
112. P. H. Doyle (consultant)
113. U. Fano (consultant)
114. T. D. Strickler (consultant)
115. J. C. Frye (consultant)
116. G. M. Fair (consultant)
117. R. S. Platzman (consultant)
118. J. B. Hursh (consultant)
119. E. P. Odum (consultant)
120. H. O. Wyckoff (consultant)

EXTERNAL DISTRIBUTION

121. R. W. McNamee, Union Carbide Corporation, New York
122. Physics and Engineering Group, Balcones Research Center, RFD 4, Box 189, Austin, Texas
123. G. E. Thoma, St. Louis University Hospital, 135 South Grand Boulevard, St. Louis, Missouri
124. Vanderbilt University (Physics Library)
125. Paul Jones, U.S. Geological Survey, Washington, D.C.
126. Lola Lyons, Librarian, Olin Industries, Inc., East Alton, Illinois
127. Jack Story, Health Physicist, North Carolina State College, Raleigh, North Carolina
128. J. H. Ebersole, USS Nautilus, c/o Fleet Post Office, New York, New York

129. David S. Smith, Health and Safety Division, U.S. Atomic Energy Commission, Chicago Operations Office, P.O. Box 59, Lemont, Illinois
130. Research and Development Division, AEC, ORO
131. S. C. Sigoloff, Edgerton, Germeshausen and Grier, Inc., P.O. Box 98, GoLeta, California
132. Robert Wood, Department of Physics, Memorial Center, 444 E. 68th St., New York 21, New York
133. John Wolfe, Division of Biology and Medicine, U.S. Atomic Energy Commission, Washington, D.C.
134. Orlando Park, Department of Biology, Northwestern University, Evanston, Illinois
135. W. T. Ham, Medical College of Virginia, Richmond, Virginia
136. F. H. W. Noll, Department of Physics, Berea College, Berea, Kentucky
137. Herbert E. Stokinger, Bureau of State Service, Department of Health, Education and Welfare, Penn 14 Broadway, Cincinnati 2, Ohio
138. J. B. Lackey, University of Florida, Gainesville, Florida
139. J. J. Davis, Biology Operation, Hanford Atomic Power Operations, Seattle, Washington
140. Robert B. Platt, Department of Biology, Emory University, Atlanta, Georgia
141. C. H. Bernard, Physics Department, Texas A&M, College Station, Texas
142. C. E. Dady, Watertown Arsenal, Ordnance Material Research Office, Watertown, Massachusetts
143. John I. Hopkins, Davidson College, Department of Physics, P.O.Box 327, Davidson, North Carolina
144. W. J. Lacy, Office of Civil Defense, Pentagon, Washington, D.C.
145. G. A. Andrews, Oak Ridge Institute of Nuclear Studies, Oak Ridge, Tennessee
146. E. P. Resner, States Marine Lines, c/o New York Shipbuilding Corp., Camden, New Jersey

147–151. Walter Belter, Division of Reactor Development, AEC, Washington, D.C.

152. H. J. Carey, Jr., The Carey Salt Company, Hutchinson, Kansas
153. C. Orr, Georgia Institute of Technology, Atlanta, Georgia
154. E. F. Gloyna, Department of Civil Engineering, University of Texas, Austin 12, Texas
155. J. S. Cragwall, Jr., U.S. Geological Survey, Surface Water Branch, 823 Edney Building, Chattanooga, Tennessee
156. H. H. Waesche, AEC Liaison Officer, Geochemical and Petrology Branch, U.S. Geological Survey, Naval Gun Factory, Building 213, Washington 25, D.C.
157. S. Leary Jones, Tennessee Department of Public Health, Cordell Hull Building, Nashville, Tennessee
158. H. C. Thomas, Chemistry Department, University of North Carolina, Chapel Hill, North Carolina
159. Glenn Gentry, Fish Management Division, Game and Fish Commission, Cordell Hull Building, Nashville, Tennessee
160. Vincent Schultz, Environmental Sciences Branch, Division of Biology and Medicine, U.S. Atomic Energy Commission, Washington 25, D.C.
161. O. W. Kochtitzky, Tennessee Valley Authority, 717 Edney Building, Chattanooga, Tennessee
162. Leslie Silverman, Industrial Engineering, Department of Industrial Hygiene School of Public Health, Harvard University, 55 Shattuck Street, Boston 15, Massachusetts
163. J. Wade Watkins, U.S. Bureau of Mines, Washington, D.C.
164. Kansas State Board of Health, Topeka, Kansas (Dwight F. Metzler)
165. Kansas State Geological Survey, Lawrence, Kansas (Lee Mays)
166. Linn Hoover, Executive Secretary, Division of Earth Sciences, National Academy of Sciences–National Research Council, Washington, D.C.
167. C. S. Shoup, Biology Division, U.S. Atomic Energy Commission, Oak Ridge, Tennessee
168. L. Garcia, Naval Research Laboratory, Washington, D.C.
169. J. A. Lieberman, Division of Reactor Development, AEC, Washington, D.C.
170. Conrad Straub, Robert A. Taft Sanitary Engineering Center, Cincinnati, Ohio
171. M. Vidmar, Boris Kidric Institute, Vinča, Yugoslavia
172. Warren J. Kaufman, University of California, Berkeley, California
173. Sakai Shimizu, Institute for Chemical Research, Kyoto University, Kyoto, Japan
174. Toshio Aoki, J. A. E. R. I., Tokai-Mura, Naka-Gun, Ibaraki-Ken, Japan
175. K. A. Mahmoud, Radiation Protection and Civil Defense Department, Atomic Energy Establishment, Abou-Zaabal Post Office, Cairo, U. A. R., Egypt

176–862. Given distribution as shown in TID-4500 (22nd ed.) under Health and Safety category (100 copies – OTS)